UNIVERSIDADE D
COIMBRA

Adriana Costa Leal

TOWARDS THE CHARACTERISATION OF THE PREICTAL STATE USING NEURO-CARDIOVASCULAR INFORMATION AND UNSUPERVISED LEARNING

Doctoral thesis submitted in partial fulfilment of the PhD in Informatics Engineering, Intelligent Systems, supervised by Professor César Alexandre Domingues Teixeira, Professor Maria da Graça Cristo dos Santos Lopes Ruano, and Professor Anna Maria Bianchi, and presented to the Department of Informatics Engineering of the Faculty of Sciences and Technology of the University of Coimbra.

September 2022

Towards the characterisation of the preictal state using neuro-cardiovascular information and unsupervised learning

Adriana Costa Leal

September, 2022

The studies presented in this thesis were carried out at the Centre for Informatics and Systems of the University of Coimbra (CISUC) at the Informatics Department, Faculty of Sciences and Technology, University of Coimbra, Portugal. The research was performed with financial support of the following institutions/programs:

- Grant from European Union project LINK (H2020-692023).
- Grant from national project lookAfterRisk (POCI-01-0145-FEDER-030290).
- Ph.D. grant SFRH/BD/147862/2019 from the FCT – Foundation for Science and Technology, I.P..
- Project CISUC (UID/CEC/00326/2020) and project RECoD (PTDC/EEI-EEE/5788/2020), both financed by national funds through the FCT – Foundation for Science and Technology, I.P..

Faculty of Sciences and Technology

University of Coimbra

Towards the characterisation of the preictal state using neuro-cardiovascular information and unsupervised learning

Adriana Costa Leal

Supervisor:
César Teixeira

Co-supervisors:
Maria da Graça Ruano
Anna Maria Bianchi

Dissertation presented to obtain a Ph.D. degree in Informatics Engineering, Intelligent Systems, at the Faculty of Sciences and Technology of the University of Coimbra

Dissertação de Doutoramento apresentada à Faculdade de Ciências e Tecnologia da Universidade de Coimbra, para prestação de provas de Doutoramento em Engenharia Informática, Sistemas Inteligentes

September, 2022

Abstract

Pre-seizure alterations have been long captured in the electroencephalography (EEG) trace. Typical seizure prediction models aim at discriminating interictal brain activity from pre-seizure patterns. The lack of a preictal clinical definition implicitly imposes an imprecision that is the artificial consideration of a fixed interval in the vast majority of studies. Recent studies reporting preictal interval selection among a range of fixed intervals show inter- and intra-patient preictal variability, reflecting the heterogeneity of the seizure generation process. Obtaining accurate labels of the preictal interval can be used to train supervised prediction models and, hence, avoid assuming a fixed preictal interval for all seizures within the same patient. Unsupervised learning methods hold great promise for exploring preictal alterations on a seizure-specific scale.

Additionally, pre-seizure patterns were also observed in non-neurological biosignals, such as electrocardiography (ECG). The potential prediction value stemming from these signals is further heightened by the comfort of their ambulatory collection. Wearable devices based on preictal changes in cardiac parameters, including heart rate and heart rate variability (HRV), are some of the focuses of current research.

The problem of the preictal identification in brain-heart data was addressed here using unsupervised learning methods. The data were collected from a group of 41 patients with drug-resistant temporal lobe epilepsy undergoing presurgical evaluation. This dataset, provided by the EPILEPSIAE database, comprised scalp EEG and ECG signals acquired simultaneously.

This thesis's first contribution consisted of exploring HRV to investigate the discriminative power of its features in identifying the preictal interval. Information characterising the linear and nonlinear dynamics of the HRV signals was analysed. Unsupervised learning methods were applied to each three-by-three feature combination of the HRV features. Preictal patterns were assumed to manifest predominantly

in the two hours before seizure EEG onset. Distinguishable preictal behaviour was identified in 90% of the patients and 41% of the seizures. The preictal intervals occurred 62.7 ± 36.7 minutes before seizure onset and lasted for 14.2 ± 18.8 minutes.

In the second contribution, multivariate and univariate linear and nonlinear features were extracted from scalp EEG signals. Nonlinear dimensionality reduction was performed for each group of features and each seizure. Similarly to the previous contribution, different clustering methods were applied in searching for preictal clusters. Preictal patterns were identified in 90% of the patients and 51% of the inspected seizures. The preictal clusters manifested a seizure-specific profile with varying duration (22.9 ± 21.0 minutes) and starting time before seizure onset (47.6 ± 27.3 minutes). Analysis of the reduced univariate linear features evidenced the existence of multiple clusters across the analysed 4.5 hours of data before the seizure onset, suggesting the presence of multistate dynamics.

The last contribution consisted of evaluating the impact of using preictal interval information from the first two contributions on the performance of prediction models developed for EEG and HRV separately. Performance of the EEG- and HRV-based models were compared to the homologous control seizure prediction models that use only grid-search to define preictal intervals. Results show that models using the preictal intervals determined with unsupervised learning and control models performed comparably. The patient-specific predictors, evaluated quasi-prospectively, returned performance above chance level in 55% and 30% of 40 patients using EEG and ECG data, respectively. HRV-based models yielded performance above chance level for seven patients who were not statistically validated using EEG.

Searching for preictal patterns on both the EEG and the ECG traces using unsupervised methods showed that it is possible to identify seizure-specific preictal signatures for some patients and some seizures within the same patient. Using this information, when available, avoids the need to assume a fixed preictal interval in seizure prediction models and might improve prediction performance. Findings also encourage the development of cardiac-based prediction wearable devices that provide a less cumbersome option for seizure monitoring and control in day-to-day settings.

Keywords: Epilepsy, Preictal Interval, Electroencephalography, Electrocardiography, Unsupervised Learning, Seizure Prediction.

Resumo

Durante muitos anos, a maior fonte de informação acerca alterações pré-crise foi a electroencefalografia (EEG). Os modelos de previsão comuns visam distinguir actividade cerebral do estado interictal, de padrões do estado preictal. Dado que não existe uma definição clínica do intervalo preictal, estes modelos são tipicamente desenvolvidos usando um intervalo preictal fixo artificialmente definido. Estudos recentes reportam a seleccão de um intervalo preictal de entre um conjunto de intervalos fixos de acordo com o desempenho de previsão. Os resultados mostram uma grande variabilidade do intervalo preictal entre doentes e entre crises anotadas para o mesmo doente, evidenciando a heterogeneidade do processo de geração de crises epilépticas. Assim, treinar modelos de previsão de crises usando a informação correcta acerca do início do intervalo preictal evitaria assumir a existência de um intervalo fixo para todas as crises e doentes. Esta informação pode ser explorada usando métodos de aprendizagem não-supervisionada aplicados a cada crise.

Padrões pre-crise foram também observados em sinais não-neurológicos como é o caso da electrocardiografia (ECG). Ao potencial valor de previsão destes biosinais, acrescenta o conforto da sua aquisição em ambulatório. Actualmente estão a ser desenvolvidos dispositivos de monitorização vestíveis com base em alterações pre-crise detectadas em parâmetros cardíacos, incluindo ritmo cardíaco e variabilidade do ritmo cardíaco (acrónimo em inglês HRV).

O problema da identificação do intervalo preictal em dados neuro-cardiovasculares foi abordado com recurso aos métodos de aprendizagem não-supervisionada. Os dados analisados nesta tese foram adquiridos durante a fase de avaliação pré-cirúrgica de 41 doentes com epilepsia refractária do lobo temporal. Este conjunto de dados, proveniente da base de dados EPILEPSIAE, contém sinais de EEG de escalpe e ECG adquiridos em simultâneo.

A primeira contribuição desta tese consistiu na análise da HRV com vista à avaliação da respectiva capacidade de identificação do intervalo preictal. Extraiu-se informação que caracteriza a dinâmica linear e não-linear dos sinais de HRV. Métodos não-supervisionados foram aplicados aos dados de cada crise, e, por sua vez, a cada combinação três-por-três de caraterísticas extraídas para a HRV. Assumiu-se que os padrões de preictal iriam ocorrer predominantemente nas duas horas que precedem o início da crise. O estado preictal, identificado em 90% dos doentes e 41% das crises, ocorreu 62.7 ± 36.7 minutos antes do início da crise e durou 14.2 ± 18.8 minutos.

Na segunda contribuição, características univariadas, lineares e não-lineares, assim como características multivariadas foram extraídas dos sinais de EEG de escalpe. Um método de redução da dimensionalidade foi aplicado aos dados de cada crise, seguido da identificação do intervalo preictal com métodos não-supervisionados. Os padrões de preictal, identificados em 90% dos doentes e 51% das crises, manifestaram-se de forma distinta entre crises, com grande variabilidade em termos de duração (22.9 ± 21.0 minutos) e localização antes do início da crise (47.6 ± 27.3 minutos). A análise das características univariadas lineares revelou a existência de vários grupos de amostras ao longo das 4.5 horas de dados analisadas para cada crise, sugerindo uma dinâmica de multi-estados.

A última contribuição consistiu na avaliação do impacto do uso das anotações dos intervalos preictais (obtidas nas contribuições anteriores) no desempenho de previsão de modelos desenvolvidos com base em dados de EEG e HRV, separadamente. Os modelos de previsão baseados em EEG e HRV foram comparados com modelos de controlo homólogos em que o preictal é seleccionado de acordo com o desempenho. Os resultados mostram que modelos desenvolidos com as anotações de preictal (resultantes da aprendizagem não supervisionada) levaram a um desempenho semelhante aos modelos de controlo. Os modelos específicos ao doente foram avaliados quase-prospectivamente resultando num desempenho de previsão estatisticamente significativo em 55% e 30% dos 40 doentes usando EEG e ECG, respectivamente. Os modelos com base em HRV validaram sete doentes que não foram validados usando os dados de EEG.

A procura de padrões preictais usando métodos não-supervisionados em dados de EEG e ECG demonstrou ser possível identificar um estado preictal, específico à crise,

em alguns doentes e em algumas crises registadas para o mesmo doente. O uso desta informação, quando disponível, dispensa a definição de um intervalo preictal fixo durante o desenvolvimento de modelos de previsão, podendo melhorar o desempenho dos mesmos. Os resultados também incentivam o desenvolvimento de modelos de previsão com base na actividade cardíaca. Dispositivos de monitorização vestíveis que integrem tais modelos surgem como alternativas não-invasivas que permitem a monitorização de crises epilépticas de forma menos aparatosa e passível de ser usada no dia-a-dia dos doentes.

Palavras-chave: Epilepsia, Intervalo Preictal, Electroencefalografia, Electrocardiografia, Aprendizagem Não-supervisionada, Previsão de Crises.

Acknowledgements

To my supervisors, César Teixeira, Maria da Graça Ruano and Anna Bianchi I express my thanks, for all the guidance and advice.

I would like to express my sincere thanks to Professors António Dourado, Jorge Henriques and Paulo de Carvalho for all the thoughtful revisions.

I gratefully acknowledge FCT, the Human Capital Operational Program (POCH) and the European Union (EU) for supporting this research work under Ph.D. grant SFRH/BD/147862/2019.

I thank the Centre for Informatics and Systems of the University of Coimbra (CISUC) for hosting my research.

I acknowledge the Laboratory for Advanced Computing at the University of Coimbra for providing computing resources that have contributed to the research results reported within this thesis.

My thanks to Centro Hospitalar e Universitário de Coimbra (CHUC), particularly the refractory epilepsy centre, the sleep monitoring unit, and Dr Francisco Sales, for all the insight.

I dearly thank my colleagues and friends Mauro Pinto and Fábio Lopes for the fruitful discussions and team work.

Lastly, I thank my family and my friends for all the support throughout the completion of this thesis.

Contents

List of Acronyms

AEDs anti-epileptic drugs 1, 27, 28, 30, 34, 61, 62

AH agglomerative hierarchical clustering 103, 104, 122, 124, 139

ANS autonomous nervous system 3, 4, 26, 27, 35, 59, 61, 94, 99, 104, 115, 210, 235–238, 244

AUC area under the receiver operating characteristic curve 42, 43, 83, 147, 148, 155

CD correlation dimension 240, 260, 263

DBSCAN density-based spatial clustering of applications with noise 103–105, 107, 112, 122, 124

DFA detrended fluctuation analysis 239, 249, 251, 258, 264

DI Dunn's index 105–107, 123, 124

DL deep learning 62, 67, 73–75, 78, 91

DRE drug-resistant epilepsy 1, 2, 4, 28–31, 35, 37, 39, 43, 59, 62, 63, 83, 84, 93, 94, 114, 118, 134, 138, 210

ECG electrocardiography 3–5, 8, 11, 24, 25, 35, 36, 53, 60, 62, 63, 73, 93, 94, 99–101, 104, 114, 115, 118, 131, 139, 141, 143, 146, 149–151, 153–155, 157, 158, 161, 163, 164, 217, 233–236, 284

EEG electroencephalography 3–5, 8, 9, 11, 13–18, 20–25, 29, 30, 33–40, 44, 46, 47, 51–53, 55, 56, 59, 62, 63, 66, 67, 70, 71, 73, 75, 78, 79, 83, 86–88, 91–94, 97, 99, 100, 104, 112–115, 117–120, 124, 127, 131, 132, 134–136, 138–143, 146, 147, 149–151, 153, 154, 156–158, 161, 163, 164, 205, 206, 209, 217, 235, 255–258, 260, 261, 264, 270–272, 284, 290, 292, 300

FBTC focal to bilateral tonic-clonic 14

FOA focal onset aware 14

FOIA focal onset impaired awareness 14, 38, 60, 109, 110, 210

FPR/h false prediction rate per hour 40–43, 45, 83, 148–151, 153, 156, 157

GMM expectation-maximisation clustering using Gaussian mixture models 103, 104, 107, 112, 122, 124, 129, 139

HDBSCAN hierarchical density-based spatial clustering of applications with noise 122, 139

HF high frequency 103, 113, 235, 237–239, 248–251

HR heart rate 25–27, 53, 59–62, 86, 99, 209, 210, 235, 238

HRV heart rate variability 4, 9, 25–27, 53, 59–61, 99, 100, 102–104, 112–114, 146, 147, 155, 210, 233, 235–239, 244, 249, 251

IC independent component 119

IEA interictal epileptiform activity 56, 86, 88, 90

ILAE International League Against Epilepsy 11–14, 17, 28

KM K-means clustering 103, 104, 122, 124, 129, 139

LF low frequency 235, 237–239, 251

LLE largest Lyapunov exponent 240, 260, 263, 264

ML machine learning 34, 41, 45, 62, 74, 75, 78

RQA recurrence quantification analysis 112, 113, 240, 241, 249, 251

SOP seizure occurrence period 40–45, 49, 61, 144

SPH seizure prediction horizon 40–43, 61, 67, 70, 93, 97, 104, 107, 114, 120, 144, 149

SS seizure sensitivity 40–45, 148–151, 153, 156, 157

SVMs support vector machines 78, 147, 148, 155–157, 160, 291

TLE temporal lobe epilepsy 16, 30, 59, 61, 94, 99, 100, 210

UMAP uniform manifold approximation and projection for dimension reduction 120–124, 129, 139

VLF very low frequency 103, 237, 238, 248, 250, 251

List of Figures

List of Tables

Chapter 1

Introduction

Pre-seizure alterations captured in electrographic signatures have paved the way for the development of seizure prediction algorithms. Even though many efforts have been devoted to seizure prediction over the last four decades, many challenges remain to address, among them the understanding of the transition from seizure-free brain activity to seizure. In this chapter, the problem of the limited understanding of such transition is introduced, and, on that basis, the main objectives of the thesis are outlined.

1.1 Motivation

Being one of the most common neurological diseases, epilepsy affects about 1% of people worldwide [1, 2]. Despite the availability of surgery and more than 30 licensed treatments, including anti-epileptic drugs (AEDs) [3] and neuromodulation devices [4], approximately 30% of people with epilepsy do not achieve seizure control, being diagnosed with drug-resistant epilepsy [5]. These people refer to the apparent unpredictability of seizures as the most debilitating aspect of the disease. Adding to that, epilepsy is singularly characterised by the rare occurrence of high-impact seizures. Even though these events are, in most cases, not frequent and, therefore, the time spent with clinical manifestations is very low, the effects of seizures profoundly mark the lives of patients and caregivers. It then becomes evident the burden associated with drug-resistant epilepsy (DRE) in terms of day-to-day limitations (e.g., crossing roads or driving) and social stigma resulting from seizures' clinical symptoms. Additionally, comorbidities including depression, anxiety, migraine and increased mortality considerably affect patients with DRE beyond the severity of seizures themselves [6].

The emergence of new AEDs over the last several decades has not reduced the percentage of patients with DRE [7]. In the face of the insufficient effect of antiseizure medication, there is a demand for improved therapeutic strategies that minimise (i) possible injuries resulting from a seizure discharge and (ii) anxiety levels resulting

from the unpredictability of epileptic seizures. A possible solution encompasses the identification of seizure precursors and the development of prediction algorithms based on them. These algorithms can be further integrated into implanted or wearable devices for on-demand intervention (e.g., controlling seizures through neuromodulation or, at least, the patient taking preventive measures against accidents). Additionally, monitoring non-neurological epileptic data may increase device adherence as patients with DRE may be more willing to use wearable devices delivering warnings of impending seizures rather than invasive implantable devices [8, 9].

Seizure prediction is considered a promising research field that has been widely explored but still presents challenges related to the prospective application of prediction devices.

1.1.1 Limitations on seizure prediction using supervised learning models

Most seizure prediction approaches proposed to date are based on supervised learning techniques. Being supervised approaches, prediction models require the existence of labels to discriminate at least between two brain states: seizure-free (interictal) state and pre-seizure (preictal) state. Consequently, correctly identifying the preictal interval to optimally label data can greatly contribute to the success of seizure prediction approaches. However, the preictal interval has no clinical definition or specific biomarker that can be used across patients [10–12]. For this reason, when developing seizure prediction algorithms, a straightforward approach is to artificially define a fixed preictal interval for all patients [11, 13].

Different studies considered different fixed preictal intervals, ranging from 2 to 90 minutes [11]. As a result of this variability in the definition of a fixed preictal interval, seizure precursors have been reported to occur over different time scales, setting the basis for exploring a range of preictal intervals for each patient. In 2005, authors started reporting the exploration of a range of preictal intervals for each patient-specific seizure prediction model [14]. The chosen model integrates the preictal interval leading to the highest prediction performance. Clear differences have been found for the duration of these intervals for different patients and even from seizure to seizure occurring in the same patient [12, 15–17]. These findings are in line with the reported heterogeneity of the seizure generation process (among patients and within the same patient) [16, 18]. Even though performing a patient-specific preictal search over a range of intervals is considerably more informative than using a fixed interval, it still may not address the existence of diverse paths of seizure evolution among different seizures (reported for the same patient).

On this basis, the correct estimation of preictal intervals may bring enormous benefits to developing supervised seizure prediction algorithms and understanding the seizure generation mechanisms.

1.1.2 Non-neurological pre-seizure alterations

Naturally, the electroencephalography (EEG) signal has been the primary source of explicit brain activity changes during epileptic events. In addition, epileptic seizures have implicit manifestations of other body functions. Namely, seizure discharges that arise from or spread to areas in the central autonomic function will induce modifications in the normal functioning of the autonomous nervous system (ANS). As a consequence, the normal response of the parasympathetic and sympathetic systems will be disturbed, leading to alterations in cardiorespiratory parameters, including respiratory rate, blood flow, blood pressure, and heart rate [19, 20].

Even though autonomic dysfunction is commonly observed during a seizure discharge, cardiac parameters such as heart rate and heart rate variability have been the first parameters reported to change before and after the seizure onset and offset, respectively. Besides the existing evidence of preictal cardiac changes, another relevant aspect heavily weighs on directing efforts to inspect the heart-brain interaction over the seizure generation process. Specifically, smartwatches or other commercially available devices can be used to continuously monitor physiological parameters, including cardiac activity [21, 22], without requiring a complicated and uncomfortable electrode setup. Consequently, recent years have witnessed a growing interest in using data collected with minimally invasive or wearable devices [23]. Also, patients' willingness to participate in long-term data collection is strongly dependent on the usability of the acquisition devices [8, 24]. Noninvasive devices are also less expensive and involve fewer clinical personnel than the scalp and intracranial EEG. These characteristics are desirable when considering a broader application of wearable devices for epilepsy management in low-income countries. The burden of epilepsy is mostly concentrated in low- and middle-income countries [25, 26]. More than seizure control, wearable devices could become a possible solution to improve the diagnosis and management of epilepsy for people living in these countries where even presurgical evaluation lacks resources to be performed [27].

1.2 Expected goals and contributions

In this thesis, it was hypothesised that, by using unsupervised learning to determine the existence and characterisation of the preictal interval for each seizure, it would be possible to overcome the problem of using a fixed, user-defined, preictal interval in supervised seizure prediction models. This hypothesis was raised for the independent analysis of EEG and electrocardiography (ECG) data in order to compare the prediction potential of the preictal brain and cardiac alterations. Using seizure-specific information can potentially improve seizure prediction performance while addressing the heterogeneity of the seizure generation process.

To fulfil this purpose, EEG and ECG data simultaneously recorded during

presurgical monitoring of patients with DRE were explored. These data were provided by the European Epilepsy Database [28, 29], the most complete database regarding continuous electrographic data acquired during presurgical monitoring. The database comprises long-term signals as well as patient and seizure metadata.

This investigation aimed to provide solutions that expand the current understanding of the preictal state and the consequent impact on seizure prediction algorithms. In addition to brain activity, the analysis of cardiac information was intended to provide evidence for the potential of using data acquired with a less invasive and more user-friendly modality compared to EEG.

In sum, this thesis reports for the first time an extensive study on the existence of preictal alterations on brain-heart data and their consequent impact on seizure prediction. The resulting conclusions might prove helpful in designing future prospective seizure prediction applications that would open new avenues for the real-time management of seizures in patients with DRE.

The investigation was subdivided into three major contributions, described in the following subsections.

1.2.1 Preictal interval estimation based on ECG

The first part of this thesis refers to the analysis of the ECG signal aiming at identifying preictal changes resulting from a seizure's impact on the autonomic function. Heart rate variability (HRV), being considered the proxy to the cardiac autonomic control [20, 30], was extracted from the ECG signals. Signals were preprocessed before extracting linear and nonlinear HRV features. Afterwards, unsupervised learning methods were used to search for a preictal pattern on the HRV dataset. Clustering solutions containing two clusters were sought in the three-by-three feature combination spaces to quantify how many seizures evidenced an interictal state separation from the preictal state. When such solutions were identified, it was assumed that a putative preictal interval existed. Such intervals were then properly characterised in terms of duration and starting time before the seizure onset.

Besides inspecting clustering solutions in searching for a preictal signature, the results were interpreted physiologically to understand the influence of the sympathetic and parasympathetic ANS across the pre-seizure interval.

1.2.2 Preictal interval estimation based on EEG

The second main task aimed at exploring alterations of the brain activity captured by the EEG signal towards the seizure-specific identification of the preictal interval. The EEG signals were firstly preprocessed. After that, a comprehensive feature engineering procedure was conducted to obtain a feature dataset comprising univariate, linear or nonlinear, and multivariate measures of brain activity. Given the large dimensionality of the dataset, feature reduction methods were further applied. The

preictal interval search was carried out on the three-dimensional reduced dataset obtained for each group of features and each seizure. After applying unsupervised learning methods, clustering solutions were characterised to identify preictal patterns. In this case, applying feature reduction methods allowed for the feasibility of inspecting solutions containing more than two clusters that might evidence the occurrence of distinct brain states.

1.2.3 Impact of unsupervised learning in seizure prediction

The third part of the thesis was designed to evaluate the impact of using unsupervised preictal labels on supervised seizure prediction models. Having identified seizure-specific preictal intervals, it is possible to develop strategies to integrate those labels into supervised seizure prediction models. The first step consisted of performing a metadata analysis to determine the existence of similar preictal intervals among the same type of seizures or seizures that occurred while the patient was awake or asleep. In other words, if stratification of the preictal intervals proved successful, it would be possible to build, for instance, seizure-type-specific prediction models [16]. Otherwise, a solution would reside in taking the average preictal interval to train a patient-specific prediction model. This task was performed independently for ECG and EEG, using the corresponding information about the unsupervised preictal intervals. These models were then compared to a control prediction pipeline, also developed for each signal, that searches for an optimal preictal interval for each seizure using a grid-search procedure.

1.3 Scientific outcomes

During this thesis, several contributions to the field of epilepsy seizure prediction were made. These include publishing main authored and co-authored articles in international peer-reviewed journals, participating in international and national conferences, and co-supervising a master's degree thesis. These are enumerated in the following sections.

Educational and scientific contributions in other research fields were also made. These include giving classes to students, attending summer schools and presenting at international conferences.

Peer-reviewed journal articles

J1 **Leal, A.**, Pinto, M. F., Lopes, F., Bianchi, A. M., Henriques, J., Ruano, M. G., Carvalho, P., Dourado, A., and Teixeira, C. A. Heart rate variability analysis for the identification of the preictal interval in patients with drug-resistant epilepsy. *Scientific Reports*, 2021, 11, 5987.

J2 **Leal, A.**, Curty, J., Lopes, F., Pinto, M. F., Oliveira, A., Sales, F., Bianchi, A. M., Ruano, M. G., Dourado, A., Henriques, J., and Teixeira, C. A. Unsupervised EEG Preictal Interval Identification in Patients with Drug-resistant Epilepsy. In preprint and accepted for publication in *Scientific Reports* journal.

J3 Pinto, M. F., **Leal, A.**, Lopes, F., Dourado, A., Martins, P., and Teixeira, C. A. A personalized and evolutionary algorithm for interpretable EEG epilepsy seizure prediction. *Scientific Reports*, 2021, 11, 3415.

J4 Lopes, F., **Leal, A.**, Medeiros, J., Pinto, M. F., Dourado, A., Dümplemann, M., Teixeira, C. A. Automatic Electroencephalogram Artifact Removal using Deep Convolutional Neural Networks. *IEEE Access*, 2021, 9, 149955-149970.

J5 Pinto, M. F., **Leal, A.**, Lopes, F., Pais, J., Dourado, A., Sales, F., Martins, P., and Teixeira, C. A. Interpretable EEG seizure prediction using a multiobjective evolutionary algorithm. *Scientific Reports*, 2022, 12, 4420.

J6 Lopes, F., **Leal, A.**, Pinto, M. F., Dourado, A., Dümplemann, M., Teixeira, C. A. Ensemble Deep Neural Network for Automatic Classification of EEG Independent Components. *IEEE Transactions on Neural Systems and Rehabilitation Engineering*, 2022, 30, 559-568.

J7 Pinto, M. F., **Leal, A.**, Lopes, F., Pais, J., Dourado, A., Sales, F., Martins, P., and Teixeira, C. A. On the clinical acceptance of black-box systems for EEG seizure prediction. *Epilepsia Open*, 2022, 00, 1-13.

J8 Lopes, F., **Leal, A.**, Medeiros, J., Pinto, M. F., Dourado, A., Dümplemann, M., and Teixeira, C. A. EPIC: Annotated epileptic EEG independent components for artifact reduction. *Scientific Data*, 2022, 9, 512.

Journal articles submitted or in preparation

J8 **Leal, A.**, Martinho, B., Lopes, F., Pinto, M. F., Sales, F., Bianchi, A. M., Ruano, M. G., Dourado, A., Henriques, J., and Teixeira, C. A. Preictal interval labelling with unsupervised learning may improve seizure prediction models. *Manuscript under preparation to be submitted to a peer-reviewed journal* (2022).

J9 Pinto, M. F., Batista, J., **Leal, A.**, Lopes, F., Oliveira, A., Dourado, A., Sales, F., Martins, P., Teixeira, C. A.. Explaining Machine Learning models for EEG seizure prediction. *Manuscript under preparation to be submitted to a peer-reviewed journal* (2022).

1.3.1 Other scientific publications

O1 *Poster presentation in international conference:* **Leal, A.**, Pinto, M. F., Bianchi, A. M., Ruano, M. G., Henriques, J., Carvalho, P., and Teixeira, C. A. "Heart Rate Variability Analysis in Drug-resistant Epilepsy Patients Towards Seizure-specific Preictal Time Assessment", *International Conference for Technology and Analysis of Seizures (ICTALS2019)*, 2019

O2 *Poster presentation in international conference:* **Leal, A.**, Pinto, M. F., Lopes, F., Curty, J., Oliveira, A., Sales, F., Ruano, M. G., Dourado, A., Bianchi, A. M., Henriques, J., and Teixeira, C. A. "Can unsupervised preictal labelling improve seizure prediction?", *International Conference for Technology and Analysis of Seizures (ICTALS2022)*, 2022

O3 *Presentation in national conference:* **Leal, A.**, Bianchi, A. M., Ruano, M. G., and Teixeira, C. A."Heart Rate Variability Analysis for the Identification of the Preictal Interval in Patients with Drug-resistant Epilepsy", *33º Encontro Nacional de Epileptologia (ENE) – CONGRESSO VIRTUAL DA Liga Portuguesa Contra a Epilepsia (LPCE)*, 2021

O4 *Poster presentation in national conference:* **Leal, A.** Bianchi, A. M., Ruano, M. G., Henriques, J., Carvalho, P., and Teixeira, C. A., "Towards the characterisation of the preictal state using neuro-cardiovascular information and unsupervised learning", *encontro Ciência '19*, 2019

O5 *Poster presentation in international summer school:* **Leal, A.**, Bianchi, A. M., Ruano, M. G., and Teixeira, C. A. "Heart Rate Variability Analysis in Drug-resistant Epilepsy Patients. Towards seizure-specific preictal time assessment.", *COST Action Training School*, 2019

O6 *Poster presentation in international summer school:* **Leal, A.**, Bianchi, A. M., Ruano, M. G., and Teixeira, C. A. "Towards the characterisation of the preictal state using neuro-cardiovascular information and unsupervised learning.", *IEEE International Summer School on Technologies and Signal Processing in Perinatal Medicine*, 2018

1.3.2 Master's degree co-supervision

Martinho, B. "Epilepsy Seizure Prediction Based on HRV Analysis", *Master Thesis dissertation, Faculty of Science and Technology of the University of Coimbra* (2021).

1.4 Research team & context

This investigation is integrated into a broader project that is driving a skilled research team. Joint efforts are being undertaken to improve seizure prediction models in adherence to the current research guidelines in this field of study. The work reported herein was carried out from 2017 to 2022, at the Center for Informatics and Systems of the University of Coimbra (CISUC). Table 1.1 describes the team members and their corresponding roles.

Table 1.1: Epilepsy research team members.

Role	**Name**	**Research group**
Supervisor	César Teixeira	CISUC
Co-supervisor	Maria da Graça Ruano	CISUC/UALG
Co-supervisor	Anna Maria Bianchi	POLIMI
Scientific Advisor	António Dourado	CISUC
Scientific Advisor	Jorge Henriques	CISUC
Scientific Advisor	Paulo de Carvalho	CISUC
Clinical Advisor	Francisco Sales	RERC
PhD Student	Mauro Pinto	CISUC
PhD Student	Fábio Lopes	CISUC
MSc Student	Tiago Coelho	CISUC
MSc Student	Mariana Tavares	CISUC
MSc Student	Beatriz Martinho	CISUC
MSc Student	Ana Oliveira	CISUC
BSc Student	Juliana Curty	CISUC

CISUC: Center for Informatics and Systems of the University of Coimbra; POLIMI: Politecnico di Milano; UALG: University of Algarve; RERC: Refractory Epilepsy Reference Centre, Centro Hospitalar e Universitário de Coimbra, EPE, Coimbra.

1.5 Thesis Outline/Structure

The remainder of this thesis proposal is structured as follows.

Chapter 2 provides background information related to some concepts referred to in the following chapters. Namely, the field of epilepsy is introduced, including clinical definitions, current treatments, data acquisition modalities and guidelines considered when developing seizure prediction algorithms.

Chapter 3 presents state of the art regarding the supervised seizure prediction methodologies proposed so far and their current pitfalls, including the preictal interval definition. EEG- and ECG-based studies are the focus of the literature review.

Specifically, findings related to the cardiovascular changes occurring during epileptic events are extensively reviewed.

Chapter 4 describes the dataset analysed in this thesis.

Chapter 5 includes the unsupervised learning process carried towards identifying preictal patterns in the HRV data.

Chapter 6 refers to the unsupervised learning search for the preictal interval on the EEG signals.

In Chapter 7, the information on preictal interval gathered in the previous two chapters is used to design seizure prediction models. The impact of using unsupervised preictal labels on seizure prediction performance was evaluated by comparing the results with a standard seizure prediction methodology.

The studies described in Chapters 5, 6 and 7 are complemented with an extended description of the methods and results in Appendices D, E and F, respectively. The studies' details were included in the appendix to enhance this thesis's readability.

Finally, the thesis is concluded in Chapter 8 by providing an overview of the main findings resulting from this research and what it adds to the current knowledge on the preictal state. The results from the different studies are comprehensively analysed, and future directions are outlined.

Chapter 2

Epilepsy background: concepts and management

In this chapter, epilepsy-related background concepts are presented. Section 2.1 presents the definition of epilepsy and seizure. Sections 2.2 and 2.3 describe the biosignals analysed in this thesis, the electroencephalography (EEG) and electrocardiography (ECG), respectively, as well as the physiological background behind each biosignal. Section 2.4 covers the current epilepsy treatment and management options. Section 2.5 provides information on the technical concepts required to develop seizure prediction models. Concept drifts are introduced in Section 2.6. Lastly, Section 2.7 presents a summary of some key concepts that should be retained from the background chapter.

2.1 Epilepsy and epileptic seizure concepts

Epilepsy is one of the most common neurological diseases affecting the brain. Idiopathic epilepsy[1] has been ranked fifth after stroke, migraine, dementia, and meningitis in the 2016's global burden of neurological disorders [1]. Also, in 2016, a systematic analysis estimated that 45.9 million people were affected by epilepsy in the world [31]. Prevalence was reported to vary with age (it increases at ages 5–9 years and in people older than 80) and sociodemographic status (it is more prevalent in low-income countries) [31].

2.1.1 Definition of epilepsy and seizure

The conceptual definition of both seizure (Box 1) and epilepsy (Box 2) was proposed by the Task Force of the International League Against Epilepsy (ILAE) in 2005 [32].

[1] Epilepsy resulting from a genetic cause or epilepsy for which the diagnostic assessment was not clear with regards to its origin. Conversely, secondary epilepsy corresponds to epilepsy due to structural, metabolic, infective, or immune causes.

Box 1 - Conceptual definition of seizure (as defined by the Task Force of the ILAE in 2005 [32])

"An epileptic seizure is a transient occurrence of signs and/or symptoms due to abnormal excessive or synchronous neuronal activity in the brain."

Box 2 - Conceptual definition of epilepsy (as defined by the Task Force of the ILAE in 2005 [32])

"Epilepsy is a disorder of the brain characterised by an enduring predisposition to generate epileptic seizures, and by the neurobiological, cognitive, psychological, and social consequences of this condition. The definition of epilepsy requires the occurrence of at least one epileptic seizure."

In 2014, a practical clinical definition of epilepsy was formulated by the ILAE, aiming to be applied in clinical diagnosis [33]. According to this new update, epilepsy, commonly defined by the occurrence of a minimum of two unprovoked seizures separated by more than 24 hours, can also be diagnosed by two other conditions (see Box 3).

It is important to note that the underlying brain mechanisms leading to seizure onset and subsequent termination are yet not well-understood [34]. Still, research, mainly based on animal models, has revealed that epilepsy is not defined by the arising of a single symptom resulting from the abnormal activity of a single neuron. Instead, it is a brain network disease manifesting in a specific brain location or covering hemispherically separated locations [34–36].

Patients with epilepsy can present a wide range of symptoms which differ according to the affected brain region [34]. The varying clinical phenomenology includes objective signs and/or subjective symptoms (e.g., loss of awareness, stiffening, jerking, a smell of burnt rubber or déjà vu) [37].

Box 3 - Diagnostic criteria for epilepsy (as defined by the Task Force of the ILAE in 2014 [33])

"Epilepsy is a disease of the brain defined by any of the following conditions:

1. *At least two unprovoked (or reflex) seizures occurring >24 h apart.*
2. *One unprovoked (or reflex) seizure and a probability of further seizures similar to the general recurrence risk (at least 60%) after two unprovoked seizures, occurring over the next 10 years.*
3. *Diagnosis of an epilepsy syndrome."*

2.1.2 Classification of seizures and the epilepsies

In 2017, the ILAE proposed a revised framework for the classification of epilepsies [38] and an operational classification of seizure types [36].

The new framework for the classification of epilepsies (see Figure 2.1) comprises the three stages of diagnosis: (i) identification of the seizure types, (ii) followed by the epilepsy types, and (iii) the epilepsy syndromes. The diagnostic process might include the assessment of medical history, physical examination, video and/or EEG, and neuroimaging [37]. Specifically, video-EEG is required to differentiate epileptic seizures from other similar clinical events [39]. EEG signals provide information regarding (i) epileptic brain activity occurring during seizure-free periods (inter-seizure or interictal state) and (ii) the seizure period (ictal state). When there is no access to EEG, video and neuroimaging studies, it might only be possible to perform the classification according to the seizure type [38].

A brief description of the classification of epilepsies based on those three stages will be presented in the following subsections. Notably, most databases on epilepsy data provide information regarding the seizure type and the epilepsy type while missing epilepsy syndrome information.

The clinician can use information collected over the three stages to determine the underlying causes of the patient's epilepsy (aetiology) and possible comorbidities. The cause of epilepsy, although often unknown, might be included in the following categories: structural (e.g., stroke or brain tumours), genetic (e.g., mutations in the SCN1A gene diagnosing for Dravet syndrome), infectious (e.g., bacterial or viral brain infections), metabolic (e.g., porphyria, uremia, aminoacidopathies or GLUT1 [2] deficiency) and immune (e.g., multiple sclerosis or autoimmune encephalitis) diseases [37, 38]. Comorbidities, including learning, psychological, and behavioural problems, are often associated with epilepsies [38, 40]. Given the severe impact of some comorbidities on the patient's quality of life, sometimes exceeding the seizure

[2] Solute carrier family 2, facilitated transporter member 1.

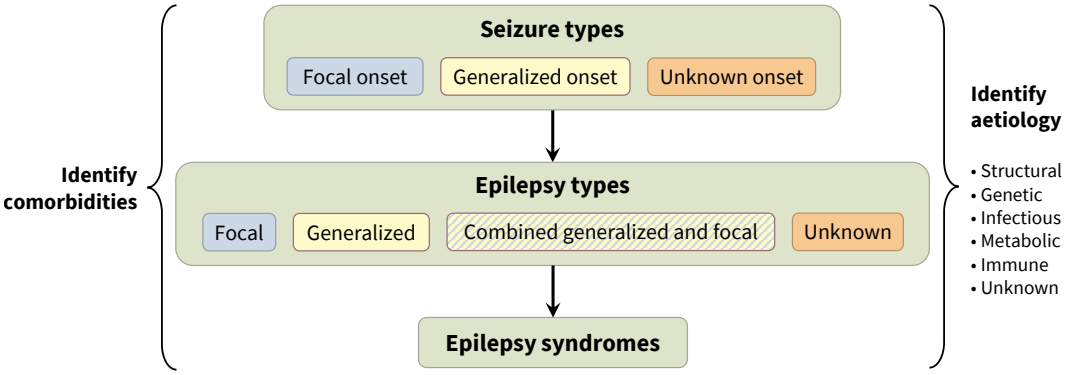

Figure 2.1: ILAE 2017 multilevel classification of epilepsies. Adapted from Sheffer *et al.* 2017 [38] and Devinsky *et al.* 2018 [37].

discharge, it is critical to assess its existence over the three levels of diagnosis, this way allowing for early identification, diagnosis, and proper management [40].

Seizure types

Assuming that the hypothesis of diagnosing a nonepileptic event has been discarded, the clinical diagnosis starts by determining the type of epileptic seizure affecting the patient. Given the insufficient knowledge regarding epilepsy's pathophysiologic mechanisms, the classification of seizure types proposed by the ILAE is an operational (practical) classification intended for clinical use [36]. Epileptic seizures can be classified into focal, generalised, or unknown onset (see Figure 2.2), based on how and where they begin in the brain.

Focal onset seizures are the ones for which the first clinical and EEG analysis point to a start in a specific location in the brain limited to one cerebral hemisphere [36, 41]. This seizure type can occur with or without the patient's awareness of self and environment, being classified as focal onset aware (FOA) and focal onset impaired awareness (FOIA), respectively [3]. Moreover, a focal seizure can optionally be classified into motor or nonmotor onset depending on the occurrence of motor or nonmotor signs and symptoms at the onset. The seizure can be specifically characterised by the name of the first motor or nonmotor onset symptom [36]. Classification based on awareness and motor or nonmotor symptoms may not always be possible. In other words, some seizures may be classified according to both characteristics, whereas others are directly named based only on the motor or nonmotor symptoms [36].

Seizures characterised by the occurrence of a focal onset followed by the propagation of the seizure pattern to another location in the brain are denoted focal to bilateral tonic-clonic (FBTC) seizures. During this epileptic event, motor changes, such as body stiffness (tonic) and jerking movements (clinic), typically occur [36]. FBTCs[4] can occur with awareness or impaired awareness, and with or without motor manifestations [42].

Generalised seizure onset is characterised by the involvement in both sides of the brain, not necessarily the entire brain but part of it on each side [36, 41]. In other words, such onset is characterised by the engagement of bilateral networks. Generalised tonic-clonic seizures are the most common seizure type seen in patients with epilepsy and are associated with the highest morbidity and mortality [43, 44]. These seizures usually involve impaired awareness, or complete loss of consciousness [44].

When the seizure onset cannot be determined with $\geq 80\%$ confidence by the clinician, but the event is associated with motor or nonmotor features, it is classified

[3] FOA and FOIA correspond to simple partial and complex partial seizures in the previous notation, respectively.

[4] FBTC corresponds to secondarily generalised seizures in the previous notation.

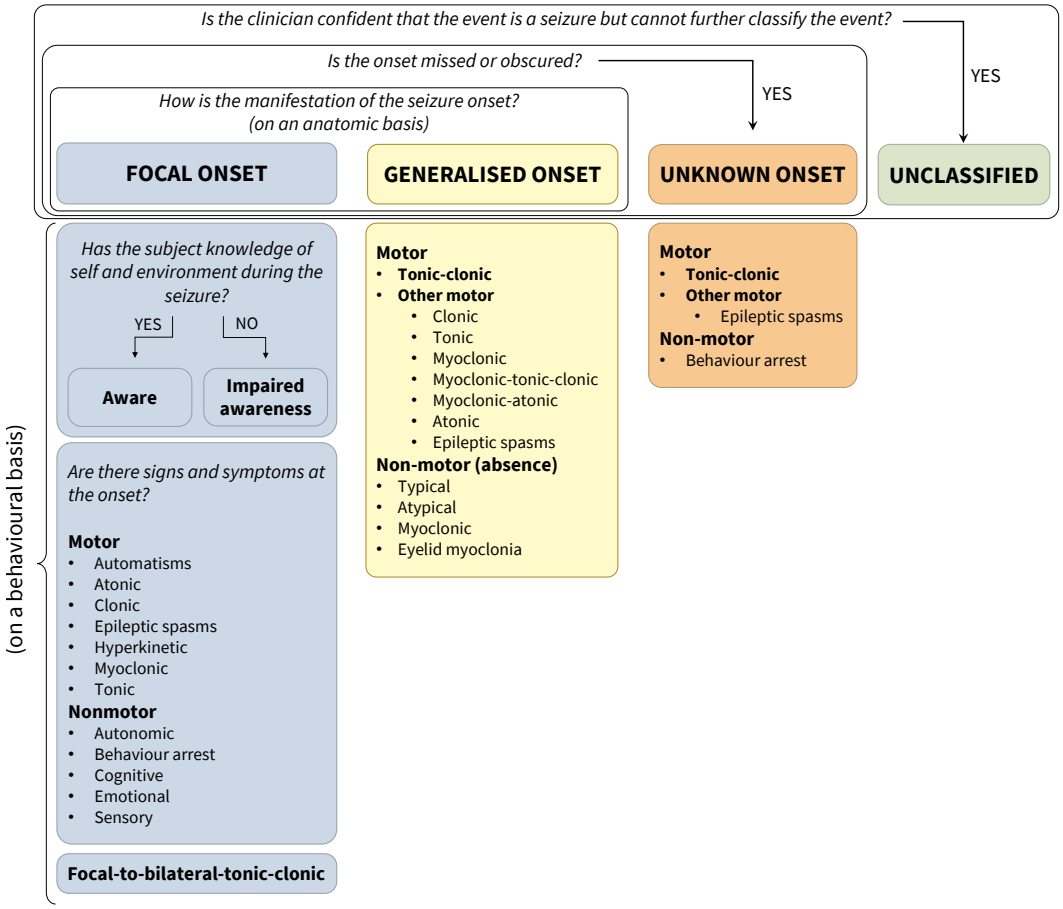

Figure 2.2: ILAE 2017 classification of seizure types. The clinician can use a basic (in bold) or an expanded seizure classification, depending on the level of expertise in diagnosing and treating epilepsy. Adapted from Fisher *et al.* 2017 [36] and Devinsky *et al.* 2018 [37].

as unknown onset. At the extreme, the lack of information regarding either the seizure's nature or diagnosis data may lead to the categorisation of the seizure as unclassified [36].

Epilepsy type

If the patient has been diagnosed with epilepsy, according to the 2014 definition in Box 3, the second step in clinical diagnosis can be taken: identifying the type of epilepsy affecting the patient [38]. As can be seen in Figure 2.1, four categories exist for the type of epilepsy:

- Focal epilepsies, accounting for 60% of all epilepsy [37], are typically characterised by focal epileptiform discharges captured during interictal EEG and include unifocal and multifocal[5] disorders and seizures involving one hemisphere. Seizure types that are more likely to occur include focal aware seizures, focal impaired

[5] A seizure is considered unifocal if it arises uniquely from a brain network, even though with the possibility of multiple clinical manifestations. When multiple seizures, triggered by different networks, occur, it corresponds to a multifocal event.

awareness seizures, focal motor seizures, focal non-motor seizures, and focal to bilateral tonic-clonic seizures.

- Generalised epilepsies manifest through generalised spike-wave activity captured on EEG. Seizure types such as absence, myoclonic, atonic, tonic, and tonic-clonic seizures are typically associated with this epilepsy type.
- Combined generalised and focal epilepsies are seen in patients presenting with both generalised and focal seizures identified in the interictal EEG by generalised spike-wave and focal epileptiform discharges, respectively.
- Epilepsies are classified as unknown when the clinician is not provided with enough information. For instance, EEG data may not be available or may be similar to a normal subject.

Temporal lobe epilepsy (TLE) is the most common type of focal onset epilepsy and is characterised by focal seizures arising from lesions in, or mediated by, the temporal lobe [41, 45]. Temporal lobe epilepsies can be divided into two types: mesial temporal lobe epilepsy (MTLE) and neocortical or lateral TLE.

MTLE is the most prevalent type of TLE, and MTLE with hippocampal sclerosis is the most common type of MTLE. Most patients diagnosed with MTLE are resistant to antiseizure medication, being often referred for resective surgery. A definitive diagnosis of MTLE is reached when the patient with drug-resistant epilepsy (see Section 2.4.1) is considered for surgical treatment. Being the epilepsy type for which most surgeries are performed, the real MTLE prevalence is, however, unknown due to the limited diagnosis assessment for the cases of adequately or poorly controlled seizures [34, 45, 46].

Epilepsy syndrome

Identifying the epilepsy syndrome represents the third level of diagnosis and may inform about aetiology, treatment and prognosis [38,40]. There are different epilepsy syndromes which possibly originate from different pathological processes [35]. An epilepsy syndrome is defined by the occurrence of clusters of features identified by collecting information, including seizure type(s), EEG characteristics, aetiology and imaging studies [38, 40]. Additionally, age-dependent features such as age at onset and remission, seizure triggers, and diurnal variation are often identified among these clusters of electroclinical features [38].

2.1.3 Seizure frequency

Seizures are considered rare events that, despite that, may have profound effects on the patient's life [16, 47].

Due to the low frequency of seizure events, clinicians often rely on patient-reported seizure counts to assess seizure frequency and further aid in the diagnosis

and management of seizure disorders [48].

Seizure frequency can also be determined by observing the occurrence of seizures in the EEG trace [49]. The number of seizures identified in continuous intracranial EEG has been reported to considerably exceed the patient-reported seizures [49, 50].

Table 2.1 presents the seizure frequency reported in some comprehensive studies, based on patient-reported seizure counting or electrographic seizure identification.

Importantly, the reliability of daily seizure counts remains controversial due to underreporting and overreporting (e.g., nonseizure events) [47, 48, 51].

Table 2.1: Seizure frequency.

Study	Demographics	Type of seizure	Mean (median) seizure frequency per month
Karoly *et al.* 2021 [51]	31 subjects (Focal: 22; Generalised: 9)	Patient-reported (seizure mobile diaries from Seer App) during presurgical monitoring	Focal: 11.1 (-) Generalised: 17.4 (-)
Ferastraoaru *et al.* 2018 [52]	10 186 subjects; 1 037 909 seizures	Patient-reported (seizure mobile diaries from Seizure Tracker)	Children: 16.1 (3.5) Adults: 7.7 (2.7)
Cook *et al.* 2013 [50]	14 patients with drug-resistant focal epilepsy	Patient-reported (seizure diaries or audio recordings) and iEEG seizures	Patient-reported: 5.5 (1.1) iEEG: 29.5 (10.2)
Bauer & Burr 2001 [53]	63 patients with drug-resistant focal epilepsy	Patient-reported (seizure diaries)	3 (-)

iEEG: intracranial EEG.

2.1.4 Seizure clusters

There is no standard definition of seizure clusters, also known as acute repetitive seizures. In fact, seizure clustering is not listed by the ILAE Commission on Classification and Terminology [54, 55]. The definition of seizure clusters varies among patients, caregivers and healthcare professionals. Nevertheless, seizure clustering is mainly recognised by inspecting seizure frequency within a given interval [54, 56].

When several seizures occur consecutively, within short interictal intervals (of hours or even minutes), the patient is suffering from a seizure clustering episode. However, the number of seizures and the duration of the interictal period considered for this clinical definition varies widely among clinical studies. Seizure clusters, defined by the occurrence of three or more seizures within 24 hours (equivalent to an interictal interval of eight hours or less), is the most frequently reported definition in clinical studies [54–56].

Additionally, statistical definitions have also been proposed, describing seizure

clusters as an increase in seizure occurrence compared to the patient's average seizure frequency [54, 56]. Seizure occurrence can also be described by a Poisson (random) distribution, which considers seizures as independent events (or lead seizures). When the seizures' frequency deviates from this model, it might be possible to identify seizure regularity (hence the potential for seizure prediction) and seizure clusters [54].

It is important to note that these definitions are mainly based on the seizure frequency documented for patients in presurgical monitoring, which might be an overestimation of the real seizure frequency [56]. In fact, the prevalence of seizure clusters in patients with epilepsy increases in studies conducted in epilepsy centres and hospitals. The prevalence also varies depending on the considered definition, with estimates being higher when using the clinical definition rather than the statistical one. Seizure cluster prevalence estimates in prospective studies range from 21.7% to 42.5%, whereas estimates made for seizure clusters identified in epilepsy centres and hospitals range from 14.9% to 57.1% [55].

Besides being necessary to assess the clinical burden [55], the concept of seizure clusters is also crucial when developing seizure prediction algorithms (see Section 2.5). Namely, most studies define a given inter-seizure interval to proceed to the analysis of data from lead seizures. This topic is detailed in Section 2.5.2.

2.2 Electroencephalography

The EEG time series are used to capture the electrical activity in the brain. They record the voltage potentials resulting from the summated excitatory and inhibitory postsynaptic potentials, which in turn are produced mainly by cortical pyramidal cells with parallel geometric orientation [34, 57–59]. Such parallel arrangement of the neurons allows for establishing a layer of cortical dipoles that dominates the EEG [57].

Although EEG measurement of the brain's electrical activity can capture fast changes in current flows, rendering it with a high temporal resolution, it lacks spatial resolution. The latter depends on the number of electrodes and how and where they are placed in the head [34, 58]. Additionally, being characterised as a nonlinear and nonstationary signal, the EEG is considered complex and hard to interpret [60, 61].

2.2.1 Electrical brain activity

Broadly speaking, two types of potentials can be captured by EEG: oscillations and transients (see Figure 2.3). Oscillations correspond to rhythmic fluctuations in the excitability of populations of neurons in the cortex. There are normal oscillations: sleep spindles and delta (0.5-4 Hz), theta (4-8 Hz), alpha (8-13 Hz), beta (13-30 Hz), lower gamma (30-80 Hz), and upper gamma (80-150 Hz) frequency band activities. Abnormal oscillations include seizure occurrence [57–59, 62].

Delta band oscillations are chiefly associated with deep sleep. Theta band activity has been reported to arise during drowsiness states, creative inspiration, and deep meditation [63]. Alpha waves, usually observed over the occipital lobe, are the most

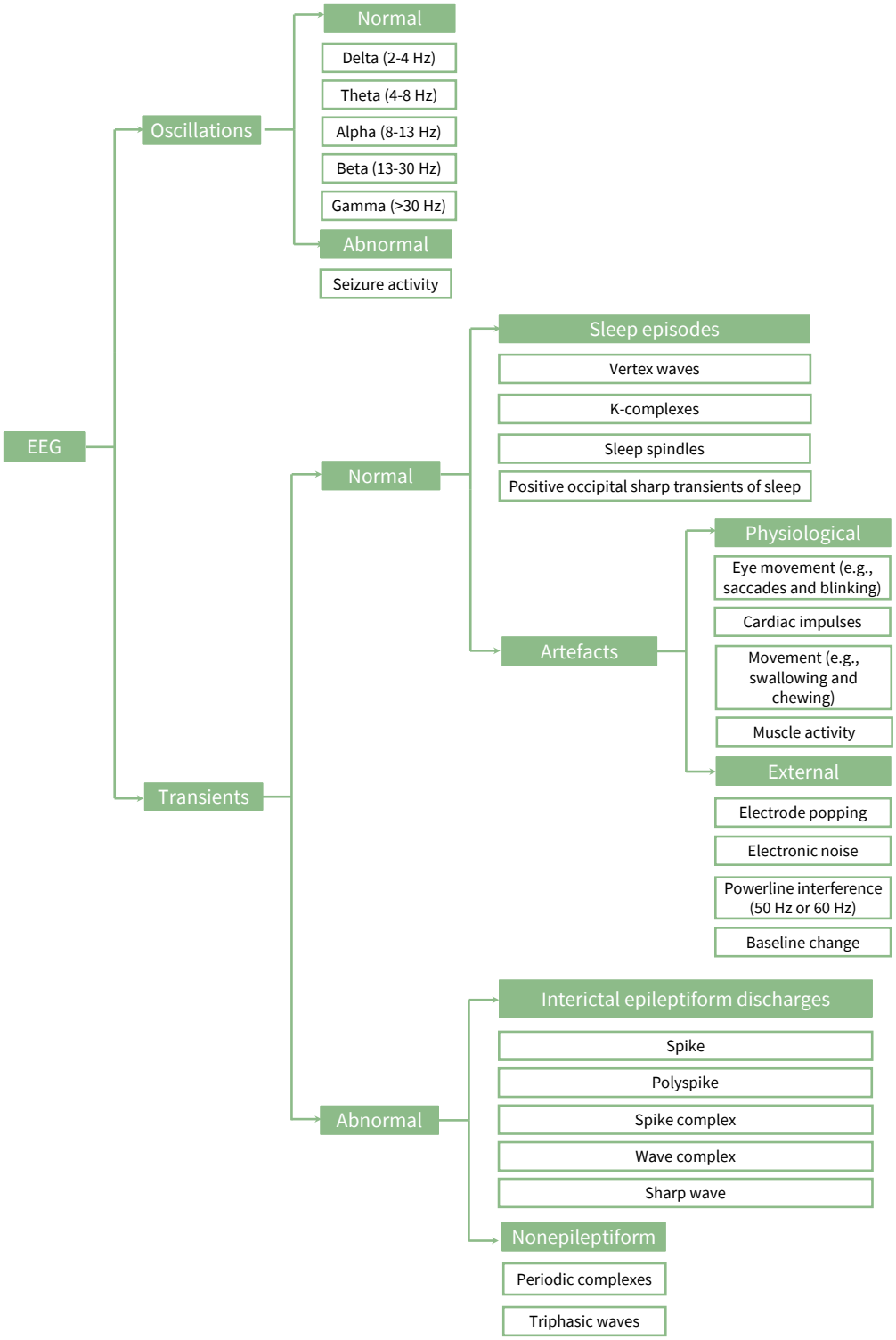

Figure 2.3: Categorisation of EEG activity. Adapted from Sanei & Chambers 2021 [63].

prominent brain rhythm. These waves arise mainly in adults while they are quietly awake but with their eyes closed and without attention or concentration [62, 63]. Beta band activity is observed for mental and cognitive tasks (e.g., active thinking and attention engagement) and during anxious and alert states, mainly over the frontal and central brain regions [62, 63]. Gamma oscillations are rare and may be clouded by the presence of artefacts, including muscle artefacts [57, 63].

Normal sharp transients captured by EEG include both cerebral (such as sleep-related potentials) and noncerebral potentials or artefacts (such as eye blinks, chewing, cardiac impulses and movement of the scalp musculature). Besides these physiological artefacts, EEG records, particularly the scalp ones, can also present other external artefacts resulting from ambient electromagnetic interference and improper attachment of the electrodes to the scalp [57, 58].

Abnormal transients, also called interictal epileptiform potentials, are typically identified for diagnostic purposes. Interictal epileptiform discharges are found in the first EEG in 29-55% of patients with epilepsy, a percentage that increases to 92% by the fourth EEG [59, 64]. The distinct morphological characteristics observed among the different types of abnormal transients help identify them: spikes, polyspikes, spike and wave complexes, sharp waves, sharp and slow waves discharges, and high-frequency oscillations [57, 59, 65]. Interictal epileptiform activity has been studied with regards to its potential in determining seizure risk (refer to Section 2.5.4) with some studies reporting fluctuations of interictal epileptiform discharges with circadian and multidien rhythms [49, 66–69].

2.2.2 Scalp EEG

Being a minimally invasive method, scalp EEG has been widely used both in diagnosis and continuous bedside monitoring of epileptic patients in intensive care units and epilepsy monitoring units during presurgical evaluation [34, 37, 64]. Additionally, analysis of the scalp EEG, in combination with other noninvasive methods, is necessary to plan and guide the electrode placing when intracranial monitoring is required [64, 70].

The scalp EEG signals, also denoted channels, result from the measurement of a voltage difference between two electrode sites, one active electrode and a reference electrode. To highlight different signal aspects, different electrode arrangements or montages can be chosen: bipolar or referential (see Section A.1 in Appendix A for more details on each montage) [34, 58, 73]. Scalp EEG therefore corresponds to multichannel recordings obtained by placing electrodes over the scalp using an electroconductive gel or paste [59]. Placing the electrodes across the entire scalp can provide large-scale information, which can be useful for studying neural mechanisms triggered in different brain areas [74]. In Figure 2.4, it is possible to observe the three existing international systems used to place the EEG electrodes on the scalp [59, 71].

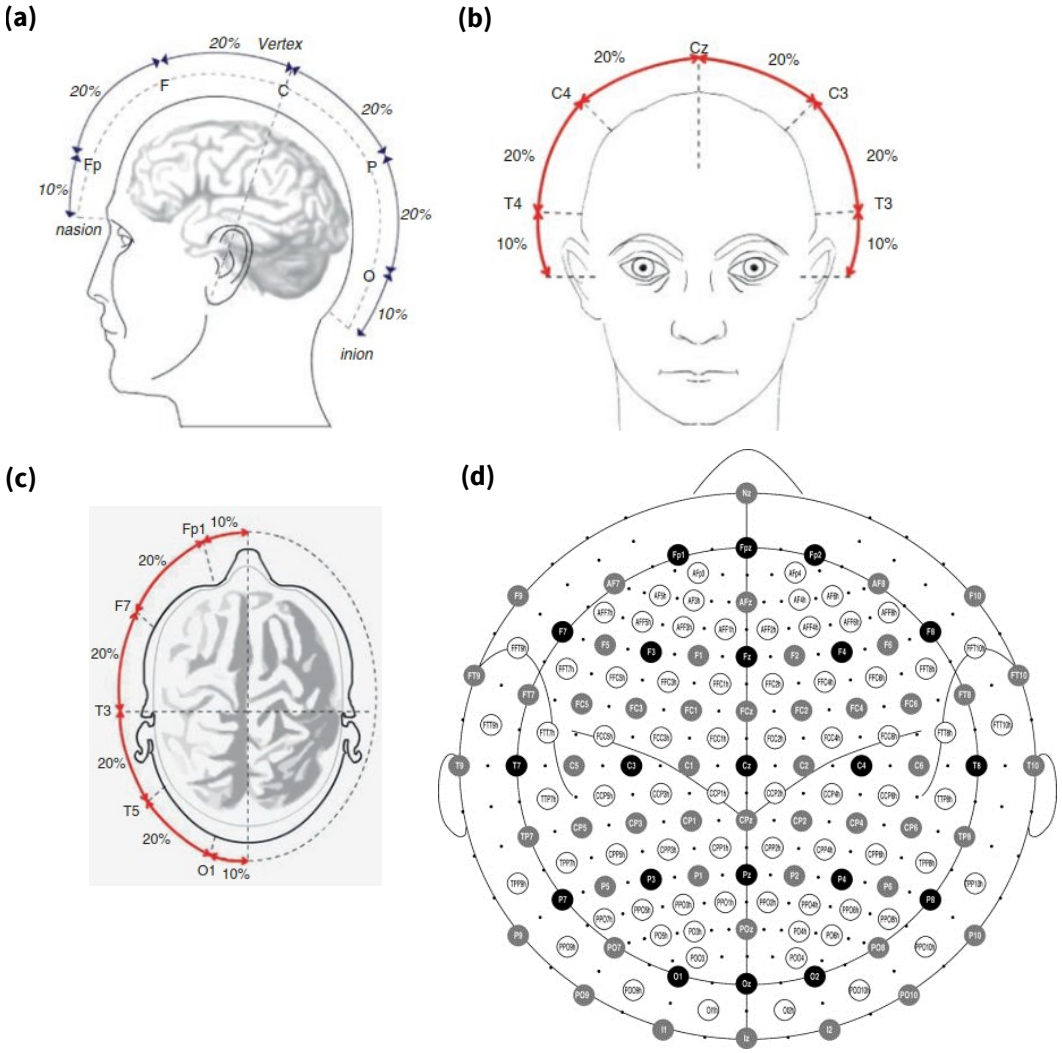

Figure 2.4: Scalp electrode placement. According to the International 10-20 system, electrodes are displayed along (a) the anteroposterior mesial arc, connecting nasion and inion, (b) the latero-lateral coronal arc, and (c) the sagittal lateral longitudinal arc, connecting nasion and inion. (d) Scalp electrode placement according to the modified combinatorial nomenclature for the International 10-10 and 10-5 systems, which have renamed four electrodes: T3 to T7, T4 to T8, T5 to P7 and T6 to P8. Letters correspond to the lobe of the brain where the electrode is placed (F: frontal, T: temporal, P: parietal or posterior temporal, O: occipital, and A: auricular). The numbers of electrodes increase with the distance to the midline, which can be identified by the suffix "z" in the electrodes' name. The left and right sides are indicated by odd and even numbers, respectively. Adapted from Mecarelli *et al.* 2021 [71] and Oostenveld & Praamstra 2001 [72].

These differ depending on the number of electrodes placed at defined distances from anatomical landmarks. The 10-20 International System was the first system used for scalp EEG recording, consisting of the placement of 21 electrodes over the scalp. This system is considered adequate for most patients, including during ambulatory or presurgical monitoring.

Potentials measured by scalp EEG result from cortical potentials volume conducted across the head and, therefore, severely attenuated by the intermediate layers

separating the neural tissue and the electrodes (including cerebrospinal fluid, dura matter, bone and the scalp) [34,63,64]. In fact, the synchronous neural activity of a large amount (at least 6 cm^2 of cortex) of neurons is typically required to allow scalp EEG effective recording and analysis, increasing to at least 10-20 cm^2 to capture pathological epileptiform potentials [34,57,59,64]. Accordingly, EEG activity may not be detectable in mesial temporal regions, interhemispheric frontal lobe structures and the thalamus [57,71]. Adding to these limitations of scalp EEG is the fact that low amplitude fast oscillations in the beta and gamma bands are often contaminated by extracranial (mainly muscle) artefacts [57].

The demand for minimally invasive, wearable or mobile EEG solutions has prompted the development of promising noninvasive devices for long-term ambulatory EEG monitoring. Efforts have been directed towards the decrease in the number of electrodes used for scalp EEG data collection, this way, decreasing patient discomfort and stigma levels. Specifically, current solutions include placing one to four electrodes behind the ear(s) and/or on the forehead aiming at capturing focal epilepsy manifestations [75].

2.2.3 Invasive EEG

EEG can also be recorded invasively using (i) intracranial electrodes recording directly from the brain (either from the surface or within the cortex) or (ii) subscalp electrodes implanted subcutaneously between the scalp and the bone [76]. When the EEG is recorded invasively with an implanted device over months to years, it is denoted chronic EEG [65,66].

Intracranial electrodes comprise three types of electrodes, widely used to record seizure onset and propagation (independently or in combination): depth electrodes, subdural strips and subdural grids (see Figure 2.5) [39,79]. These types of electrodes can be distinguished by the parts of the brain where they can be implanted, the method of insertion and the risks of implantation [79]. Subdural electrodes require a craniotomy to be placed over the cortex's surface and allow electrocorticography (ECoG) recording [39,79,80]. Depth electrodes enable the recording of brain activity from all structures, including deep brain structures within the cortex (such as the insula, cingulum, hippocampus, amygdala, orbitofrontal and medial occipital regions) [39,79,81]. Depth electrodes are stereotactically implanted (through small burr holes) in combination with subdural electrodes or independently defining a method for the three-dimensional analysis of a given brain zone named stereoelectroencephalography [79–81].

Compared to scalp EEG, intracranial EEG recordings provide information from a restrictive brain location instead of a more extensive area, therefore, being more sensitive to local generators of brain activity [57,70,79]. In fact, intracranial recordings can capture brain activity from a few millimetres (in the order of 4 mm^2) [34].

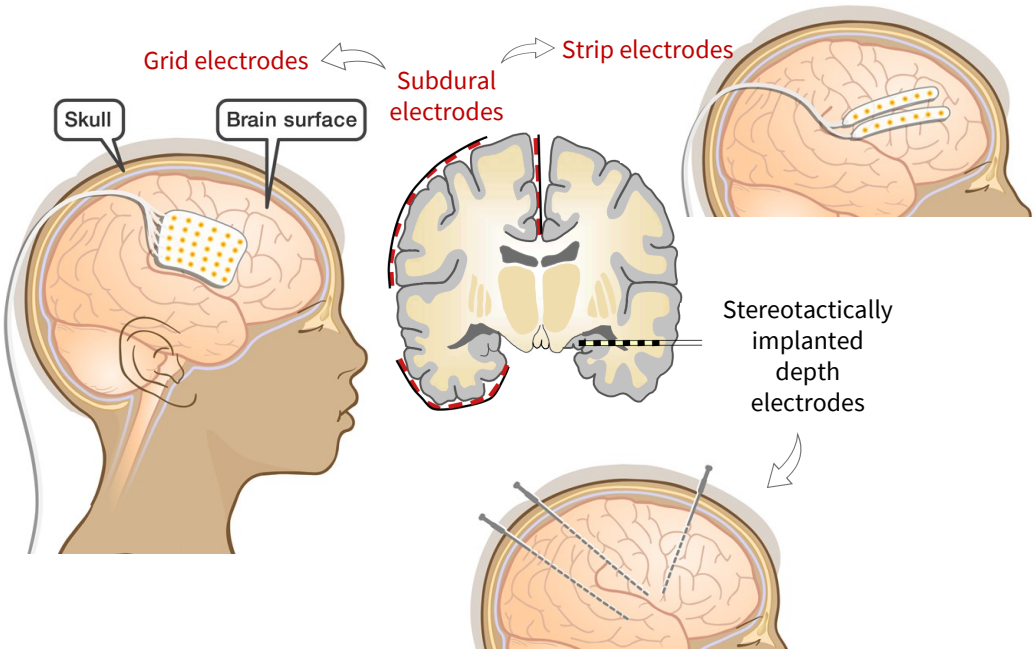

Figure 2.5: Invasive EEG monitoring. EEG can be invasively recorded using a subdural grid, a subdural strip, and/or depth electrodes. Adapted from *About Kids Health 2017* [77] and Noachtar & Rémi 2009 [78].

However, as the covered brain is considerably more restricted than the scalp EEG range across the brain, an invasive study may also yield insufficient information on a given brain area [79]. The proximity between the electrodes and the signal source is considerably higher compared to scalp EEG, resulting in the acquisition of intracranial recordings far less contaminated by artefacts and with higher improved signal-to-noise ratio [70, 79, 82]. When the seizure originates and terminates in the same brain area, EEG onset and offset times can be determined more accurately [83].

Nevertheless, invasive EEG monitoring carries associated risks. Implanting intracranial electrodes can lead to serious complications, including hemorrhage, infection, cerebrospinal fluid leaks, and cerebral edema [70]. An infection rate of 0.8% and a 1% prevalence of hemorrhage per electrode has been reported for stereoelectroencephalography, with a prevalence of about 3% for all complications [70]. Similarly, intracranial haemorrhage is also the main complication resulting from implanting subdural strips or grids, with a mean infection rate of 4% [84] and an overall complication rate of 2.5%-19% [70].

Subscalp (or subcutaneous) electrodes are implanted subcutaneously via a minimally invasive surgical procedure. While a few electrodes might be implanted in the focus (often in the temporal lobe) under local anesthesia, there is also the option for increasing electrode coverage to the entire head by resorting to general anaesthesia [76]. This is a less invasive procedure recently developed for ultra-long-term brain monitoring [22, 69, 76, 85]. Subscalp EEG and scalp EEG similarly capture background activity with closed and open eyes, showing a similar signal-to-noise

ratio. Additionally, subscalp EEG recordings present improved signal quality compared to scalp EEG, particularly during body movements that produce interferences due to the movement of wires [22,69,76]. Conversely, subscalp EEG may be affected by other types of artefacts such as muscle activity [69].

2.3 Electrocardiography

The ECG provides a way of recording the action potentials of the atrial and ventricular muscle cells of the heart over time. It uses a galvanometer to measure the current corresponding to depolarisation and repolarisation waves. When a depolarisation wave approaches the positive electrode, a positive voltage is produced, whereas when it goes away, a negative voltage is recorded. The ECG profile is determined by the type of wave, its direction and its intensity (see Figure 2.6). To be noticed that the more muscle mass exists where the wave is produced, the higher the amplitude registered by the ECG instrumentation.

Furthermore, different sensor locations in the chest will correspond to different

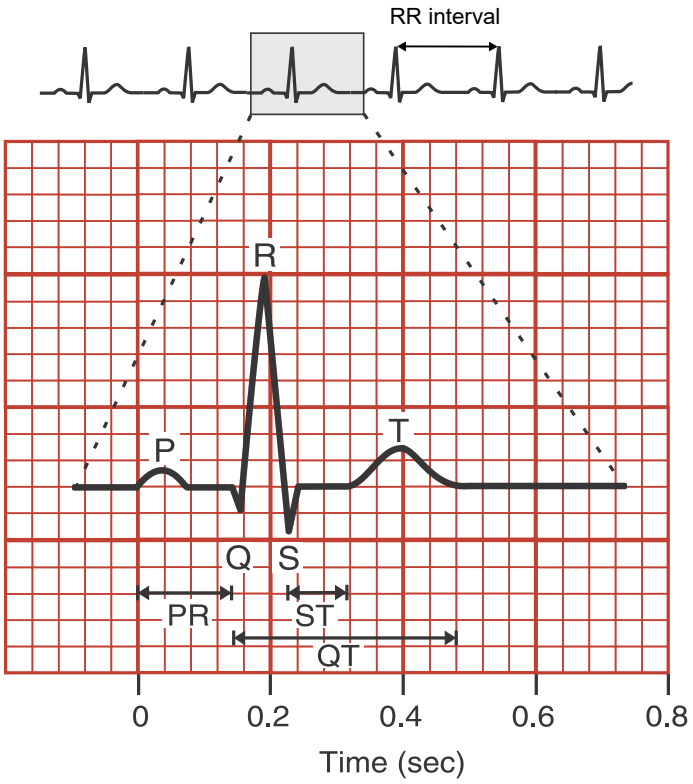

Figure 2.6: Example of an ECG trace comprising six heart cycles. Computing the distance between successive R peaks yields the RR interval series. Each heart cycle is described as the sequence of a P wave, a QRS complex and a T wave, corresponding to atrial depolarisation, ventricular depolarisation, and ventricular repolarisation, respectively. As the ventricles are associated with more muscle mass, the QRS complex waves are more pronounced than the P wave. Each small square corresponds to 1 mm. Source: Klabunde 2012 [86].

perspectives of heart activity. The different sensor configurations, named leads, are depicted in Figure 2.7.

The ECG trace shows a higher signal-to-noise ratio compared to EEG, which allows for the easy identification of heart cycle waves [89]. When this signal is acquired in noncontrolled environments, such as presurgical evaluation in an epilepsy monitoring unit, it might only be possible to identify the QRS complex on the contaminated signals (see Figure 2.7). With such information, it is possible to conduct studies on the heart rate (HR) and heart rate variability (HRV) changes over time. An HRV analysis consists of the computation of the RR interval series using the location of the R peaks. Each point in the non-evenly sampled RR interval series corresponds to the interval between adjacent R peaks [90]. When the ECG has not been contaminated with artefacts, the resulting HRV is observed for the computation of the normal-to-normal (NN) interval. Decreasing HRV is observed when HR increases, as the beat-to-beat intervals are shorter; hence, variability is less prone to occur [91].

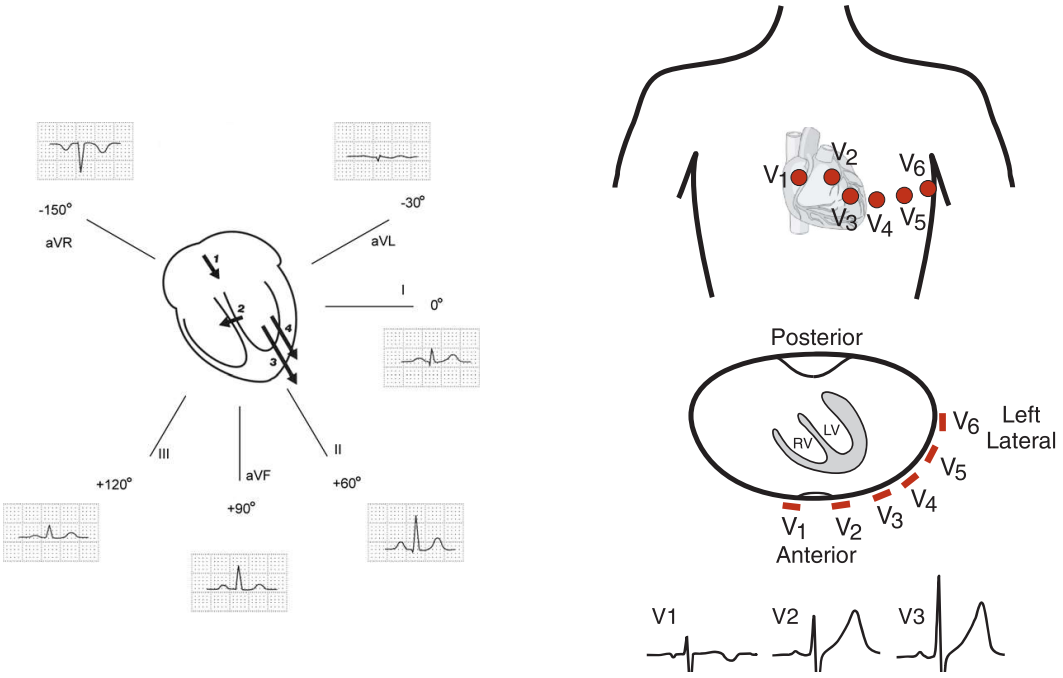

(a) **(b)**

Figure 2.7: Possible ECG electrode configurations. (a) Six limb leads, including I, II and III bipolar leads and AVR, AVF and AVL augmented unipolar leads, displayed in the frontal plane of the heart. The force vectors indicated by numbers 1, 2, 3 and 4 represent the average direction and intensity of the four main waves registered by the ECG (1 - depolarisation wave resulting from atrial contraction, 2 - depolarisation of the ventricular septum, 3 - depolarisation wave from the ventricular muscle tissue and 4 - wave triggered by ventricular repolarisation). Source: Foster 2007 [87]. (b) Unipolar chest (or V) leads capture information from the transverse or horizontal heart perspective. Source: Klabunde 2012 [88].

The guidelines for the analysis of the HRV were published in 1997 by the Task Force of The European Society of Cardiology and The North American Society of Pacing and Electrophysiology [92]. According to these guidelines, the HRV can be measured using linear time-domain and frequency-domain and nonlinear methods. These measures and corresponding physiological significance are detailed in Appendix D.2.

2.3.1 Autonomous nervous system

The autonomous nervous system (ANS) is the part of the nervous system responsible for maintaining homeostasis through the regulation of HR, respiration, micturition, digestion and reproduction [20, 30, 42].

Autonomic responses are regulated by several brain structures integrating the central autonomic network: (i) cortical limbic areas including the amygdala, anterior, insula, anterior cingulate cortex, and posterior orbito-frontal cortex), and (ii) cortical regions including the hypothalamus, periaqueductal grey matter, parabrachial region in the pons, solitary tract nucleus, and ventrolateral medulla [19, 30, 42, 93].

The parasympathetic and sympathetic reflex centres are subdivisions of the ANS which act in concert to balance autonomic function. Alterations to the normal autonomic function will be reflected in the antagonistic responses of both parasympathetic and sympathetic systems. Activation of the parasympathetic system predominates during relaxation. Consequently, there is a decrease in HR, atrio-ventricular conduction and ventricular excitability, such responses being mediated by the vagus nerve (starting in the medulla oblongata). Increased automatism of the sinus node, increase in atrio-ventricular conduction and ventricular excitability and contractility are the consequences of activating the sympathetic system. This response to the heart predominates during physical exercise, being mediated by neurons from the rostral ventrolateral medulla [19, 20, 30, 86, 93, 94].

Accordingly, cardiac parameters such as blood pressure, HR and HRV have been widely used as a proxy to the functioning of ANS [30]. Oscillations in HR can evolve to the occurrence of specific cardiac events. Tachycardia corresponds to the significant increase in HR comparing to a resting HR range. The upper threshold of this range depends on the patient's age and decreases with it. For instance, for subjects over 15 years, an HR superior to 100 beats per minute (bpm) indicates ictal tachycardia [42, 88, 93]. The threshold increases to 169 bpm for children 6-11 months of age [93].

Conversely, when the HR decreases below 50 or 60 bpm, the resting sinus rhythm, the subject is experiencing an abnormal rhythm named bradycardia [88, 95]. This threshold is also dependent on the subject's physical condition. For instance, an athlete's resting state HR may be lower than 60 bpm [88].

Assessment of the HRV is being increasingly documented as it can provide impor-

tant information regarding the effects of the ANS on the heart. In fact, unlike HR, measuring HRV has been undertaken to determine if and to which extent are sympathetic and parasympathetic systems involved in autonomic control. A simplistic analysis of HRV allows for the general observation that an increase in HRV results from parasympathetic system predominance while a decrease indicates increasing activation of the sympathetic system [96]. Analysis of the evolution of HR over time is useful to indicate the changes in autonomic control. However, it is not possible to determine which autonomic subsystem is responsible for these changes [30]. As a result, HRV measurements have been used as the standard parameter when studying cardiac autonomic control [30].

The proximity of the ANS centres to the cerebral cortices explains the prevalence of autonomic manifestations in the temporal lobe and insular lobe epilepsies. Autonomic dysregulation has been observed mainly during a seizure event, with some studies also reporting altered autonomic parameters before [30] and after [97] seizures. Cardiac measures have been widely assessed to inspect changes in autonomic function associated with seizure activity [30]. Details regarding changes in autonomic function occurring before and close to the seizure onset are provided in state-of-the-art Section 3.2.

2.4 Epilepsy treatment and management

The first line of treatment for patients with epilepsy consists of the administration of anti-epileptic drugs (AEDs). When this primary treatment fails to reduce seizure occurrence and severity, patients can resort to other treatment options, including trying additional AEDs, resective surgery, neurostimulation and dietary therapies [37].

2.4.1 Antiepileptic drugs

AEDs development is based on the understanding that epilepsy is characterised by hyperexcitatory or hypersynchronous neuronal activity resulting from disturbances in the normal balance between excitation and inhibition. Currently, there are approximately 30 AEDs that can be used to control seizures either by dampening excitatory mechanisms or boosting inhibitory ones (see Figure 2.8). However, administration of AEDs might not be successful and result in the diagnosis of drug-resistant epilepsy or the worsening of epilepsies in some patients [3].

Pharmacological treatment has evolved hand in hand with the increased knowledge regarding mechanisms of epilepsy at molecular and cellular levels. Additionally, epilepsy is also known to involve dysfunction at the circuit level, although limited information exists about the underlying mechanisms. Future endeavours concern understanding circuit-level mechanisms toward the enhancement of current phar-

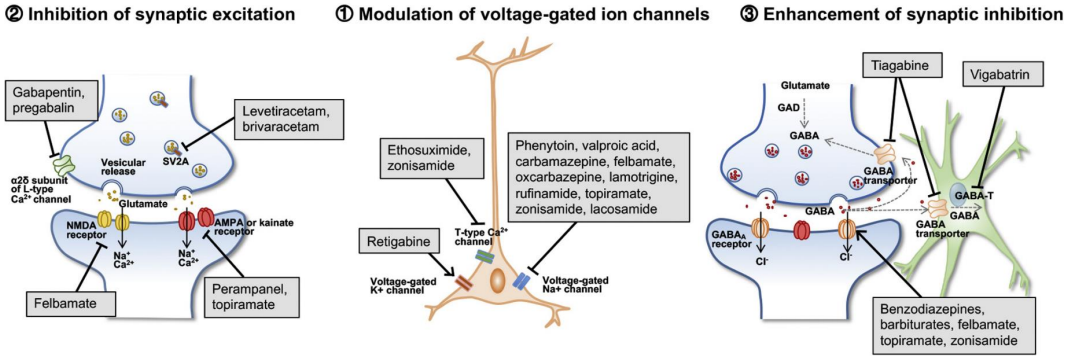

Figure 2.8: Molecular targets of available AEDs. Key mechanisms of AED action can be categorised according to three aspects: (1) modulating voltage-gated ion channels (that determines the intrinsic firing ability of a neuron), (2) dampening excitatory or (3) boosting inhibitory synaptic transmission (that determines the extrinsic neural signal input). Source: Wang & Chen 2019 [3].

macological treatment [3].

Drug-resistant epilepsy

According to the operational definition proposed by the ILAE, patients are diagnosed with drug-resistant epilepsy (DRE) when the treatment with at least two seizure medications does not lead to seizure freedom (see Box 4). Seizure freedom is achieved when all types of seizures cease to happen for 12 months or three times the inter-seizure interval observed before treatment started [98].

A recent systematic review reported 32.4% overall pooled prevalence of DRE. This study's meta-analysis also showed that DRE was more prevalent in focal epilepsy [5]. The introduction of new AEDs over the last decades has not considerably changed the proportion of patients with DRE [3, 5, 7]. However, even though the efficacy of the new proposed AEDs has not considerably improved over the years, a decrease in the subsequent side effects has been reported [3].

Patients with DRE can see their quality of life significantly reduced as they can be continuously exposed to the harmful consequences of seizure discharges. Namely, these people commonly present with a neurologic impairment such as memory loss and behavioural problems such as depression [7]. In addition to the treatment consequences, the occurrence of seizures can originate severe injuries resulting in falls and loss of consciousness that might contribute to increased social stigma [6,37]. The mortality rate for DRE is 5–10 times higher than that of the general population [7].

Box 4 - Diagnostic criteria for drug-resistant epilepsy (as defined by the Task Force of the ILAE in 2010 [98])

"Drug-resistant epilepsy may be defined as failure of adequate trials of two tolerated and appropriately chosen and used antiepileptic drugs schedules (whether as monotherapies or in combination) to achieve sustained seizure freedom."

The vast majority of people with DRE are not referred to epilepsy centres to be evaluated by a team of epilepsy experts. In the United States of America, it has been estimated that less than 1% of DRE patients are referred to an epilepsy centre. In addition, there is a span of 20 years, on average, from the onset of seizures to the date of referral, that often results in irreversible psychological and social disability despite post-surgical successful seizure elimination [7].

2.4.2 Surgery

Patients with DRE can achieve seizure control by resorting to epilepsy surgery. This treatment option consists of resecting or disconnecting the brain zone involved in the process of seizure generation, i.e., the epileptogenic zone. The success of resective surgical treatment is dependent on the correct identification of the epileptogenic zone, which is based on clinical, neuropsychological, and neuroimaging data. Assessment of such data is performed during presurgical monitoring (see Figure 2.9) [26, 39, 99–101].

During the first phase of presurgical evaluation, clinicians inspect the structural magnetic resonance imaging (MRI) to identify the structural abnormality of the brain, i.e., the epileptogenic lesion, that might be causing epileptogenic activity. Additionally, they commonly inspect the scalp EEG trace and seizure phenomenology (through video and scalp EEG observation). Complementary investi-

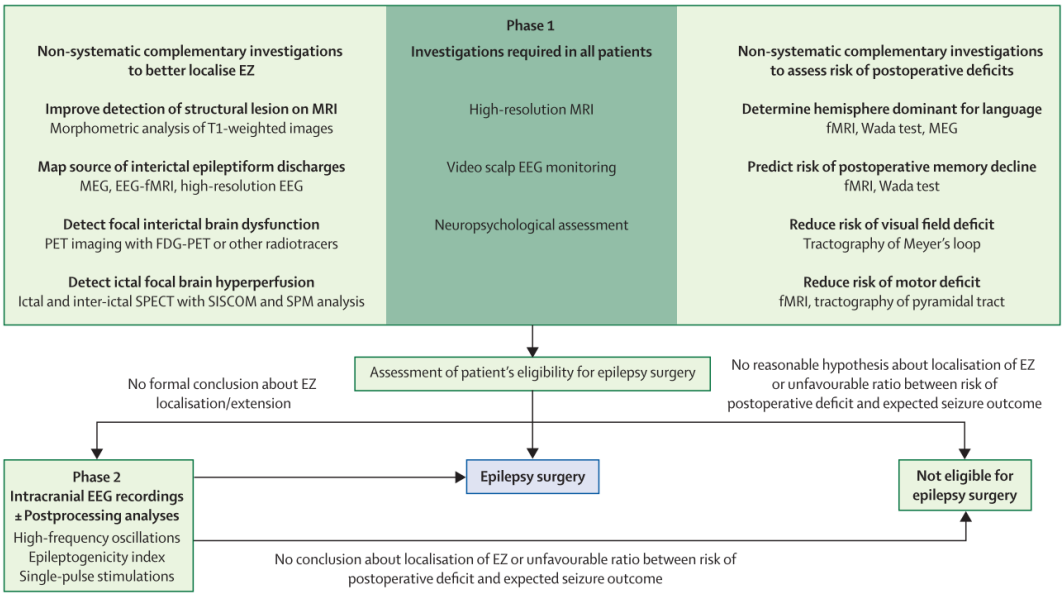

Figure 2.9: Patient assessment during presurgical monitoring. Phase 1 investigations are conducted to localise the epileptogenic zone and determine if the patient is a candidate for surgery. Phase 2 investigations are recommended to improve the localisation of the epileptogenic zone if the risk/benefit ratio is acceptable. ^{18}F-FDG: ^{18}F-fluorodeoxyglucose. fMRI: functional MRI. MEG: magnetoencephalography. SISCOM: subtraction ictal SPECT coregistered with MRI. SPECT: single-photon emission computed tomography. SPM: statistical parametric mapping. Source: Ryvlin *et al.* 2014 [99].

gations can be undertaken to identify and characterise (i) the brain areas manifesting interictal spikes (irritative zone) and the functional role of these areas, using magnetoencephalography and EEG-fMRI and (ii) the brain areas where seizures seem to arise (ictal onset zone) using single-photon emission computed tomography [26, 39, 99–101].

Structural MRI is the primary tool for identifying epileptogenic lesions such as hippocampal sclerosis, focal cortical dysplasia or neocortical mass [37, 100]. When the MRI lesion is difficult to localise, possibly a consequence of the epileptogenic zone falling outside the temporal lobe, the success rate of surgery is considerably lower [26, 37, 99]. In fact, the second phase of presurgical evaluation is performed when video-EEG and MRI studies are discordant, no clear epileptogenic lesion has been identified in MRI or when the ictal onset zone is located over or near the eloquent cortex (i.e. language cortex and primary motor and sensory cortex) [26, 37, 99]. During this phase, required for up to a quarter of presurgical patients, intracranial EEG electrodes are implanted to identify the irritative zone and ictal onset zone, even though at the expense of increased risk of morbidity and mortality [26, 37, 99, 101].

To be noticed that routine presurgical evaluation begins by initiating activation procedures such as AEDs tapering or sleep deprivation, in order to precipitate seizures and reduce costs of hospital stay [59, 64, 102]. Considerable evidence indicates that AEDs withdrawal influences seizure propagation, but not the seizure onset characteristics observed in the video-EEG [102]. However, AEDs withdrawal might increase the risk of experiencing clusters of seizures (see Section 2.1.4) which in turn deteriorate the patient's condition. Additionally, AEDs withdrawal has been reported to trigger a generalised tonic-clonic seizure in patients that previously did not experience this type of seizure [64, 102, 103]. The effects of medication withdrawal are yet to be established as they depend on several factors, including the rate of withdrawal, drug interactions and the experience of the clinician in charge [64, 102, 103]. Sleep deprivation protocols are also frequently employed in epilepsy centres to induce seizures despite some evidence exist showing sporadic efficacy [64].

Epilepsy surgery is still considered the most effective treatment option that leads to long-term seizure freedom in patients diagnosed with drug-resistant focal seizures [37, 99]. Patients with MTLE are the most frequently referred DRE patients for epilepsy surgery, as this treatment strategy exceeds continued medication regarding seizure freedom and quality of life [37, 104]. A large range of outcomes can be seen after TLE surgery, as evidenced by the 49% to 83% rate of seizure freedom at 10 years after surgery [99].

Surgical treatment has seen improvements over time, in part, due to the recent development of neuroimaging techniques. Consequently, the eligibility criteria for surgery have also widened, including patients with normal MRI (i.e., with no identifiable lesion on MRI) [99, 100, 104]. However, achieving long-term seizure freedom has been reported to vary significantly among patients that underwent surgery. For

instance, a survey from 2008 reported that postoperative seizure freedom after one year of follow-up ranged from 53 to 84% in patients with mesial temporal lobe sclerosis [105]. Additionally, epilepsy surgery has not seen a considerable increase over the last decade, particularly in adults and in western countries [99]. Besides being the direct result of the low number and late referrals, surgery underuse might be related to the existence of misconceptions and fears both from clinicians and patients [7, 26, 99, 100].

2.4.3 Neurostimulation

When patients are not eligible for resective surgery, they can be offered neurostimulation as an alternative therapy. In contrast to a potentially curative surgical treatment (seizure freedom), neurostimulation is considered a palliative option (seizure reduction) as only a few patients become seizure-free for more than 12 months. The patient is implanted with a neurostimulation device which delivers electrical pulses to peripheral nerves, such as the vagus nerve or the trigeminal nerve, or specific brain areas of the central nervous system to prevent potential seizures (see Figure 2.10) [4, 26, 106–108].

Currently, there are several neurostimulatory techniques available for DRE that can be primarily divided into invasive and noninvasive, depending on the need to implant a device through surgery. Additionally, stimulation can be provided in a scheduled manner (open-loop) or response to seizure activity (closed-loop) [26]. Invasive modalities include vagus nerve stimulation (VNS), deep-brain stimulation (DBS), and responsive neurostimulation (RNS). Noninvasive treatments, yet to be

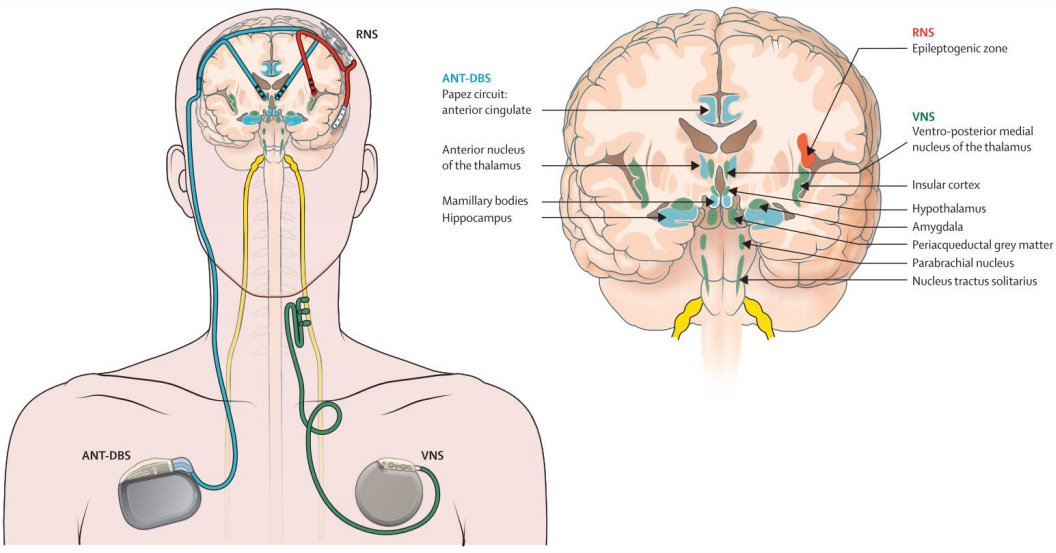

Figure 2.10: Approved neurostimulation therapies for treating drug-resistant focal epilepsy. ANT-DBS: deep brain stimulation of the anterior nucleus of the thalamus. RNS: responsive neurostimulation. VNS: vagus nerve stimulation. Source: Ryvlin *et al.* 2021 [4].

approved, include transcutaneous vagus nerve stimulation, trigeminal nerve stimulation and transcranial magnetic stimulation [4,106–108]. Drug-resistant focal epilepsy can be treated using one of the following approved invasive stimulation devices: VNS, DBS of the anterior nucleus of the thalamus (ANT-DBS), and RNS of the epileptogenic zone or zones (see Table 2.2) [4]. The following paragraphs will focus on these three modalities.

VNS originally operated in an open-loop manner by delivering stimulus to the left vagus nerve according to predefined schedules, typically 30 s every 5 min [4]. Additionally, patients or caregivers can pass a magnet over the implanted device to either stop stimulation at any particular situation or deliver a single stimulation on demand [4,107]. VNS was later implemented in closed-loop, delivering stimulus upon the detection of predefined changes in heart rate triggered by the seizure generation process [4, 114]. The basis for the detection of heart rate derives from reports of

Table 2.2: Approved invasive neurostimulation therapies for drug-resistant epilepsy [4, 107, 109].

	VNS	**ANT-DBS**	**RNS**
Approval	Open-loop: FDA and EU in 1997; Closed-loop: FDA and EU in 2015	EU in 2010, FDA in 2018	FDA in 2013
Stimulation target	Left vagus nerve (neck)	Anterior nucleus of the thalamus (bilaterally)	Ictal onset zone (cortex)
Stimulation placement	Subcutaneous, left pectoral/sub clavicular	Subcutaneous, abdominal	Within the skull
Stimulation mode	Open-loop (stimulus delivered during 30 s every 5 min); heart rate responsive closed-loop; on demand	Open-loop (stimulus delivered during 1 min every 5 min)	Ictal intracerebral EEG responsive closed-loop
Age	Children $\geq$ 4 years, adults	Adults	Adults
Type of seizure	Focal and generalised	Focal	Focal
Epileptogenic focus or foci	Non-localisable, multifocal, or not resectable	Bitemporal, multifocal, or non-localisable	Bitemporal or eloquent focus
AED requirements	Resistance to 2 AEDs	Resistance to 3 AEDs	Resistance to 2 AEDs
Double-blind, multicenter, randomised controlled trial	[110, 111]	[112]	[113]

EU: European Union; FDA: United States Food and Drug Administration.

increased heart rate during seizures (defined as ictal tachycardia) in about 82% of seizures [93]. VNS is an extracranial procedure associated with minimal surgical risk and tolerable symptoms and was the first procedure approved for epilepsy treatment [4, 6, 37].

DBS uses intracranial electrodes to deliver open-loop stimulation to specific brain structures (e.g., anterior nucleus of the thalamus) assumed to manifest seizure activity [6, 108]. Although the exact mechanisms of action of ANT-DBS remain unknown, it is accepted that high-frequency stimulation can disrupt pathological synchronisation of brain activity and epileptic networks [107, 108, 115].

RNS consists in intracranially implanting a neurostimulator connected to depth electrodes, or subdural cortical strip leads to deliver closed-loop stimulation directly to the seizure focus (which might include one or two epileptogenic brain regions). Cortical stimulation occurs as a result of the detection of seizure onset activity in the EEG signals (enhanced rhythmicity, changes in frequency, or amplitude) [4, 6, 26, 108, 115]. The seizure detection model integrating the clinically approved RNS system was developed based on EEG features and the definition of a threshold that, once exceeded, triggers stimulation to the seizure focus or foci [116].

No randomised direct comparisons of the efficacy and tolerability of the stimulation techniques mentioned above exist. Summing this gap to the lack of consensus across epilepsy centres leads to the absence of guidelines for when and which modality to adopt for a given patient [4, 106, 108, 115]. Long-term outcomes of neurostimulation therapies have been reported in some studies, requiring however careful comparison due to the wide range of study biases (e.g., trial design, stimulation parameters, changes in epileptic medication and studied populations) [4, 117]. Overall, these studies suggest that ANT-DBS and RNS seem to overcome VNS in terms of seizure freedom rates, even though at the expense of a more invasive procedure. However, despite being the most available treatment (used in 100 000 people with epilepsy), VNS tends to be chosen given the more favourable risk/benefit ratio and, therefore, the preference for less invasiveness over efficacy [4, 6]. The 50% responder rate [6] at one year is 37%, 43% and 44% for VNS, ANT-DBS and RNS, respectively. After 7 to 9 years of follow-up, the 50% responder rate increased to 73-74% for ANT-DBS and RNS. When the influence of cofactors is reduced the 50% responder rate decreases to 50% or less [4].

Nevertheless, all modalities involve a surgical procedure, battery replacement, frequent clinical appointments to adjust stimulation parameters and limitations regarding MRI safety after device implantation [4]. Concerns have also been raised regarding the closed-loop neurostimulation approaches. For the case of the RNS system, there are reports of over 99.9% stimulations without clinical manifestation of seizures, evidencing the tuning of the detection models towards seizure sensitivity [117]. The efficacy of both RNS and tachycardia-responsive VNS is suspected

[6] Ratio of individuals achieving a reduction of at least 50% of their baseline seizure frequency.

to arise from frequent stimulation, possibly yielding a long-term neuromodulatory effect rather than from detecting clinical and electrographic seizures alone [115, 117]. Closed-loop neurostimulation is therefore highly dependent on the development of accurate seizure detection algorithms. Both closed-loop RNS and VNS are based on detecting alterations in EEG features and heart rate, respectively, above a given threshold [114, 116]. Developing machine learning (ML) detection approaches has been pointed to as a solution to improve current detection performance in closed-loop systems [4, 117].

2.4.4 Rescue medication

Administration of acute medication has been performed with different purposes: (i) to achieve seizure freedom through combined effect with other AEDs, (ii) reduction of the continuous AEDs dose, and (iii) prevent seizure clusters and prolonged seizures [7] [119]. Timely administration of medication may prevent side effects of long-term systemic therapy using multiple AEDs [43, 90].

Benzodiazepines are the most common type of emergency medication due to their rapid and effective antiepileptic effect, which, when administered continuously, may trigger secondary adverse effects [119, 120].

Diazepam rectal gel was approved by the FDA in 1997 as a rescue medication for out-of-hospital treatment for seizure clusters [120]. Despite the complaints regarding the necessity of a proper environment and acceptance for its administration, diazepam rectal gel remained the only solution for seizure clusters until 2019, being mainly used for younger children [120]. Recently two other routes of administration have been proposed to prevent seizure clusters: a midazolam nasal spray for patients with epilepsy aged 12 years and older and a diazepam nasal spray for patients aged 6 years and older [120].

Buccal midazolam was approved in 2011 in the European Union for the treatment of prolonged seizures in children younger than 18 years [55, 120].

As can be seen in Table 2.3, the different routes of emergency medication are associated with different times to start taking effect (onset of action) and to reach the maximum effect (peak level).

Intranasal routes of administration have been widely explored due to a number of advantages, including being a noninvasive and easy-to-access route, having a rapid onset of action and avoiding social discomfort [120].

2.4.5 Dietary therapies

Dietary treatments, including the ketogenic and modified Atkins diets, have been reported to reduce seizure frequency [6, 37]. The ketogenic diet is an established

[7] Prolonged seizures are identified when the convulsive phase of convulsive seizures (e.g. tonic-clonic seizures) continues for more than five minutes [118].

Table 2.3: Rescue medication approved for out-of-hospital treatment.

Drug	Route	Onset action	Peak level	Approval
Diazepam [121]	Rectal	5-10 min	10-45 min	FDA, 1997, for seizure clusters
Midazolam [119]	Buccal	< 5 min	20-30 min	EU, 2011, for prolonged seizures in children younger than 18 years
Midazolam [122]	Intranasal	< 10 min	15-120 min	FDA, 2019, for seizure clusters in patients with epilepsy aged 12 years and older
Diazepam [121]	Intranasal	< 5 min	> 60 min	FDA, 2020, for seizure clusters in patients with epilepsy aged 6 years and older

EU: European Union; FDA: United States Food and Drug Administration.

treatment for DRE children and people with epilepsy caused by metabolic derangements such as the GLUT1 deficiency syndrome [37]. According to two randomised controlled trials conducted in children with DRE, there is a greater than 50% reduction in the number of seizures (at three months) for 38% [123] and 50% [124] of patients when treated with the ketogenic diet. Even though, the modified Atkins diet shows more adherence in adults comparing to the ketogenic diet, the effectiveness and long-term safety of these dietary treatments still remain to be assessed [37].

2.4.6 Warning devices

The use of intervention devices has been explored in several healthcare applications, including epilepsy, where it has been making use of seizure prediction (Subsection 2.5), seizure detection (Subsection 2.5.3), and, more recently, seizure forecasting (Subsection 2.5.4). The ability to predict or detect an upcoming seizure can be used to automatically deliver an alarm to the patient or the caregiver and enable behavioural or therapeutic intervention (rescue antiseizure medication or neurostimulation) [26, 43, 125]. Additionally, continuous monitoring of biosignals in patients with epilepsy can be useful in improving diagnosis and seizure foci localisation [76, 90].

Wearable warning devices are designed to integrate algorithms that perform an automated analysis of long-term biosignals. The influence of the seizure generation process on the ANS (see Section 2.3.1) has prompted the analysis of biosignals other than EEG. Specifically, researchers are considering the acquisition of multimodal data, including actigraphy (using accelerometers), electrodermal activity, blood volume pulse (using photoplethysmography), muscle activity (using electromyography), body temperature, and heart rate (using ECG). Algorithms must be able to auto-

matically exclude data segments containing artefacts or non-physiological information [125].

The choice of the modality to use in epilepsy management may be related to the type of seizure experienced by patients [125,126]. For instance, noninvasive detection of tonic-clonic seizures, associated with pronounced motor clinical manifestations and high morbidity and mortality, has been performed using mainly accelerometry, electrodermal activity, and surface electromyography [43, 126–130]. While there is evidence of higher detection performance for motor seizures compared to non-motor seizures [126], there are reports of no differences between focal and generalised onset seizures [128]. Sweat level changes occurring for tonic-clonic and focal seizures can be captured by electrodermal activity [76, 127, 130]. Heart rate features (typically computed from ECG recordings) are widely explored for the detection of focal seizures [76, 130, 131].

However, device adherence is still limited as a result of problems such as inherent design deficiencies, signal quality and invasiveness [125, 132, 133]. For instance, long-term monitoring of brain activity using scalp or invasive EEG is simultaneously strongly informative but also severely limiting for patients with epilepsy [76]. Namely, scalp EEG can only be collected continuously for periods of a maximum of 1-2 weeks in epilepsy monitoring units, a narrow time window for infrequent seizures. Patients are typically in presurgical evaluation, which involves activation procedures (e.g., medication withdrawal or sleep deprivation) to provoke seizures [59]. These seizures might not correspond to the spontaneous seizures patients typically experience during their daily lives, hindering clinicians' interpretation [16, 76, 82, 126, 134]. Additionally, this method requires the use of a cap or an adhesive to ensure skin-electrode adherence and consequent recording quality for further analysis [76]. This setup causes discomfort to the patient and precludes its use during the patient's daily life due to resulting stigmatisation [13, 76, 128, 129, 132]. Invasive EEG allows for longer periods of acquisition, however, risking the development of complications including infections, lead migration, fracture and skin erosion [76].

Some of these problems can be mitigated by resorting to (i) minimally invasive EEG, noninvasive scalp EEG or extracerebral multimodal sensing, all options useful both during ambulatory or in-hospital monitoring. Despite ongoing research efforts to mitigate this need, design issues continue to arise from such devices. For instance, patients with epilepsy expressed a considerable preference for wrist-worn devices comparing to other types of sensors placed on the chest, arm, or forehead [125, 135, 136].

Minimally invasive systems concern the collection of subscalp ultra-long-term EEG in ambulatory settings. These systems have been designed primarily to improve seizure counting and localisation of the seizure onset zone [76, 137]. Noninvasive scalp EEG devices are emerging as alternatives to conventional scalp EEG by providing patients with more comfort and usability [75]. Nevertheless, the field of subscalp and

noninvasive EEG devices still require assessment of the true clinical value, including large-scale clinical trials [76, 137–139].

Regarding non-EEG sensors, there is high-quality evidence for the applicability of non-EEG-based wearables to the detection of generalised tonic-clonic and focal-to-bilateral tonic-clonic seizures [43,130,140]. Even though these are seizures associated with the highest morbidity and mortality [43, 44], there is also a pressing need to develop non-EEG-based wearable devices that are capable of detecting nonconvulsive seizures such as nocturnal or focal impaired awareness seizures (often unnoticed during sleep) [43, 76, 130, 133, 141]. Such devices exist on the market, although their clinical utility remains to be proved [130].

Lastly, it should be noted that despite the more than four decades dedicated to developing seizure prediction models, to date, there is only one prospective trial of a seizure prediction advisory system [50]. This first-in-human clinical trial, published in 2013, documents the performance of a seizure advisory system (Neurovista) implanted in 15 patients with DRE. The study was conducted over two phases. During the first phase, the device was implanted for data acquisition until a sufficient number of seizures occurred. The acquired data was then used to develop patient-specific models, which returned the likelihood of an upcoming seizure (high, moderate, or low). Of the 15 people implanted with the device, only 10 entered the second phase, during which the prediction algorithm's performance was prospectively assessed over four months. Seizure prediction was successful in four out of ten patients, demonstrating that seizure prediction based on long-term recordings can have a positive impact, at least for some patients.

2.5 Seizure prediction

Seizure prediction models are developed to recognise seizure precursors and raise an alarm whenever such patterns are detected in new data. This alarm informs the patient with epilepsy or the caregiver that a seizure will occur within a given time window, rather than informing about the exact time of seizure onset [11, 13, 82].

Seizure prediction relies on correctly identifying seizure precursors that reflect the transition from the interictal (seizure-free) brain state to the ictal (seizure) state. This transition corresponds to the preictal state (see Figure 2.11). Additionally, after the seizure's EEG offset, there might be a period during which the electrographic trace returns to interictal (baseline) activity, known as the postictal interval [83,142]. In focal onset seizures, this interval is often characterised by a rhythmic attenuation and slowing in the theta and delta frequency bands of the scalp EEG [14, 83, 142].

The ictal phase of an epileptic event has been reported to last from a few seconds to several minutes [143, 144]. In one study [52], seizure duration, assessed for a total of 751 625 seizures, ranged from one second to one day with a median duration of 30 seconds.

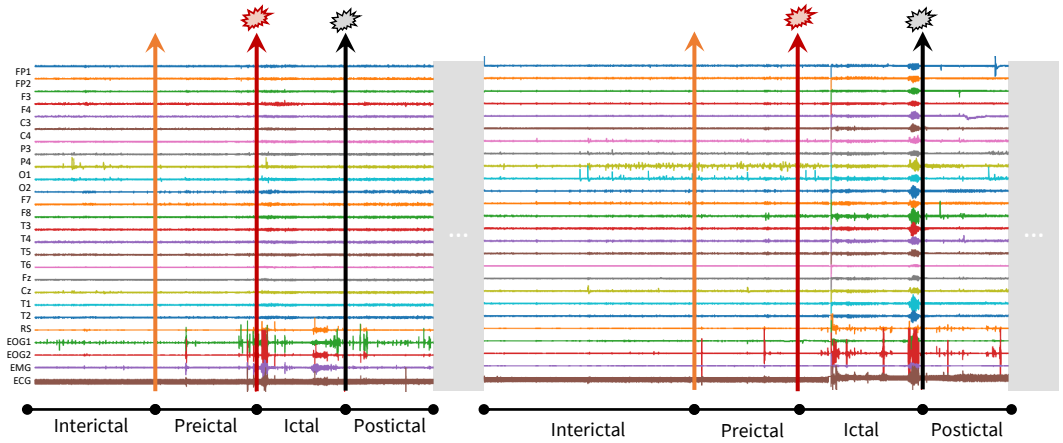

Figure 2.11: Example of the possible location of the brain states in scalp EEG recordings. The ictal interval is limited by the EEG or clinical onset at the beginning and the EEG or clinical offset at the end. Onset and offset times are annotated by clinicians or experienced technicians. Preictal and postictal intervals are typically defined by researchers in seizure prediction studies. Adapted from Cui *et al.* 2018 [145].

Both the preictal and postictal periods are not characterised by any recurrent pattern, being associated with high inter- and intra-patient variability. Although there is clinical evidence of these intervals' existence, no clinical or operational definition of these periods is known [10, 142, 146]. Additionally, there could be seizures which are not preceded or followed by any apparent alteration in the EEG records [10, 30, 61, 83].

The lack of a preictal interval definition significantly complicates the design of seizure prediction models. Ideally, if a preictal interval could be defined and used widely, it could be possible to predict the exact time of seizure occurrence. However, given the uncertainty associated with the preictal interval, this is currently unattainable [147].

2.5.1 Seizure onset

Seizure prediction methodologies are developed through the analysis of EEG data together with annotations of the onset and offset of seizures obtained by video-EEG inspection.

Seizures can be characterised by two types of onset and offset: (i) the clinical onset/offset identified by the neurophysiologists when looking at the behavioural symptoms and (ii) the EEG onset/offset also observed by the neurophysiologists and corresponding to the first/last ictal changes in the electrographic trace [13, 143]. The EEG onset may not coincide with the clinical onset, being often annotated seconds or minutes earlier [13, 34, 82]. Prediction algorithms are usually based on EEG onset/offset since (i) these models are based on the tracking of EEG signal alterations over time and (ii) clinical onset/offset is not always identifiable, particularly in FOIA and nonmotor seizures [13, 82].

Throughout this thesis, the EEG onset will be extensively refereed, being interchangeably used with simple seizure onset.

2.5.2 Lead seizure

A considerable number of seizures should be analysed to enable a reliable assessment of the seizure prediction performance. Conversely, the interval separating consecutive seizures should also be addressed so that seizures are considered independent events [82]. This is particularly important for seizure clusters (see Section 2.1.4), from which it is hard to distinguish preictal and/or postictal states [14,37,56,82,118].

Given the lack of consensus regarding the definition of seizure clusters, there are also varying interictal intervals used to define lead seizures among studies. One of the most adopted definitions of seizure cluster consists of the occurrence of three or more seizures in 24 hours (i.e., interictal intervals of 8 hours or less) in patients with DRE [54, 56]. Nevertheless, recent studies have defined lead seizures as consecutive seizures separated by 1 hour [148], 1.5 hours [149], 2 hours [128, 150], 3 hours [151], 4 hours [134, 152–155], 4.5 hours [156, 157], 5 hours [17] and 8 hours [50]. This variability inherently derives from the paucity of data to train and test prediction algorithms that would result, for instance, from the analysis of seizures separated by more than 8 hours.

2.5.3 Seizure prediction vs detection

Seizure detection was initially aimed at providing clinicians with information on the onset of seizures suffered by patients during presurgical monitoring (for diagnosis and treatment management). With seizure detection the reviewing process could then be sped up, avoiding the need for the time-consuming task of annotating hours to days of EEG data [22, 89, 146, 158]. Later, seizure detection became also known as the task of detecting the EEG seizure onset some seconds before the first clinical symptoms (early detection) [13, 82]. This time window evidenced the potential of seizure detection for a fast intervention such as closed-loop systems that provide on-demand feedback [89]. Contrarily, seizure prediction aims to identify a preictal interval located minutes to hours before the EEG onset that provides enough time for the patient to prepare for the seizure [11, 13, 82]. In other words, the main difference between detection and prediction consists in the fact that the latter provides a longer warning time that enables the patient or the caregiver to limit the debilitating consequences of the seizure [13, 34].

Seizure detection is, therefore, considered a useful tool for timely delivery of fast-acting medication or neurostimulation triggered through closed-loop (responsive) systems [13, 82, 93, 133, 146].

Seizure detection has been proven feasible when using intracranial EEG rather than scalp EEG due to the lower specificity of the latter resulting from the delay in

capturing seizure effects on a large area of the scalp [11, 34].

2.5.4 Seizure prediction vs forecasting

Even though the term forecasting has been primarily used interchangeably with prediction and anticipation [13, 82], it has been recently associated with the identification of periods of increased seizure risk (proictal states) that are not necessarily followed by the occurrence of a seizure [66]. In practice, there is a shift from developing models able to distinguish interictal and preictal samples of EEG data to developing probabilistic models fed with long-term information on cycles of epileptic EEG activity [159]. The latter is supported by patient-specific studies revealing that circadian and multidien rhythms often modulate seizures and interictal epileptiform activity [49, 66–68, 160].

Being based on identifying circadian and multidien cycles of EEG activity, seizure forecasting provides information regarding periods of increased seizure risk on a scale of days and hours [68, 161]. This is an essential difference with regard to seizure prediction, as the preictal interval is typically set to last for minutes to hours [159].

Since seizure forecasting has been recently addressed in several studies, this subject will be detailed in the state-of-the-art Section 3.4.

2.5.5 Seizure prediction characteristic

The first prediction algorithms returned a time-resolved output, typically determined by the evolution of a given feature with respect to a defined threshold. Such threshold-based algorithms, therefore, involve issuing an alarm whenever the feature crosses that threshold (see Figure 2.12) [82, 162].

In 2003, the need to evaluate and compare different prediction methodologies led Winterhalder *et al.* [147] to introduce the seizure prediction characteristic. According to this general framework, the performance of a given seizure prediction model should be evaluated in terms of seizure sensitivity (SS) and false prediction rate per hour (FPR/h), two metrics adapted to the context of developing alarming devices (and detailed in the next section). Additionally, two other concepts should be considered: seizure prediction horizon (SPH) and seizure occurrence period (SOP) (see Figure 2.12) [82, 147, 162–164]. SOP corresponds to the period where the seizure is expected to occur. If an alarm occurs during SOP, it is considered a true alarm. Otherwise, it is a false alarm (refer to Figure A.1 in Appendix A for some examples). The SPH corresponds to the period of intervention that allows the patient to react to an alarm. It starts when the alarm is fired and ends at the beginning of the SOP.

The SOP and SPH values can vary according to the impact on the patient as well as the envisioned application, respectively. For instance, an implanted neurostimulation device only requires an SPH of a few seconds to prevent the seizure. For the case of a warning device, the SPH should be long enough (e.g., 10 minutes) to allow

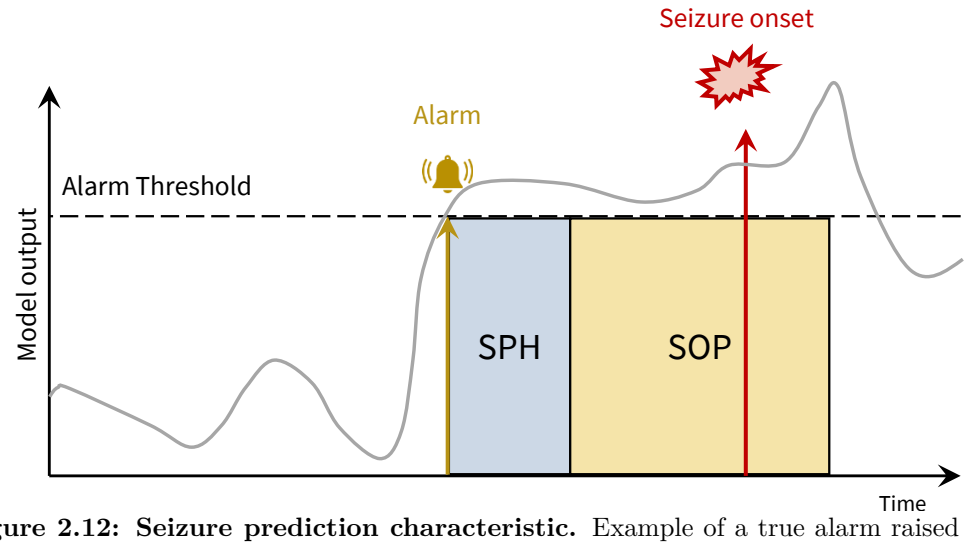

Figure 2.12: Seizure prediction characteristic. Example of a true alarm raised considering the SPH and SOP. Adapted from Winterhalder *et al.* 2003 [147].

for a behavioural adjustment that prevents the occurrence of accidents [147].

The SOPs found in the literature range from several minutes to a few hours [82]. With regards to the impact on patients, when a SOP of two hours is considered, it can induce stress states in the patient who is waiting for a seizure that, in case of a false alarm, may never happen [165]. Additionally, considering a long SOP may lead to the automatic exclusion of some seizures, e.g., if a seizure prediction model is developed using an SOP of six hours, seizures that are spaced less than that interval will never be predicted.

In sum, the performance of a given prediction model should be covered by the seizure prediction characteristic $SS(FPR/h, SPH, SOP)$ which reflects the dependence of the seizure sensitivity on the false prediction rate (detailed in the next section), the SPH and the SOP. Considering the concept of seizure prediction characteristic allows for a fair comparison of prediction models designed for different clinical applications [147].

Performance assessment

As previously mentioned, the performance of a seizure prediction model should be presented using two descriptive measures: SS and FPR/h [147]. These measures were adapted from the measures used to evaluate the performance of standard ML problems: sensitivity and specificity, which, in turn, are defined based on the confusion matrix (see Table 2.4).

If seizure prediction would be considered a classic ML problem, then the binary classification of interictal vs preictal would be evaluated using sample sensitivity (SE in equation 2.1) and sample specificity (SP in equation 2.2):

$$SE = \frac{TP}{TP + FN} \times 100 \tag{2.1}$$

Table 2.4: Confusion matrix for evaluating sample performance of supervised learning models.

		Predicted labels	
		Preictal	Interictal
True labels	Preictal	True Positive (TP)	False Negative (FN)
	Interictal	False Positive (FP)	True Negative (TN)

$$SP = \frac{TN}{TN + FP} \times 100 \tag{2.2}$$

Each sample corresponds to points in a raw time series or points in a feature time series, the latter obtained by windowing a raw time series and extracting some measure from each window. Performance is also often reported using the sample area under the receiver operating characteristic curve (AUC) metric to plot the SE versus one minus the SP.

These metrics were adjusted to the context of seizure prediction to better convey information about the number of correctly predicted seizures rather than just sample classification. Namely, SS is given by the number of true alarms divided by the total number of seizures under analysis (see equation 2.3).

$$SS = \frac{\#true\ alarms}{\#seizures} \times 100 \tag{2.3}$$

The specificity is replaced by the false alarm rate per hour, which consists of the number of false alarms divided by the time during which false alarms can be fired. In prospective testing, whenever an alarm is issued, an interval equal to the duration of SOP and SPH is considered when evaluating prediction models, during which the patient is waiting for the impending seizure. Throughout this interval ($\Delta_{SPH} + \Delta_{SOP}$), also known as the refractory period, the prediction algorithm stops analysing data, preventing the triggering of any other alarm. The patient realises that it was a false alarm only at the end of the refractory period [13]. The FPR/h is therefore computed by considering the duration of the interictal interval ($\Delta_{Interictal}$) minus the duration of SOP and SPH associated with every false alarm (see equation 2.4) [13, 82, 149].

$$FPR/h = \frac{\#false\ alarms}{\Delta_{Interictal} - \#false\ alarms \times (\Delta_{SPH} + \Delta_{SOP})} \tag{2.4}$$

Additionally, it should be noted the more informative nature of FPR/h when compared to sample specificity. In other words, reporting a 98% sample specificity may be seen as a good performance, however, it corresponds to a poor performance of a 2.4 FPR/h (considering the analysis of portions of signal with 30 seconds of duration) [146]. When considering the practical application, whenever an alarm is raised, an intervention occurs. As such, a measure of performance able to inform

about the number of false alarms that a prediction system might trigger in a given period of time, allows the clinician to decide on the number of false alarms that might be tolerated by each patient.

The overall algorithm performance may also be quantified and ranked using the AUC metric adapted to seizure prediction. It corresponds to plotting the SS versus the proportion of time in false warning [12, 68, 166].

The optimal performance of a seizure prediction model would be 100% SS, i.e., all seizures would have been predicted, and zero FPR/h, meaning that no false alarms would have been fired. In practice, such a scenario is very unlikely, with prediction performance being the result of a trade-off between SS and FPR/h (see Figure 2.13). Typically, an increase in SS is achieved at the cost of issuing a higher number of false alarms [82, 146, 147]. Tuning the model towards one of the two performance metrics may be dependent on the purpose of the seizure prediction. For instance, when considering warning systems, high values of FPR/h translate to the patient spending more time expecting an upcoming seizure and therefore increasing levels of anxiety or, conversely, losing confidence in the warning system and ending up being unprepared for seizures [146, 147, 162]. For the case of an intervention system, there might be more tolerance to a higher number of false alarms, depending on the system invasiveness and on the side effects of neurostimulation or on-demand medication [82, 147]. Additionally, in 2003, Winterhalder *et al.* [147] proposed maximum values of FPR/h depending on the monitoring conditions. Patients with focal DRE monitored during normal daily life, reported a mean seizure frequency of about three seizures per month, yielding a maximum FPR/h of 0.0042 h^{-1} [53]. During presurgical evaluation, the maximum average seizure frequency increases to 3.6 seizures per day (or 0.15 seizures per hour), as a result of medication tapering or other activation procedures [167].

Regarding seizure sensitivity, one study showed that the majority of patients considered that a seizure prediction device would be useful when at least 90% of seizures could be predicted [24]. Additionally, it is important to note that, as shown in Figure 2.14, seizure sensitivity increases with the SOP duration (for a fixed SPH and different fixed values of FPR/h) [162].

2.5.6 Statistical validation

Another requirement to propose a seizure prediction algorithm is for it to significantly overcome the performance of a chance predictor model [13]. Even though different strategies (analytical or bootstrap-based) have been proposed for developing chance prediction models [11, 162, 164], the two most widely adopted are the analytic random predictor [11, 12, 162, 168] and the seizure time surrogates [11–13, 162, 168].

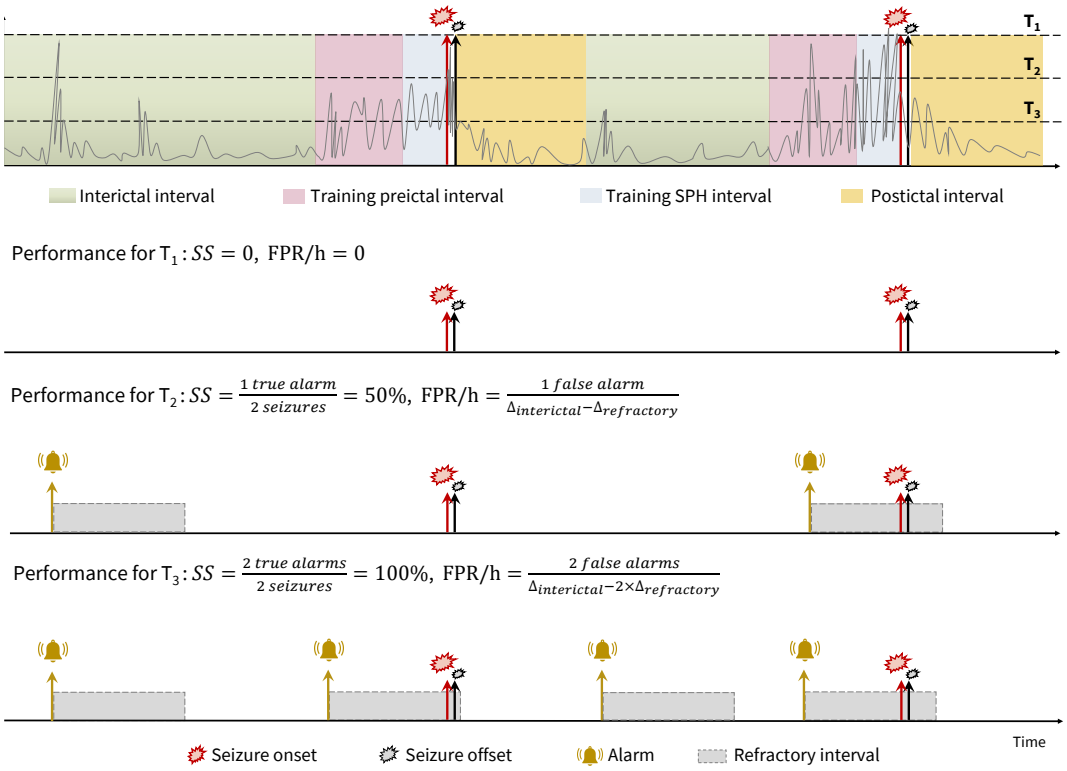

Figure 2.13: Example of the performance obtained for a given model output. Alarms are triggered whenever the feature crosses a certain threshold. The performance of a seizure prediction model is presented for three thresholds T_1, T_2 and T_3. With this example, it is possible to observe the trade-off between SS and FPR/h. By decreasing the threshold, it was possible to correctly predict two seizures (SS = 100%), however at the cost of increasing the number of false alarms and, consequently, the value of FPR/h. Adapted from Winterhalder *et al.* 2003 [147].

The analytic random predictor

The random predictor is an analytic technique first proposed by Winterhalder *et al.* [147] in 2003. This technique considers that alarms are raised randomly without analysing information contained in the EEG recordings.

The probability, p, of firing an alarm during a small interictal interval I is given by:

$$p = FPR/h \times I \tag{2.5}$$

For a longer interval, W, the probability P of raising at least one alarm is given by:

$$P = 1 - (1 - FPR/h \times I)^{W/I} \approx 1 - e^{-FPR/h \times W} \; for \; I \ll W \tag{2.6}$$

By setting $W = SOP$, it is possible to obtain the SS of a random prediction method as it represents the probability of issuing at least one alarm during the SOP.

Schelter *et al.* [163] later proposed an analytic random predictor based on a homogeneous Poisson process for false predictions. Accordingly, the probability of raising an alarm at each sample of a feature time series is given by:

$$P_{Poisson} = \frac{\#false\ alarms}{\#samples} \tag{2.7}$$

At this point, let us consider a time interval equal to SOP and that the product FPR/h×SOP is considerably smaller than one, which is reasonable to assume as the patient should not be submitted to continuous warning [162]. Under these assumptions, the probability P, from equation 2.6, of firing at least an alarm within SOP can be approximated to:

$$P \approx 1 - e^{-FPR/h \times SOP} \approx FPR/h \times SOP \tag{2.8}$$

The probability P of randomly predict k out of K independent seizures follows a binomial distribution given by:

$$P_{binom,d}(k, K, P) = 1 - \left[\sum_{j \geq k} \binom{K}{j} P^j (1-P)^{K-j} \right]^d \tag{2.9}$$

Importantly, the random predictor was first proposed considering the statistical validation of threshold-based prediction models. In that context, the goal was to compare the predictive power of the different electrodes and extracted features (d in equation 2.9). Increasing the number of channels or extracted features increases the probability of randomly detecting pre-seizure patterns in any of those time series and, therefore, the probability of successfully predicting a seizure [162]. Accordingly, equation 2.9 shows the probability of predicting k of K seizures using the information of at least one of d independent features (extracted for each channel). In the context of this thesis, only ML models were developed. As a consequence, the multidimensional input is followed by a single output vector ($d = 1$) [149]. The value of d can increase when several ML models are applied simultaneously.

For a given significance level α, it is possible to determine the critical value of seizure sensitivity (σ) for the random predictor [169]:

$$\sigma_{rand} = \frac{max\{k | P_{binom}(k, K, P) > \alpha\}}{K} \times 100\% \tag{2.10}$$

The seizure sensitivity value then consists in the ratio between (i) the maximum number of seizures, k, for which the probability given by the equation 2.9 is higher than the chosen α, and (ii) the total number of seizures, K. In other words, equation 2.10 provides information about the minimum number of seizures that need to be predicted to ensure that performance above chance level is achieved [149, 163]. The goal is to develop a seizure prediction algorithm with an SS higher than the upper critical SS value of a random predictor [170].

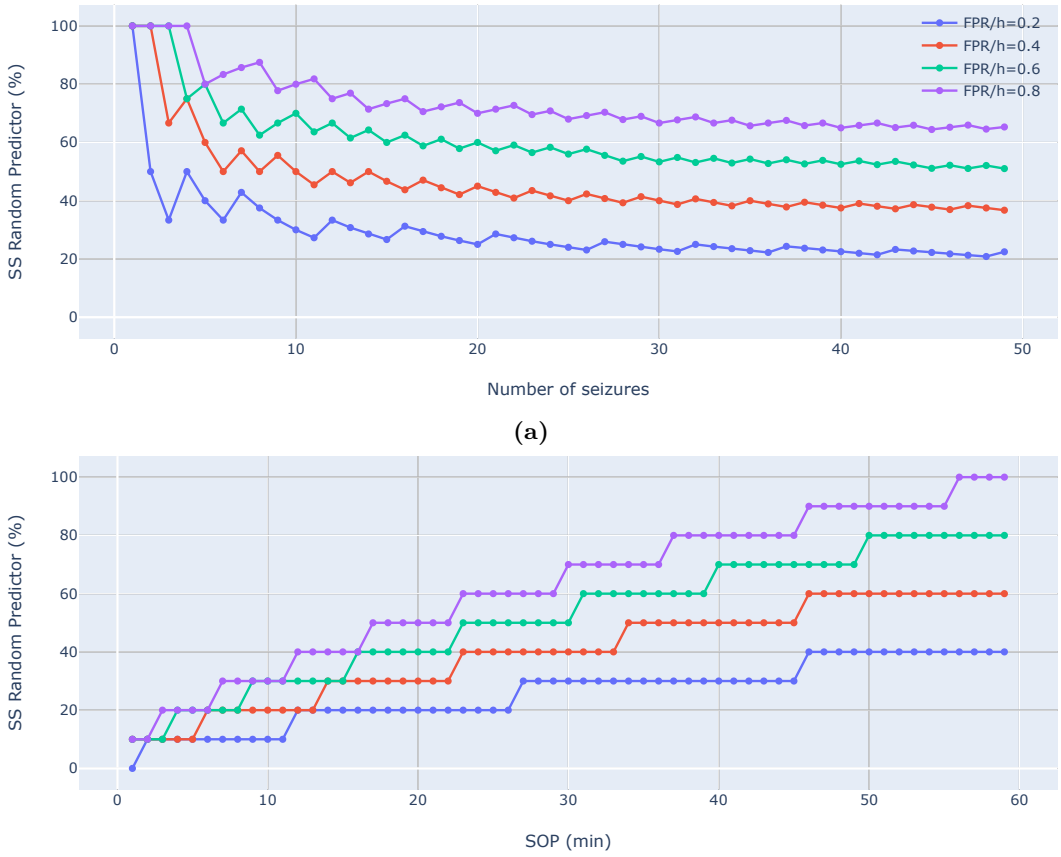

Figure 2.14: Seizure sensitivity analysis of a random predictor. The SS, computed for different values of FPR/h, is shown to depend on the (a) number of seizures (fixing SOP to 40 minutes) and on the (b) SOP interval (fixing the number of seizures to 10). A significance level of 5% was considered. Adapted from Schelter *et al.* 2006 [163] and Schelter *et al.* 2008 [162].

As can be concluded from the previous explanation, statistical validation using the random predictor makes no use of EEG (or other biosignals), which contributes to decreasing the computational cost of the method [12, 147, 162, 163]. Additionally, this method may not be suitable when a low number of seizures is being tested (see Figure 2.14), which is often the case in epilepsy and, particularly, in patient-specific approaches [163]. Also, the assumption that the intervals between seizures follow a Poisson distribution may not correctly address recent findings supporting the nonrandom occurrence of seizures [12, 168, 171].

Seizure time surrogates

The bootstrapping (or Monte Carlo based) techniques consist in generating constrained randomisations of the original data (either the seizure onset times [172], the alarms raised by the prediction models [173] or the raw data/feature time series [174]) to construct surrogate data [168]. Below a brief explanation is provided

for surrogate data based on seizure onset times, as it has been considered to be the method that is better adjusted to different prediction settings [162, 168].

In 2003, Andrzejak *et al.* [172] introduced the concept of seizure time surrogates. This method consists of randomly shuffling the original labels of inter-seizure intervals (random permutation without replacement) while maintaining the original feature profiles (see Figure 2.15). If the performance of the original seizure predictor is better, with statistical significance than the performance of the predictor surrogates, the null hypothesis (see Box 5) is rejected [13, 162, 173].

Seizure times surrogates are therefore based on the EEG (or other biosignals) pattern recognition to assess if a given seizure prediction model performs above chance level. Additionally, artificial seizure onset times are generated under the constraints of preserving the distribution of intervals between consecutive seizures, the total number of seizures and the clustering of the seizures. However, a low number of seizures and the presence of gaps in the EEG records can make it difficult to generate a sufficient number of independent surrogates needed to obtain significance [13, 162, 172, 173]. Despite being more time-consuming than the analytic random predictor, this method is still considered to provide more confidence than the random predictor in assessing the performance above chance level [12].

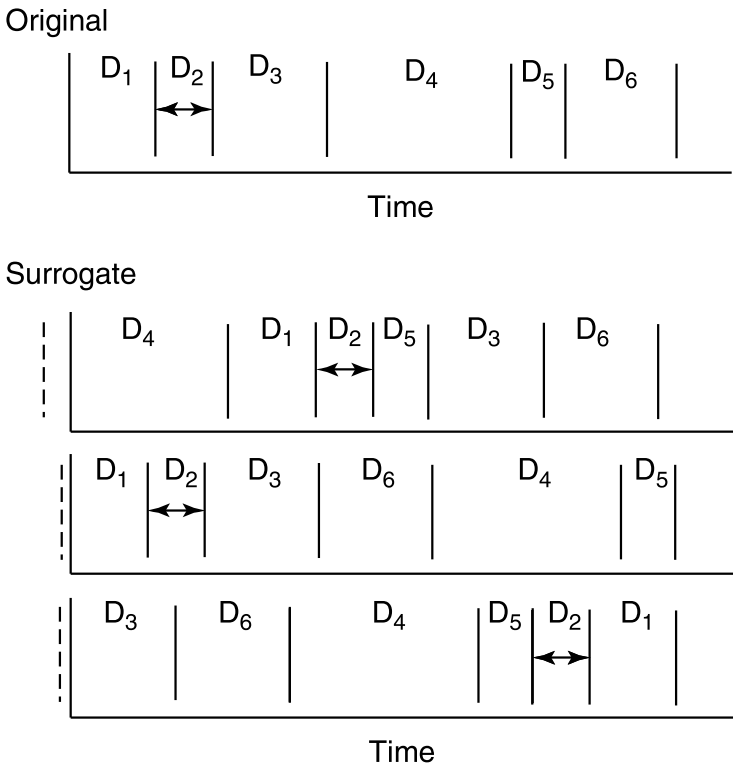

Figure 2.15: Example of seizure times surrogates. Considering a continuous EEG recording, D_1 corresponds to the interval between the recording starting time and the first seizure onset. D_2, .., D_S denote the intervals between consecutive seizures. Three seizure time surrogates were obtained by randomly shuffling the inter-seizure intervals. A random offset is also added to the first interval preventing the last seizure onset time from always coinciding with the original one. Source: Schelter *et al.* 2008 [162].

Box 5 - Null hypothesis for seizure times surrogates [172]

"The transition from the interictal to the ictal state is an abrupt phenomenon. An intermediate preictal state does not exist."

2.5.7 Postprocessing

The output of a binary classifier that was trained to distinguish interictal from preictal samples considers each sample individually, without taking into account the temporal relationship between each sample and the previous ones [11, 175]. Consequently, if the classifier's output were taken as the final prediction outcome, an alarm would be raised for every sample misclassified as preictal. Each sample reflects brain or extracerebral activity changes in a few seconds window. The resulting rate of fluctuations over the extracted feature samples may lead to the generation of several alarms over time, many of which correspond to noisy alarms. This noisy behaviour tends to aggravate when analysing long-term data [144, 175].

In order to constrain the number of alarms and, consequently, improve the model's specificity, postprocessing (or regularisation) methods are often applied [11, 176]. Two of the most used postprocessing techniques that take into account temporal signal dynamics are the Kalman filter [176] and the firing power [177].

Kalman filter

Chisci *et al.* [176] first applied the Kalman filter as a postprocessing method in a seizure prediction framework. The method consists of the estimation of the states s_k of a linear dynamical system, at the instant k, where z_k is the output variable of the model, w_k and v_k correspond to zero mean white noise vectors, and T_p represents the prediction interval (in equation 2.11). An alarm is raised whenever the Kalman filter output increases (samples are classified as preictal) and crosses a zero-threshold [176, 178, 179].

$$\begin{cases} s_{k+1} = \begin{bmatrix} 1 & T_p \\ 0 & 1 \end{bmatrix} s_k + w_k \\ z_k = \begin{bmatrix} 1 & 0 \end{bmatrix} s_k + v_k \end{cases} \tag{2.11}$$

Firing power

The firing power method was introduced by Teixeira *et al.* [177] and consists of applying a moving average filter to the output of the binary classifier chosen for prediction (see Figure 2.16). The firing power is then a measure of the number of samples classified as preictal in a given window. Considering that $o[k]$ is the output of the classifier (taking 0 for interictal and 1 for preictal) and τ is the filter window

which corresponds to the number of samples of the preictal interval, the output of the firing power $fp[n]$ at the discrete-time n is given by:

$$fp[n] = \frac{\sum_{k=n-\tau}^{n} o[k]}{\tau} \tag{2.12}$$

The value of $fp[n]$ ranges from zero to one, with zero and one meaning that all the samples in the preceding preictal interval were classified as interictal and preictal, respectively.

An alarm is issued only when the firing power is above a given threshold, which sets the maximum tolerance for the predictor error (see equation 2.13 where $O[n]$ is the prediction output). Increasing the threshold leads to a more conservative prediction performance. As previously explained, a new alarm can only be raised after the SOP (or preictal interval duration). After that, if the firing power remains above the threshold, a new alarm can be issued [153].

$$O[n] = \begin{cases} alarm & if\ fp[n] \geq threshold \\ no\ alarm & if\ fp[n] < threshold \end{cases} \tag{2.13}$$

A comparison between both regularisation methods [178] has evidenced a more pronounced reduction of false alarms with the firing power. This method is more conservative in issuing alarms compared to the Kalman filter. This behaviour stems from the ability to keep a longer memory of past samples (which depends on the duration of the preictal interval).

In addition, due to the lower complexity of the firing power, the implementation

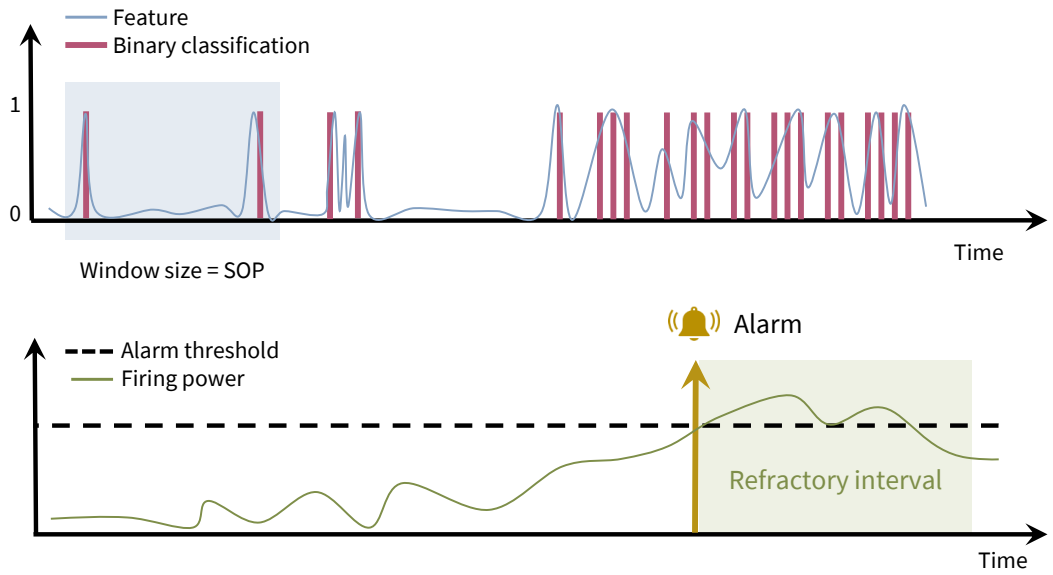

Figure 2.16: Illustrative example of how to compute the firing power. The binary output of the machine learning model is low-pass filtered using a window with a duration equal to the SOP. The alarm raised after threshold crossing is followed by the refractory interval during which the model is on hold and no alarm can be raised.

of this method is more straightforward when compared to the Kalman filter.

2.6 Concept drifts

Concept drift is a phenomenon characterised by data distribution changing over time or, in other words, by a nonstationary, dynamic behaviour of data. It may not be possible to observe these changes directly on the available data as such changes occur in a hidden context [180–182]. Disregarding such fluctuations in the underlying distribution of data may lead to poor model predictive performance [180, 183, 184].

Among the possible types of concept drifts (see Figure 2.17), some might occur in the context of epileptic seizure prediction. In fact, the availability of long-term data acquired over days, months or even years has led to the discovery of concept drifts that influence seizure frequency. The latter has been reported to fluctuate according to circadian rhythms (reflected in the variation of cardiovascular parameters and sleep-wake state over the 24-hour day) and activation procedures used in presurgical monitoring (such as medication tapering) [16]. For instance, seizure frequency considerably increases during presurgical monitoring compared to normal daily life [147]. The identification and tackling of concept drifts have been the subject of current investigation in the seizure prediction field and will be further explored in state-of-the-art Section 3.5.

2.6.1 Rhythms in epilepsy

Circadian, ultradian or multidien rhythms can influence seizure susceptibility (see Box 6) [16, 185].

A circadian rhythm is defined as an oscillation of any behavioural or physiologic activity roughly within a 24-hour interval [186]. Such oscillations of endogenous nature are associated with variations in physiological parameters. The sleep-wake cycle, hormonal production and oscillations in body temperature, heart rate and blood pressure are examples of circadian rhythms [170, 187, 188].

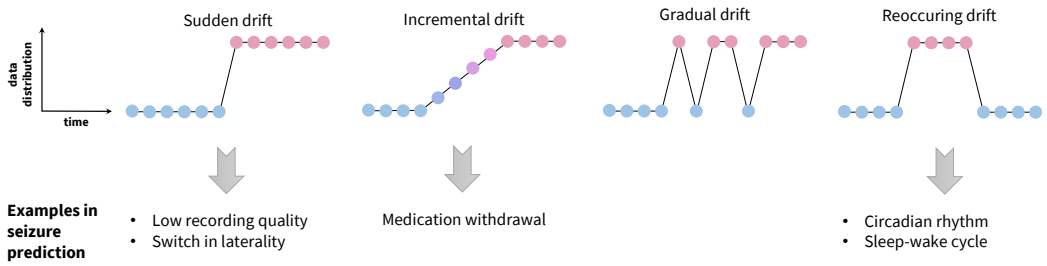

Figure 2.17: Types of concept drift. Association of concept drifts to its possible occurrence in data acquired for seizure prediction. Adapted from Gama *et al.* 2014 [181] and Lu *et al.* 2018 [180].

Ultradian cycles include the non-REM-REM cycle that lasts approximately 90 minutes in humans [185, 188, 189]. Multidien (or infradian) cycles, spanning, for example, weeks, are named circaseptan cycles and have also been recently studied in seizure prediction [160, 190].

In the context of epilepsy, it is also possible to identify a circadian pattern of seizure occurrence in some patients. Accordingly, circadian rhythms' influence on seizure frequency has been evidenced by the higher risk of seizure at specific day times such as the evening while going to sleep or the morning while waking up [16, 188, 190].

2.6.2 Sleep-wake cycle

Sleep is currently regarded as a brain state characterised by distinct behavioural and physiologic traits of the patient while asleep compared to a waking brain's electrical activity. Behavioural manifestations include lack of mobility or little mobility, closed eyes, sleeping posture, reduced response to external stimulation, impaired cognitive function, and a reversible unconscious state [191]. The EEG is typically inspected in search of physiologic sleep features. Specifically, the existence of activity in specific frequency bands in the EEG, together with behavioural criteria, helps define two sleep stages: Non-Rapid Eye Movement (NREM) sleep, accounting for 75-80% of the total sleep time, and Rapid Eye Movement (REM) sleep. REM cyclically follows NREM stage, with each cycle lasting from 90 to 110 minutes. Adults experience four to six cycles during normal sleep (see Figure 2.18) [191, 192].

One-third of a healthy subject's life is spent sleeping. The remaining two-thirds are spent in the waking state, also known as wakefulness, which is predominated by the alpha rhythm and a small amount of beta rhythm [191, 192].

The NREM stage can be further divided into three substages: N1, N2, and N3,

Box 6 - Definition of circadian, multidien and ultradian rhythms (as defined by Khan *et al.*, 2018 [185] and Karoly *et al.*, 2021 [65])

Ultradian rhythm: *"Refers to rhythms with periods of less than 24 h; ultradian rhythm cycles can occur with a frequency of more than once per day." [185]*

Circadian rhythm: *"A biological rhythm is considered to be a circadian rhythm if it meets three criteria: the rhythm should have an endogenous free-running (approximately) 24 h period, should be entrainable (i.e., be capable of phase reset by environmental cues and synchronisation to the 24 h day), and should exhibit temperature compensation." [185]*

Multidien rhythm: *"A recently coined term noting or pertaining to biological cycles that are likely to be generated endogenously with a period of >2 days to several weeks." [65]*

Circannual rhythm: *"Noting or pertaining to biological cycles of around 1 year that are likely to be generated endogenously." [65]*

according to the American Academy of Sleep Medicine guidelines (proposed in 2007 and updated in 2020) [194]. During the N1 stage, the EEG captures mainly theta and some delta frequencies and vertex waves. Theta and some delta frequencies, K-complexes and sleep spindles can be found during the N2 stage. N3 is characterised by the presence of slow-wave activity, with the main contribution from the delta rhythm [191, 192].

Finally, during the REM stage, the EEG captures low-amplitude mixed frequency signals, such as beta and theta rhythms. Additionally, alpha rhythms lasting for a few seconds may also be observed [191, 192].

Sleep and epilepsy are known to share a centuries-old bidirectional relationship. On one hand, patients with epilepsy may develop some sleep disorders such as obstructive sleep apnea [195–197]. On the other hand, sleep disruption is considered a significant risk factor to elicit seizures as well as influence the development, frequency and distribution of interictal activity [195–197]. For instance, interictal epileptiform discharges have been found to predominantly manifest during stage three NREM sleep stage in patients with focal epilepsy [195, 197].

2.7 Summary

Given the extension of the previous sections regarding epilepsy-related concepts, the following paragraphs summarise the most important concepts to be taken into account when reading the remaining of this thesis.

Epilepsy

Epilepsy is a neurological condition characterised by the seemingly random occurrence of seizures. It is a rather heterogeneous condition, as is evident by the different types of seizures, types of epilepsy and epilepsy syndromes. Seizures can

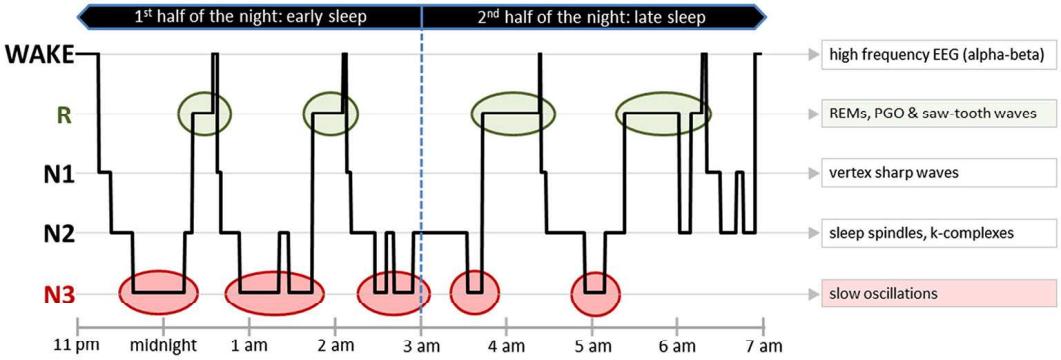

Figure 2.18: Sleep cycle in a healthy human. Example of a hypnogram showing the sleep stages in a healthy human over 8 hours of sleep time. The N3 stage predominates in early sleep, while the REM stage contribution increases by the end of sleep time. PGO: Ponto-Geniculo-Occipital Waves. Source: Blume *et al.* 2015 [193].

be categorised according to the corresponding subject's signs and symptoms, state of awareness and epileptic focus localisation (lobe and hemisphere). Focal seizures mostly arise from the temporal lobe, which is also the location associated with the highest autonomic seizure-related symptoms. Seizure prediction algorithms represent a solution to improve the quality of life of patients with epilepsy resistant to antiseizure medication. Predicting seizures minutes before the onset might provide time for the patient to take action (either by taking rescue medication or simply by avoiding dangerous or embarrassing situations).

EEG and ECG

The EEG has long been the primary source of electrical brain activity, being widely screened during presurgical monitoring. The EEG can be acquired on the scalp or intracranially. The latter is an invasive method associated with considerable risk (up to 19%) of developing complications such as infection and haemorrhage.

The voltage potentials captured in EEG can be categorised into two main groups: oscillations and transients. Oscillations refer to rhythmic patterns (showing in different frequency bands), while transients correspond to sharp transitions, which may be normal (e.g. eye blinks) or abnormal (e.g., seizures).

The effect of seizures on autonomic function can be assessed using the ECG signal. Namely, HR and HRV can be extracted from ECG recordings to develop detection or prediction models to integrate into neuromodulation or warning devices, respectively.

Seizure prediction

Supervised seizure prediction algorithms require the accurate labelling of the preseizure intervals, during which alterations in the brain or cardiac parameters become evident in the physiological signals. The ability to correctly discriminate interictal from preictal intervals would allow for predicting an upcoming seizure within a given occurrence period. The patient is provided with a defined seizure prediction horizon so that actions can be taken to prevent seizure-related accidents.

The performance of seizure prediction algorithms should be presented using seizure sensitivity (ratio of correctly predicted seizures) and the false positive rate per hour. Additionally, statistical validation should be performed in order to evaluate if the algorithm performs above chance level with statistical significance. The surrogate seizure predictor will be used in this thesis instead of the random seizure predictor. The former is a pattern recognition approach that takes into account the EEG information, whereas the latter is a probabilistic approach that works under more restricted assumptions.

Finally, the presence of concept drifts, including circadian rhythms and the sleep-wake cycle, should be considered when evaluating the performance of seizure pre-

diction approaches.

Chapter 3

State of the Art

This chapter presents the state of the art regarding several topics that were addressed throughout this thesis. Particular attention was given to the different stages of a typical seizure prediction pipeline based on the analysis of electroencephalography (EEG) data. Section 3.1 presents current knowledge on the brain dynamics during seizure generation. Section 3.2 addresses the impact of ictogenesis on the autonomous nervous system and the available evidence for a preictal behaviour in cardiac parameters. Section 3.3 addresses the seizure prediction framework, including literature on preprocessing, feature extraction and classification steps. In this section, emphasis was placed on the existence and characterisation of the preictal interval in EEG data (Section 3.3.4). Recent findings regarding seizure forecasting and concept drifts are briefly presented in Sections 3.5 and 3.4, respectively. Finally, a brief summary of the literature overview performed in this chapter is presented in Section 3.6.

3.1 Brain seizure dynamics

Nonlinear dynamical systems and the bifurcation theory have been used to explain the transitions between different stages of the seizure [198]. In fact, increasing exploration of electrographic alterations in epilepsy has prompted the development of computational models of brain activity that may help understand the complexity of seizures [12]. With that knowledge, it might be possible to understand seizure-controlling mechanisms, including closed-loop neurostimulation [12, 198]. These mechanisms are being studied via smaller (metabolic changes) and larger (electrophysiological recordings) scale networks [199].

3.1.1 Concepts in dynamical systems

Some concepts should be introduced before diving into the underpinnings of seizure dynamics in epilepsy. The theory of dynamical systems describes the qualitative behaviour of a given system over time. Accordingly, the state of a system at any

given time corresponds to a single point (or phase point) position in multidimensional space (or phase space). The system's evolution is reflected in the movement of the phase point, which is represented by a trajectory in the phase space [199].

The evolution of the system over time can occur either by changing the system's state (i.e., changing the phase point position) or the system's internal dynamics (i.e., the landscape over which the phase point rolls). When the internal dynamics change, a bifurcation occurs, meaning that there is a qualitative change in the system's behaviour. A qualitative behaviour is perceived by assessing properties such as conditions to maintain a system (i) in equilibrium, (ii) displaying periodic oscillations or (iii) showing chaotic behaviour. A critical transition is observed when fundamental changes occur due to the system passing a bifurcation. In other words, a critical transition occurs when the system crosses a threshold (or tipping point) and suddenly transitions from a stable state to an alternative state. Critical transitions have generic properties recognised in systems such as climate transition, species extinction, and financial markets [199–201].

Additionally, there is also the property of multi-stability in system dynamics: multiple attractors simultaneously reside in the phase space. The system evolves to either of these attractors depending on the initial conditions [202].

Box 7 - Definitions in dynamical system theory [203]

State variable: *"In a dynamical model, state variables are the values that change with time."*

Trajectory: *"In a dynamical model, the trajectory is the path that is followed by the n-state variables through the n-dimensional state space. This is a higher-dimensional generalisation of the notion of trajectory as a term that is commonly used to describe motion. However, trajectories in models of motion include velocities as well as locations."*

Attractor: *"The set of stable trajectories of a dynamical system in state space. If a trajectory is perturbed away from an attractor, it will tend to move back to it."*

3.1.2 The epileptic brain as a dynamical system

Computational models have been developed in the context of focal and generalised epilepsies to reproduce and explain epileptiform activity occurring in interictal and ictal intervals [198, 203, 204]. Developing such models can help discover associations between a set of empirical observations (e.g., the electroencephalographic trace) and possible seizure mechanisms [205]. Accordingly, epileptic seizures being represented by transitions between different states might translate to changes in amplitude and frequency of EEG oscillations and/or changes in signal correlation among brain regions [205]. The same rationale might be applied to the occurrence of interictal epileptiform activity (IEA): these transients might represent "ghosts" of surrounding bifurcations and might increase when transitions between states are approaching

[205, 206].

Early studies on the basic mechanisms underlying neural network evolution toward a seizure [210, 211], propose three possible paths that can lead to abnormal ictal dynamics: (i) an abrupt change caused by a fast trajectory convergence to the ictal state, assuming a system having interictal and ictal attractors simultaneously (scenario 1 in Figure 3.1), (ii) a continuous sequence of states reflecting a gradual transition from an interictal to an ictal attractor (scenario 2 in Figure 3.1), or (iii) a combination of both [16, 159, 209]. External or endogenous factors can influence the three types of transition to the ictal state. Generally, the nonlinear dynamic evolution towards a seizure has been described using deterministic models. Accord-

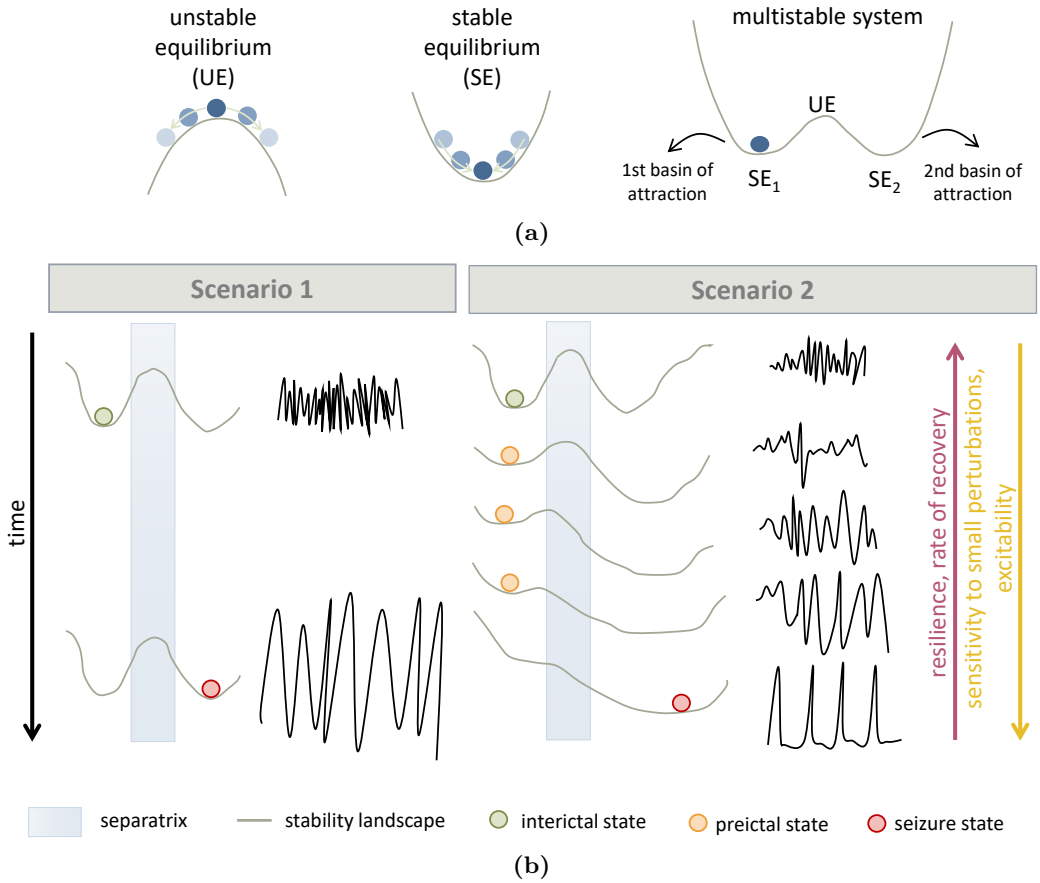

Figure 3.1: Possible routes to epileptic seizures. (a) The ball analogy: the EEG trace can be represented as the movement of the ball (state point) in a through or a hill (landscape). A small perturbation leads the ball to roll-off from the top of the hill (unstable equilibrium). In contrast, the same perturbation in the through leads to the ball returning to its original position (stable equilibrium). (b) Scenario 1 describes the system in a bistability dynamic. Transition to seizure occurs due to random perturbations kicking the system over the seizure threshold. In scenario 2, the ictogenesis process unfolds as the landscape changes. Initially, the troughs are deep, requiring a large perturbation to reach the tipping point and shift from one state to another (high resilience). As the through flattens, there is less resilience to the transition, and the EEG shows an increase in amplitude and a decrease in frequency. Adapted from: Skourtis-Cabrera 2021 [207], van Putten & Hofmeijer 2015 [208], Baud *et al.* 2020 [159], Jiruska *et al.* 2013 [209] and Zubler *et al.* 2014 [199].

ingly, such evolution is represented as the crossing of a threshold, or separatrix, between interictal and ictal states [159, 206, 210, 211]. Once the threshold is crossed, the system goes through a bifurcation, meaning that a seizure will occur.

In scenario 1, the transition might result from an abrupt random perturbation that makes prediction difficult to conduct if not impossible (precluding the existence of a preictal interval) [16, 203, 210]. This scenario has been represented by models of generalised (or absence[1]) seizures manifesting in absence epilepsy [203, 210]. In this scenario, it is interesting to compare the system's bistability occurring for nonepileptic and epileptic brains. In the case of a nonepileptic brain (see Figure 3.2a), the attractor of the normal brain activity (central trajectories) is clearly separated from the attractor of seizure activity (outer trajectories). This means that, upon a stress condition, anyone can have a seizure (as a consequence of, e.g. fever, ischaemia, hypoglycaemia or insomnia). However, the system is stable, being resilient against random perturbations [203, 206]. In an epileptic brain (see Figure 3.2b), the attractors are deformed due to a parameter change leading to lower separation between each attractor and the separatrix. As a result, there is a higher susceptibility to minor perturbations reflected in a higher frequency of random transitions to the ictal state [203, 210]

In scenario 2, as the landscape changes, the system becomes gradually more unstable to the point that minor perturbations will lead to a state transition [159, 209]. This type of seizure transition has been identified using models applied to mesial

[1] "Absence seizures are brief episodes of loss of consciousness without convulsions." [203]

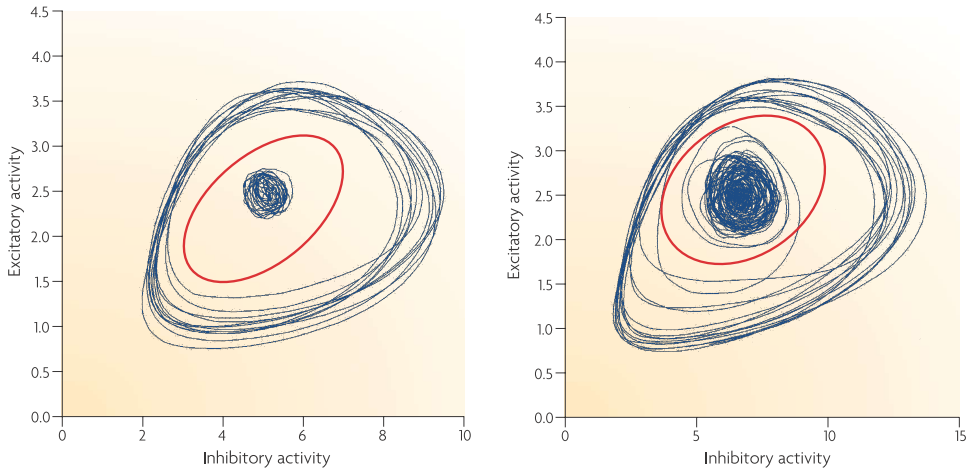

(a) **(b)**

Figure 3.2: State space representation of a deterministic neural mass model of absence epilepsy. Sample trajectories (blue lines) are represented for (a) normal and (b) epileptic models. Cortical excitatory activity and cortical inhibitory activity are the state variables. The normal activity attractor (inner trajectory) is separated by the seizure attractor (outer trajectory associated with higher-amplitude activity) by the separatrix (red line). The higher separation observed for the normal model indicates the lower probability of a random perturbation resulting in a transition between states. Source: Lytton *et al.* 2008 [203].

temporal lobe epilepsy [203]. The gradual transition may allow for identifying a pre-ictal state: the system getting close and away from the separatrix without reaching the bifurcation [206]. The change in the landscape translates to a decrease in the system's resilience to small perturbations, which in turn increases the probability of transition. Importantly, when considering multi-stability, stochastic perturbations may not directly lead to a state switch but induce a change in the landscape. Increased sensitivity to perturbations is considered one of the early warning indicators that a critical transition is gradually approaching [209]. The evolution of a system towards instability can also be characterised by another feature: slowing down of recovery from a perturbation. Also known as critical slowing down, this feature reflects the tendency of a system to require more time to return to equilibrium [132, 201, 209]. Seizures may be preceded by signatures of critical slowing down, including an increase in autocorrelation and variance of EEG signals [201]. To be noticed that there are also studies showing no evidence of such early warning signals [212, 213]. This lack of consensus may be related to the analysed temporal scale in [201] (hours and days) compared to [212, 213] (seconds to minutes).

3.2 Brain-heart dynamics in epilepsy

As the epileptic seizures arise from or propagate to the autonomous nervous system (ANS) structures involved in autonomic control, it is very likely that such abnormal events can lead to functional disturbances in the normal autonomic function [19,20,30,42,93]. Autonomic typical symptoms occurring during seizures include cardiorespiratory, gastrointestinal and respiratory abnormal manifestations, palpitations, polyuria, piloerection, and sweating [19, 30, 42]. Such patterns of autonomic ictal dysfunction have been long reported, with heart rate (HR) changes being one of the earliest and, to date, most reported manifestations found in the literature (refer to Section B.1 in Appendix B for more details) [30, 42]. Specifically, when the sympathetic nervous activity is triggered during seizures, it typically results in increased HR and blood pressure and the possible occurrence of tachycardia and tachypnea [19, 20, 42]. On the other hand, when the parasympathetic system response predominates, the normal cardiorespiratory function is altered regarding the decrease of heart and respiration rates and blood pressure [19, 20]. Additionally, alterations in heart rate variability (HRV) measures have also been explored during seizures [95, 96].

Autonomic modulation occurs not only during the seizure discharge but also during the interictal period. Reduced parasympathetic and increased sympathetic responses are reflected in the reduced interictal HRV [19, 95, 96]. Patients with temporal lobe epilepsy (TLE) and patients with drug-resistant epilepsy (DRE) verify a more severe decrease in HRV, which contribute to an increased risk of cardiac arrhythmias [19, 20, 214, 215].

Preictal manifestations have been observed in HR and HRV data suggesting the potential of cardiac information in seizure prediction [21,95,96]. The advent of wearable devices may also explain the growing interest of the research community in HR and HRV alterations during epileptic brain states. Long-term continuous monitoring using less invasive and user-friendly modalities such as electrocardiography (ECG) is more likely to be accepted by patients with epilepsy [21,216]. Accordingly, there are two studies that used wearable smartwatches to track HR and inspected the potential of HR cycles to improve seizure forecasting [148,217]. Karoly *et al.* [217] reported the existence of circadian, about-weekly and about-monthly cycles in HR [217]. Authors verified that, in some patients with epilepsy, seizure occurrence was in phase with their HR cycles. Stirling *et al.* [148] showed that using cyclic features (HR cycles and previous seizure timing) improved seizure forecasting performance.

3.2.1 Changes in heart rate and heart rate variability

In the more than 30 years of research on HR and HRV changes before and during epileptic events, the vast majority of studies have compared HR and HRV parameters among healthy controls and patients with epilepsy or interictal vs ictal intervals. An early 1999 study reporting HRV time-frequency analysis revealed the first evidence of autonomic modulation occurring several minutes before the clinical seizure onset of patients with temporal lobe focal onset impaired awareness (FOIA) seizures [218]. In 2005, Kerem & Geva's comprehensive study [219] reported the occurrence of preictal changes in the RR intervals from 11 min to 1.5 min before seizure onset. Results showed considerable inter-patient and intra-patient variability. Since then, other studies have investigated changes in cardiac measures before, during, and after the seizure onset envisioning different applications. In fact, given the large amount of research showing HR increase at seizure onset, seizure detection models based on HR have been widely developed, for example, in vagus nerve stimulation [89,131,133,140,220,221].

The identification of changes in HR occurring minutes before seizure onset also motivated the development of seizure prediction models based on this information. Table 3.1 presents details regarding preictal interval and performance of studies on seizure prediction algorithms based on HRV analysis. Information regarding the analysed datasets and methodology are presented in appendix Tables B.1 and B.2. It is evident that the number of HRV-based prediction studies is still limited. Even though high seizure sensitivity values have been reported, the false prediction rate remains too high to envision a prospective seizure prediction application. No postprocessing method has been applied to the classifier's output in any of the studies. Consequently, these false prediction rates may reflect the existence of noisy samples rather than a considerable number of falsely predicted samples suggesting an effective alteration in the features.

Table 3.1: HRV seizure prediction studies.

Study	Preictal (min)	Performance
Fujiwara *et al.* 2016 [223]	15	SS = 0.91, FPR/h = 0.70 h^{-1}
Pavei *et al.* 2017 [225]	10	SS = 0.94, FPR/h = 0.49 h^{-1}
Billeci *et al.* 2018 [224]	15	SE = 0.89, FPR/h = 0.41 h^{-1}
Yamakawa *et al.* 2020 [222]	15	SS = 0.86, FPR/h = 0.62 h^{-1}, SS above chance level

n.s.: not specified. SE: sample sensitivity. SP: sample specificity. SS: seizure sensitivity. FPR/h: number of false positives divided by the number of interictal hours.

Furthermore, state-of-the-art studies often lack proper validation. Some studies do not report the standard seizure sensitivity and false alarm rate per hour. No study considered seizure occurrence period (SOP) and seizure prediction horizon (SPH) when evaluating prediction algorithms. Only one study [222] performed a statistical validation to assess if the results were above chance. Lastly, only two studies [223, 224] reported patient-specific prediction performance. Current literature limitations demand additional extensive studies on HR and HRV modulation across interictal to preictal states, including prospective studies [43].

3.2.1.1 Confounding factors

Many studies have reported high variability of results regarding the individual contribution of one or both sympathetic and parasympathetic autonomic subsystems during epileptic seizures and the consequent changes in cardiorespiratory parameters. Such variability can be mainly explained by the difficult task of isolating the cardiac effects of seizures from the effect of, e.g., anti-epileptic drugs (AEDs), emotional states, or increased motor activity. Furthermore, the differences across studies can also be explained by several other variables, including the type of seizure, type of epilepsy, location and size of the seizure onset zone, timing of seizures, patients' age and gender, and time to diagnosis [21, 23, 42, 93, 95, 146, 215, 226, 227]. For instance, disturbances in the ANS manifested predominantly in studies involving TLE patients, which is in agreement with the localisation of most of the structures responsible for cardiovascular autonomic regulation [42, 91, 93].

As another example, it is known that there is a prominent increase in HR in seizures happening during sleep in comparison to the ones occurring in an awake state [42]. Consequently, the predictive potential of autonomic function monitoring may be more evidenced during sleep time, as there are fewer confounders that lower the specificity of the measures capturing changes in autonomic functioning [30].

Based on the above, multimodal signal acquisition has been suggested as a solution to isolate and more accurately interpret the seizure effects in HR. For instance, EEG and ECG seizure monitoring should ideally also encompass the simultaneous acquisition of accelerometer and electrodermal activity signals [89, 146, 228, 229].

Lastly, autonomic alterations must also be interpreted considering the circadian pattern associated with the cardiac parameters that reflect those changes and, even more importantly, the effect of administration of AEDs in patients with DRE [93, 133].

3.3 Seizure prediction using supervised learning models

Seizure prediction algorithms are developed by following a more or less consensual framework (see Figure 3.3). Namely, researchers should consider four main steps when developing machine learning (ML) prediction algorithms: signal preprocessing, feature engineering, classification and postprocessing [11, 230]. The preprocessing and feature engineering steps may be absent when choosing a deep learning (DL) framework. These steps are detailed in the following sections, being preceded by a Section referring to the current databases used to perform seizure prediction or detection.

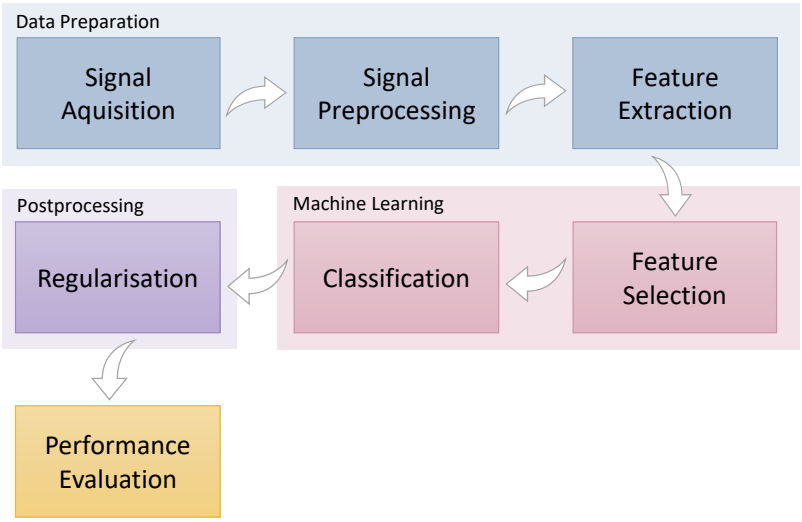

Figure 3.3: Seizure prediction framework. Adapted from Bou Assi *et al.* 2017 [11] and Kuhlmann *et al.* 2018 [12].

3.3.1 Epilepsy databases

Seizure prediction studies have long been conducted on databases containing predominantly EEG data. Over the last years, these databases have been improved in

terms of the recordings duration and number of patients. The current requirement of using continuous long-term annotated datasets to develop seizure prediction models is in line with the need for prospective validation of models [12, 230]. Additionally, several attempts have been made at using non-neurological information to predict seizures, hence the inclusion of other signals rather than EEG in recent databases. In fact, accelerometry, electrodermal activity or ECG are examples of noninvasive and user-friendly methods used for long-term monitoring.

Table 3.2 contains information on the databases used in studies conducted over the past 10 years in seizure prediction. These major impact studies concern patient-specific methodologies. EPILEPSIAE database, explored in this thesis and described in more detail in Chapter 4, is the most complete database regarding data collected during presurgical monitoring. Similarly, Freiburg and Children's Hospital Boston from the Massachusetts Institute of Technology (CHB-MIT) databases also contain recordings collected during presurgical evaluation. The Freiburg database was merged into the EPILEPSIAE database [231]. The CHB-MIT scalp EEG database is publicly available and includes data from 23 pediatric subjects with DRE.

Databases comprising data collected while the patients are outside the hospital, experiencing normal day-to-day activities, are currently the subject of extensive studies. Collecting ambulatory data over long periods (spanning months to years) more truthfully reflects a real prediction scenario. This way, it might be possible to take into account factors such as the sleep-wake cycle or circadian cycles (see Section 3.5) that naturally influence data distribution and, therefore, the prediction performance [12].

The NeuroVista Seizure Advisory System (NCT01043406) provided a comprehensive collection of ultra long-term continuous intracranial EEG recordings in an ambulatory setting [50]. Data was collected over a maximum of two years per patient, totalling about 16 years of continuous recordings across the 15 patients. Once the NeuroVista trial was concluded, no investment was made to commercialise the device leading to the end of data collection in humans [166]. A "Melbourne-University AES-MathWorks-NIH Seizure Prediction Challenge" was later held at Kaggle.com using data from the NeuroVista trial, specifically, data from the three patients verifying the lowest seizure prediction performance [232].

The NeuroPace RNS® system (NCT00572195) is another device used for long-term continuous monitoring (but not continuous storing) of intracranial EEG during patients' daily lives [116]. Clips of data are stored when specific events occur. The clinician may choose which events may trigger data storage: detection, responsive stimulation, time of day, and magnet swipe, among others. The maximum storage capacity corresponds to 90-second four-channel intracranial EEG segments. If this limit exceeds, the oldest data is replaced by the new data [116]. While intracranial EEG data may be used to provide an indication of seizure activity identified by a certified epileptologist, extracerebral data has also been collected using wrist-worn

Table 3.2: Databases used for patient-specific seizure prediction over the past 10 years.

Study	Database	#Pt	TUA	#Sz	Biosignal	Electrodes
Valderrama *et al.* 2012 [233]	EPILEPSIAE	12	132 days*	108*	sEEG, iEEG, ECG	sEEG: 4-27, iEEG: 0-58; ECG: 1-4
Cook *et al.* 2013 [50]	NeuroVista	15	≈ 16 years	1392	iEEG	16
Rasekhi *et al.* 2013 [234]	EPILEPSIAE	10	31 days*	46*	sEEG, iEEG	3 in focal region and 3 far from local region
Teixeira *et al.* 2014 [175]	EPILEPSIAE	278	2031 days	2702	sEEG, iEEG	F7, FZ, F8, T5, PZ, T6; 6 random; 6 in focal region
Alvarado-Rojas *et al.* 2014 [149]	EPILEPSIAE	53	531 days	558	iEEG	n. s.
Rasekhi *et al.* 2015 [144]	EPILEPSIAE	10	58 days	86	sEEG, iEEG	3 in focal region and 3 far from local region
Bandarabadi *et al.* 2015 [235]	EPILEPSIAE	24	150 days*	183*	sEEG, iEEG	3 in focal region and 3 far from local region
Direito *et al.* 2017 [236]	EPILEPSIAE	216	697 days*	1206*	sEEG, iEEG	F7, FZ, F8, T5, PZ, T6; 6 random; 6 in focal region
Karoly *et al.* 2017 [17]	NeuroVista	9	10.35 years	1458	iEEG	16
Kuhlmann *et al.* 2018 [232]	NeuroVista	3	442 days	211	iEEG	16
Tsiouris *et al.* 2018 [237]	CHB-MIT	12	40 days	185	sEEG	n. s.
Truong *et al.* 2018 [238]	Freiburg, CHB-MIT, Kaggle (AES)	13 13 2	13 days 8.7 days 26 days	59 64 48	sEEG, iEEG	6 22 12

#Pt: number of patients. #Sz: number of seizures. TUA: time under analysis. iEEG: intracranial EEG. sEEG: scalp EEG. AES: American Epilepsy Society. CHB-MIT: Children's Hospital Boston from the Massachusetts Institute of Technology. ZUH: Zealand University Hospital. KCl: King's College London. BVP: blood volume pulse. ACC: accelerometry. EDA: electrodermal activity. TEMP: temperature. HR: heart rate. The asterisk indicates that information corresponds to the testing dataset in a given study. n. s.: not specified.

Continued on next page

Study	Database	#Pt	TUA	#Sz	Biosignal	Electrodes
Kiral-Kornek *et al.* 2018 [239]	NeuroVista	15	16.29 years	2817	iEEG	16
Truong *et al.* 2019 [152]	Freiburg, CHB-MIT, EPILEPSIAE	13 13 30	12.95 years 8.7 years 120 years	59 64 261	sEEG, iEEG	6 22 19
Daoud & Bayoumi 2019 [240]	CHB-MIT	8	n. s.	43	sEEG	n. s.
Ozcan & Erturk 2019 [151]	CHB-MIT	16	19.4 days	77	sEEG	22
Meisel & Bailey 2019 [150]	EPILEPSIAE	10	54 days	60	sEEG, iEEG, ECG	sEEG: 21, iEEG: 30-114, ECG: 1
Zhang *et al.* 2020 [241]	CHB-MIT	22	n. s.	182	sEEG	n. s.
Nasseri *et al.* 2021 [134]	NeuroPace	6	4 years	278	ACC, BVP, EDA, TEMP, HR	Wrist-worn band
Stirling *et al.* 2021 [148]	Personal	11	13.5 years	1493	HR, sleep stages, step counts	Smartwatch
Usman *et al.* 2021 [242]	CHB-MIT	23	27 days	198	sEEG	n. s.
Pinto *et al.* 2021 [153]	EPILEPSIAE	19	29.6* days	49*	sEEG	19
Pinto *et al.* 2022 [157]	EPILEPSIAE	93	153.6 days*	238*	sEEG	19
Viana *et al.* 2022 [243]	ZUH, KCL	6	594 days	82	Subscalp EEG	n. s.

#Pt: number of patients. #Sz: number of seizures. TUA: time under analysis. iEEG: intracranial EEG. sEEG: scalp EEG. AES: American Epilepsy Society. CHB-MIT: Children's Hospital Boston from the Massachusetts Institute of Technology. ZUH: Zealand University Hospital. KCl: King's College London. BVP: blood volume pulse. ACC: accelerometry. EDA: electrodermal activity. TEMP: temperature. HR: heart rate. The asterisk indicates that information corresponds to the testing dataset in a given study. n. s.: not specified.

devices (Empatica E4, Empatica Inc., Boston MA) [134]. This dataset has been used to conduct studies on seizure forecasting [68, 134].

Lastly, there are ongoing efforts to obtain EEG data using minimally invasive methods. That is the case of the SeizeIT2 clinical trial (NCT04284072), where scalp EEG signals were acquired using two behind-the-ear channels connecting to a wearable device [244]. Another example is the subscalp EEG monitoring of patients with epilepsy using the 24/7 EEG SubQ (UNEEG Medical A/S, Denmark). With this device, implanted unilaterally behind the ear, researchers obtained EEG data from (i) a cohort of nine patients from Zealand University Hospital, Denmark [85] and (ii) a group of two patients undergoing an observational study (NCT04061707) in King's College London [243].

3.3.2 EEG signal preprocessing

Seizure prediction models should be developed using long-term EEG signals. Different types of artefacts can alter the normal EEG trace. As a result, instead of capturing mainly neural information of interest, the multi-channel EEG recordings will probably also contain artefacts, including environment interferences and experimental errors [156, 245]. Physiological artefacts are also frequently present in EEG signals, regardless of the acquisition environment. These types of noise stemming from physiological activity (e.g., routine tasks such as eating, sleeping, talking and walking) include eye movements, muscle activity, and cardiac pulse [60, 246]. It is therefore recommended to preprocess the EEG before conducting any further analysis [11, 230]. However, care should be taken as there is a trade-off between removing noise from the EEG signals and maintaining the relevant information. When the signals contain saturated segments or segments with electric flatlines, these segments can be removed without the loss of potentially important information. For other types of artefacts, researchers have developed several methods for noise removal of attenuation while trying to keep neural information [246].

Table 3.3 presents the preprocessing details of patient-specific seizure prediction studies published over the past ten years. It is noticeable that some studies document minimum or even no preprocessing methodologies indicating which might be indicative of the challenging task of correctly preprocessing complex signals such as the EEG without compromising the analysis of neural information.

Before handling artefacts, the signals are segmented into windows that are further discarded or denoised and then features are extracted from each denoised or clean window. When considering offline data analysis, signal segmentation may be undertaken after or before artefact handling. However, this step needs to be performed before inspecting the existence of noise when considering an online real-time application. In literature, signals are typically segmented into 5-second non-overlapping windows. Such window duration has been considered a fair trade-off

between the assumption of stationarity and the ability to identify patterns of interest [11].

Denoising

Denoising approaches applied to EEG data include filtering methods, blind source separation methods (BSS), and DL architectures. Linear filtering methods are widely used in seizure prediction studies (as can be seen in Table 3.3). Specifically, signal denoising may start with the basic step of removing the power line interference caused by the alternating current power supply. The power line component corresponding to the 50 Hz or 60 Hz (and corresponding harmonics) frequency peaks may, therefore, be attenuated using a notch filter. Low-pass, high-pass and band-pass filters are also often used to isolate the frequency bands of interest [11, 247]. Typically, the frequency components corresponding to the direct current (DC) component and the breathing artefacts are removed using a high-pass filter, whereas the high-frequency and likely noisy frequency content is attenuated using a low-pass filter [246]. The cut-off frequencies for both types of filters may vary among studies depending on the defined frequencies of interest. Additionally, it is important to note that the filtering methods may not be the ideal approach due to the overlapping frequencies of both neural and noisy content (verified for experimental errors and physiological artefacts) [60, 245].

There are other, more complex, types of filtering methods: adaptive filters, Wiener filters, and Kalman filters. In addition, source decomposition methods such as wavelets and empirical mode decomposition can also be considered to separate neural from noisy information in the EEG signals. All these approaches are rarely used in seizure prediction due to several reasons: overlapping frequencies of interest, high computational complexity and/or threshold tuning [60, 156, 245, 246].

The blind source separation (BSS) methods, despite being widely used in many research areas, are not often considered for EEG denoising in seizure prediction. Nevertheless, it is worth noting that these are considered robust methods for artefact removal, not requiring training or calibration [248]. The independent component analysis (ICA) is the most common BSS algorithm [246]. This method attempts to separate the signals into their independent sources, requiring, however, visual inspection to identify brain and noisy signals. Such limitations have prompted the development of DL architectures to automatically remove or attenuate artefacts in long-term signals [156, 230, 248].

3.3.3 Seizure prediction horizon

Information regarding the preictal interval and the SPH considered in each study is also presented in Table 3.3, as the two intervals should also be defined at an initial stage of a seizure prediction study. The SPH (detailed in the background Section

Table 3.3: Preprocessing steps, preictal duration and SPH in patient-specific EEG seizure prediction studies conducted over the past 10 years.

Study	EEG sliding window	EEG filtering	Preictal interval	SPH
Valderrama *et al.* 2012 [233]	5 s, no overlap	n. s.	[5, 10, 20, 30, 45, 60] min	n. s.
Cook *et al.* 2013 [50]	5 s, no overlap	Octave-wide digital and notch filters at 8-128 Hz	minutes to hours	n. s.
Rasekhi *et al.* 2013 [234]	5 s, no overlap	50 Hz notch filter	[10, 20, 30, 40] min	n. s.
Teixeira *et al.* 2014 [175]	5 s, no overlap	50 Hz notch filter	[10, 20, 30, 40] min	10 s
Alvarado-Rojas *et al.* 2014 [149]	5 s, no overlap	8th-order Butterworth band-pass filter in the bands of interest, Hilbert transform	60 min	1 min
Rasekhi *et al.* 2015 [144]	5 s, no overlap	50 Hz notch filter	[10, 20, 30, 40] min	n. s.
Bandarabadi *et al.* 2015 [235]	5 s, no overlap	50 Hz notch filter	[10, 20, 30, 40] min	n. s.
Direito *et al.* 2017 [236]	5 s, no overlap	50 Hz notch filter	[10, 20, 30, 40] min	10 s
Karoly *et al.* 2017 [17]	60 s, 50% overlap	1-140 Hz band-pass filter	30 min	1 min
Kuhlmann *et al.* 2018 [232]	0 s to 10 min, 0 to 50% overlap	n. s.	55 min	5 min
Truong *et al.* 2018 [238]	30 s, no overlap	Notch-filter, DC component removal	30 min	5 min
Tsiouris *et al.* 2018 [237]	5 s, no overlap	n. s.	[15, 30, 60, 120] min	n. s.
Kiral-Kornek *et al.* 2018 [239]	5 s, no overlap	Octave-wide digital and notch filters at 8-128 Hz	15 min	1 min
Truong *et al.* 2019 [152]	28 s, no overlap	Notch filter, DC component removal	30 min	5 min
Daoud & Bayoumi, 2019 [240]	5 s, no overlap	n. s.	60 min	n. s.

n. s.: not specified.

Continued on next page

Study	Sliding window	Filtering	Preictal interval	SPH
Ozcan & Erturk 2019 [151]	4 s, 50% overlap	DC component removal, power line at 60 Hz excluded from frequency analysis	[30, 60] min	1 min
Meisel & Bailey 2019 [150]	30 s, no overlap	50 Hz notch filter	20 min	10 min
Zhang *et al.* 2020 [241]	5 s, no overlap	5th-order Butterworth band-pass filter at 5-50 Hz	30 min	n. s.
Nasseri *et al.* 2021 [134]	1 s and 4 s	n. s.	60 min	15 min
Stirling *et al.* 2021 [148]	5 s and 60 s, no overlap	Butterworth band-pass filter, Hilbert transform	1 hour and 24 hours	n. s.
Usman *et al.* 2021 [242]	29 s, no overlap	Empirical mode decomposition	32 min	n. s.
Pinto *et al.* 2021 [153]	5 s, no overlap	50 Hz notch filter, 0.1–120 Hz band-pass filter	[40, 50, 60] min	10 min
Pinto *et al.* 2022 [157]	5 s, no overlap	50 Hz fourth-order notch filter, fourth-order Butterworth high-pass filter at 0.5 Hz	[30, 35, 40, 45, 50, 55 60, 65, 70, 75] min	10 min
Viana *et al.* 2022 [243]	60 s, no overlap	0.5-48 Hz band-pass and 25 Hz low-pass filters, 40 dB attenuation filter	60 min	5 min

n. s.: not specified.

2.5.5) has not been defined in about half the studies presented in Table 3.3. When designing seizure prediction studies to be prospectively tested in a real-life scenario, an SPH interval needs to be defined. Its duration depends on the envisioned clinical application [11, 13].

3.3.4 Preictal state

The transition between interictal brain activity and seizure manifestations (either behaviourally or on the electrographic trace) has been the subject of great interest for the scientific community engaged in seizure prediction. Identification of such transition, known as the preictal state, presents serious challenges stemming partly from the highly complex brain dynamics [61] and also from the current limitations on the available data collection techniques. The preictal state is indeed the brain state associated with the lowest understanding in epilepsy [249], and yet its delimitation is considered crucial to the success of seizure prediction models. Typically, this preictal state can be easily distinguished from ictal manifestations, particularly when considering clinical symptoms. However, its beginning may be difficult to observe, often not being associated with clinical manifestations [10]. Currently, besides no clinical definition exists also, there is no specific pattern or set of patterns able to discriminate between this period and the interictal stage [10–12, 133]. Although no widely accepted evidence of the preictal interval has been presented to date, widespread confidence in its existence is suggested by the predictability of seizures [10, 12, 30, 61].

Studies on EEG-based seizure prediction started by assuming a fixed preictal interval. Typically, such interval took a value in the range of 2 to 90 minutes [11, 13]. The different duration of fixed preictal intervals used to train the first seizure prediction models led to a range of performances later regarded as overoptimistic in a 2007 critical review [13]. The failure to report appropriate performance measures (seizure sensitivity and FPR/h) and the lack of statistical validation (assessment of performance above-chance) often overshadowed the true performance of predictive models [13]. As such, the prediction potential of the assumed preictal interval in those early studies has been addressed in recent rigorous studies, which show little evidence for a (quasi-) prospective above-chance prediction [12, 13, 250].

The variability seen in model performance for different choices of preictal duration prompted researchers to compare the prediction potential of different values of the preictal intervals. This inspection has been performed using statistical and algorithmic approaches [13, 82]. Statistical approaches correspond to the comparison of preictal and interictal feature distributions. When inspecting different preictal durations, the one leading to the highest value of a given comparison metric holds the highest prediction potential. Algorithmic approaches consist of inspecting a set of intervals (grid-search), with the interval corresponding to the best performance

being integrated as the preictal interval in the final prediction algorithm. Table 3.4 presents information on studies reporting the assessment of the prediction potential for different values of the preictal interval. Tables B.3, B.4, B.5, and B.6, in the appendix, present further details on these studies, regarding the dataset analysed, preprocessing methods, extracted features and classification algorithms, respectively.

According to Table 3.4, it is possible to conclude that the best performances, either statistical or algorithmic, have been achieved when preictal intervals started 28 to 60 minutes before seizure onset. However, in some of these studies, the longest preictal interval considered lead to the best performance in some patients [149,233,236]. With longer preictal intervals, the class imbalance problem (addressed in Section 3.3.7) is attenuated, indicating that there is a natural tendency for the machine learning models to become optimal for longer preictal intervals. The two statistical approaches found in the literature report the computation of feature amplitude distribution histograms of interictal and preictal samples [14,251]. Mormann *et al.* [14] used receiver operating characteristic (ROC) curves to assess the predictive power of different sets of features and preictal intervals. The duration of the selected preictal interval was found to vary among univariate and bivariate features [2]. Bivariate features were associated with longer preictal intervals, possibly indicating a higher sensitivity to long-term seizure dynamics. Bandarabadi *et al.* [251] searched for an optimal preictal interval in the range of 5 to 180 minutes (with 1-minute increments) before seizure onset. Evidence for preictal alterations was found for 70% of seizures and in the range of 5 minutes up to 173 minutes. Additionally, the optimal preictal intervals varied from seizure to seizure, even for seizures experienced by the same patient.

In all studies in Table 3.4, the seizure prediction models were trained for each patient individually. The variability seen in the prediction performance among patients further supports the heterogeneity of the seizure generation process, even for patients experiencing the same type of seizures. Nevertheless, performing a patient grid-search on the previously defined set of preictal intervals may still be regarded as a limited, user-dependent approach to the problem of preictal identification.

The variability observed in all these studies for the preictal interval across patients has established consensus on developing patient-specific prediction models [12,15,16]. Additionally, the preictal heterogeneity observed within seizures for the same patient supports the exploration of seizure-specific preictal profiles [16,17]. Finding correlations between preictal characteristics and different types of seizures (or other metadata) can translate, for instance, into training seizure prediction models for each seizure type [16,132]. The existence of a large number of epilepsy syndromes (resulting in considerable heterogeneity concerning aetiology and clinical manifestations) and non-cerebral confounders may explain the variability observed

[2]Univariate features are extracted for a given time series (e.g., a given EEG channel). Bivariate features correspond to measures quantifying the relationship between two time series [13]

Table 3.4: Seizure prediction studies with preictal interval grid-search performed for each patient.

Study	Preictal (minutes)	Average preictal (minutes)	Signal	SS (%)	FPR/h (h^{-1})	Above chance prediction
Mormann *et al.* 2005 [14]*	$t = [5, 30, 120, 240]$	Univariate features: $t = 5 - 30$; Bivariate features: $t = 240$	iEEG	n. s.	n. s.	n. s.
Valderrama *et al.* 2012 [233]	$t = [5, 10, 20, 30, 45, 60]$	$t = 37.50 \pm 14.54$, $r = [20, 60]$	sEEG+iEEG+ECG	33.38±26.44	n. s. 8	9 patients out of 12
Rasekhi *et al.* 2013 [234]	$t = 10 : 10 : 40$	n.s.	iEEG sEEG	68.70 76.67	0.33 0.08	
Teixeira *et al.* 2014 [175]	$t = 10 : 10 : 40$	$t = 30.47$	iEEG sEEG	67.66±21.83 73.55±24.83	0.39±0.37 0.28±0.28	
Alvarado-Rojas *et al.* 2014 [149]	$t = [10, 30, 60]$	$t = 60$	iEEG	68.00	0.33	
Rasekhi *et al.* 2015 [144]	$t = 10 : 10 : 40$	$t = 31$	iEEG sEEG	50.0 66.7	0.08 0.12	
Bandarabadi *et al.* 2015 [251]*	$t = 5 : 1 : 180$	$t = 44.3$	sEEG+iEEG	–	–	–
Bandarabadi *et al.* 2015 [235]	$t = 10 : 10 : 40$	$t = 30$	iEEG sEEG	78.36 73.98	0.15 0.06	
Direito *et al.* 2017 [236]	$t = 10 : 10 : 40$	$t = 28$	iEEG sEEG	28.47 41.42	0.25 0.19	
Tsiouris *et al.* 2018 [237]	$t = [15, 30, 60, 120]$	$t = 120$	sEEG	100.00	0.02	
Pinto *et al.* 2021 [153]	$t = 40 : 10 : 60$	$t = 58.5 \pm 7.07$	sEEG	37±24	0.69±0.46	7 patients out of 19
Pinto *et al.* 2022 [157]	$t = 35 : 5 : 90$ sEEG	$t = 50.7 \pm 1.86$	sEEG	16±11	0.21±0.08	30 patients out of 93

t: preictal starting time before seizure EEG onset. When the considered preictal intervals were defined as a vector of successive values, separated by a step, that information was presented as: [starting preictal:step:ending preictal]. r: range of preictal starting time. Average preictal: average preictal period corresponding to the best performance. iEEG: intracranial EEG. sEEG: scalp EEG. The asterisk indicates a statistical rather than an algorithmic approach. n. s.: not specified.

for the preictal interval across patients and even seizures [252].

Unsupervised learning methods have been scarcely employed to automatically identify preictal activity (see Table 3.5). The first studies were conducted in 2005. Le Van Quyen *et al.* [253] reported the use of the K-means clustering algorithm to build a library of interictal patterns based on the analysis of the degree of phase synchronisation. The interictal recordings were found to generally fit into 5 to 10 clusters, suggesting the existence of recurrent patterns of interictal activity. The results varied widely among patients [253]. Kerem & Geva applied a fuzzy clustering algorithm to search for the preictal interval in the RR interval series extracted from the ECG [219]. The authors reported seizure-specific preictal clusters.

From 2019 onward, the use of unsupervised learning methods for preictal determination was resumed [254–256]. Results across studies indicate that the preictal interval may manifest in human EEG data only for some seizures (ranging from 38% to 70% [253, 254, 256]). Importantly, the studies report the analysis of recordings collected from small groups of patients [253, 254, 256] (or canines [255]) and consequently reduced the number of seizures.

3.3.5 Feature engineering

After preprocessing phase, the segmented EEG and ECG signals are ready for feature extraction. Characteristics (or features) are typically computed from each signal window, this way capturing essential changes occurring in the raw signals [12,13,158]. Studies mainly differ on the choice of the features to extract, which might reflect the lack of a predictive feature or group of features that is able to generally characterise the preictal state [12].

EEG feature engineering can be performed on single- or multi-channel data. For instance, features can be computed from (i) a single channel (univariate) or (ii) several simultaneously acquired channels (bivariate in the case of two channels and multivariate in the case of more than two channels) [13]. Multivariate EEG features are obtained based on the assumption that the preictal state manifests as an increase in neural synchronisation between brain regions [158]. However, these measures require a considerably large computational time which might explain their reduced use in prediction studies. One study reported that combining univariate and multivariate features increased prediction performance [14].

EEG features can also be categorised as linear or nonlinear (see Table 3.6). Although no consensus has been reached regarding the difference in the predictive potential of each group, nonlinear measures are associated with a considerably higher computational cost compared to the linear features [11]. Literature indicates that linear features are widely extracted in seizure prediction studies (see Table 3.7). Although less frequent, some DL studies also report handcrafted [151] or automatic [240, 242] feature extraction before classification. Automatically extracting

Table 3.5: Studies reporting unsupervised learning for preictal characterisation.

Study	Dataset	Features	Clustering	Results
Kerem & Geva, 2005 [219]	8 patients with TLE in presurgical evaluation, 21 FOIA seizures, ECG recordings lasting from 9.8 to 38.8 min	RR interval series	Fuzzy clustering	Preictal activity in 86% of the seizures, range: 1.5 to 11 min
Le Van Quyen *et al.*, 2005 [253]	5 patients with mesial TLE, 52 seizures, iEEG, interictal recordings with 5 to 24 h	Bivariate feature (phase-locking value)	K-means applied to interictal data, with $K = [5 : 10]$	Preictal activity in 70% of the seizures, mean±std: 187±56 min
Li *et al.*, 2019 [254]	13 patients with epilepsy, 29 seizures, one hour sEEG recordings	Multivariate features (characteristic path length, clustering coefficients, global efficiency and local efficiency)	K-medoids, K-means, fuzzy C-means, and hierarchical clustering, with $K = 2$	Preictal activity in 69% of the seizures, range: 25±14 min
Nasseri *et al.*, 2020 [255]	6 dogs with epilepsy, 127 seizures, chronic iEEG, recordings lasting from 28 to 241 days	Cross-channel correlation coefficient in time and frequency domains, entropy of power-in-band for frequency bands up to 30 Hz, FFT magnitude with logarithmic scaling for frequency band from 0.5 to 48 Hz, Higuchi fractal dimension, Petrosian fractal dimension, and Hurst exponent	Hierarchical clustering	Improved results for time in warning and false positive rate for some dogs.
Quercia *et al.*, 2021 [256]	21 children with DRE (CHB-MIT dataset), 74 seizures, sEEG, recordings lasting from 9 to 42 h	Bivariate feature (phase-locking synchrony value)	K-means, with $K = 2$	Preictal activity in 38% of the seizures, range: 25 to 90 min

DRE: drug-resistant epilepsy; iEEG: intracranial EEG; sEEG: scalp EEG; TLE: temporal lobe epilepsy; FOIA: focal onset impaired awareness; CHB-MIT: Children's Hospital Boston from the Massachusetts Institute of Technology; FFT: fast Fourier transform.

features using DL methods might, however, be less informative on the seizure generation process than computing informed-based features using ML methods. It is

also important to mention that the recent transition from ML to DL approaches is reflected in the use of raw data, time-frequency data obtained with time-frequency methods, such as the short-time Fourier transform and new data components obtained with common spatial pattern. Lastly, it is possible to notice that researchers have been taking into account circadian rhythms by using features such as the time of day when a given seizure occurred and cardiac and sleep features.

3.3.6 Feature selection

High-dimensionality datasets may result from the feature engineering step, particularly when analysing multi-channel EEG signals. High-dimensional datasets should be assessed regarding redundant or irrelevant features that may further degrade the prediction performance. Feature selection, therefore, contributes to reducing the model's computational cost while avoiding overfitting [11, 230, 260]. The goal is to remove (i) features with lower predictive power (maximise relevance) and (ii) fea-

Table 3.6: EEG-derived features.

Group	Linear	Nonlinear
Univariate	Statistical moments	Entropy
	Accumulated energy	Correlation dimension
	Decorrelation time	Largest Lyapunov exponent
	Hjörth parameters	
	Energy of wavelet coefficients	
	Relative spectral power (delta, theta, alpha, beta and gamma)	
	Spectral edge power	
Bivariate	Relative normalised spectral power [235]	Mutual information
	Coherency	Shannon entropy index
	Correlation	Dynamical entrainment [11, 13]
	Granger causality index [257]	Conditional probability index
	Maximum of normalised cross-correlation [13]	Correlation on the probability of recurrence [177]
		Intersite phase clustering (or mean phase coherence or phase locking value) [58, 257, 258]
Multivariate		Directed transfer function [259]
		Partial directed coherence [177]
		Shannon entropy index
		Conditional probability index

All features that are not followed by a citation were mentioned in Bou Assi *et al.* [11] comprehensive survey.

Table 3.7: Feature extraction in patient-specific seizure prediction studies conducted over the past 10 years.

Features		Studies																								
		Valderrama *et al.* 2012 [233]	Cook *et al.* 2013 [50]	Rasekhi *et al.* 2013 [234]	Teixeira *et al.* 2014 [175]	Alvarado-Rojas *et al.* 2014 [149]	Rasekhi *et al.* 2015 [144]	Bandarabadi *et al.* 2015 [235]	Direito *et al.* 2017 [236]	Karoly *et al.* 2017 [17]	Kuhlmann *et al.* 2018 [232]	Truong *et al.* 2018 [238]	Tsiouris *et al.* 2018 [237]	Kiral-Kornek *et al.* 2018 [239]	Truong *et al.* 2019 [152]	Daoud & Bayoumi, 2019 [240]	Ozcan & Erturk, 2019 [151]	Meisel & Bailey 2019 [150]	Zhang *et al.* 2020 [241]	Nasseri *et al.* 2021 [134]	Stirling *et al.* 2021 [148]	Usman *et al.* 2021 [242]	Pinto *et al.* 2021 [153]	Pinto *et al.* 2022 [157]	Viana *et al.* 2022 [243]
Linear univariate	Statistical moments	x		x	x		x		x		x						x						x	x	
	Spectral band related	x		x	x		x	x	x		x						x	x					x	x	
	Wavelets	x		x	x		x		x		x													x	
	Linear modelling	x		x	x		x		x		x														
	Energy		x	x	x		x		x	x	x														
	Hjorth parameters	x		x	x		x		x		x						x							x	
	Decorrelation time	x		x	x		x		x		x														
Nonlinear univariate	Energy																								
	Entropy																								
	Line length		x							x															
Linear bivariate	Ratio							x																	
Nonlinear bivariate	Intersite phase clustering										x														

Continued on next page

Features		Studies																							
		Valderrama *et al.* 2012 [233]	Cook *et al.* 2003 [50]	Rasekhi *et al.* 2013 [234]	Teixeira *et al.* 2014 [175]	Alvarado-Rojas *et al.* 2014 [149]	Rasekhi *et al.* 2015 [144]	Bandarabadi *et al.* 2015 [235]	Direito *et al.* 2017 [236]	Karoly *et al.* 2017 [17]	Kuhlmann *et al.* 2018 [232]	Truong *et al.* 2018 [238]	Tsiouris *et al.* 2018 [237]	Kiral-Kornek *et al.* 2018 [239]	Truong *et al.* 2019 [152]	Daoud & Bayoumi, 2019 [240]	Ozcan & Erturk, 2019 [151]	Meisel & Bailey 2019 [150]	Zhang *et al.* 2020 [241]	Nasseri *et al.* 2021 [134]	Stirling *et al.* 2021 [148]	Usman *et al.* 2021 [242]	Pinto *et al.* 2021 [153]	Pinto *et al.* 2022 [157]	Viana *et al.* 2022 [243]
Synchrony											x							x							
Other EEG	Phase interaction with HFO					x																			
	Raw data												x			x				x					x
	FFT/PSD data																	x							x
	Common spatial pattern																		x						
	Spectrogram													x											
	STFT spectrogram											x			x							x			
Other non-EEG	Time of the day													x						x	x				
	Heart rate features	x																		x	x				
	HRV features	x																x			x				
	Sleep features																				x				
	ECG PSD data																	x			x				

HFO: high-frequency oscillations; FFT: fast Fourier transform; STFT: short-time Fourier transform; HRV: heart rate variability. PSD: power spectral density.

tures with similar evolution (minimise redundancy). Some of the most used feature selection methods include minimum redundancy maximum relevance (mRMR), and genetic algorithms [11]. In the group of studies presented in Tables 3.2, 3.3, and 3.8, only a few performed feature selection using a filter-based approach [17,50,144,235], others reported a channel selection to search for the most informative EEG channels [175, 236, 240] and others included an automatic search for discriminative features in the model design, as was done by evolutionary algorithms [153,157]. Studies with DL approaches do not require feature extraction and selection steps.

Additionally, instead of selecting features, authors might opt for dimensionality reduction: a high-dimensional dataset is transformed into a low-dimensional subspace. The principal component analysis (PCA) is one of the most popular unsupervised dimensionality reduction methods. Applying PCA consists in obtaining new relevant features through orthogonal linear combinations of the original features. These new components represent the maximum variance in the original high-dimensional dataset [261, 262].

3.3.7 Classification

As can be seen in Table 3.8, a wide plethora of classifiers have been used in seizure prediction studies to distinguish interictal from preictal samples. These classifiers range from simple thresholding methods to more complex DL approaches. The increase in the models' complexity has been observed over the years with a clear transition from the common use of support vector machines (SVMs) to long short-term memory (LSTM) artificial neural networks capable of dealing with time series long-term dependencies [263]. In the 2016 Kaggle contest, the top teams predominantly applied ensembles of different ML algorithms. Also, different algorithms were found to reach maximum performance for different patients evidencing the patient-specific profile of seizure prediction [232]. These results should, however, be carefully interpreted given the lack of proper statistical validation to assure that the models are performing above chance level [12].

Dealing with imbalanced data

Seizure prediction is considered a rare event problem meaning that there are far more interictal samples than preictal samples. This is a problem of class imbalance that has been addressed differently across studies. The majority of researchers choose to discard interictal samples (or undersampling), [17,175,232–236,240,241] whereas a few others opt for (i) designing cost-sensitive learning classifiers [11, 179, 238], (ii) using an oversampling technique aiming at artificially generating new preictal samples (e.g. using generative adversarial networks [152, 241, 242], or (iii) noise-adding copies of preictal samples [134,243]).

3.3.8 Training and testing

In 2007, Mormann *et al.* [13]'s major review alerted to the problem of in-sample optimisation. Specifically, early seizure prediction studies presented overestimated performance results, likely due to the use of training samples during the testing phase. Consequently, when these prediction models are applied to new data, the results will hardly be reproducible. It is therefore, advisable to evaluate the true performance of a seizure prediction model on out-of-sample data, i.e., data that has not been used before. Additionally, selecting models based on their performance in the testing dataset is also considered a biased evaluation of the prediction performance (known as selection bias). This problem is inherent to the retrospective evaluation of models developed in different studies using the same database. In order to reliably assess the true predictive potential of a given model, a prospective evaluation should be sought [12]. While aiming at prospective testing, retrospective studies should first assess the quasi-prospective out-of-sample performance by testing the models on unseen data [13].

To perform out-of-sample testing, it is necessary to separate the whole dataset into training and testing sets. Given the patient-specific nature of brain activity, developing a general prediction model using data from a group of patients and testing it on the remaining data has been gradually discouraged [12]. Interestingly, a few recent studies are reporting the assessment of prediction performance for generalised cross-patient forecasting models developed using new datasets comprising non-neurological data [128] and two-channel subscalp EEG data [263]. Even though these studies showed better than chance prediction performance for some patients, seizure sensitivity and time in warning results are not superior to similar patient-specific studies [243].

Table 3.8 contains information on patient-specific prediction algorithms that were initially developed, choosing the first seizures of a given patient for training and the remaining for testing. More recently, there is a tendency to perform a leave-one-seizure-out cross-validation procedure or a chronological retraining and retesting to mimic a clinical application (that also deals with the presence of concept drifts).

3.3.9 Postprocessing

In terms of postprocessing, no significant changes have been observed over time. The Kalman filter and the firing power are the most used approaches to attenuate the number of false alarms returned by the classifiers [11]. It is worth noting that some studies present a moving average filter to postprocess the classifier's output which is quite similar to the firing power rationale (see Section 2.5.7 in background Chapter 2).

Table 3.8: Classification and postprocessing in patient-specific seizure prediction studies conducted over the past 10 years.

Study	Training/Testing data	Classifier	Postprocessing	Performance	Statistical Validation
Valderrama *et al.* 2012 [233]	First 1/2 of data/Last 1/2 of data	Multiclass SVM	n. s.	SS=0.33, FPR=0.24	Seizure time surrogates, 9 in 12 (75%)
Cook *et al.* 2013 [50]	First 4 months/Remaining data	kNN + Decision Trees	Filtered classifier output	SS=0.61, TiW=0.23	Time-matched predictor, 9 in 10 (90%)
Rasekhi *et al.* 2013 [234]	First 3 seizures/Remaining seizures	SVM	Firing power	SS=0.74, FPR/h=0.15	–
Teixeira *et al.* 2014 [175]	2 to 3 seizures/Remaining seizures	SVM, ANN	Firing power	SS=0.74, FPR/h=0.28	Statistical comparison between methods
Alvarado-Rojas *et al.* 2014 [149]	First 4 seizures and at least 10 hours of data/Remaining seizures	Thresholding	Kalman filter	SS=0.68, FPR/h=0.33	Analytic random predictor, 7 in 53 (13%)
Rasekhi *et al.* 2015 [144]	First 3 seizures/Remaining seizures	SVM	Firing power	SS=0.61, FPR/h=0.11	Analytic random predictor, 5 in 10 (50%)
Bandarabadi *et al.* 2015 [235]	First 3 seizures/Remaining seizures	SVM	Firing power	SS=0.76, FPR/h=0.10	Analytic random predictor, 23 in 24 (96%)
Direito *et al.* 2017 [236]	2 to 3 seizures/Remaining seizures	SVM	Firing power	SS=0.38, FPR/h=0.20	Analytic random predictor, 24 in 216 (11%)
Karoly *et al.* 2017 [17]	Day 100-200/Day 200 onwards	Logistic regression	Bin width of 1 h	SS=0.60, TiW=0.23	Time-matched predictor, 9 in 9 (100%)

SVM: support vector machine; kNN: k-nearest neighbours; ANN: artificial neural networks; GLM: generalised linear model; CNN: convolutional neural network; LSTM: long short-term memory; GAN: generative adversarial network; SE: sample sensitivity; SP: sample specificity; SS: seizure sensitivity; FPR/h: false positive rate per hour; TiW: time in warning; AUC: area under the receiver operating characteristic curve, based on the proportion of preictal samples correctly classified (true positive rate) and the proportion of interictal samples incorrectly classified as preictal (false positive rate). When not stated otherwise, the analytic random predictor has been derived as a function of the false positive rate.

Continued on next page

Study	Training/Testing data	Classifier	Postprocessing	Performance	Statistical Validation
Kuhlmann *et al.* 2018 [232]	Training and testing clips	GLM, SVM, CNN, Decision trees, Ensembles, Boosting	–	AUC=0.75, FPR/h=0.58	–
Truong *et al.* 2018 [238]	Leave-one-seizure-out	CNN	Kalman filter	SS=0.79, FPR/h=0.14	Analytic random predictor, 28 in 31 (90%)
Tsiouris *et al.* 2018 [237]	K-fold with recordings	LSTM	–	SS=0.99, FPR/h=0.02	–
Kiral-Kornek *et al.* 2018 [239]	First 2 months/Remaining data	CNN	–	SS=0.69, FPR/h=0.00	Random predictor, 15 in 15 (100%)
Truong *et al.* 2019 [152]	Leave-one-seizure-out	GAN, CNN	–	AUC=0.81	Hanley-McNeil AUC test, 51 in 56 (91%)
Daoud & Bayoumi 2019 [240]	Leave-one-seizure-out	DCNN, Bi-LSTM	–	SS=0.99, FPR/h=0.004	–
Ozcan & Erturk 2019 [151]	Leave-one-seizure-out	CNN	1-minute causal moving average filter	SS=0.86, FPR/h=0.10, TiW=0.10	Analytic random predictor as function of the fraction of TiW, 15 in 16 (93.7%)
Meisel & Bailey 2019 [150]	5-fold cross validation (70%/30%)	DNN, k-NN, SVM	–	AUC=0.90	Randomly shuffled test set labels, 10 in 10 (100%)
Zhang *et al.* 2020 [241]	Leave-one-seizure-out	CNN	Kalman filter	SS=0.92, FPR/h=0.12	Statistical comparison between methods

SVM: support vector machine; kNN: k-nearest neighbours; ANN: artificial neural networks; GLM: generalised linear model; CNN: convolutional neural network; LSTM: long short-term memory; GAN: generative adversarial network; SE: sample sensitivity; SP: sample specificity; SS: seizure sensitivity; FPR/h: false positive rate per hour; TiW: time in warning; AUC: area under the receiver operating characteristic curve, based on the proportion of preictal samples correctly classified (true positive rate) and the proportion of interictal samples incorrectly classified as preictal (false positive rate). When not stated otherwise, the analytic random predictor has been derived as a function of the false positive rate.

Continued on next page

Study	Training/Testing data	Classifier	Postprocessing	Performance	Statistical Validation
Nasseri *et al.* 2021 [134]	First 2/3 of data/Last 1/3 of data	LSTM	Kalman filter	AUC=0.80	Analytic random predictor as function of the fraction of TiW, 5 in 6 (83%)
Stirling *et al.* 2021 [148]	Retraining and testing chronologically and iteratively	LSTM+Random Forest+Logistic Regression	Kalman filter	AUC=0.74	Random forecast, 11 in 11 (100%)
Usman *et al.* 2021 [242]	K-fold cross validation with seizures	CNN+LSTM	–	SE=0.93, SP=0.92	–
Pinto *et al.* 2021 [153]	First 60% seizures/Last 40% seizures	Logistic regression	Firing power	SS=0.37, FPR/h=0.80	Seizure time surrogates, 6 in 19 (32%)
Pinto *et al.* 2022 [157]	First 3 seizures/Remaining seizures	Logistic regression	Firing power	SS=0.16, FPR/h=0.21	Seizure time surrogates, 30 in 93 (32%)
Viana *et al.* 2022 [243]	First 1/3 of data/Last 2/3 of data	LSTM	1h smooth	SS=0.73, TiW=0.34	Analytic random predictor as function of the fraction of TiW, 5 in 6 (83%)

SVM: support vector machine; kNN: k-nearest neighbours; ANN: artificial neural networks; GLM: generalised linear model; CNN: convolutional neural network; LSTM: long short-term memory; GAN: generative adversarial network; SE: sample sensitivity; SP: sample specificity; SS: seizure sensitivity; FPR/h: false positive rate per hour; TiW: time in warning; AUC: area under the receiver operating characteristic curve, based on the proportion of preictal samples correctly classified (true positive rate) and the proportion of interictal samples incorrectly classified as preictal (false positive rate). When not stated otherwise, the analytic random predictor has been derived as a function of the false positive rate.

3.3.10 Performance assessment

According to the available guidelines [12, 13], the performance of seizure prediction algorithms should be evaluated using seizure sensitivity and the false prediction rate per hour (FPR/h) in addition to the correct statistical validation to assess if the performance is above chance level. Most studies present such metrics, except for some authors who opted for the area under the receiver operating characteristic curve (AUC) or the sample sensitivity and specificity (described in Section 2.5.5). Presenting only these metrics might not be sufficient to provide the required information on seizure sensitivity and the number of false alarms per hour that allows for a correct assessment of the impact on the patient that might be subjected to an intervention.

The metric time in warning is used in studies proposing seizure forecasting algorithms (see Section 3.4 below). As the occurrence of false alarms is regarded differently in seizure forecasting, presenting this metric is not adequate for this type of study [13, 16].

When evaluating the performance of seizure prediction according to the explored database, conflicting results might be observed. That is the case with the EPILEPSIAE database, for which highly heterogeneous results have been observed. Such discrepancies might be explained by the different criteria used to select data among the available 278 patients dataset. Specifically, different groups of patients may be analysed when considering the percentage of noise in the signals, the seizure onset lobe, and the inter-seizure distance, among others.

Additionally, the best prediction results also seem to be database-dependent. That is the case of the CHB-MIT database, for which researchers consensually have reached the highest seizure sensitivity and the lowest FPR/h. Despite being the only online available database currently in use, it might not be relevant to derive more prediction models using these data.

3.4 Seizure forecasting

Seizure forecasting has been recently explored in patients with DRE. This framework is based on identifying patient-specific cycles of epileptic brain activity that modulate the risk of seizure occurrence. Accordingly, the long-term continuous recording of EEG data may allow for exploring seizure likelihood states, named proictal states. These states, characterised by a sufficiently high probability of transition to an ictal state, may not evolve towards a seizure or can even persist after a seizure [12, 15, 16, 23, 65, 66, 159]. Table 3.9 contains the key differences between forecasting and prediction frameworks (briefly discussed in the following subsections). It is important to note that prediction and forecasting are not mutually exclusive; on the contrary, both approaches might be required to enable clinical

application [68, 159, 166]. As such, the two concepts presented in Table 3.9 were individually characterised only to provide a better understanding of the two frameworks.

The driving study

The hallmark study of Cook and colleagues [50] presented the first prospective study on seizure prediction during which patients with DRE were informed whether the likelihood of an upcoming seizure was high, moderate, or low. The study was a breakthrough in proving seizure prediction possible and encouraged the adoption of the forecasting perspective in subsequent studies (see Table 3.10).

Meaning of false positives

Starting in the early 1990s, with the application of the mathematical theory of nonlinear dynamics, the preictal interval became associated with the state during which the brain activity evolves deterministically towards the seizure [18, 264]. In other words, once the brain enters this state, a "point of no return" has been passed, meaning that the seizure will inevitably occur [13, 15, 18]. However, the deterministic perspective on seizure occurrence might overlook the existence of corrective regulatory mechanisms in the brain. Specifically, false positives identified by deter-

Table 3.9: Main differences between seizure forecasting and seizure prediction frameworks.

Parameter	Prediction	Forecasting
Concept	Preictal state	Proictal state
Prediction horizon	Minutes to hours	Hours to days
Seizure dynamics	Deterministic (seizure will occur)	Probabilistic (seizure may not occur)
Algorithm [68, 166]	Assign a label to each data sample	Optimise conditional probability of observing a label giving a data sample.
Information to the patient	A seizure will occur within a given prediction horizon	There is a probability or risk that a seizure will occur
Intervention [166]	Adoption of rapid safety procedures	Patients and caregivers can plan their lives according to periods of increased seizure risk
State duration	Ends at seizure onset	Can persist after the seizure offset
Metrics [68, 166]	Sensitivity, false alarm rate, area under the curve	time in warning, reliability curve, calibration, resolution, skill, Brier score, Brier skill score

Table 3.10: Seizure forecasting studies.

Study	Database	Patients	Signal	Results
Meisel *et al.*, 2020 [128]	Empatica E4	69 patients with DRE, with focal and generalised seizures	ACC, BVP, EDA, TEMP	Average prediction horizon across patients with forecasting performance better than chance: 31.6±1.68 minutes, ranging from 12.3 to 54.55 minutes.
Karoly *et al.*, 2020 [265]	NeuroVista & Seer App	15 patients with focal DRE and 50 patients with self-reported seizures	iEEG	Using self-reported cycles in forecasting models was predictive of EEG seizures in about half the validation cohort. On average, 69.1% of seizures occurred during high-risk states and 10.5% of seizures occurred in low-risk states
Stirling *et al.*, 2021 [148]	Personal	11 patients with DRE, with generalised and focal seizures	BVP, sleep stages	Forecasting performance better than chance: (i) in all patients for an hourly prediction horizon and (ii) in 10 out 11 patients for a daily prediction horizon. Average prediction time before seizure onset was 37 minutes in the hourly forecast and 3 days in the daily forecast.
Stirling *et al.*, 2021 [69]	ACTRN 12619001587190 trial	5 patients with DRE, with generalised, focal and multifocal seizures	Subscalp EEG	Forecasting results for one participant with 119 testing seizures: 99 (83%) seizures occurred in high risk, 8 (7%) seizures occurred in medium risk and 12 (10%) seizures occurred in low risk. Median time spent in the high risk state before a seizure occurred was 28 hours.
Proix *et al.*, 2021 [68]	NeuroPace	175 patients with focal DRE, 18 patients with EEG seizures and 157 patients with self-reported seizures.	Chronic iEEG	Forecasting horizon of (i) one day in 83% patients; (ii) three days in 11% of patients and (iii) one hour in 100% of patients (in the cohort with EEG seizures). Proictal state lasting 3 to 5 days in most patients.
Nasseri *et al.*, 2021 [134]	NeuroPace and Empatica E4	6 patients with DRE, with focal and generalised seizures	Chronic iEEG, ACC, BVP, EDA, TEMP	Forecasting performance better than chance in 5 out 6 patients. Average forecasting time before seizure onset was 33 minutes, ranging from 28 to 42 minutes.
Viana *et al.*, 2022 [243]	ZUH, KCL	6 patients with focal DRE	Subscalp EEG	Forecasting performance better than chance in 3 out 5 patients. Median duration of preictal period ranged from 16 minutes to 2 hours and 52 minutes.

DRE: drug-resistant epilepsy; iEEG: intracranial EEG; sEEG: scalp EEG; ZUH: Zealand University Hospital; KCl: King's College London; BVP: blood volume pulse; ACC: accelerometry; EDA: electrodermal activity; TEMP: temperature; n. s.: not specified; Chronic EEG: EEG collected over months to years [66].

ministic frameworks may reflect the presence of epilepsy-related alterations in the EEG trace that are mitigated by the activation of brain processes to resume normal brain activity and prevent seizure occurrence [16].

Proictal state

In practice, supervised seizure prediction algorithms are developed to discriminate between interictal and preictal samples in the EEG signals. Contrarily, forecasting frameworks consist in using probabilistic algorithms based on the estimation of seizure risk (e.g., by tracking cycles of seizures or cycles of IEA). For instance, a Bayesian approach may consider the information on proictal states as priors to draw a probability of seizure occurrence. Importantly, interictal to ictal transitions during proictal states result from the alignment of proictal factors together with the occurrence of random perturbations [159].

Proictal factors

In addition, the transition to an ictal state can be conditioned by proictal factors (see Figure 3.4). Namely, circadian and multidien (weekly and monthly) rhythms of seizures and interictal epileptiform activity may help explain the occurrence of peaks of seizure susceptibility [12, 65, 66, 159, 185]. These cycles of brain activity might be in phase with the sleep-wake cycle, the cortisol levels, or cyclic oscillations of other non-neurological parameters such as HR, body temperature, blood pressure, and blood oxygen levels [12, 23, 65, 66]. Hence, correctly identifying periods of increased seizure risk is critical to the success of seizure forecasting (refer to Section 3.5 for more information on this topic).

Practical implications for the patient

With seizure forecasting comes a shift in the prediction horizon, which has a different impact on the patient's life. In seizure prediction, the patient is informed that a seizure will occur within a given time interval (minutes to hours). With this information, the subject can prepare himself for the upcoming event or take on-demand medication that promptly prevents the seizure. Under a seizure forecasting perspective, the patient is informed that there is an increased risk of seizure occurrence within, e.g., the next three days. Under such a forecasting horizon, the patient may opt for the administration of a benzodiazepine during the period of high seizure risk. By targeting optimal medication timing (chronotherapy), it might be possible to reduce the chances of habituation and dependence caused by chronic medication [159, 185].

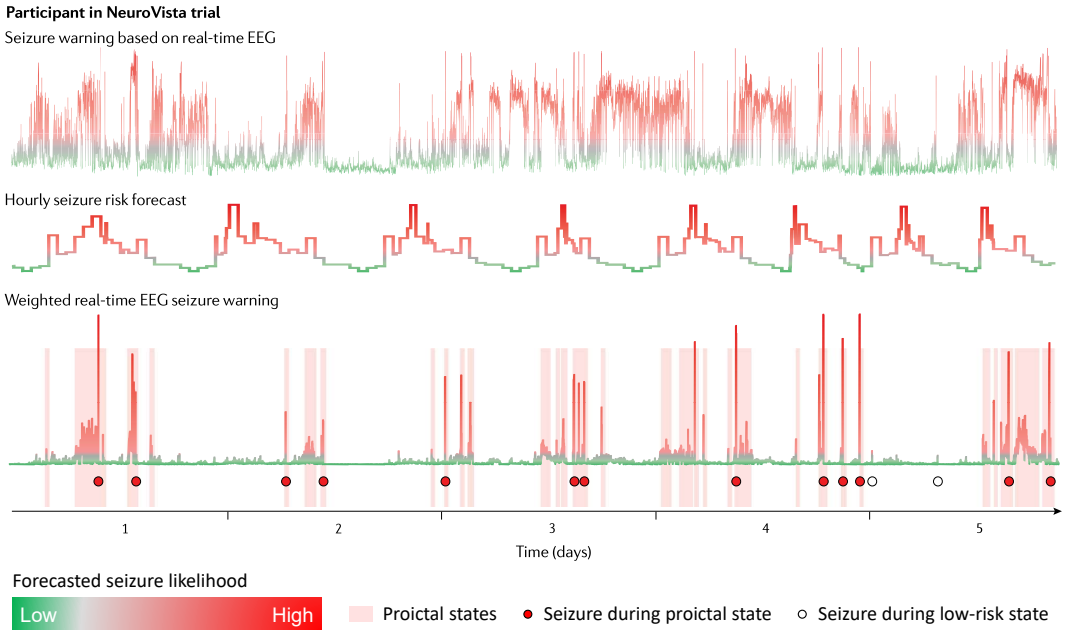

Figure 3.4: Example of seizure forecasting. Intracranial EEG data were collected during the NeuroVista trial. The top trace corresponds to the seizure warning resulting from using only real-time EEG-based prediction. The second trace shows the hourly circadian profile of seizure risk updated for each seizure timing. The bottom trace shows the seizure warning resulting from weighting the real-EEG prediction with the prior hourly seizure risk. Source: Karoly *et al.* 2021 [65].

Combining preictal and proictal information

Combining prediction and forecasting frameworks has been suggested to account for the multiple timescales of epileptic brain activity. First, there is a proictal estimation within the scale of hours to days based on identifying circadian and multidien cycles. Second, by taking into account these forecasted prior probabilities, a preictal state might be identified in the minutes to hours preceding each seizure onset [65, 68, 159, 161]. By combining both approaches, it might be possible to consider the multiple timescales manifesting epileptic activity [161].

Interestingly, a pseudo-prospective study presenting a seizure prediction algorithm based on EEG features showed an increase in performance when incorporating information about seizure risk (given by the circadian seizure distribution) [17].

Recent main findings

Some general conclusions can be extracted from studies detailed in Table 3.10. Pseudo-prospective forecasting studies taking into account circadian and multidien rhythms lead to higher forecasting performance. Prediction horizons typically vary from approximately 12 minutes to three hours. When testing different forecasting horizons [68, 148], shorter horizons result in better than chance forecasting for more patients.

3.5 Concept drifts

Following the previous section, literature findings regarding the existence of concept drifts and their influence on seizure prediction and forecasting performance are presented hereafter.

Concept drifts can manifest, for instance, as a result of medication changes during presurgical evaluation (incremental drift), accompanying circadian cycles or vigilance states (reoccurring drift), as a consequence of implanting a neurostimulation device (incremental drift), and/or following a switch in laterality of the seizure onset (sudden drift) [158].

Depending on the type of concept drift, different options may be considered to tackle such changes in signals' statistics or target distribution. For instance, a gradual drift characterised by the temporal sequence of two concept drifts (see Figure 2.17 in the Background chapter) may be addressed by training two classifiers for each concept. Incremental drifts might be dealt with by continuously retraining the classifiers. Reoccurring drifts might be addressed similarly to gradual drifts by training different classifiers for each of the drifts. For instance, train a classifier for each vigilance state. Another option is to compute a state detector that can later weight the seizure prediction classifier [158].

Over the last 10 years, several studies have been conducted towards identifying cyclical patterns of seizure occurrence manifesting over different timescales, including circadian, multidien and circannual. Such patterns were first observed in the frequency of seizures of some patients: seizure diaries indicate higher seizure incidence at specific times of day, days of the month and even during certain seasons of the year. Then, the analysis of long-term EEG also provided evidence for the existence of IEA following circadian organisation [65, 266]. Table 3.11 presents results for the most relevant and comprehensive studies on seizure cycles.

Seizure cycles based on seizure recurrence

Seizure diaries have been long used to uncover seizure cycles. The patient self-reporting of seizure times is now facilitated by the development of online diaries (e.g., the SeizureTracker) and mobile applications. The high percentage of identified circadian cycles, more than 80% [52, 160], should, however, be carefully interpreted due to the limitations and biases of individual self-reporting [48, 266].

The annotation of electrographic seizures can mitigate such biases [266]. Circadian cycles have also been identified in seizure counts obtained from chronic EEG, with a prevalence ranging from 86% to 92% [49, 67, 160]. This fact may advocate for the non-random occurrence of seizures and the consequent implication of the inter-seizure intervals not simply following a Poisson distribution [159, 171].

The sleep-wake cycle may also explain the frequency of seizures observed over 24

Table 3.11: Studies on seizure occurrence cycles in epilepsy.

Study	Patient data	Seizure cycle prevalence
Karoly *et al.*, 2018 [160]	EEG seizures: 2-year spanning, 12 patients with drug-resistant focal epilepsy (NeuroVista study) Self-reported seizures: 9-year spanning, 1118 patients (SeizureTracker)	Circadian cycles: at least 80% of SeizureTracker patients and 92% of NeuroVista patients. Circaseptan (weekly) cycle: between 7% (77 of 1118) patients and 21% (233 of 1118) patients.
Baud *et al.*, 2018 [67]	37 patients with drug-resistant focal epilepsy with EEG (NeuroPace).	Circadian cycles: 86% (12 out of 14) patients. Multidien cycles: 93% (13 out of 14) patients. Circadian and multidien cycles may equally influence seizure timing. Seizures predominate in the rising phase of mutidien IEA cycle.
Ferastraoaru *et al.*, 2018 [52]	Self-reported seizures, spanning up to more than 8 years, from 10 186 patients (SeizureTracker) with different epilepsy syndromes	Circadian pattern: higher seizure frequency between 07:00 a.m. and 10:00 a.m. and lower overnight. Multidien pattern: different weekly seizure reporting (higher seizure frequency on Monday through Friday than Saturday or Sunday).
Leguia *et al.*, 2021 [49]	222 patients with drug-resistant focal epilepsy: 194 patients with only seizure diaries; 186 patients with seizure diaries and EEG (NeuroPace) and 85 patients with only EEG (NeuroPace).	Circadian cycles: 89% (76 of 85) of patients. Multidien (about-weekly to about-monthly) cycles: 60% (112 of 186) of patients. Circannual (about 1 year) cycles: 12% (24 of 194) of patients.
Karoly *et al.*, 2021 [217]	31 patients with drug-resistant epilepsy and 15 healthy controls (Tracking Seizure Cycles study). Heart rate obtained with smartwatch (PPG)	Heart rate cycles in all epilepsy/control subjects: circadian (N=31/15), about-weekly (N=17/8) and about-monthly (N=9/4).

PPG: photoplethysmography.

hours in some types of seizures (see Figure 3.5). For instance, seizures experienced during sleep are more frequent in patients with focal epilepsy than in patients with generalised epilepsy. Increasing evidence also suggests that seizure occurrence is

probably more influenced by the vigilance state than by the time of day [185]. In fact, in focal epilepsy, focal lobe seizures often occur during sleep (during the day and night), whereas seizures with temporal lobe onset may occur according to the circadian rhythm, regardless of the vigilance state. Occipital and parietal lobes lack sufficient data to achieve robust conclusions [65, 185].

Observations at the population level show that peaks of seizure occurrence often coincide with sleep-wake transitions (late evening and early morning). Nevertheless, the sleep-wake cycle not always explains seizure frequency around specific times of the 24-h period, suggesting a tight coupling with the circadian cycle [65, 266]. For instance, some patients suffering mainly from diurnal seizures show a peak in seizure frequency in the afternoon. Additionally, the sequence of NREM and REM sleep stages may not explain that patients diagnosed with sleep-related epilepsy verify high seizure incidence at the beginning and/or end of the sleep period [65].

In sum, both the circadian and sleep-wake cycles seem to modulate the pattern of seizure occurrence. Interestingly, seizures do not always occur at every circadian cycle, suggesting that there are no sufficient conditions for ictal transition despite the existent propensity for seizure triggering [65].

Seizure cycles based on interictal epileptiform activity

Increased IEA can also be observed during the sleep stage of the sleep-wake cycle, with the NREM sleep verifying the highest IEA predominance compared to REM sleep (regardless of the seizure onset location) [65, 185, 268]. Besides being predominantly modulated by the sleep-wake cycle, the IEA shows a consistent daily circadian modulation [65]. IEA also oscillates over subject-specific multidien cycles, with seizures occurring predominantly during the rising phase of the multidien IEA

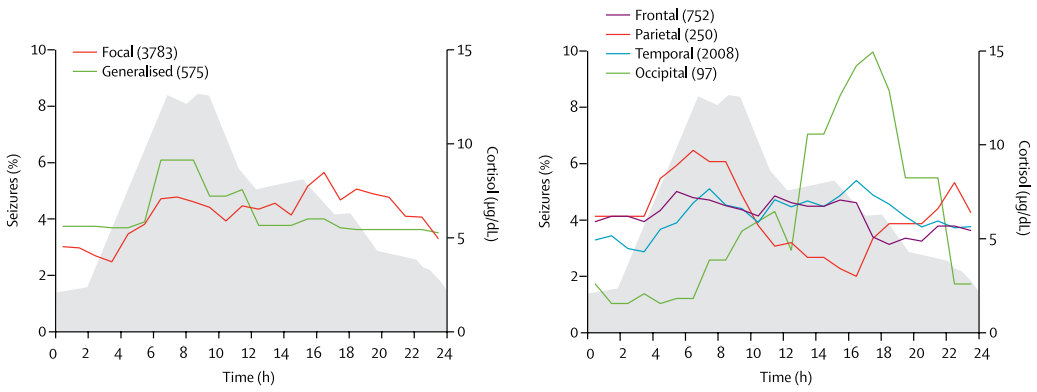

(a) **(b)**

Figure 3.5: Seizure frequency over 24h. The circadian seizure frequency is displayed along with the standard curve of plasma cortisol concentration (in grey). (a) Seizure frequency for focal onset and generalised onset. (b) Seizure frequency for the different lobes of origin in focal seizures. The figures were obtained from a systematic review of 15 studies [267]. The numbers in brackets correspond to the number of each seizure type. Source: Khan *et al.* 2018 [185].

cycles [67].

Prediction studies considering concept drifts

Information on the identified circadian rhythms of seizure occurrence has been used to leverage seizure prediction performance.

Schelter *et al.* [170] analysed the rate of false predictions over the sleep-wake cycle for two threshold-based seizure prediction algorithms (a mean phase coherence and a dynamic similarity index). Models were developed using a dataset comprising intracranial EEG records (each lasting 24 to 26 hours) from 21 patients with drug-resistant focal epilepsy undergoing presurgical monitoring. They found that 86% and 68% of the false predictions returned by the dynamic similarity index and the mean phase coherence predictors, respectively, occurred while patients were asleep. When considering the information on the sleep-wake cycle (awake and sleep states) for developing the dynamic similarity index predictor, the number of false positives was reduced by 50% while maintaining seizure sensitivity.

Karoly *et al.* [17] also studied the impact of the circadian cycles on prediction performance. The analysed data comprise intracranial EEG records (lasting on average 320 days) collected with an implantable seizure warning device (NeuroVista) from nine patients with focal onset seizures. The authors evaluated the performance of two logistic regression classifiers, each with and without considering prior information on the circadian rhythm of seizure timing. An increase in seizure prediction performance was observed when accounting for the circadian seizure distribution.

Kiral-Kornek and colleagues [239] proposed another solution to handle the presence of concept drifts. They analysed intracranial EEG data acquired over about 16 years (NeuroVista cohort) and chose to retrain their prediction models every new month. The retraining interval was defined according to each patient's seizure rate (90 days for some patients and 30 days for the remaining). The ability of the models to automatically re-adapt over time evidenced the advantages of using DL architectures. Authors, however, recognise that training DL prediction models can be challenging due to the small number of seizures experienced by some patients.

3.6 Summary

The transition from interictal to preictal state might occur as an abrupt random perturbation or as a result of a gradual change in the system that turns it more susceptible to small perturbations. In the second scenario, the system might exist in an identifiable preictal state or in a multistate that includes a preictal state.

Seizure prediction models are highly dependent on the correct identification of pre-seizure patterns. Such patterns have been shown to vary among patients and among seizures experienced by the same patient. Supervised seizure prediction mod-

els may compromise future prediction performance by assuming a fixed preictal interval for all patients. This assumption likely does not address inter- and intra-patient variability inherent to the ictogenesis process.

The normal functioning of the autonomous nervous system has been reported to change before, during and after an epileptic seizure. Accordingly, the research community has directed efforts towards the analysis of noninvasive, easy-to-record signals that have prediction potential. Cardiac parameters have been receiving special attention, with results showing evidence of preictal heart rate variability alterations.

The occurrence of false positives in seizure prediction may be explained in light of a forecasting perspective. Accordingly, perturbations of the system may not be strong enough to drive the system across the threshold. As such, alterations of brain activity may be captured in the EEG indicating that the brain was in a proictal state during which there is a higher probability of seizure occurrence. The seizure generation process occurring in a proictal state may be stopped by other brain mechanisms.

Lastly, the analysis of long-term ambulatory recordings imposes the development of seizure prediction models able to deal with the presence of concept drifts. Alterations in raw data or extracted features should be addressed as these might result from the influence of circadian rhythms in physiological processes. As such, the assumption that seizures randomly occur is contradicted by the evidence of cycles of epileptic activity manifesting at multiple timescales.

Chapter 4

Dataset description

This chapter provides information on the data analysed in this thesis, to avoid repeating information in the next chapters. The details concerning the source of the dataset, the EPILEPSIAE database, are provided in Section 4.1. Sections 4.2, 4.3 and 4.4 describe the dataset under analysis, including patient and seizure metatada, respectively. An explanation concerning the choice of the seizure prediction horizon (SPH) interval considered throughout the thesis is also provided in Section 4.5.

4.1 The EPILEPSIAE database

The dataset used in this study was selected from the European Epilepsy Database, also known as the EPILEPSIAE database (www.epilepsy-database.eu) and created on behalf of the FP7 EPILEPSIAE project (www.epilepsiae.eu).

The database contains long-term and simultaneously acquired electroencephalography (EEG) and electrocardiography (ECG) recordings from patients with drug-resistant epilepsy (DRE) undergoing presurgical monitoring at the epilepsy centres of Epilepsiezentrum, Universitätsklinikum Freiburg (Germany), Centro Hospitalar e Universitário de Coimbra (Portugal), and Hôpital de la Pitié-Salpêtrière, Paris (France) [28, 29]. The dataset also contains a vast amount of information regarding patient etiologies and medication and seizure characteristics (including classification, vigilance state and EEG and clinical onset times). Whenever seizure onset is mentioned throughout this thesis, it refers to the seizure EEG onset.

Data acquisition and further research use were approved by the local ethics committees of the three hospitals involved in the database development (Ethik-Kommission der Albert-Ludwigs-Universität Freiburg; Comité consultatif sur le traitement de l'information en matière de recherche dans le domaine de la santé, Hôpital de la Pitié-Salpêtrière; and Comité de Ética do Centro Hospitalar e Universitário de Coimbra). Informed consent was obtained from patients and the parents and/or legal guardians of patients under 18 years of age. All methods were performed

following the relevant guidelines and regulations.

4.2 Analysed dataset

From the EPILEPSIAE database, a group of patients with temporal lobe epilepsy (TLE), was selected for analysis in the present thesis. This choice was based on two facts: (i) TLE is the most frequent type of focal epilepsy in adults [46] (and thus the predominant temporal lobe in EPILEPSIAE) and (ii) disturbances in the autonomous nervous system (ANS) manifest predominantly in patients suffering from seizures originating from the temporal lobe. Most of the structures responsible for autonomic cardiovascular regulation are localised to the same cranial region [21]. Additionally, the dataset comprising data from 41 patients with DRE (24 males; age range: 13-67 years; mean age: 41 ± 15 years) was collected at the Epilepsiezentrum, Universitätsklinikum Freiburg. Patient data contains scalp EEG and ECG signals recorded simultaneously and sampled at 256 Hz. Scalp EEG data was obtained from 19 electrodes (Fp1, Fp2, F7, F3, Fz, F4, F8, T7, C3, Cz, C4, T8, P7, P3, Pz, P4, P8, O1, and O2) were analysed. ECG data was acquired using only one electrode. A total of 388 seizures were annotated in this group of patients.

4.3 Patient metadata

Table 4.1 contains information regarding the group of patients with temporal lobe DRE analysed in this study. The table includes information on sex, age at hospital admission and onset age (corresponding to the occurrence of the first epilepsy event), epilepsy foci lateralisation, the total number of annotated seizures and the number of seizures analysed for each patient (lead seizures), according to the considered minimum inter-seizure interval.

4.4 Seizure metadata

Table C.1 in Appendix C contains a description of metadata collected for each analysed seizure. This information, available in the EPILEPSIAE database [28, 29], was annotated by experienced professionals by inspecting both video and EEG data. The table then includes information about seizure type, vigilance state determined 10 seconds before the seizure onset, and EEG onset time over the 24h period. Seizures were classified according to the International League Against Epilepsy (ILAE) nomenclature [36]. The vigilance state corresponds to one of the following states of alertness and responsiveness: wakefulness, non-rapid eye movement sleep (NREM sleep, further subdivided into three sleep stages N1–3) and rapid eye movement (REM) sleep [65]. Information about the seizure type, vigilance state and EEG onset time is also depicted in Figure 4.1.

P	ID	Sex	Onset Age (years)	Admission Age (years)	Lat.	#Sz	#LSz ECG	#LSz EEG
1	402	F	10	55	L, R	5	5	5
2	8902	F	23	67	L	5	5	5
3	11 002	M	21	41	R	8	5	4
4	16 202	F	43	46	L, R	8	7	7
5	21 902	M	44	47	L	6	4	4
6	23 902	M	36	36	L	5	5	5
7	26 102	M	15	65	L	8	4	4
8	30 802	M	28	28	L, R	9	8	8
9	32 702	F	33	62	L, R	6	5	5
10	45 402	F	13	41	L, R	5	4	4
11	46 702	F	13	15	R	5	5	5
12	50 802	M	2	43	L	5	5	5
13	52 302	F	13	61	L	7	5	4
14	53 402	M	0	39	L, R	8	5	4
15	55 202	F	3	17	R, B	9	8	8
16	56 402	M	18	47	L, R	7	6	4
17	58 602	M	17	32	L	22	7	6
18	59 102	M	17	47	R	7	5	5
19	60 002	M	47	55	L, R	8	6	6
20	64 702	M	3	51	R	6	5	5
21	75 202	M	10	13	R	8	7	7
22	80 702	F	14	22	B	10	7	6
23	81 102	M	5	41	R	13	5	3
24	85 202	F	4	54	L	10	5	5
25	93 402	M	40	67	L	7	5	5
26	93 902	M	43	50	R	9	6	6
27	94 402	F	29	37	R	11	7	7
28	95 202	F	13	50	L	14	7	7
29	96 002	M	21	58	L, R	9	7	7
30	98 102	M	2	36	L	5	5	5
31	98 202	M	3	39	R	10	7	7
32	101 702	M	44	52	L, R	6	5	5
33	102 202	M	0	17	L	28	7	7
34	104 602	F	8	17	L	5	5	5
35	109 502	M	40	50	L, R	10	5	4
36	110 602	M	6	56	R	8	5	5
37	112 802	M	47	52	L	6	6	6
38	113 902	F	16	29	R	25	7	6
39	114 702	F	31	22	R	25	9	8
40	114 902	F	15	16	L, R	12	7	7
41	123 902	F	7	25	L, R	8	5	5
Mean			19	41		9	6	6
SD			15	15		6	1	1
Total						388	238	226

P: patient index. ID: patient identifier. Sex: female (F) or male (M). Lateralisation (Lat.): L: left, R: right, B: bilateral. #Sz: total number of seizures annotated per patient. #LSz: number of leading seizures, obtained as a result of the analysis of 4 and 4.5 hours of inter-seizure ECG and EEG data, respectively. SD: standard deviation.

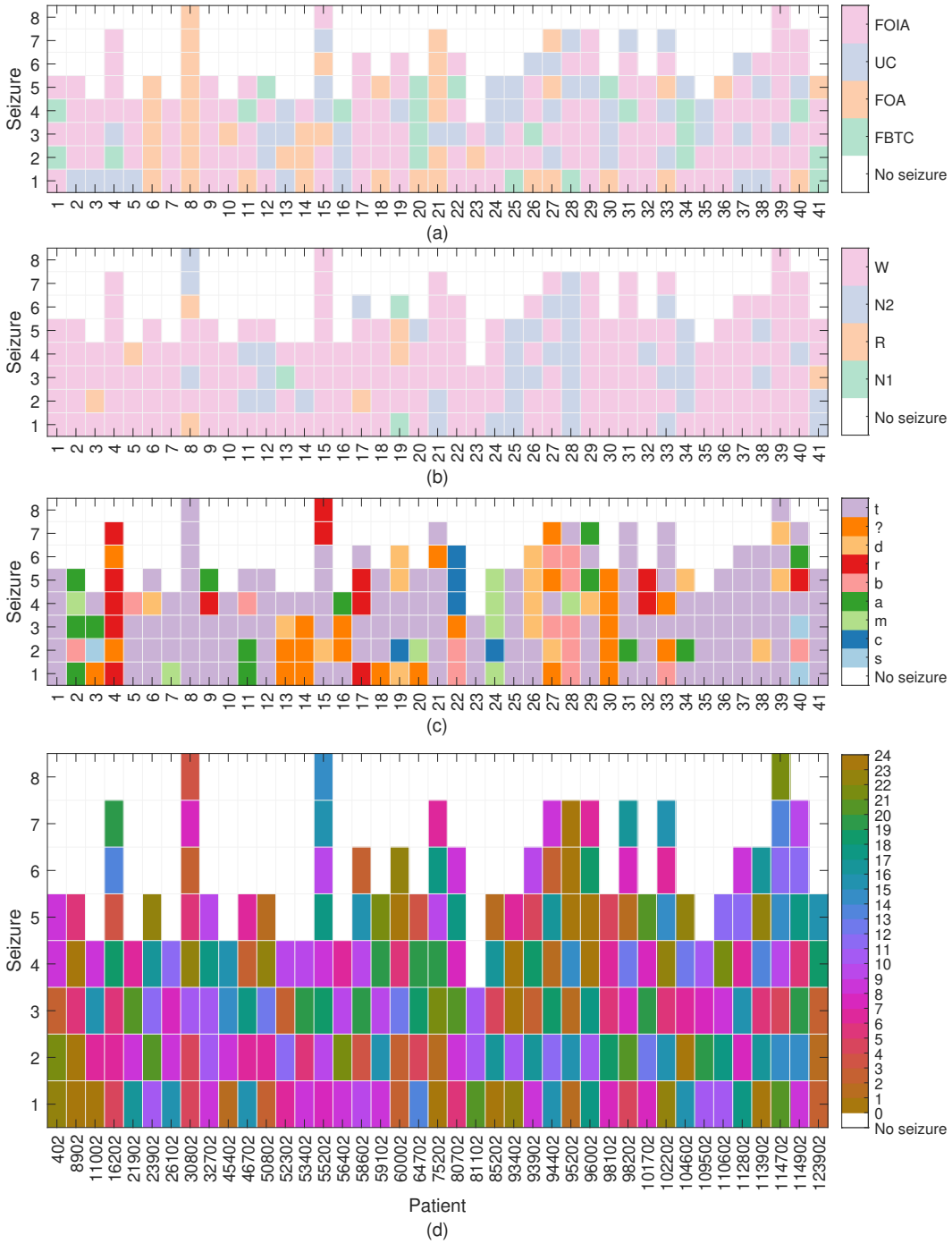

Figure 4.1: Information regarding each seizure in the group of patients selected for this study. (a) Seizure ILAE classification: focal onset aware (FOA), focal onset impaired awareness (FOIA), focal to bilateral tonic-clonic (FBTC) and unclassified (UC). (b) Seizure vigilance state: W: wakefulness, R: REM sleep stage, N1: NREM sleep stage I, N2: NREM sleep stage II. (c) Seizure activity pattern: rhythmic alpha waves (a), rhythmic beta waves (b), cessation of interictal activity (c), rhythmic delta waves (d), amplitude depression (m), repetitive spiking (r), rhythmic sharp waves (s), rhythmic theta waves (t), unclear (?). (d) Seizure onset hour across the 24-hour day.

4.5 The seizure prediction horizon

The duration of the SPH, set to 10 minutes in this study [150, 153, 157], was defined according to the future clinical application. Since scalp EEG data were being analysed, the treatment strategies were limited to (i) acute drug administration to prevent an imminent seizure or (ii) the patient taking action to avoid accidents resulting from seizure occurrence. As addressed in Section 2.4.4, rescue medication takes effect at most five to ten minutes after administration (as is the case of diazepam rectal gel).

Treatment strategies requiring the intracranial device implantation to deliver brain electrical stimulation typically define SPH intervals of a few seconds. However, given the considerable differences between scalp and invasive EEG, neurostimulation was not considered in the range of future applications [147, 165]. A longer SPH interval of 10 minutes was then defined so that, when envisioning future studies, seizure prediction models enable the patient to have enough time, after receiving the alarm, to prepare for an upcoming seizure [147].

Chapter 5

Unsupervised preictal activity search: an ECG-based approach

This chapter presents the search for preictal patterns on the electrocardiography (ECG) data using unsupervised methods. It is worth noting that this was the first study conducted in this PhD. The reason behind this choice is that, firstly, the ECG is a fairly well-behaved signal compared to the electroencephalography (EEG), which is far more complex and difficult to interpret. Secondly, literature already presented standalone studies on the heart rate variability (HRV) data in the context of epilepsy which then would allow for a fruitful discussion of the results.

The content of this chapter is based on a journal article published in *Scientific Reports* [155]. Section 5.1 presents a brief context of this study. Section 5.2 contains the methodology developed here. Sections 5.3 and 5.4 report and discuss the findings of this study, respectively.

5.1 Study context

As addressed in state-of-the-art Section 3.2, in addition to the pre-seizure brain manifestations captured in the EEG, it might also be possible to observe non-neurological preictal alterations. Given the anatomic proximity of the autonomous nervous system (ANS) structures to the temporal lobe, cardiac parameters such as heart rate (HR) and HRV have been reported to capture heart rhythm oscillations in seizures typically occurring in patients with temporal lobe epilepsy (TLE) [96]. The emergence of such extracerebral alterations across the pre-, post- and ictal periods [19–21, 93], concurrent with EEG profile changes, has prompted the acquisition of other biosignals, namely, ECGs, for performing seizure prediction [216]. This growing interest by the scientific community can be explained by the advent of wearable devices that allow the continuous acquisition of physiological signals in a more comfortable and user-friendly mode for the patients [21, 216].

Despite the increasing number of studies documenting seizure detection and prediction models based on other modalities, established evidence for the use of non-EEG wearable systems has only been reported for the detection of generalised tonic-clonic seizures [43, 130, 140]. The potential of extracerebral information to detect or predict focal seizures remains largely unexplored. Specifically, there are only a few studies reporting the use of HRV alone to develop seizure prediction models [222–225]. Of these, only one study provides a comprehensive analysis of HRV indices and demonstrates some concerns on the appropriate validation of the prediction model [224]. Additionally, although unsupervised learning methods have already been considered to inspect preictal changes in EEG data [253–256], there is only one study that has attempted to inspect the existence of preictal activity in the RR interval series using fuzzy clustering [219]. Even though the scarcity of the aforementioned studies might be related to the difficulty in interpreting the source of the altered ECG trace, the current effort to develop wearable devices based on non-neurological data demands for appropriate assessment of their prediction potential [12].

Based on the above, the present study was designed to provide a deeper understanding of the preictal period using easy-to-record information from HRV. First, 32 HRV features were extracted from 5-minute windows located until four hours before seizure onset [236, 269]. Second, different clustering methods were applied to all three-feature combinations of the HRV features to identify and characterise a seizure-specific preictal interval in the two hours preceding seizure onset.

5.2 Methodology

The next sections comprise all steps conducted towards the identification of preictal patterns in HRV data. ECG data were collected from patients with drug-resistant TLE, undergoing presurgical monitoring (as described in Chapter 4). Figure 5.1 presents the flow diagram of the proposed methodology. The ECG signals were firstly preprocessed to identify data segments not containing noise. The HRV was computed using the information on the R-peaks. Afterwards, different clustering methods were applied to the three-dimensional combination of the extracted HRV features. The obtained clustering solutions were inspected regarding the presence of the preictal state. Whenever a small cluster occurred in two-cluster solutions, it was assumed that it corresponded to a preictal interval that was later characterised in terms of starting time, duration and time continuity.

All calculations were performed in MATLAB R2019b, running on WINDOWS 10 Pro with an INTEL Core i7-4790K CPU at GHz and 32 GB RAM. The MATLAB source code developed for this study is publicly available on GitHub via adrianaleal/HRV-Preictal-Identification-Epilepsy.git.

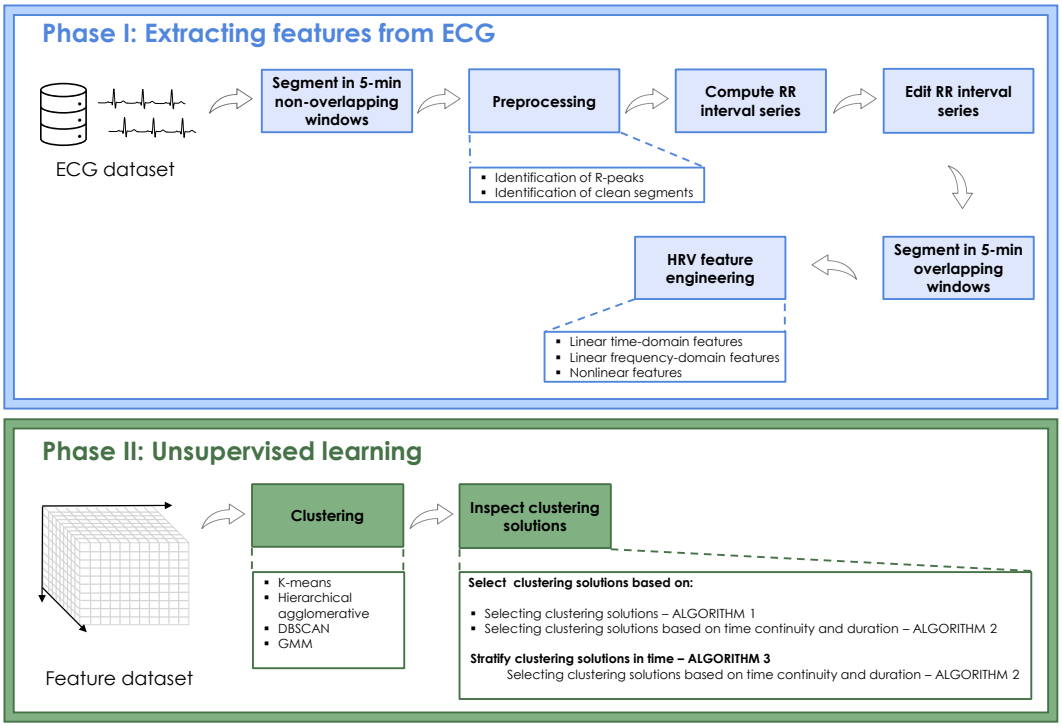

Figure 5.1: Block diagram of the proposed methodology. The study started by preprocessing the ECG signals, followed by RR interval series computation and editing and, lastly, HRV feature extraction. The study's second phase consisted in applying unsupervised learning methods to the feature dataset followed by preictal interval inspection.

5.2.1 Lead seizures

To investigate the existence of a preictal period before seizure onset, only the four hours (240 minutes) preceding the seizure event were analysed. It was assumed that seizures separated by at least 240 minutes were considered independent events [134, 152, 154]. As a result, 150 seizures separated by less than 240 minutes were discarded from a total of 388 seizures, leading to the 238 seizures considered in this study.

5.2.2 ECG signal preprocessing

The ECG preprocessing started by applying a 50 Hz notch filter to each 5-minute non-overlapped windows of data. Next, the Discrete Wavelet Transform was used to extract information on the frequencies up to 45 Hz.

Afterwards, an R-peak detection method, based on the Pan & Tompkins algorithm [270], was used to obtain the intervals between subsequent R-peaks (or RR intervals), yielding the RR interval series. The latter was then edited by identifying and correcting abnormal RR intervals.

These steps are thoroughly described in Appendix D Section D.1.

5.2.3 HRV feature engineering

Linear time- and frequency-domain and nonlinear measures were extracted from 5-minute HRV windows (see Table 5.1) [92, 271, 272]. Section D.2 in Appendix D includes additional details on how each feature was obtained. From the feature engineering step (see Figure 5.1), a three-dimensional matrix, $M(f, s, w) \in \mathbb{R}^3$, where

$f = 1 : F, \quad F = 32$ features;

$s = 1 : S, \quad S = 238$ seizures;

$w = 1 : W, \quad W = 2768$ 5-minute 98.33% overlapping windows.

An analysis of feature redundancy was performed using Pearson's correlation coefficient and average mutual information (refer to Section D.3). This analysis showed a strong agreement between both redundancy assessment methods regarding features capturing sympathetic and parasympathetic activity over the analysed 240 minutes preceding each seizure. From the wide range of measures extracted from the RR interval series, one may observe high redundancy among features capturing short-

Table 5.1: HRV-derived features.

Linearity/ Domain	Features
Linear/Time domain	• Number and percentage of RR intervals that last more than 50 ms (NN50 and pNN50); • Standard deviation of RR intervals (SDNN); • Square root of the mean squared differences of successive RR intervals (RMSSD); • Standard deviation of the differences between successive RR intervals (SDSD); • Minimum, maximum, mean and variance of the RR intervals (RRMin, RRMax, RRMean and, RRVar).
Linear/Frequency domain	• Total power; • Very low frequency (VLF) power; • Low frequency (LF) and high frequency (HF) powers and the ratio between the two features (LF/HF); • LF norm and HF norm.
Nonlinear	• Standard deviation of length and width of the ellipse fitted to the Poincaré plot (SD_1 and SD_2) and the ratio between the two features (SD_1/SD_2); • Detrended fluctuation analysis (DFA) slope α_1 and α_2; • Approximate and sample entropies (ApEn and SampEn); • Largest Lyapunov exponent (LLE) and correlation dimension (CD); • Recurrence quantification analysis (REC, L, TT, DET, LAM, ENT, L_{max}).

term HRV oscillations (SDSD, SD_1, high frequency (HF) Power, NN50, pNN50 and RMSSD). In addition, very low frequency (VLF) Power and RRVar features (not yet associated with physiological interpretation, to the best of our knowledge) presented strong redundancy with features capturing overall variability (Total Power, SDNN and SD_2).

5.2.4 Unsupervised learning (Clustering)

The clustering task was conducted for all three-feature combinations from among the $F = 32$ feature dataset:

$c = 1 : C, \quad C = 4960$ combinations of three features resulting from C_3^F.

In this way, it might be possible to understand which features are more frequently present among the best clustering solutions and, therefore, by preserving the original semantics of the feature dataset, provide a simple interpretation of the clustering results. Additionally, the probability of discovering interesting solutions was maximised by combining features three-by-three instead of only examining the two-dimensional feature space.

The following clustering methods were applied to each of the 4960 three-dimensional feature spaces:

1. K-means clustering (KM), a partitioning method typically successful in detecting spherically shaped and well-separated clusters.

2. Agglomerative hierarchical clustering (AH) is often used to identify structured clusters. Here, the distance between clusters was measured using the Ward method and the Euclidean distance metric [273].

3. Density-based spatial clustering of applications with noise (DBSCAN) is considered appropriate for identifying structured clusters while distinguishing noisy samples or outliers. Two parameters should be defined: the minimum number of samples in clusters, $MinPts$, and a radius Euclidean distance, ε, that allows the establishment of a neighbourhood among samples [274, 275]. Here, $MinPts$ was set to six, which is twice the dimensionality of the feature space according to Sander *et al.* [276]. Four different values of ε were tested after data normalisation and analysis of the k-distance plot (resulting in $DBSCAN_\varepsilon$, with $\varepsilon = 1$, 2, 3 and 4) [274].

4. Expectation-maximisation clustering using Gaussian mixture models (GMM) [277], applied by assuming clusters follow a Gaussian distribution and are therefore described by a mean and standard deviation (both parameters estimated using the expectation-maximization algorithm).

5.2.5 Searching for preictal patterns

The existence of a preictal interval, characterised by changes in HRV in the two hours before seizure onset, was investigated using unsupervised learning. It was assumed that the preictal state is mainly influenced by the cardiac changes observed within the 120 minutes before the seizure onset and that the data in the 240–120-minute interval would be representative of the interictal state. The screening of the 120-minute interval is supported by the literature (as addressed in Section 3.3.4).

In addition to the preictal interval duration, the present study also aimed to elucidate about the localisation of this interval. In other words, it was hypothesised that the preictal interval might not manifest for all features simultaneously but rather at different timestamps for distinct groups of features. Additionally, assuming the existence of a preictal brain state in different time windows for different groups of features, this state may only manifest over an interval separated from the seizure onset instead of strictly near the seizure event. This means that a cerebral trigger might be issued as an indication of the transition from the normal brain state (interictal) to an "abnormal, hypersynchronous ictal" state [35], which in turn can induce an abnormal state in the ANS. This trigger may be responsible for a short-term alteration in the feature values and may be expressed minutes to hours before seizure onset. Additionally, when translating this knowledge to the implementation of seizure prediction models, it might be ideally expected for the preictal interval to be located in the time preceding the seizure prediction horizon (SPH) (see Section 4.5 for more details). Given the potential to integrate the preictal interval in the seizure prediction methodology to allow for the patient or the caregiver to prepare for an upcoming seizure, optimally, the preictal interval should be found before this SPH interval [165]. In this work, an SPH of 10 minutes was considered suitable for a practical application [147, 150, 153, 157, 165].

The hypotheses mentioned above are reflected in the analysis of the results obtained after performing clustering on the feature dataset.

Selecting clustering solutions

This step was conducted under the assumption that the preictal interval can be represented by a single cluster, clearly separated from the remaining samples. Accordingly, the mandatory input argument defining the number of clusters in KM, AH, and GMM methods was set as $k = 2$, and clustering solutions with two clusters were selected among all DBSCAN clustering solutions. Additionally, given the higher probability of a preictal interval lasting less than an interictal interval, the smaller cluster found in each two-cluster solution represented the preictal interval. This interval may not occur strictly near the seizure onset but could be captured as an ECG-related event eventually preceding an EEG seizure onset. A visual representation of these assumptions is depicted in Figure 5.2.

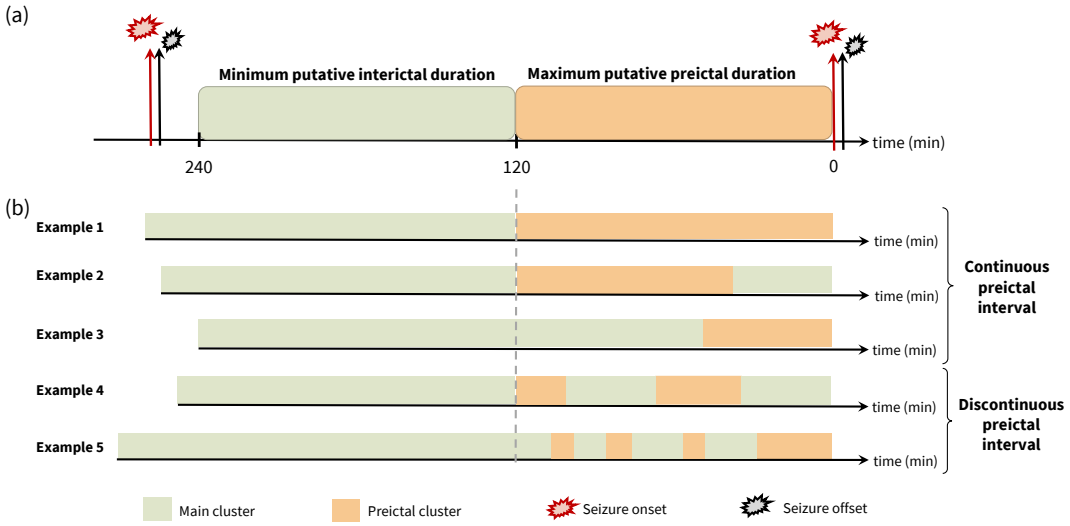

Figure 5.2: Examples of preictal location and duration along the 240 minutes of analysed HRV data. (a) Representation of two seizures separated by more than 240 minutes. (b) Some examples of clustering solutions containing continuous and discontinuous preictal clusters are presented.

Solutions containing noisy samples, sometimes returned by DBSCAN, were also discarded from the analysis. When the assumed preictal interval, corresponding to the smaller of the two clusters with the lowest number of samples (see Figure 5.3), was found to contain less than 1.58 minutes of information (less than 20 samples), it was also considered noise and therefore excluded from the results [278]. The clustering solutions previously obtained were then evaluated using Dunn's index (DI) [279]. Clustering solutions representing compact and well-separated clusters were characterised by high DI values. A minimum DI value was defined to accept a given clustering solution [280]. Specifically, if a solution presented a DI equal to or above 0.15 (defined according to Mahallati *et al.* [280] and by visual inspection of solutions across all patients), then it was assumed to identify a preictal interval. Lastly, clustering solutions were considered to contain a preictal pattern when the identified smaller cluster started after the 120 minutes of data recorded before the seizure onset. With this strategy, the initial set of 4960 clustering solutions, inspected for each seizure and clustering method, was drastically reduced by considering the aforementioned criteria for accepting solutions (see algorithm 1 in Appendix D Section D.4). Specifically, only 0.92% of the solutions were selected in this step.

Selecting clustering solutions based on time continuity and duration

Given that different feature combinations and clustering methods could yield more than one clustering solution, the solutions selected in the previous step were differentiated using two indicators: time continuity and duration (i.e., number of samples). The preictal interval was then classified (see algorithm 2 in Appendix D Section D.4) as continuous if the samples in the smaller cluster were sequential over time

and discontinuous otherwise.

The first criterion, time continuity, was considered by reasoning that a given clustering solution represented a preictal interval occurring continuously over time. If no time continuity was observed for the smaller cluster, it might indicate the existence of "jumps" from a preictal interval to an interictal state evolving towards seizure onset. In addition, solutions containing a continuous smaller cluster were selected over discontinuous clusters since a continuous preictal interval meant that a clearer and permanent change occurred before seizure onset.

When more than one solution was found (after selection by time continuity), and when those solutions comprised smaller clusters of different sizes, the solution for which the smaller cluster had the highest number of samples was chosen, as it provided more statistical confidence in the presence of a preictal state.

Stratifying clustering solutions in time and selecting clustering solutions based on time continuity and duration

Finally, another analysis was performed to provide quantitative information regarding the location of the assumed preictal interval (see algorithm 3 in Appendix D Section D.4). To this end, the timing of the samples defining the smaller cluster was registered and stratified into the following intervals: 120 to 80 minutes, 80 to 40 minutes and 40 to 0 minutes before seizure onset. This analysis aimed at quantifying the number of clustering solutions comprising a smaller cluster (assumed as the preictal interval) starting in one of the three 40-minute intervals near the seizure. When more than one solution was found for each interval, algorithm 2 was applied to select the clustering solutions according to time continuity and duration.

5.3 Results

Figure 5.3 depicts an example of the clustering solutions returned for patient 5. Evidence of a preictal interval was found for three of the four seizures; the interval was continuous over time for the second and fourth seizures. For this patient's first seizure, it was not possible to find clustering solutions complying with the conditions of the first selection process. In other words, for this seizure, there were no clustering solutions comprising a smaller cluster with a minimum of 20 non-noisy samples (or lasting for at least 1.58 minutes) and a cluster validity index, in this case, DI, over 0.15.

Selecting clustering solutions based on time continuity and duration

Figure 5.4 shows the clustering results obtained by selecting solutions according to time continuity and duration for the smaller cluster. Solutions were accepted for a total of 97 seizures out of 238 (41%). Additionally, 26 of the represented

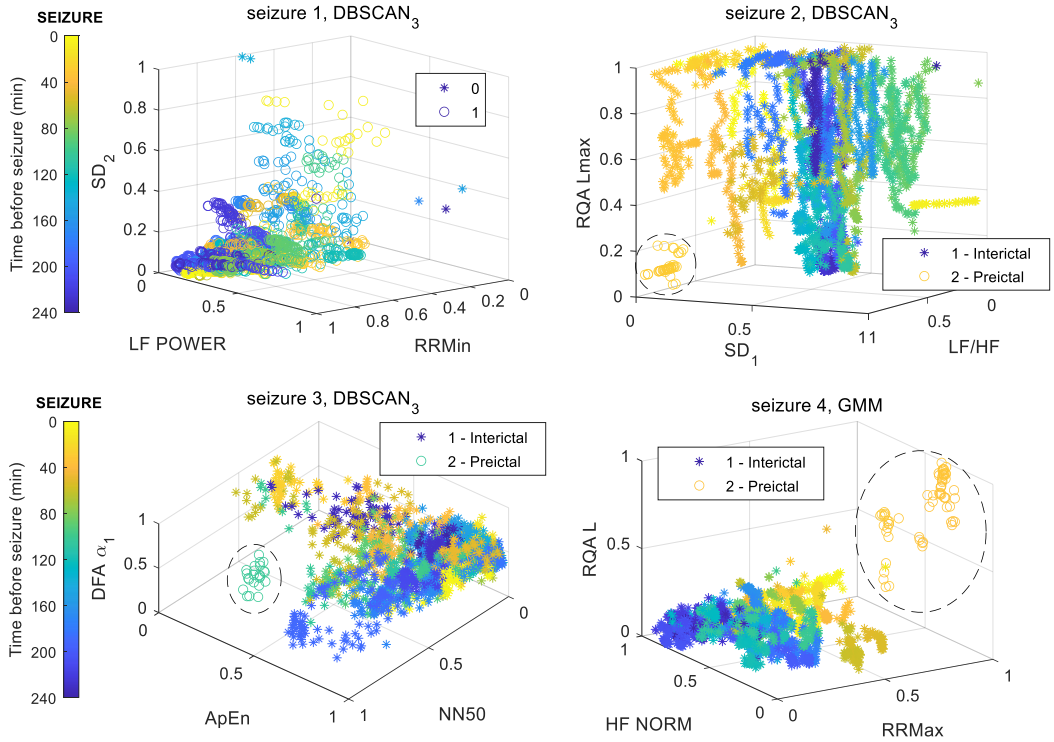

Figure 5.3: Representation of clustering solutions for patient 5. The smaller clusters (identified with dashed lines) found for the second and fourth seizures are continuous, lasting for 3.50 and 5.42 minutes (or comprising 43 and 66 samples), respectively. The smaller cluster for the third seizure is discontinuous and lasts for 1.83 minutes (i.e., 23 samples). The three accepted solutions (for the last three seizures) correspond to DI values of 0.1555, 0.1576 and 0.1585, respectively. No clustering solutions were accepted for the first seizure; a solution containing noisy samples was randomly selected and is represented here.

solutions contain a smaller cluster that occurred or just ended in the SPH interval of 10 minutes before seizure onset. Specifically, the putative preictal intervals (i) started and ended before the SPH interval for 71 seizures (30%), (ii) started and ended before and after the beginning of the SPH interval, respectively, for 24 seizures (10%) and (iii) started and ended in the SPH interval for two seizures (1%).

According to Figure 5.4, the smaller cluster can be characterised in terms of the starting time before seizure onset, duration, clustering methods used in its generation and time continuity (see Table 5.2).

In terms of time continuity, 52 solutions were continuous over time (54%). Additionally, the continuous smaller clusters were found to last from 1.58 minutes (20 samples) to 35.83 minutes (431 samples). The duration of discontinuous clusters usually fell in the range of 1.58 minutes (20 samples) to 80.75 minutes (970 samples). Among the clustering methods, DBSCAN_3, DBSCAN_2 and GMM returned the vast majority of accepted clustering solutions (34%, 22% and 19%, respectively). Finally, the starting time of the smaller cluster demonstrates high variability. Therefore, to better quantify the smaller clusters' starting time, the solutions were stratified into three intervals, as described in the following section.

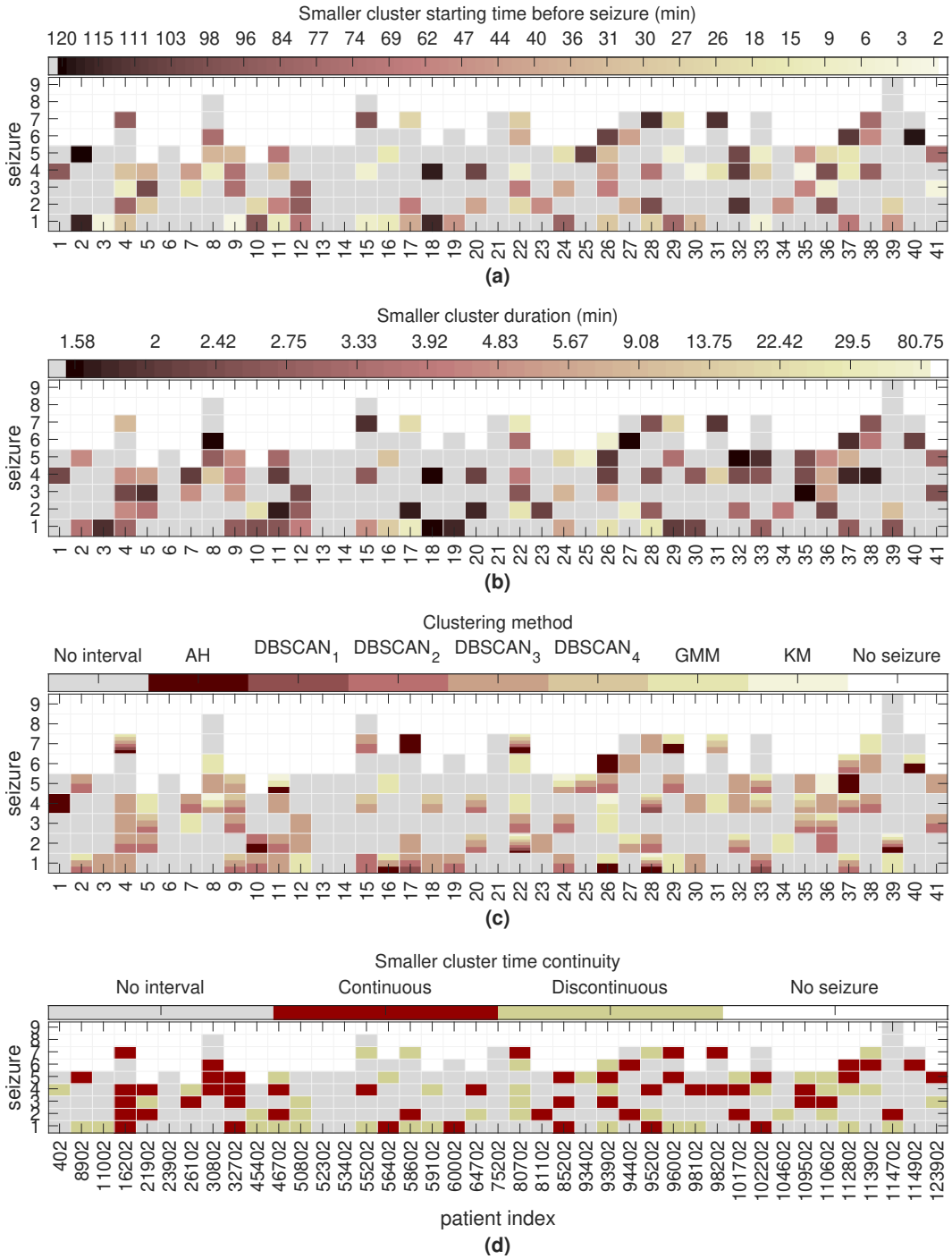

Figure 5.4: Results for the selection of clustering solutions based on time continuity and duration. The smaller cluster from the selected two-cluster solutions found for 97 seizures was characterised. The colours in the figure indicate (a) the smaller cluster starting time before seizure onset (0 minutes); (b) the duration of the smaller cluster; (c) the clustering methods returning the clustering solutions, and (d) the continuity over time of the smaller cluster (54% were continuous clustering solutions). See the colour scale for each subfigure. The x-axis and y-axis in all plots contain the patient and seizure indexes, respectively. For example, the clustering solution accepted for seizure 1 of patient 24 was returned by DBSCAN_2 and DBSCAN_3 and comprises a continuous smaller cluster that starts 84 minutes before seizure onset and lasts for 5.67 minutes.

Table 5.2: Preictal characterisation in terms of starting time and duration.

Condition	#Sz	%Sz	Starting time (min)		Duration (min)	
			Mean	SD	Mean	SD
Preictal intervals ending before SPH	71	30%	74.5	34.5	12.3	19.9
Preictal intervals ending before or after SPH starting time	95	40%	62.7	36.7	14.2	18.8
All preictal intervals	97	41%	61.6	37.1	13.9	18.7

#Sz and %Sz correspond to number and percentage of seizures, respectively, for which a preictal cluster has been found. SD: standard deviation.

Stratifying and selecting clustering solutions based on time continuity and duration

The clustering results were subsequently stratified into three 40-minute-long intervals occurring before seizure onset (120-80, 80-40 and 40-0). The results, presented in Figure 5.5, indicate that for 89 seizures out of 238 (37%), it was possible to find clustering solutions comprising a smaller cluster suggestive of the existence of a preictal interval. In fact, 15 solutions found in the previous subsection could not be stratified into the intervals considered. However, for seven of those seizures, other accepted solutions were found to fit in those intervals. These solutions contained a smaller cluster that was discontinuous and/or had a shorter duration than the solution selected in the previous subsection. No clustering solution fit in the 40-minute intervals for the remaining eight seizures.

Whereas no clustering solutions were found for any of the seizures from four patients, there were 12 patients for whom it was possible to determine solutions for 50% or more of the seizures. Additionally, 40–0-minute intervals were more prominent (found for 47 seizures, 53%) than the other two intervals (120–80-minute intervals found for 21 seizures, 28%, and 80–40-minute intervals found for 25 seizures, 24%).

The results were cross-checked with metadata provided by the EPILEPSIAE database, including the four variables characterising each patient: sex (male and female), epileptic focus lateralisation (right, left, and both hemispheres), age at hospital admission and age at the time of the first epileptic seizure (onset age). However, no correlation was found between the results and these variables, which, for the case of lateralisation, is in line with the literature [21, 93].

The metadata characterising each seizure were also analysed (see Figure 5.6 (a)-(c)). Seizures that occurred in the awake stage and focal onset impaired awareness (FOIA) seizures, were predominant among the accepted clustering solutions. However, seizures occurring when the patient was awake were the most frequent among

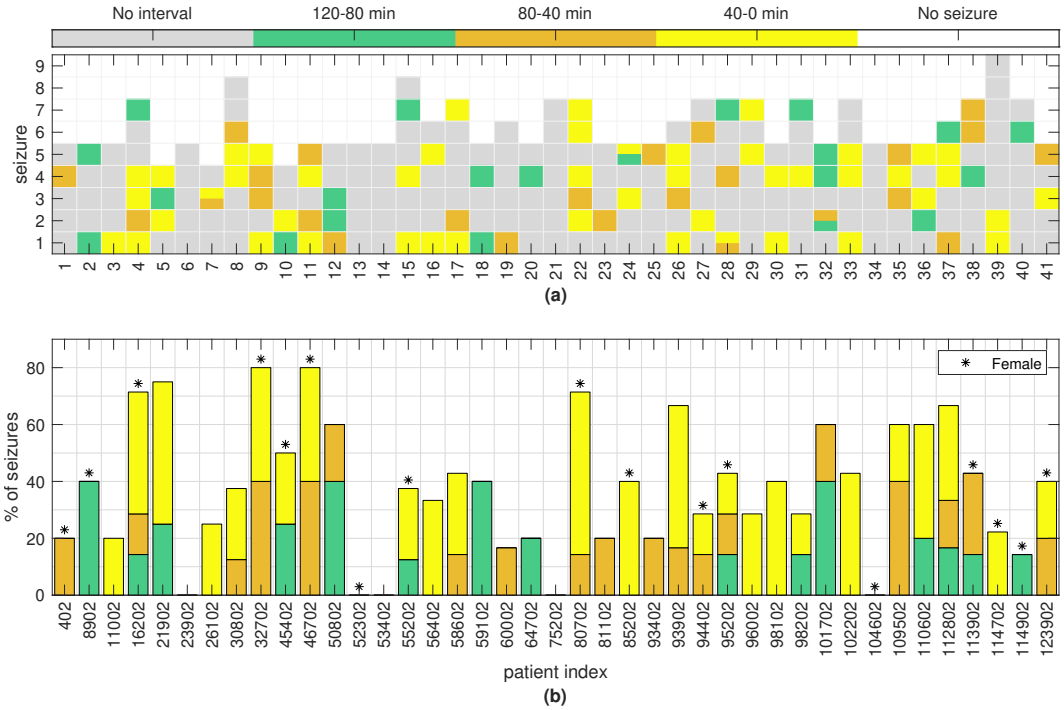

Figure 5.5: Results for the stratification and selection of clustering solutions based on time continuity and duration. (a) Information regarding the existence of clustering solutions for each patient (x-axis) and each seizure (y-axis, in chronological order) for the three different intervals considered: 120-80, 80-40 and 40-0 minutes before seizure onset (occurring at 0 minutes). There were four seizures (third seizure in patient 7, fifth seizure in patient 24, first seizure in patient 28, and second seizure in patient 32) for which clustering solutions were found in more than one interval. (b) The percentage of seizures for which at least one clustering solution was found is depicted for each patient and each 40-minute interval considered. An asterisk indicates female patients. It is important to note that when clustering solutions were found in more than one interval, the interval nearer the seizure was considered for computing the percentage for each patient in this subfigure.

all 238 seizures (76%). The same occurred with FOIA seizures, which were the most frequent type of seizure (50%). When interpreting the results according to the seizure onset time, no strong conclusion could be drawn, apart from a slight tendency for the seizures to occur early in the morning among those clustering solutions that were accepted, specifically for the 40–0-minute interval before seizures.

The smaller clusters observed among the two-cluster non-noisy solutions (assumed to represent preictal intervals) were further characterised in terms of the most frequent features and clustering methods, as shown in Figure 5.6 (d) and (f), respectively. All the obtained solutions were also analysed in terms of the duration and continuity of the smaller cluster (see Figure 5.6 (e) and (g), respectively). Here, it is important to note that the numbers on the axis for (d)-(g) do not add up to the number of seizures for which several clustering solutions were accepted (as occurs in (a)-(c)). In fact, for the same seizure, it was possible to find clustering solutions complying with the preictal interval requirements for different (i) 40-minute intervals (see patients 7, 24, 28 and 32 in Figure 5.5), (ii) clustering methods and (iii)

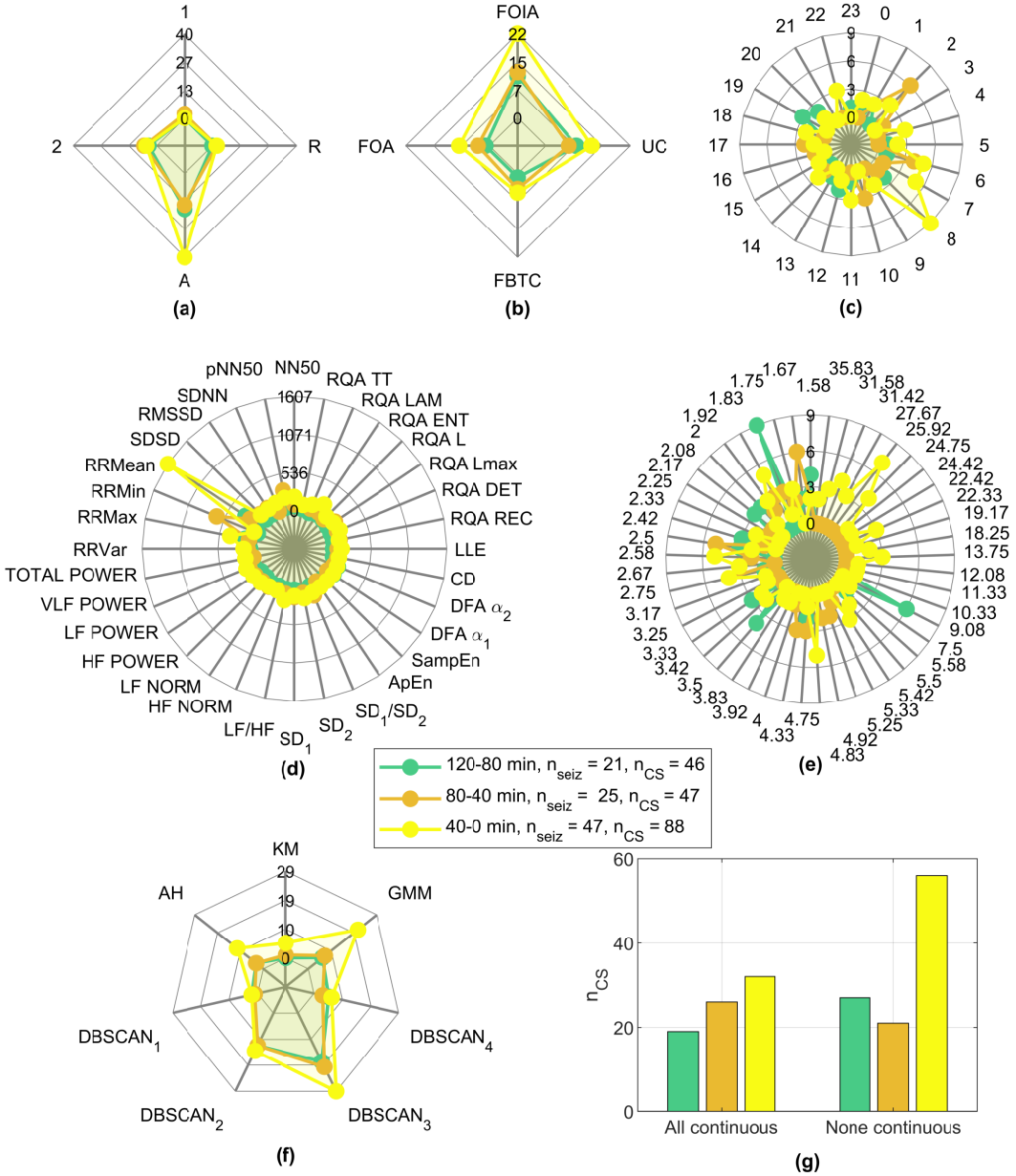

Figure 5.6: Characterisation of the clustering results for each 40-minute interval. (a) Seizure vigilance state (A: awake, 1: sleep stage I, 2: sleep stage II, R: REM sleep), (b) seizure type (FOA: focal onset aware, FOIA: focal onset impaired awareness, FBTC: focal to bilateral tonic-clonic, UC: unclassified), (c) seizure onset time, (d) most frequent features, (e) duration of the smaller cluster (minutes), (f) most frequent clustering methods and (g) time continuity of the smaller cluster ("All continuous" was assigned when all solutions found for that seizure were continuous and "None continuous" if no solution was continuous). n_{CS} indicates the number of clustering solutions found in each interval, including when more than one solution was found for each seizure.

feature combinations.

Regarding the features most frequently appearing in the accepted clustering solutions, it is clear that time-domain features such as RRMax, RRMin and RRMean are strongly predominant. LF/HF, pNN50, NN50 and recurrence quantification analysis (RQA) ENT also stand out. It is also worth noting the differences between the profile presented for 40-0 minute intervals and that for the other two 40-minute intervals, as clearly manifested, for example, in features RRMean, RRMin, RRMax and pNN50. Such differences might indicate the occurrence of HRV changes over time that is captured by different groups of features in distinct time intervals. The fact that the mean, minimum and maximum of the RR intervals were often observed among the accepted clustering solutions may indicate the presence of EEG confounds unrelated to the occurrence of epileptic seizures.

Concerning the tested clustering methods, it can be seen that methods GMM and DBSCAN (applied with $\varepsilon = 2$ and $\varepsilon = 3$) returned the majority of accepted solutions. These methods might, therefore, be most suitable for searching for preictal intervals among clustering solutions of diverse shapes and duration.

With regard to the duration of the smaller cluster, no one cluster duration demonstrates clear prevalence, which means that when assuming a preictal interval corresponding to this smaller cluster, it is likely to have a duration that lasts from 1.58 minutes (20 samples) up to a maximum of 35.83 minutes (431 samples). It is worth noting that this limit applies for the 40–0-minute interval, whereas a maximum number of samples corresponding to 9.08 minutes (110 samples) and 5.42 minutes (66 samples) was returned for 120–80- and 80–40-minute intervals, respectively. It can also be observed that the duration of the clustering solutions was found to range from 1.58 to 9.08 minutes for 100% of the clustering solutions found for the 120–80- and 80–40-minute intervals and in 58% of the solutions fitting 40–0-minute intervals. These results further support the hypothesis that different seizures, possibly associated with the same patient, are characterised by different preictal dynamics [12, 16].

Finally, a larger percentage of discontinuous clustering solutions was found for the 40–0-minute interval than for the other intervals. This observation indicates that cardiac events triggered as a result of an oncoming seizure, located until 40 minutes before the seizure, most likely do not occur continuously but rather as a sequence of heart rhythm alterations occurring towards the seizure onset. It is worth mentioning that the noise detection method may introduce missing values responsible for pseudo-discontinuities.

5.4 Discussion

This study is a proof of concept that systematically applied unsupervised learning methods to HRV-derived features in characterising the preictal interval. Evidence

of this interval was found in 41% of the seizures analysed and in 37 out of 41 patients. In addition, preictal intervals ending before the seizure prediction horizon of 10 minutes were found for 30% of the seizures. A total of 54% preictal intervals were continuous over time. Furthermore, 53% of the preictal intervals occurred in the 40 minutes before seizure onset, which is in line with the mean duration and location of preictal intervals leading to the best seizure prediction performances in previous studies [14, 149, 175, 233, 235, 236, 251]. For the majority of the clustering solutions, the duration of the preictal interval ranged from approximately 2 to 9 minutes. The results also show the high variability of this interval both between and within patients, reinforcing the need for patient-specific approaches in treating epilepsy [12, 16].

5.4.1 Key aspects

With regard to the most relevant features identified in this study, there was a clear prevalence of time-domain features such as RRMax, RRMin and RRMean, along with a mild presence of LF/HF, pNN50, NN50 and RQA ENT among the accepted clustering solutions. These results are aligned with those presented in an HRV-based seizure prediction study [224]. Billeci *et al.* [224] proposed a prediction model based on HRV features, using a preictal interval of 15 minutes and at least 50 minutes of interictal data. This was the only study presenting a comprehensive analysis of an HRV feature dataset in terms of the number and importance of each of those features in distinguishing interictal from preictal epileptic stages. In fact, after applying a feature selection method, the authors found that features obtained from the time (RRMean, pNN50) and frequency (HF power and LF/HF) domains, together with nonlinear measures (RQA LAM and coefficient of SampEn), were relevant in characterising the preictal interval.

While identifying a preictal stage in 41% of seizures is not sufficient for developing a seizure prediction model, observing cardiac changes for all seizures would not be expected [12, 30, 251]. It might not even be possible to find preictal patterns in electroencephalographic data, as reported in similar studies using statistical or clustering approaches [251, 253, 254, 256]. Specifically, preictal interval was identified on EEG data in 38% [256], 69% [254] and 70% [251, 253] of seizures, respectively. In sum, monitoring autonomic changes might prove useful in seizure prediction only for some patients or even for specific seizures recorded for the same patient [12].

5.4.2 Study limitations

Additionally, the results reported herein should be understood in light of the limitations of this study. Namely, the assumptions regarding the search for the preictal interval, taken for the sake of finding acceptable solutions, may have made the unsupervised approach not completely unsupervised. The analysis of 240 minutes of

EEG data may also weaken confidence in the existence of a sufficient amount of interictal cardiac screening. However, in addition to the two studies in the literature reporting the EEG and EEG analysis of this time interval [236, 269], the vast majority of supervised studies in the literature indicate that the preictal interval is located within an hour before the seizure onset [149, 175, 233, 235, 236, 251]. Accordingly, results show that more than 53% of seizures manifested preictal HRV changes in the 40–0-minute interval before seizure onset. These findings support the assumption that, despite not considering the existence of a postictal interval, a representative interictal interval was analysed for each seizure, simultaneously allowing the fast computation of the results. New studies should, however, take into account the possible manifestation of the postictal state on the 240 minutes of data preceding seizure. Assuming that the 120 minutes farthest from the seizure onset contain mainly interictal activity might not be correct for seizures separated by exactly 240 minutes of ECG signal, due to postictal manifestations.

It is important to highlight that new studies are required to confirm the existence of preictal intervals in certain seizures using HRV data. In fact, new research on both cardiac and brain information can uncover the types of seizures for which pre-seizure changes are common. New endeavours in the unsupervised characterisation of the preictal interval are also encouraged, as this new perspective might potentially reveal key aspects related to neurophysiological knowledge of the preictal state.

5.5 Conclusions

The following sections elaborate on this chapter's final reflections and provide suggestions for further research.

5.5.1 Final reflections

To summarise, unsupervised learning was applied here to search for preictal patterns in HRV data acquired in patients with drug-resistant epilepsy (DRE). The study showed that it might be possible to find evidence of a putative preictal interval in the two hours of ECG data preceding some seizures. The results indicate that the assumed preictal alterations were observed for 90% of patients and 41% of seizures, with a seizure-specific profile. In all but two seizures, the preictal interval ended before the beginning of the SPH interval. More than half of the identified preictal intervals manifested in the 40 minutes before seizure onset. The results demonstrate the potential of applying clustering methods to HRV features to deepen the current understanding of the preictal state.

5.5.2 Future work

Additional information regarding cardiac preictal changes could improve seizure prediction methodologies, particularly in the context of multimodal approaches. Accordingly, the methodology described herein should be applied to the EEG recordings of the same group of patients (see Chapter 6) to validate the results for the preictal interval found by ECG analysis. In this way, it will be possible to overcome this study's main limitation, i.e., validation of the origin of the cardiac changes seen over the 240 minutes of data. Performing an unsupervised search of the preictal interval on EEG data could make it possible to discard potential confounders present in the EEG and ECG signals and increase confidence in the identified preictal intervals. In addition to assessing the patient's neurological condition, an EEG analysis may also allow the identification of artefacts (e.g., muscular artefacts). This information can be used to eliminate confounding factors for the unsupervised preictal interval search in ECG. For instance, muscular artefacts may result from walking or talking and may be associated with an alteration of the heart rhythm.

In sum, the characterisation of the preictal interval based on EEG and ECG will yield new preictal interval labels, which can be integrated into data fusion and seizure-specific prediction methodologies. The final results are expected to contribute to the field of epilepsy in terms of the design of prospective seizure prediction studies, recognised in the epilepsy field as a path leading to the validation of the clinical applicability of prediction models [12].

Ultimately, the evidence of preictal changes may enable the prediction of epileptic seizures sufficiently early to allow the patient to prepare for the upcoming seizure, seek a safe location to experience the seizure and avoid negative social exposure during seizure occurrence. Moreover, as the field of epilepsy progresses, the feasibility of seizure prediction might lead to the development of new strategies for treatment, such as closed-loop electrical stimulation, enabling seizure control. Given the path to such clinical applications, further studies are required to address this work's limitations regarding the analysis of data acquired during presurgical monitoring. Even though it is expected that alterations of medication will impact the normal functioning of the ANS and, therefore, induce changes in the EEG trace, considering a seizure-specific approach might contribute to a normalisation of the medication effect at the individual level.

Chapter 6

Unsupervised preictal activity search: an EEG-based approach

This chapter presents the study on the existence of preictal manifestations in the electroencephalography (EEG) data using unsupervised learning methods. Given the complexity of the EEG signals, a comprehensive assessment of pre-seizure brain alterations was performed. Although the study shares the same methodological approach as in Chapter 5, the signal's differences demanded some adjustments across the sequence of steps in methods.

The content of this chapter is based on a journal article accepted for publication in *Scientific Reports* and available as a preprint. Section 6.1 includes a short context of this study. Section 6.2 presents the methodology developed herein. The results are reported in Section 6.3 and then discussed in Section 6.4.

6.1 Study context

Seizure prediction models have been developed for more than 40 [12]. However, despite initial encouraging results, only recently have researchers proved that prospective seizure prediction is possible, at least for some patients [50]. Comprehensive reviews have provided guidelines for performance assessment and statistical validation of seizure prediction studies [12, 13]. Adopting these guidelines has demonstrated that seizure prediction models generally perform poorly, being successful for only some patients. The heterogeneity of the ictogenesis mechanisms among seizures (intra- and inter-patient) can contribute to the unsatisfactory performance of current seizure prediction models [16, 18]. As such, understanding the transition (including when it starts in time) from interictal to ictal states can greatly influence the prediction performance, demanding for a proper characterisation of the preictal interval.

A few studies have considered the use of unsupervised learning approaches to explore the existence of preictal activity in EEG data available from small cohorts

of humans [253, 254, 256] and dogs [255]. Authors inspected univariate [255], bivariate [253, 255, 256] and multivariate [254] features. Besides the analysis of a small number of subjects/dogs in these studies, it is also possible to conclude that little information is provided regarding the characterisation of the preictal interval. With such information, it might be possible to extract more knowledge on the ictogenesis mechanisms acting in each patient.

Importantly, the interpretation of the results reported in Chapter 5 for the electrocardiography (ECG) data can be enriched by observing the behaviour of the simultaneously collected EEG signals. Likely, hour-long ECG recordings capture more than just epilepsy-related events. Conversely, given the complexity of the EEG trace and its subsequent analysis, complementary information provided by other modalities might also be helpful to interpret brain manifestations.

This study explores the existence of preictal intervals in EEG data using unsupervised learning methods. First, univariate and multivariate features were extracted from 4.5 hours of EEG data recorded before seizure onset. Second, four clustering methods were applied to each seizure's feature data, obtained after dimensionality reduction. Then, a search for any pattern that could be distinguishable from interictal activity in the two hours preceding seizure onset was conducted through visual inspection. When those patterns were identified, they were characterised in terms of duration, density, and starting time.

6.2 Methodology

The following sections describe each step performed to explore the preictal interval in EEG data from patients with drug-resistant epilepsy (DRE) (see Figure 6.1). The analysed dataset is described in Chapter 4. The EEG recordings were preprocessed to minimise the effects of possible confounding artefacts. Then, meaningful features were extracted from the preprocessed EEG data. Afterwards, given the obtained high-dimensional feature space, dimensionality reduction was conducted, and four clustering methods were applied to the reduced three-dimensional feature space. Each seizure's data distribution and clustering solutions were visually inspected in search of preictal activity. When a cluster has been discovered for a given seizure in the 120 minutes before onset, it was considered as evidence of the preictal state. In that case, information on its starting time, duration, and density was collected.

6.2.1 Lead seizures

This study concerns the inspection of EEG data acquired for lead seizures, i.e., for seizures preceded by at least 4.5 hours of seizure-free interval, therefore considered as independent events [156, 157]. Given this criterion, 162 seizures separated by less than 4.5 hours were discarded from a total of 388 seizures, leading to the 226 seizures

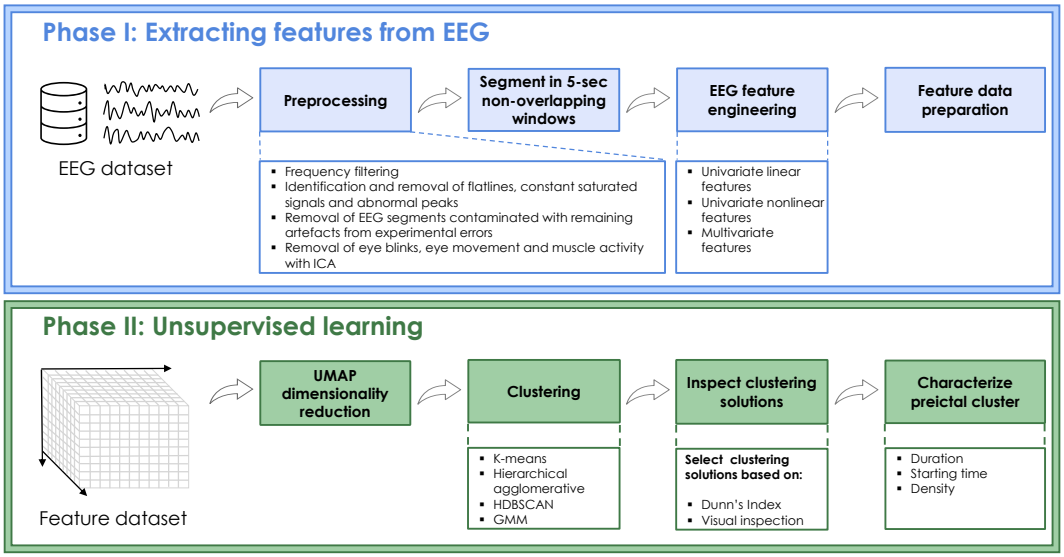

Figure 6.1: Block diagram of the proposed methodology. The study's first phase corresponded to preprocessing and feature engineering and preparation. The second phase encompassed the dimensionality reduction of each feature group (univariate linear, univariate nonlinear and multivariate), followed by the application of unsupervised learning methods and the preictal interval inspection.

considered herein.

6.2.2 EEG signal preprocessing

EEG preprocessing is crucial to allow a meaningful application of clustering methods. But it must be performed in a way that appropriately preserves the useful, brain-related information contained in the EEG. One important step is to remove artefacts naturally occurring in the non-controlled environment of presurgical monitoring. This step was performed using the algorithm developed by Lopes *et al.* [248] described below. First, the scalp EEG signals were filtered using a 0.5-100 Hz bandpass 4th-order Butterworth filter and a 50 Hz 2nd-order notch filter. Secondly, segments containing flatlines, constant saturated signals and abnormal peaks were automatically identified and discarded. Then, the 4.5-hour signals were divided into 10-minute segments. After automatically removing the remaining experimental errors, the EEG segments were re-referenced to average reference and decomposed using extended infomax independent component analysis. Some of the obtained independent components (ICs) would still contain artefacts, including eye blinks, eye movements and muscle activity. As such, a deep neural network model was used to classify the ICs as brain-related or artefact. The model was fed with the raw time series, the power spectrum density and the topographic map obtained for each independent component. The EEG signals used in the feature engineering phase then resulted from the signal reconstruction using the brain-related independent components automatically classified with the DNN model.

6.2.3 EEG feature engineering

Several features were extracted from EEG data (see Table 6.1). It is common to group features into (i) univariate linear, capturing, for example, the characteristics of the frequency spectrum in different frequency bands, (ii) univariate nonlinear, capturing the nonlinear behaviour of the EEG, and (iii) multivariate measures, measuring brain connectivity patterns (refer to Appendix E Section E.1 for more details). The frequency bands considered in univariate linear and multivariate feature extraction comprise delta (0.5-4 Hz), theta (4-8 Hz), alpha (8-13 Hz), beta (13-30 Hz), and gamma (30-47 Hz) [11, 13, 62, 233].

Each value of the features was computed from 5-second non-overlapping windows of EEG [11]. The final feature dataset comprised 42 univariate linear features per channel, 29 univariate nonlinear features per channel and 495 multivariate features.

6.2.4 Feature data preparation

Information contained in the 10 minutes before the seizure onset and the 30 minutes after the previous seizure offset was removed (the latter was removed when subsequent seizures occurred). The 30-minute interval was considered to correspond to the period following the ictal discharge, known as postictal, that may be captured in the electrographic trace [14, 83, 97, 281–283]. The 10-minute interval corresponds to the seizure prediction horizon (SPH) (see Section 4.5 for more details) [147, 150, 153, 157, 165].

Inspection of the feature dataset resulted in identifying constant and quasi-constant features in the three feature groups (univariate linear, univariate nonlinear, and multivariate). Constant features correspond to features for which all values are equal. Quasi-constant features correspond to features for which more than half of the values are equal. Constant and quasi-constant features were discarded from the analysis (refer to Appendix E Section E.2 for further details).

Afterwards, the z-score normalisation was applied to each feature group dataset.

6.2.5 Dimensionality reduction

The feature dataset of each seizure contains 741 univariate linear, 532 univariate nonlinear, and between 235 and 329 multivariate features. Dimensionality reduction was applied to obtain the three-dimensional space where clusters are further drawn. This way, it was possible to visually inspect and interpret the clustering results.

Uniform manifold approximation and projection for dimension reduction (UMAP), a recently proposed nonlinear manifold dimensionality reduction method, was used in this study. This method produces low-dimensional datasets while preserving the local and global structure of the original data [284]. The basic principle of this graph algorithm is to keep similar points close and dissimilar points apart [285]. Although other feature reduction methods have been applied (principal component analysis

Table 6.1: EEG-derived features.

Linearity/ Domain	Features
Univariate/ linear	• Statistical measures (normalised and non-normalised, mean amplitude, standard deviation, skewness, and kurtosis); • Hjorth parameters (activity, mobility, and complexity); • Decorrelation time; • Spectral power and relative spectral power in each frequency band (delta, theta, alpha, beta, and gamma); • Total power; • Alpha peak power; • Spectral edge frequency and power (at 50%); • Mean frequency; Frequency bands power ratios; • Energy of wavelet coefficients.
Univariate/ nonlinear	• Higuchi's fractal dimension; • Monofractal detrended fluctuation analysis; • Multifractal detrended fluctuation analysis; • Multifractal 1-D Wavelet Leader estimates; • Approximate and sample entropies; • Correlation dimension; • Largest Lyapunov exponent; • Recurrence quantification analysis.
Multivariate	Connectivity measures (per frequency band): • Circular omega complexity,; • Circular correlation; • Intersite phase clustering; • Phase lag index; • Weighted phase lag index; • Debiased weighted phase lag index; • Spearman's correlation coefficient; • Spearman's correlation coefficient for instantaneous power; • Normalised cross-correlation; • Normalised cross-correlation for instantaneous power; • Phase slope index. Graph indexes for connectivity: • Assortativity; • Characteristic path length; • Global efficiency; • Modularity; • Mean network degree; • Mean strength, mean closeness centrality; • Mean betweenness centrality; • Transitivity; • Mean weighted clustering coefficient; • Mean incloseness centrality; • Mean outcloseness centrality.

and t-distributed Stochastic Neighbour Embedding), it was concluded that UMAP more consistently presented separated rounded or elongated clusters. As such, the

unsupervised learning task was conducted on the UMAP-reduced data.

UMAP starts by building a high-dimensional weighted graph representation of the data where the edge weights correspond to the likelihood that two points are connected. Then a cost function is used to optimise a low-dimensional graph while maintaining the original structural similarity. UMAP has two main input parameters that control the trade-off between local and global structures: the number of nearest neighbours and the minimum distance. The former defines the number of nearest neighbours required to obtain the initial high-dimensional graph. The latter corresponds to the minimum distance between points in low-dimensional space [285].

Hyperparameter tuning was performed for UMAP (see Figure 6.2). Namely, UMAP was applied considering different values of nearest neighbours (ten values in the range of $[10, 100]$) and minimum distance (nine values in the range of $[0.1, 0.9]$). The next section describes the process of finding the best parameters in detail.

6.2.6 Unsupervised learning (Clustering)

Four clustering methods were applied to the three-dimensional datasets obtained for each seizure, resulting from applying UMAP (for each hyperparameter combination):

1. K-means clustering (KM), a widely used clustering partitioning method, is better suited to detect well-separated and similarly sized and shaped clusters [275, 286]. The initial cluster centroids were selected using the *k-means++* method [287] and the distances between points and centroids were computed using the Euclidean distance. The algorithm was run for k clusters, with $k = 2, 3, 4$.

2. Agglomerative hierarchical clustering (AH) can identify structured clusters. The Ward linkage method and the Euclidean distance were chosen [273]. The algorithm was run for k clusters, with $k = 2, 3, 4$.

3. Hierarchical density-based spatial clustering of applications with noise (HDBSCAN) (HDBSCAN) performs density-based spatial clustering of applications with noise (DBSCAN) over varying values of ϵ, which is an input argument that defines the maximum distance that can exist between two points within the same cluster [288]. HDBSCAN automatically selects the optimal clustering solution, requiring the definition of the number of samples in a neighbourhood, $MinPts$, for a point to be considered a core point [289, 290]. This parameter was set to six, corresponding to twice the dimensionality of the feature space [276]. An optional input parameter, minimum cluster size, $MinSz$, was set to 20 samples [155]. Density-based clustering algorithms can be used to identify arbitrarily shaped clusters [276, 288, 290].

4. Expectation-maximisation clustering using Gaussian mixture models (GMM) [277], besides successfully identifying round clusters, is also used to find elon-

gated clusters that follow Gaussian distributions. Mean and standard deviation are estimated using the expectation-maximisation algorithm. The algorithm was run for k mixture components (or underlying Gaussian distributions), with $k = 2, 3, 4$.

The probability of identifying preictal signatures across the different data spatial distributions (observed after dimensionality reduction for each seizure) was maximised by choosing the previous clustering methods. The different clustering methods were chosen according to each method's ability to identify a specific shape of clusters, whether it be round, elongated, or other arbitrary shapes. Whenever a clustering method was applied, the obtained clustering solution was evaluated using the Dunn's index (DI) cluster evaluation metric [279]. Specifically, the best parameter combination for UMAP was selected for each seizure by searching for the maximum DI value among the values obtained for each clustering method (see Figure 6.2).

After parameter tuning, the final UMAP-reduced data was obtained for each seizure, yielding 226 three-dimensional representations for each feature group. For each seizure's reduced data, the final clustering solution would be given by the

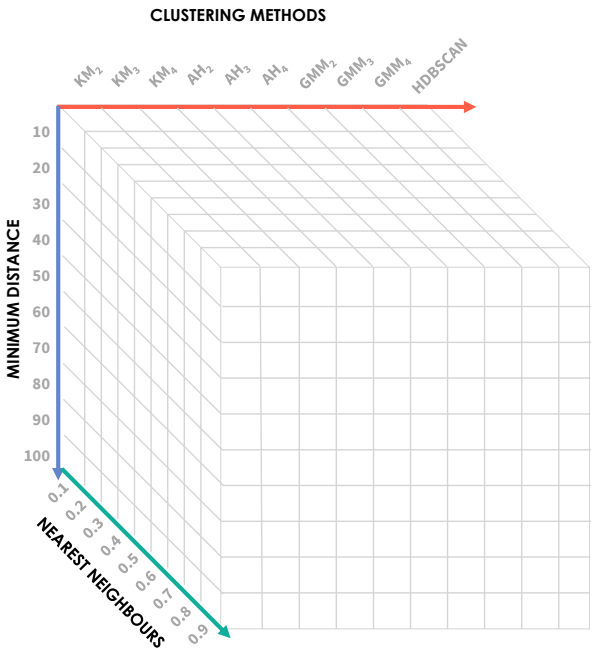

Figure 6.2: Representation of the number of clustering solutions obtained for each seizure and feature group. Four clustering methods were applied to UMAP-reduced three-dimensional datasets (KM: K-means clustering for $k = 2, 3, 4$, AH: agglomerative hierarchical clustering for $k = 2, 3, 4$, GMM: Gaussian mixture models for $k = 2, 3, 4$ and HDBSCAN). Parameter tuning was performed for UMAP (ten values of nearest neighbours and nine values of minimum distance). The final reduced data obtained before each seizure's onset and for each feature reduction method corresponds to the maximum DI obtained among the computed clustering solutions.

clustering method yielding the maximum value of DI. A visual inspection was then performed to determine if the clustering method selected with the DI matched the observed clusters. There were a few cases for which no match was achieved. In those cases, the results obtained by applying the described clustering methods were visually inspected. If none of these methods could capture the observed clusters, the number of clusters would be increased in AH, KM and GMM in trying to fit visual inspection. When a good fit was not achieved by increasing the number of clusters, DBSCAN was applied for different values of ϵ, as performed in another study [155].

6.2.7 Searching for preictal patterns

Having selected the best parameters for UMAP, the reduced datasets and the respective clustering solutions were inspected in the search for preictal alterations. Published works [149, 233, 236] report changes one hour before seizures, with significant inter- and intra-patient variability. Based on that, the preictal interval was considered to start 120 minutes before seizure onset (see Figure 6.3). A putative preictal behaviour was assumed to manifest as abnormal fluctuations in the EEG feature dataset with a higher probability of occurrence starting at the 120 minutes

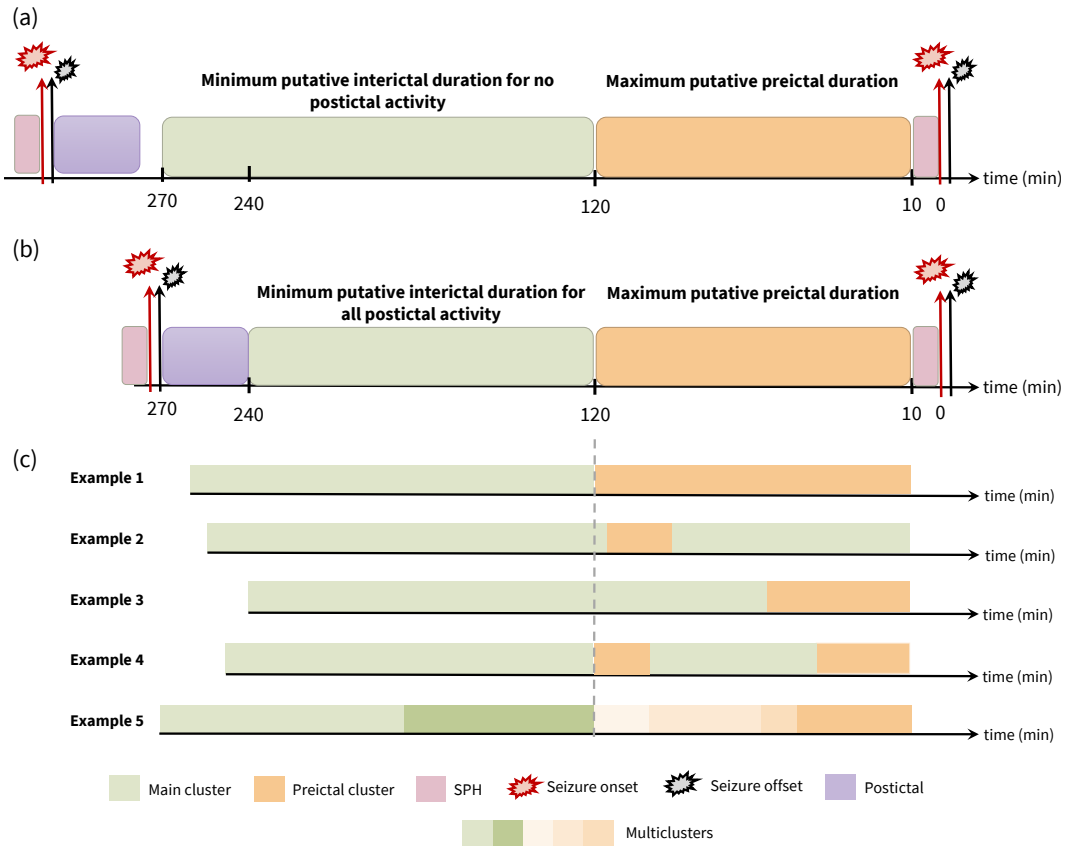

Figure 6.3: Examples of preictal location and duration for the specific case of two seizures separated by (a) more than and (b) exactly 4.5 hours (270 minutes). Examples representing clustering solutions containing differently sized preictal clusters are presented in (c).

before the seizure onset until the seizure. Data locating before the 120-minute interval were considered as enough data to predominantly contain interictal data. In addition, in the case of identifying a preictal pattern in a clustering solution with multiple clusters, that state was typically associated with the cluster that locates, in time, nearer the seizure onset but not necessarily extending to the onset time (see Figure 6.3 for some examples).

After a first visual inspection of the three-dimensional representations, it was possible to find data distributions with repeating structures across seizures and groups of features. In fact, during this visual inspection, categories of data distributions were gradually emerging, which led us to perform a categorisation task. A total of six categories were identified and are described in Table 6.2. Examples for each category are depicted in Figure 6.4. Each seizure's three-dimensional representation was then assigned to one of six categories of distributions. This categorisation enabled quantification of the different patterns arising before the seizure onset. Nevertheless, there were a few seizures for which the corresponding data distribution could be difficult to associate with a single category. Consequently, a group of five team members conducting research in the context of seizure prediction was assembled to perform this categorisation independently. Each member categorised the clustering solutions into one of the six categories. After each expert has voted, the final category would correspond to the one gathering three or more votes. If three or more votes were not assigned to a given category, the whole team would discuss over the

Table 6.2: Data distribution categories defined after data reduction and clustering solution inspection.

Category	Definition
Category 1	There is no evidence of a preictal structure. There might be a clear separation into a smaller cluster, but that either comprises samples separated in time or comprises samples strictly located previously to the 120 minutes before seizure onset.
Category 2	Separation into two evenly distributed clusters that might indicate some external interference, such as the transition of the sleep-wake cycle.
Category 3	Clear separation into two differently sized clusters, the smaller one resembling a preictal interval located within the 120 minutes before seizure onset.
Category 4	Data distribution indicating progression over time, with samples following a temporal trajectory.
Category 5	It seems that a smaller cluster can be identified, but it would be difficult to isolate it in a cluster using clustering methods.
Category 6	Category assigned when the clustering solution comprises more than two clusters that may indicate the existence of brain multistates and even progression over time. The preictal interval is represented by the cluster located within 120 minutes before seizure onset and nearest to the onset. It might be possible to observe evidence of sleep stage transition, preictal interval aside.

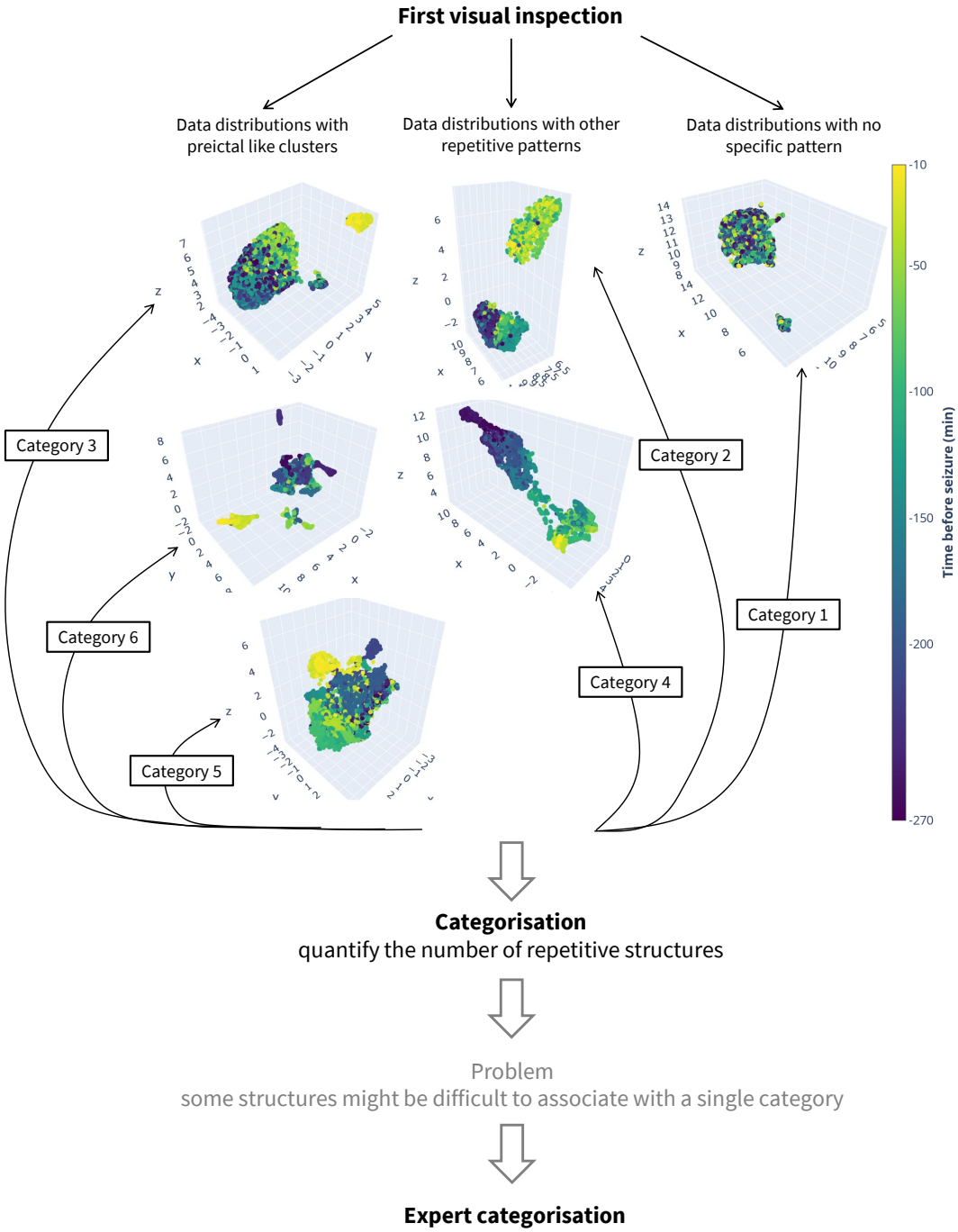

Figure 6.4: Process of searching for the preictal interval. Each example of the six data distribution categories is represented by the projected UMAP components (labelled x, y, and z). The seizure occurs at 0 minutes. Category 1 was obtained from patient 21902, seizure 4, reduced multivariate features. Category 2 was obtained from patient 98102, seizure 5, reduced univariate nonlinear features. Category 3 was obtained from patient 58602, seizure 4, reduced multivariate features. Category 4 was obtained from patient 110602, seizure 3, reduced univariate linear features. Category 5 was obtained from patient 98202, seizure 2, reduced univariate nonlinear features. Category 6 was obtained from patient 123902, seizure 2, reduced univariate linear features.

reduced data, and, through knowledge exchange, the team would agree on a final category. It is important to note that none of the team members suggested removing an existing category or adding a new category.

Evidence of preictal interval was more reliably observed in the data distribution from categories 3 and 6. After discarding noisy samples, the preictal interval starting and ending samples were registered (see Figure 6.5). With this information, three preictal characteristics were computed: interval starting time before seizure onset, interval duration, and density. The preictal density is merely an indicator of the number of preictal samples within the preictal interval defined by the starting and ending times. It corresponds to the number of preictal samples divided by the total number of samples in that interval.

6.2.8 Sleep-wake cycle detection

After performing a visual inspection of the reduced datasets and corresponding clustering solutions, particularly category 2 solutions, it was possible to observe that, in some cases, the clusters' separation would occur during day-to-night transitions and vice-versa. The oscillations observed in the EEG features during the unsupervised study may possibly reflect the copresence of other confounders rather than preictal activity, such as the sleep-wake cycle and/or other internal body circadian cycles. These normal oscillations translate to changes in EEG data distribution over time called concept drifts. In this study, the sleep-wake cycle was considered one of the most frequent types of concept drifts present in the EEG data. Based on this, a model to detect the sleep-wake cycle was used for each patient to confirm the effect of the sleep-wake cycle on the analysis [291].

Then, the *phi* coefficient (also known as Matthews correlation coefficient) [292, 293] was computed between the binary sleep-wake vector and a binary vector representing a given cluster distribution for categories 2, 3, and 6 (refer to the example in Figure 6.5). As such, for the case of categories 3 and 6, the binary vector contains ones corresponding to the cluster samples indicating preictal alterations and zeros corresponding to the remaining samples. For category 2, as the clustering solution always comprised two equivalently sized clusters, the binary vector would contain zeros and ones corresponding to the samples in each cluster.

6.2.9 Comparison with control intervals

The methodology described in the previous sections was repeated for control intervals. These intervals, of 4.5 hours duration, ended at the corresponding seizure EEG onset hour but on the day before the seizure. This way, it would be possible to compare the results for the 4.5-hour interval before the seizure onset with the results for the seizure-free intervals occurring at the same time of the 24-hour day. If similar data distributions occur in both intervals, it means that the clusters observed in the

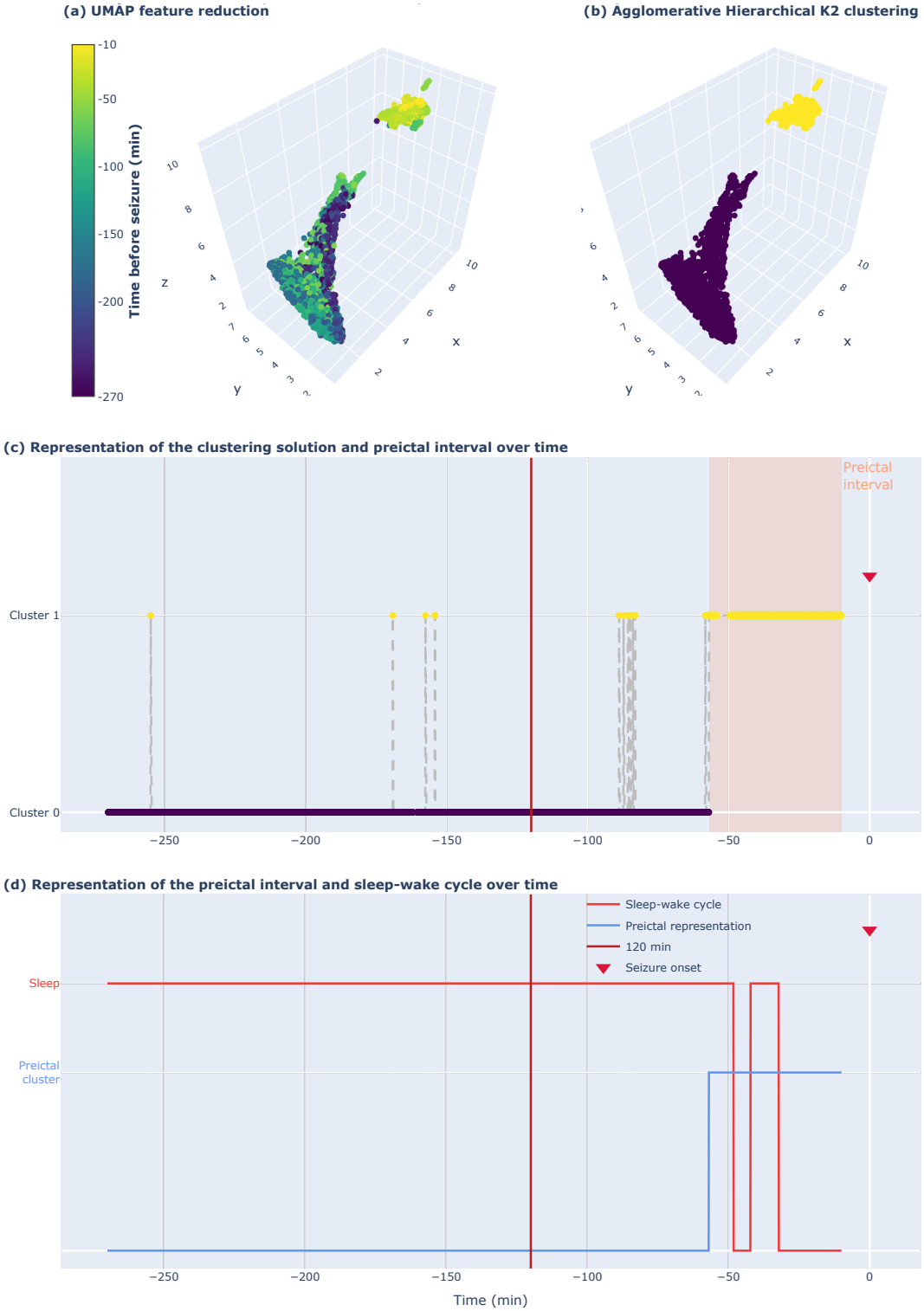

Figure 6.5: Example of clustering solution inspection. Data was acquired for patient 402 before the onset of seizure 5. (a) UMAP dimensionality reduction was performed on univariate linear features. (b) The clustering solution was obtained using agglomerative hierarchical clustering with $k = 2$. (c) Representation of the clustering solution and the preictal interval categorised as category 3. The preictal interval started 56.9 minutes before seizure onset, lasted for 46.9 minutes and verified 100% density. (d) Representation of the preictal interval and sleep-wake cycle, with a *phi* coefficient of 0.79.

two hours before the seizure onset are not related to preictal activity but instead to another unknown variable.

Selecting the control intervals from the exact same time of the 24-hour day, on the previous day controls for the effect of circadian rhythms on the data distribution. Additionally, given that a seizure-specific approach has been considered throughout the study, the control intervals are located within the interictal time before the onset of the seizure under analysis (see Supplementary Section 6.2 for some examples). Accordingly, a minimum of 33 hours of seizure-free signal is required before the onset. In other words, the control intervals start and end at 28.5 and 24 hours before the seizure onset, respectively, and are separated by at least 4.5 hours from the previous seizure. According to these criteria, 47 control intervals were analysed. These control intervals were only analysed for the univariate linear features, which require less computational time to extract.

6.2.10 Metadata analysis

This analysis aims at quantifying the association between each of the four seizure variables (vigilance state, seizure type, EEG onset hour, and percentage of noise) and the preictal characteristics (starting time, duration, and density) of the seizures for which preictal was found. Notice that the percentage of noise determined for each seizure's 4.5 hours of data was included in the analysis in order to discard the effect of obtaining a clear cluster separation due to missing feature values introduced by preprocessing. This metadata analysis was performed for each group of features.

6.2.11 Code information

Signal preprocessing and feature engineering steps were implemented in MATLAB R2019b (The MathWorks, Inc., Massachusetts, USA) and on WINDOWS 10 Pro with an INTEL Core i7-4790K CPU at 4 GHz and 32 GB RAM. The feature reduction and unsupervised search steps were implemented in Python 3.8 and on LINUX 2 x INTEL Xeon E5-2697v2 (12-core) CPU at 2.70 GHz and 96 GB RAM.

Figure 6.5, depicting reduced data, the clustering solution, and the sleep-wake cycle before onset, was obtained for each seizure's data and each feature group, for all categories. All figures and developed code are publicly available on GitHub via adrianaleal/eeg-preictal-identification-epilepsy.git. To ensure reproducible results, a random seed state was set on the following Python functions: UMAP, KM and GMM.

6.3 Results

By looking at the examples in Figure 6.4, it is possible to conclude that finding evidence of the preictal interval would correspond to obtaining reduced data and

clustering solutions categorised as either category 3 or 6. In the case of category 3, it was possible to see a smaller cluster clearly separated from the remaining samples. In the case of category 6, there are data distributions comprising small clusters clearly separated from each other, possibly indicating the existence of different brain states. Some of these states were assumed to be associated with pre-seizure alterations. To quantify the possible presence of preictal behaviour, the preictal was considered to correspond to the cluster located near the seizure. Additionally, category 5 data distributions also inform about clusters of data containing samples that are close in time. However, contrarily to categories 3 and 6, category 5 clusters could not be automatically distinguished and isolated by the clustering methods.

The results for the categorisation performed by each of the five experts are presented in Appendix E Section E.4.1. A consensus was not achieved for 8%, 7%, 8%, and 11% of the seizures for the univariate linear, univariate nonlinear, multivariate, and control univariate linear feature groups, respectively. Figure 6.6 presents the prevalence of each category in the three groups of features after analysing the doubtful seizures. Evidence of the preictal interval represented by category 3 was found for all feature groups extracted from the 4.5 hours preceding the seizure onset, with similar prevalence (8.4% in univariate linear, 11.5% in univariate nonlinear, and 9.7% in multivariate).

Additionally, data distributions showing several small and structured clusters over time (represented by category 6) were widely seen for the group of univariate linear features. Univariate nonlinear features were the largest source of category 2 data distributions. For this group of features, the clustering methods often could separate two major, evenly-sized clusters. This data distribution might indicate a clear transition between two brain states that may not be related to epileptogenic activity but other phenomena, e.g. the sleep-wake cycle.

Regarding category 5, it was possible to observe that this type of data distribution occurred in at least one-quarter of the seizures in all groups of features. At last, there is a residual prevalence of category 4 distributions. These distributions are characterised by a gradual and continuous evolution of the samples' trajectory over the analysed data. Analysis of the distributions obtained for the reduced univariate linear features group resulted in categorising the lowest number of uninformative distributions. Namely, only 16.8% of seizures in the univariate linear group belonged to category 1.

Figure 6.7 shows information about the existence of preictal behaviour for each of the analysed seizures and patients. Among the 41 patients selected for this study, there were 37 for whom at least one seizure showed a distinct pattern in the reduced data (either with univariate linear, univariate nonlinear or multivariate) that might indicate a preictal alteration (categories 3 or 6). From the 226 seizures studied, 116 seizures (51%) were categorised as containing distinctive pre-seizure information. Multivariate feature reduction led to the identification of preictal clusters in four

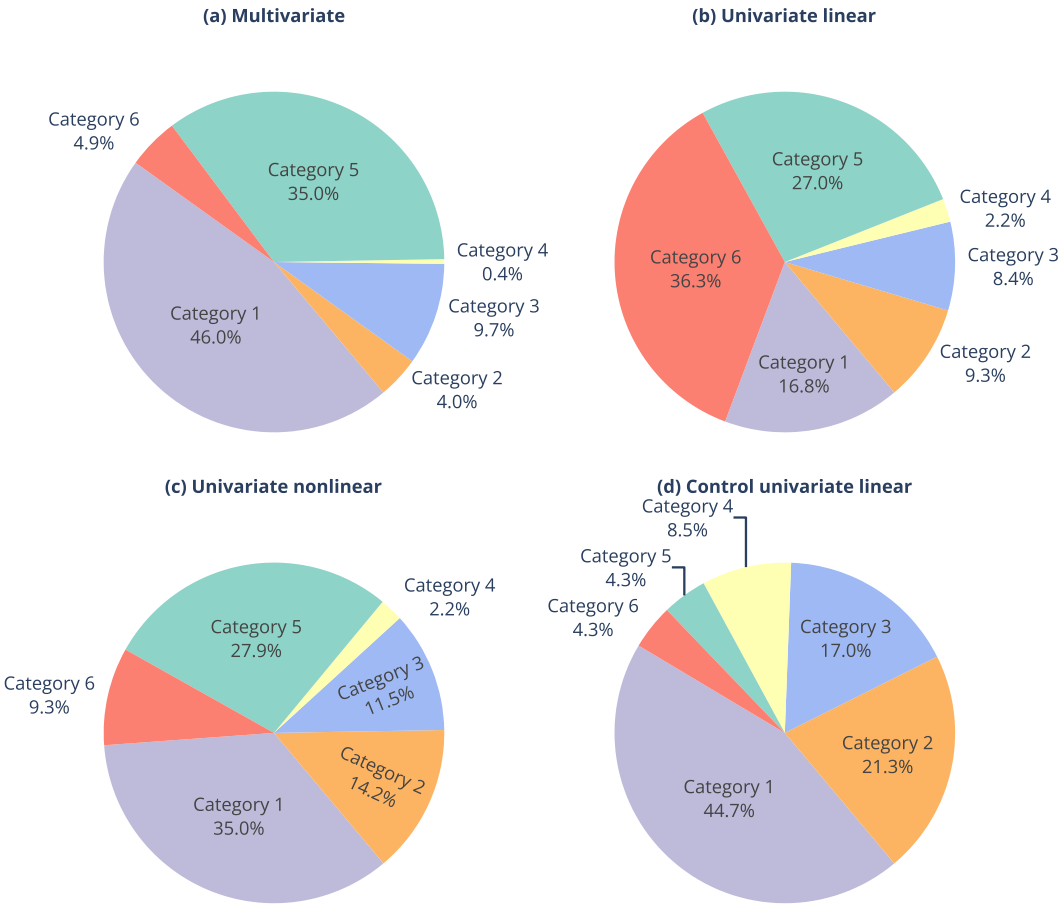

Figure 6.6: Results for data distribution categorisation. The categorisation of data distributions after experts voting and discussion of doubtful data distributions is presented for each feature group: (a) multivariate, (b) univariate linear, and (c) univariate nonlinear.

seizures for which preictal clusters were not found with univariate features. Category 5 preictal appearance is characterised by data clustered in time, however, with a less distinguishable separation from the remaining samples. If category 5 is included in preictal quantification, preictal patterns increase to a total of 183 seizures (81%) in 41 patients.

This information was compared with the results reported in Chapter 5 regarding the search for preictal patterns in ECG data (acquired simultaneously with EEG in the group of patients selected for the current study) [155]. In that work, preictal clusters were found for 41% of the seizures and 90% of the patients. As shown in Figure 6.7, the preictal interval was identified both in EEG and ECG (considering categories 3 and 6) in 50 out of 226 seizures (22%). Additionally, when comparing the starting time before the seizure onset between both modalities (see Section E.4.5 in Appendix E), it was possible to observe that while the preictal intervals started mainly 20 to 40 minutes before the onset in the EEG recordings, in the ECG there was also a large number of preictals starting from 70 to 120 minutes.

Figure 6.8 presents the statistics of the preictal interval characteristics when it

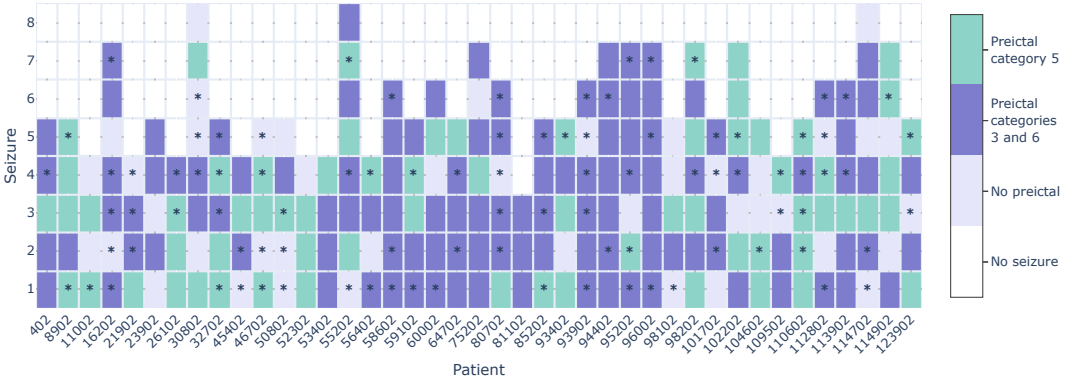

Figure 6.7: Results for preictal interval identification. The preictal interval was found for 37 patients (90%) and 116 seizures (51%). These results correspond to the evidence of preictal interval found for categories 3 and 6 (together) and category 5, when these categories were found for at least one of the feature groups. The results for category 5 were presented for a given seizure when categories 3 or 6 have not been previously assigned in any of the groups of features. Asterisks indicate seizures for which preictal patterns have also been identified in a study using ECG data concurrent with the EEG data under analysis (considering that these preictal intervals started before the SPH) [155]. Preictal patterns were found in both EEG and ECG in 22% of the seizures analysed in this study.

was found and assigned categories 3 or 6. The distributions of preictal (i) starting time before seizure onset, (ii) duration, and (iii) density are depicted. The average preictal's starting time, computed over all seizures and feature groups, was 47.6 ± 27.3 minutes (mean $\pm$ standard deviation). It started in the 40 minutes preceding seizure in 53.0% of the preictal clusters. It lasted for 22.9 ± 21.0 minutes (mean $\pm$ standard deviation) and was often nearly continuous (90% density observed for 62.4% of preictal clusters found for all groups of features). Contrarily to the other features groups, results show that the vast majority (84.8%) of preictals found for the multivariate group lasted less than 20 minutes. Additionally, preictal alterations ending at the seizure onset were observed in 45.3% of the preictal clusters identified for categories 3 and 6.

For some seizures, a preictal cluster was found for more than one feature group. To perform a comparison with state-of-the-art studies, it was necessary to select a final preictal interval to compare with. This selection was performed according to the preictal intervals' characteristics (refer to Appendix C). The average of the final preictal intervals' starting time before seizure onset found in this study (50.1 ± 28.9 minutes) falls in the range of average preictal intervals (28 to 60 minutes) obtained by performing grid-search to develop seizure prediction algorithms [14, 149, 153, 157, 175, 233, 235, 236, 251]. Additionally, the starting time of the preictal intervals identified using unsupervised learning was compared with the preictal intervals found using grid-search supervised learning on EEG data from the EPILEPSIAE database (refer to Figure E.14 and Table E.8 in Appendix E). Namely, there are two studies [153, 157] documenting results of preictal grid-search, which also report the identification number for each patient. Providing that information

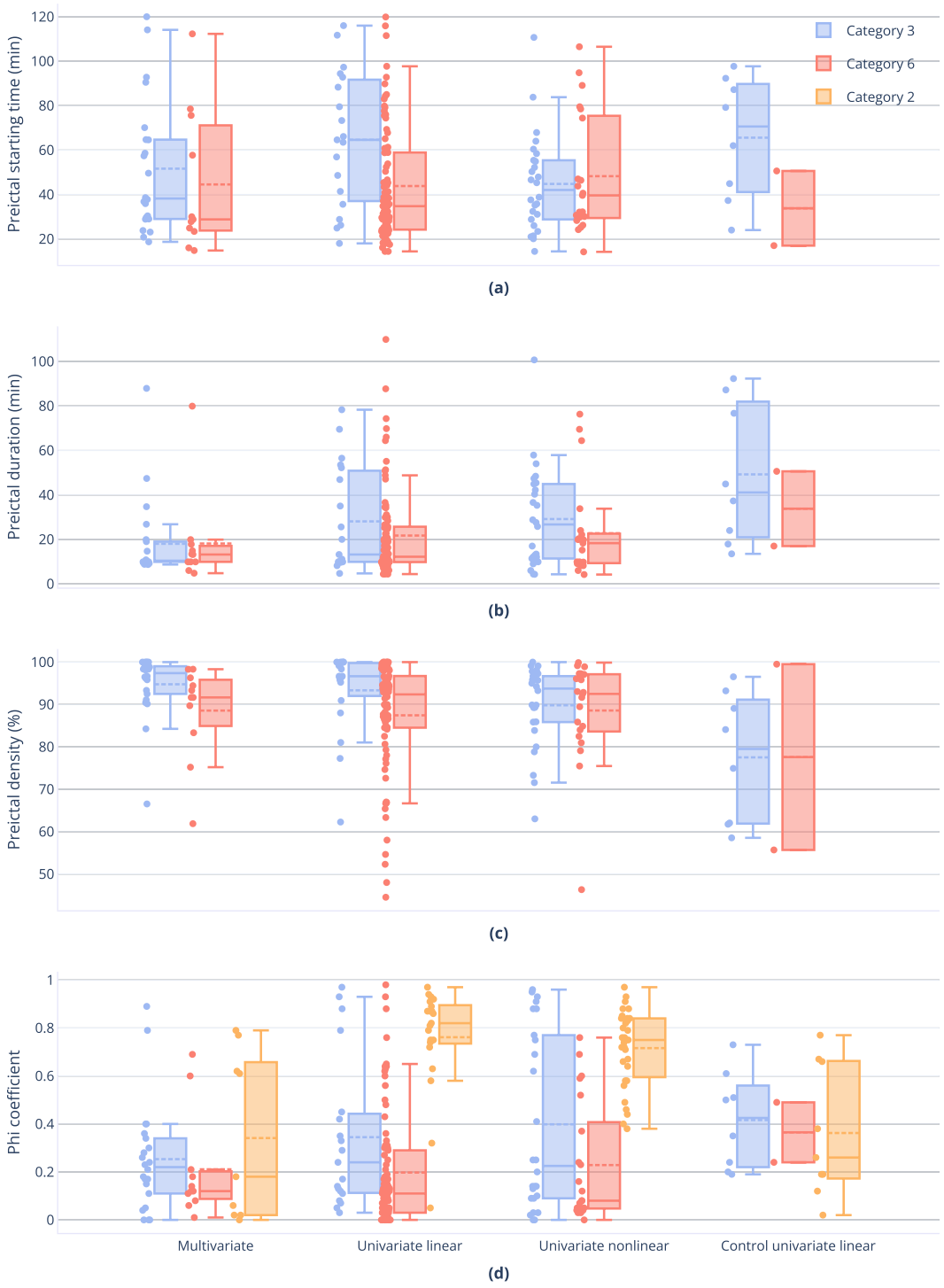

Figure 6.8: Results for preictal interval characterisation. Preictal interval was characterised for categories 3 and 6, for the three groups of features, according to three characteristics: (a) starting time before seizure onset, (b) duration, and (c) density. (d) The Phi coefficient was computed between the preictal clustering solution and the sleep-wake cycle for categories 3, 6, and 2 for the three groups of features. Dots correspond to one of the three preictal characterising variables or to the phi coefficient. Solid and dashed lines indicate medians and means, respectively. Box's tops and bottoms correspond to the 75th and 25th percentiles, respectively. Whiskers refer to the span of the preictals characteristics or the phi coefficient after discarding outliers.

allows for a more straightforward comparison, though not ideal, as seizure-specific preictal intervals were obtained only for some seizures (within the same patient) rather than all seizures. The vast majority of patient-averaged preictal intervals found in these two studies started between 65 and 40 minutes before seizure onset. Conversely, using the unsupervised learning approach led to the identification of averaged preictal patterns starting at very distinct times before seizure onset, mainly occurring between 80 and 20 minutes before seizure onset.

Figure 6.8d presents the values of the phi coefficient between the obtained putative preictal binary representation and the sleep-wake cycle for categories 3 and 6. More than 80% association between both vectors was observed in 5.9%, 12.8%, and 3.0% of the preictals in univariate linear, univariate nonlinear, and multivariate feature groups, respectively. The association between category 2 two-cluster solutions and the sleep-wake cycle was also computed. Association above 80% was found for 57.1%, 37.5%, and 0.0% of univariate linear, univariate nonlinear, and multivariate data distributions, respectively.

Comparing the results for control intervals and intervals preceding seizures for the univariate linear feature group, it was possible to conclude that the prevalence of category 6 data distributions drastically reduced in the control intervals (decreasing from 36.3% to 4.3%). However, a high prevalence of category 3 data distributions was also observed (increasing from 8.4% to 17.0%). For the eight seizures assigned category 3 in the control intervals, Figure 6.8 shows that the putative preictal starting time and duration are more spread compared to the other three feature groups. Additionally, a visual inspection was performed on the data distributions of the 4.5 hours of data preceding seizure onset and the corresponding control interval (available on the GitHub page) when the same category had been assigned. Similar data distributions were observed in three out of five seizures with the same categorisation.

Regarding the metadata analysis (refer to Appendix E Section E.5 for more details), the results showed no evident association when inspecting the relationship between four seizure variables (vigilance state at onset, seizure type, EEG onset hour, and percentage of noise) and the preictal characteristics (starting time, duration, and density).

6.4 Discussion

This study aimed to explore the existence of pre-seizure alterations in EEG data collected from patients with DRE under presurgical monitoring. Unsupervised learning methods were applied to provide new insights into the complexity of the transition from interictal activity to seizure. The success of seizure prediction models heavily relies on the accurate characterisation of the preictal interval when it manifests in the biosignal under analysis [12].

Clusters suggestive of preictal behaviour were observed in 51% of the analysed

seizures. This percentage increases to 81% if, in addition to categories 3 and 6, category 5 is also included as an indication of possible preictal activity. These findings are in accordance with previous studies that, using statistical and clustering approaches, reported preictal interval identification on EEG data in 38% [256], 69% [254] and 70% [251, 253] of seizures, respectively.

Despite the results obtained for category 3 in the control intervals (an increase from 8.4% to 17.0%), the considerable reduction in category 6 and 5 data distributions (from 63.3% to 8.6%) increases the confidence in the results on the presence of preictal activity in the 4.5 hours preceding seizures observed in the three feature groups.

6.4.1 Key aspects

Important aspects of this study are separately discussed in the next subsections.

Preictal changes in light of the nonlinear nature of brain dynamics

The preictal clusters identified in categories 3 and 6 were clearly separated from the remaining samples. For the case of category 6 data distributions, preictal clusters were also often preceded by other similarly sized clusters. The presence of these small clusters might reflect the occurrence of distinct, separated states of brain activity. This observation might be aligned with early beliefs that "neuronal networks may have bi(multi)-stable states" [210], depending on which of the different paths of brain activity lead to the seizure state (addressed in Section 3.1) [206, 210, 211]. Studies on the basic mechanisms underlying neural network evolution towards a seizure [210,211], refer to three possible paths leading to abnormal ictal dynamics: (i) a continuous sequence of states reflecting a gradual transition from an interictal to an ictal attractor, (ii) an abrupt change caused by a fast trajectory convergence to ictal state, assuming a system having interictal and ictal attractors simultaneously or (iii) a combination of both [16, 159]. In the second case, the transition might result from an abrupt random perturbation, making prediction even more difficult. External or endogenous factors can influence the three types of transition to the ictal state. The fast nonlinear dynamic evolution towards a seizure has been described as the crossing of a threshold, or separatrix, between interictal and ictal states [159, 206, 210, 211]. The three scenarios above might explain the results regarding the determination of a preictal cluster. For 49% of seizures, the occurrence of a very fast, sharp transition in brain activity may be missed by the EEG [159] or by the EEG features (e.g., due to the size of the window under analysis [17]), and, therefore, there are no seizure precursors. For the remaining 51%, it was possible to find distinguishable clusters that might reflect either a still sharp, but not so fast, transition or a gradual (possibly multistate) preictal transition [210, 294].

Nearly 20 years after Lopes da Silva *et al.* study [210], it is especially interesting

to note that the same question might still be asked: "which of all these measurable dynamical changes in the state of neuronal networks do lead to an epileptic seizure?". Particularly for the case of category 6 data distributions, it was challenging to provide preictal insight: which clusters (within the 120-minute interval) would be indicative of ictogenesis or "normal" brain function. The preictal activity was assumed to correspond to the cluster showing closer to the seizure as this assumption more closely relates to the preictal concept [159]. However, it might be possible that both the preictal and interictal intervals could comprise distinct sub-intervals that cannot be classified into normal or abnormal brain activity but rather into multi-classes representative of such sub-intervals in both main classes.

Additionally, interpreting category 3 reduced data distribution was also an arduous task. Namely, two scenarios often occurred when observing clusters within the 120 minutes before onset in category 3: (i) a gradual interictal to ictal transition reflected in a preictal interval ending on the seizure onset and (ii) a fast (but EEG perceptible) preictal interval not ending at the seizure onset (as in Figure 6.5). The first case corresponds to an increase in the features' value until the seizure onset. Supervised learning methods are typically successful when this scenario occurs as it allows for a binary classification of the data into interictal state and subsequent preictal state. In the second scenario, it was hypothesised that, even though regulatory mechanisms may have been triggered in the brain towards seizure suppression (hence the decrease in features value before the seizure onset), the seizure threshold may have been crossed, which deemed the seizure inevitable [16, 294]. Interestingly, some studies on seizure risk forecasting analysing long-term EEG data show a similar behaviour preceding seizures. Karoly *et al.* [17] noticed the existence of a peak in seizure likelihood followed by a gradual decrease until the seizure onset. This evidence is also depicted in a comprehensive survey [65], where authors present real-time EEG recorded over five days, (from the previously mentioned study [17]), weighted by the prior risk of seizures given the time of day. The corresponding proictal states and seizure timing are also depicted. Some seizures seem to occur shortly after or during a decrease in the circadian-weighted EEG, within the respective proictal state. Regarding the transition between interictal and preictal intervals, it was often possible to observe "jumps" from the main cluster, e.g., representing the interictal state, to another smaller cluster, a putative preictal state. Importantly, these "jumps" unlikely correspond to a trajectory of samples from interictal to preictal and back to interictal again, but rather a trajectory from a main, non-preictal cluster (that may contain mainly interictal samples spread over the three-dimensional feature space) to a preictal state and back to another location in the main cluster.

In this study, each cluster showing in categories 3 or 6 data distribution seems to reflect the existence of a preictal pattern. Unsupervised learning methods may leverage knowledge on the evolution of the EEG time series until the seizure onset. Simultaneously, the clusters obtained with unsupervised learning methods can

further shed light on the rate of false positives hampering the performance of supervised learning prediction models. However, new questions arise: which brain processes explain these clusters? Are those the reflection of normal brain functioning or pathological phenomena? These questions closely relate to the knowledge gap regarding the influence of, for instance, interictal brain processes (e.g., interictal epileptiform activity) during ictogenesis [18, 159, 206]. More studies should be performed to answer such questions and provide an insightful interpretation of data distributions and subsequent clustering results. Clinicians' insight would also be crucial to obtain a ground truth to validate the origin of the different clusters [154].

Influence of confounders in seizure susceptibility

As addressed in Section 3.5 in state of the art, seizure susceptibility can vary depending on the current brain state, sleep-wake cycle, circadian, and ultradian rhythms, medication tapering, stress, or other exogenous and endogenous factors [12, 14, 16, 66, 67]. The EEG features may also be subjected to a different interpretation depending on the patient's age [62] and aetiology [295]. These factors may help explain the variability observed among seizures and patients that support the development of patient-specific approaches [12, 15, 16]. Additionally, the existence of a large number of epilepsy syndromes (resulting in considerable heterogeneity concerning aetiology and clinical manifestations) and non-cerebral confounders may also contribute to such variability [18, 252]. Accordingly, the results in this study may also be heavily influenced by epilepsy-characterising aspects such as aetiology, age, and lateralisation. However, given the study's seizure-specific nature, a metadata analysis was only performed using information annotated for each seizure. The results indicate that, in the analysed dataset, there is no significant influence of the vigilance state at seizure onset, type of seizure and EEG onset hour on the obtained results. Nevertheless, future studies should continue the search for correlations between preictal characteristics and available metadata. Such analysis can translate into training models for the different concept drifts present in data (e.g., training seizure prediction models for a given epilepsy aetiology, type of medication or type of seizures) [16, 132].

Applying the unsupervised learning methods to control intervals was performed to address the existence of other variables that might be confused with preictal activity. The fact that control intervals did not exist for all seizures is a limitation arising from the analysis of data collected during presurgical evaluation characterised by an increase in seizure frequency and a consequent reduction in seizure-free time. Ideally, this analysis would be conducted on the entire seizure-free data. However, as this is a user-dependent analysis that requires a visual inspection, it would be a time-consuming task. Nevertheless, results show that, in contrast to the 4.5 hours of data preceding seizures, there is a low prevalence of data distributions with multiple

clusters in control intervals. This difference contributes to increased confidence in the reported results regarding the existence of preictal patterns.

Additionally, the scalp EEG data analysed in this article were collected while patients with DRE were in an epilepsy monitoring unit under presurgical evaluation. Consequently, rather than exploring data representative of normal ambulatory brain activity, data analysed herein were collected while the patient was hospitalised for several days [29]. During the hospital stay, patients were submitted to antiepileptic drug tapering to precipitate seizures. Thus, interpreting the results might not directly translate to DRE interictal and preictal functioning during real-world conditions [16,18]. On the one hand, medication withdrawal preceding surgery has been associated with increased seizure susceptibility [18]. On the other hand, the administration of certain types of medication, such as benzodiazepines, has been reported to increase beta wave activity in EEG recordings [62,63].

The possibility of recording long-term EEG data (days to years) has opened a new avenue in exploring circadian rhythms' influence on seizure occurrence [17,67, 185,265]. Baud *et al.* [67] found that interictal epileptiform activity fluctuations are governed by circadian and multidien rhythms, which in turn determine seizure risk in some subjects. Improved seizure forecasting was reported in Karoly *et al.* [17] study after integrating information about the circadian rhythm of seizures in patient-specific models. Identifying subjects for which seizures tend to occur during specific phases of the circadian rhythm could explain some patterns of data distributions found in this research.

The sleep-wake cycle seems to be associated with the pattern of seizure occurrence [50]. The highest number of category 3 and 6 seizures, verifying a high association between the sleep-wake cycle and the preictal cluster, was found for the univariate nonlinear features (12.8%). The highest association found for category 2 was 57.1% using the reduced univariate linear features. Such observation may motivate the use of sleep-wake cycle information when developing seizure prediction models, at least for some seizures.

Another possible confounder is the influence of postictal activity. A postictal interval of 30 minutes has been considered in this study and removed in the case of subsequent seizures. Nevertheless, despite EEG slowing or suppression occurring on average about 5 min after seizure offset, it has been reported to occur 40 to 60 minutes after the offset of some seizures [97]. Again, this aspect is more evident when analysing data collected in presurgical monitoring due to reduced interseizure interval.

Despite the thorough preprocessing performed on the scalp EEG recordings, it is important to highlight that physiological artefacts such as muscle artefacts may still be present in the data. This study's limitation results from the difficulty in distinguishing the EEG power in the frequencies of interest from the muscle artefact frequencies [57,296].

Additionally, in Chapter 5, preictal changes in heart rate variability have been reported in 41% of the seizures and 90% of the patients, evidencing the effect of seizures in the autonomous nervous system [155]. That study and the one reported in this chapter, attempted to characterise preictal patterns using unsupervised learning. However, on the former, three-dimensional combinations of ECG features were inspected, and clustering solutions comprising only two clusters were explored. In the present study, feature reduction was performed to obtain a three-dimensional dataset for each seizure and feature group. Then, clustering methods were applied to search for (i) four clusters, in the case of KM, AH, and GMM and (ii) an unlimited number of clusters in the case of HDBSCAN. These methodological differences may partly explain that preictal changes were identified in EEG and ECG in only 22% of the seizures in the analysed group of patients. Contrarily to EEG, a large number of putative preictal intervals found in ECG started between 70 to 120 minutes before onset. This might indicate that the cardiac changes captured in the ECG might not directly reflect epilepsy-related cardiac manifestations but rather result from medication oscillations and sleep stages, that induce differences in the activation of brain mechanisms (and consequent autonomic modulation) over normal to seizure transition [20, 30]. Nevertheless, such changes may still contain predictive potential.

Influence of methodological aspects

The results obtained with nonlinear feature reduction methods such as UMAP may be more suitable to reveal the nonlinear dynamical functioning of the brain. Accordingly, most studies propose nonlinear systems for epilepsy EEG modelling [11, 264]. Nevertheless, using this nonlinear method and the consequent parameter tuning could significantly impact further data interpretations [261]. Based on this, there is a need for more studies reporting similar EEG data analysis using feature reduction and clustering methods.

Regarding the different groups of features extracted, it was possible to conclude that univariate features were the major source of data distributions containing preictal clusters (and data distribution heterogeneity). The analysis of the reduced multivariate features led to the observation of preictal behaviour for only an additional four seizures compared to the univariate features. Specifically, univariate feature extraction has provided preictal information for 96.5% of the seizures.

The multivariate features are single global measures of functional brain connectivity obtained by applying graph measures to bivariate features. As such, these features reflect global changes in brain activity over time. Even though multivariate and bivariate measures have been associated with high prediction performances, some authors reported preictal alterations predominantly showing in specific channels [13, 14, 253]. In addition, when preictal clusters were identified in both reduced multivariate and univariate data, the vast majority of these intervals would start at

the same point in time and have the same duration for most seizures (see Figures E.8 and E.9 in Appendix E).

Using unsupervised learning seems to appropriately address the problem of preictal interval identification and characterisation. Given the missing knowledge regarding the sequence of brain activity leading to a seizure, it might be limiting to define fixed intervals of preictal activity for supervised seizure prediction. In fact, the preictal intervals determined in this study started in the range of 14.2 to 120 minutes before seizure onset, which is a range difficult to cover with grid-search supervised learning due to the computational load. This range of preictals' starting time demonstrates how the constraints of a preictal grid-search over a user-defined range of preictal intervals can influence results. Unsupervised approaches allow for a relaxation of these constraints and, therefore, increase the probability of finding the correct labels of the preictal interval for each seizure. Additionally, applying clustering methods to physiological data collected before a seizure might unravel seizure-specific preictal profiles that do not arise when conducting the standard interictal versus preictal binary classification.

6.4.2 Study limitations

Unsupervised learning methods are not without limitations. A potential pitfall of the unsupervised methodology corresponds to the difficulty in inferring the source of the different observed clusters. The cluster located near the seizure onset was assumed to correspond to a preictal behaviour that causally led to that seizure. However, these pre-seizure oscillations may not correspond to epilepsy manifestations but be produced by other unrelated confounders (discussed in the next section). Even though this concern was addressed by assessing the association between preictal manifestations and the sleep-wake cycle, it is advisable to obtain clinical annotations, either by video monitoring or EEG interictal close observation, in future unsupervised learning studies. Such information may be crucial to strengthen the conclusions derived from preictal interval exploration through unsupervised learning.

At last, even though this study attempted to produce a fully automatic framework for preictal interval exploration, such a goal was not fulfilled. In fact, clustering evaluation indexes were explored in search of a measure that would automatically identify preictal activity. However, due to the high variability observed among the seizures' three-dimensional representation, selecting a measure matching expert visual inspection was not possible. Such variability also explains the difficulty in categorising some seizures' data distributions into only one of the six reported categories. The contribution of the involved research team was the solution found to overcome this problem. Five experts, all working in the epilepsy field, categorised the data distributions. The problematic cases were discussed, and a final categorisation was achieved. Notwithstanding, new strategies should be sought to allow for

an automatic and user-independent unsupervised preictal interval search.

6.5 Conclusions

The following sections elaborate on this chapter's final reflections and provide suggestions for further research.

6.5.1 Final reflections

In sum, an unsupervised learning framework was used for advancing current knowledge on brain dynamics evolution toward an epileptic seizure. Electroencephalographic information recorded 4.5 hours before the seizure onset was inspected in search of preictal patterns. Seizure-specific distinct clusters have been found for 51% of seizures, suggesting that the EEG has captured preictal alterations before these events. A deeper characterisation of these intervals has been provided, aiming to achieve accurate preictal labelling for developing seizure prediction systems. Additionally, the multistate-like data distribution observed for some seizures may encourage the adoption of the seizure forecasting perspective, which provides information regarding seizure risk over time. Unsupervised learning seems to hold promise in unravelling the underlying mechanisms of seizure dynamics and, consequently, in improving seizure prediction/forecasting.

6.5.2 Future work

This study has laid the path for the retrospective identification of pre-seizure patterns using unsupervised learning methods. However, it can be challenging to envision future prospective applications. The available preictal clusters discovered during this unsupervised learning study require further validation. Specifically, it is now critical to integrate EEG and ECG preictal activity information in seizure prediction models and compare the obtained performance with the performance of a model integrating a preictal interval derived from grid-search (refer to Chapter 7). A practical application could be to train machine learning models using the preictal starting time information found using clustering methods. For instance, it might be possible to train individual models for specific types of seizures or seizures that follow a given circadian pattern if similar preictal intervals are found for these groups. This approach, however, is dependent on the analysis of a considerable number of seizures to train each model. Even though no correlation has been found between the preictal starting time and seizure metadata (vigilance state, seizure type, and EEG onset hour), it is expected that further unsupervised learning studies might reveal such a correlation when exploring other long-term databases. The problem grows more complicated when a different preictal interval is identified for each seizure within a patient, with no apparent pattern among seizures. When training

the models, it is necessary to think about a strategy to use a final preictal interval label, considering that no preictal pattern has been found for some seizures. As a suggestion, it might be possible to design a hybrid solution that consists in defining a final preictal interval to use in training and testing as the average of the clustering preictal intervals and the grid-search preictal intervals for the remaining seizures.

Less invasive procedures, such as subscalp EEG, have been recently developed for ultra-long-term brain monitoring [22, 69, 76]. The method involves implanting subscalp (or subcutaneous) electrodes, for example, unilaterally behind the ear [76]. Subscalp EEG and scalp EEG similarly capture background activity with closed and open eyes, showing a similar signal-to-noise ratio. Additionally, despite subscalp EEG may still be affected by artefacts such as muscle activity, these recordings present improved signal quality compared to scalp EEG, particularly during body movements that produce interferences due to the movement of wires [22, 69, 76]. Concomitantly, scalp EEG devices able to collect data from a few electrodes (placed, e.g. in the temporal lobe) are emerging as alternatives to conventional scalp EEG by providing patients with more comfort and usability [75]. As such, new studies should be designed towards the use of unsupervised learning to explore the capacity of, e.g., scalp EEG temporal channels to capture preictal activity.

Additionally, this research may provide evidence for a future application of unsupervised learning to obtain proictal annotations. Namely, semi-supervised annotation methods could be envisioned to facilitate the annotation of periods of seizure risk while still requiring the clinician's input to obtain the final stratification of seizure risk.

Ultimately, considering multimodal approaches might be crucial to understand seizure generation. There are clearly several factors influencing brain activity shift from normal functioning to seizure that EEG alone cannot capture. Monitoring non-neurological biomarkers such as heart rate, blood pressure, galvanic skin response, and movement might provide critical information regarding seizure triggering and driving mechanisms [12, 16, 66].

Chapter 7

Supervised seizure prediction: the impact of unsupervised preictal search

In this study, the information reported in the previous two chapters regarding the preictal interval starting time was used to develop seizure prediction models. A control seizure prediction approach was compared with a seizure prediction model that integrates preictal unsupervised information. The two approaches were independently implemented for electroencephalography (EEG) and electrocardiography (ECG) data.

The content of this chapter, submitted to a scientific journal, is based on the last study conducted in this thesis. Section 7.1 provides a short context on the study. Section 7.2 comprises the methodology followed while developing prediction models. Sections 7.3 and 7.4 report and discuss the obtained findings, respectively.

7.1 Study context

Despite evidence of autonomic modulation before, during and after a seizure event, prediction studies reporting the exploration of preictal changes in cardiac parameters are still scarce [12, 150]. Inspecting preictal alterations in different signal modalities might ultimately improve current knowledge of the pathophysiological mechanisms underlying seizures [150]. Additionally, in order to consider the single use of non-neurological information to develop seizure prediction models, the prediction potential of non-EEG-based models should be compared with the homologous EEG-based models.

Furthermore, the success of seizure prediction might be determined by the accurate characterisation of the preictal interval [12]. Using seizure-specific preictal interval labels from unsupervised learning to develop prediction models is hypothesised to overcome the traditional approach of defining a fixed preictal interval and

the often-considered approach of performing a patient grid-search on a range of intervals.

The present study aims to evaluate the impact of preictal interval unsupervised learning on the prediction performance of supervised approaches. The added value of the results obtained with unsupervised methodologies (in Chapters 5 and 6) is evaluated here by using them as labels in each patient-specific supervised learning prediction algorithm developed for 19-channel EEG and single-lead ECG data. The models were trained, and quasi-prospectively tested using all recorded data before each seizure's onset. The performance obtained with these models was compared to that obtained when applying a common seizure-specific grid-search for preictal definition. In total, four models were conceptualised and developed, considering a seizure prediction horizon (SPH) of 10 minutes. Models were statistically validated. Importantly, only the univariate linear features were extracted in this study due to computational constraints. Accordingly, only the preictals intervals found for univariate linear features in Chapter 6 were considered here.

7.2 Methodology

The labels determined using unsupervised learning techniques (in Chapters 5 and 6) were used to develop patient-specific prediction algorithms. As the preictal interval was not found for all seizures in some patients, a seizure-specific grid-search was necessary to find the missing preictal intervals. Based on that, the patient-specific prediction algorithms integrated preictal information from unsupervised learning and grid-search, and were named "Hybrid approach". Conversely, the "Control approach" corresponds to patient-specific prediction models that integrated preictal intervals resulting solely from seizure-specific grid-search (see Figure 7.1).

7.2.1 Model development

The general framework can be divided into three steps applied to each seizure: preictal interval grid-search, training and testing (see Figure F.2 in Appendix F). To respect the chronological order of the seizures and the possible inter-seizure temporal dependence, the first three seizures of each patient were assigned to the training set, while the remaining corresponded to the testing set. Accordingly, the training and the testing set comprise 120 seizures (3865 hours of data) and 103 seizures (1638 hours of data), respectively. Several parameters are optimised in the seizure-specific grid-search and then used in the training phase. In the testing phase, these models were quasi-prospectively validated on unseen data. These steps are described in the sections below.

In both the Control and Hybrid approaches, an SPH of 10 minutes was used (as addressed in Section 4.5). In addition, the seizure occurrence period (SOP) was

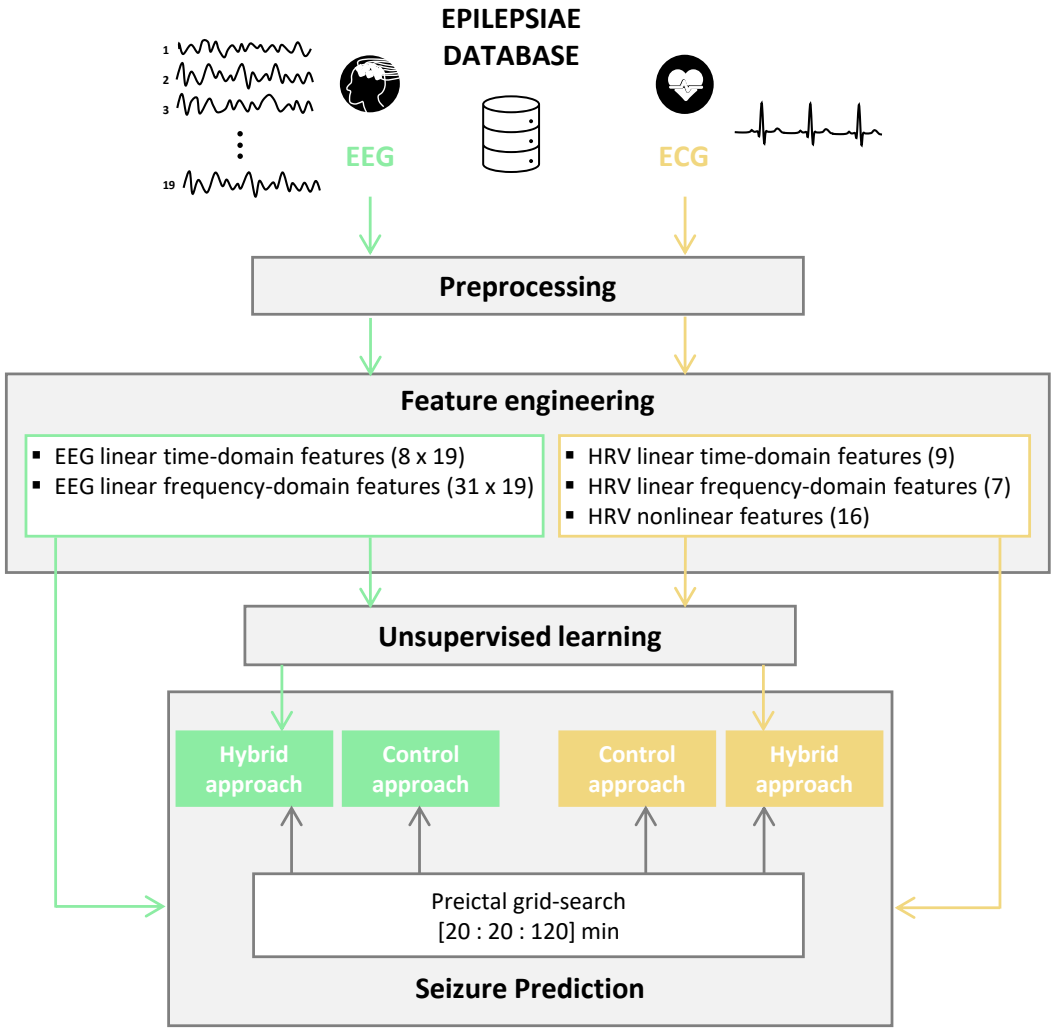

Figure 7.1: Schematic of seizure prediction models. EEG and HRV feature datasets were used to develop seizure prediction models following two approaches. The Hybrid approach uses preictal intervals found in some seizures in unsupervised learning studies and preictal intervals using grid-search for the remaining seizures. The Control approach uses solely preictal intervals obtained in grid-search.

defined as having a duration equal to the training preictal period of each seizure (refer to Figure A.1 in the appendix for some examples) [153].

Lead seizures

In this study, the entire signal preceding a given seizure was inspected. Only lead seizures, i.e., seizures occurring 4.5 hours after the preceding seizure, were considered [156, 157]. Additionally, a minimum of four seizures were required to build the prediction models for each approach and each patient. The first three chronological seizures were used to train the models, while the remaining seizures were used in the testing phase [157]. As per these criteria, only 223 seizures from 40 patients were analysed here (a total of 338 seizures from 41 patients). Seizures were separated, on average, by 24 hours and 40 minutes (standard deviation of 27 hours and 20 minutes

and a maximum of nine days, seven hours and 22 minutes). Details on patient and seizure metadata are provided in Chapter 4.

Preprocessing and feature engineering

The EEG and ECG preprocessing steps are described in detail in Section D.1 and in Lopes *et al.* [248], respectively. The heart rate variability (HRV) features and univariate linear EEG features used in this study were extracted for all the time preceding the seizure onset. Table 7.1 presents all the extracted features from HRV and EEG, which are also thoroughly described in Sections D.2 and E.1, respectively.

The samples comprised in the 10 minutes before the seizure onset and the 30 minutes after the previous seizure offset (in the case of subsequent seizures) were removed, similarly to what was done in Section 6.2.4 of Chapter 6.

Each of the two feature datasets was then standardised using z-score.

Table 7.1: Features extracted from EEG and HRV signals.

Signal	Linearity/ Domain	Features
HRV	Linear/Time domain	Number and percentage of RR intervals that last more than 50 ms (NN50 and pNN50); standard deviation of RR intervals (SDNN); square root of the mean squared differences of successive RR intervals (RMSSD); standard deviation of the differences between successive RR intervals (SDSD); minimum, maximum, mean and variance of the RR intervals (RRMin, RRMax, RRMean and, RRVar).
	Linear/Frequency domain	Total power; very low frequency (VLF) power; low frequency (LF) and high frequency (HF) powers and the ratio between the two features (LF/HF); LF norm and HF norm.
	Nonlinear	Standard deviation of length and width of the ellipse fitted to the Poincaré plot (SD_1 and SD_2) and the ratio between the two features (SD_1/SD_2); detrended fluctuation analysis (DFA) slope α_1 and α_2; approximate and sample entropies (ApEn and SampEn); largest Lyapunov exponent (LLE) and correlation dimension (CD); recurrence quantification analysis (REC, L, TT, DET, LAM, ENT, L_{max}).
EEG	Linear/Time domain	Statistical measures (normalised and non-normalised mean amplitude, standard deviation, skewness, and kurtosis); Hjorth parameters (activity, mobility, and complexity).
	Linear/Frequency domain	Spectral power and relative spectral power in each frequency band (delta, theta, alpha, beta, and gamma); total power; spectral edge power (at 50%); mean frequency; 12 frequency bands power ratios; energy of 6 wavelet coefficients.

Feature Selection

Feature selection was carried out to identify and remove features with similar and/or low prediction power (relevancy and redundancy assessment, respectively). Filter-based feature selection methods were used because they are computationally less complex when compared to embedded and wrapper methods.

Filter-based relevancy methods yield a rank of features according to their capability to discriminate between interictal and preictal classes. From this rank, the F more relevant features were chosen. The filter-based relevancy methods considered in this study were the ANOVA f-test, the area under the receiver operating characteristic curve (AUC), and the Kruskal-Wallis H test. In the grid-search step, a relevancy method is chosen, and the parameter F is optimised.

Considering features to be highly correlated if they exhibit a correlation higher than 90%, the pairwise correlation between all features was evaluated, excluding those of each pair which were more common among all pairs if they were highly correlated. Here, Pearson's correlation coefficient (linear) and Spearman's rank coefficient (nonlinear) were applied in parallel, selecting the union of the features selected by the two methods, i.e., the features selected by at least one of the methods.

The EEG and HRV feature datasets were analysed differently regarding the order of application of the relevancy and redundancy assessment methods. As the HRV feature dataset contains only 32 features, filter-based redundancy assessment methods were first applied to exclude highly correlated features. Secondly, filter-based relevancy assessment methods were used to select F features. The EEG feature dataset contains 39 features for each of the 19 acquisition channels (741 features in total). Consequently, the computationally feasible option was to first select the F most relevant features from the dataset using filter-based relevance assessment methods and then remove the redundant features.

Classification

The selected feature dataset was then fed to a linear support vector machines (SVMs) (refer to Section F.1.1 in Appendix F for more details). The class imbalance problem was addressed by assigning weights to each class (interictal and preictal) according to class frequency. Namely, each class weight is inversely proportional to the class's frequency [153, 157].

Postprocessing

The classifier's output was postprocessed using the firing power method [177] as the regularisation filter to reduce the number of false alarms (as addressed in Section 2.5.7). Importantly, the firing power proposed by Teixeira *et al.* [177] was adapted here to handle temporal gaps resulting from not concatenating windows after preprocessing. As a consequence, each gap in the classifier's output time series is assigned

zeros by the firing power (similarly to the interictal samples). The number of zeros corresponds to the duration of the gap in the SOP window divided by the 5-second window used in the feature extraction step.

In this study, the firing power threshold corresponds to 0.7 meaning that if more than 70% of samples are classified as preictal, in each SOP window, an alarm is raised [11, 175, 235, 236]. This is a more conservative firing power threshold that prevents SVMs classifier from overfitting the training samples [153, 157].

Performance metrics

To evaluate the performance of the developed prediction models on the testing seizures, the two standard measures used in seizure prediction were computed: seizure sensitivity (SS) and false prediction rate per hour (FPR/h) (as described in Section 2.5.5).

Grid-search

First, a grid-search procedure was performed to search for the optimal value of the following parameters in the seizure prediction framework:

- Preictal intervals: $P = [20, 40, 60, 80, 100, 120]$ minutes (grid-search for all seizures in the Control approach and for some seizures in the Hybrid approach);
- Relevancy assessment methods: M_{rel} =[ANOVA f-test, AUC, Kruskal-Wallis H test];
- Number of features selected in feature relevance assessment for each signal type: $F_{rel_{EEG}} = [10, 20, 30, 40, 50, 100]$ and $F_{rel_{ECG}} = [5, 10, 15, 20, 25, 30]$;
- SVMs cost: $C = [2^{-20}, 2^{-16}, 2^{-12}, 2^{-8}, 2^{-4}, 2^{0}, 2^{4}, 2^{8}, 2^{12}, 2^{16}, 2^{20}]$;

For each set of parameters, a three-fold cross-validation technique was used. In each k fold, the k^{th} seizure is used for validation, and the remaining two are concatenated yielding the training set. The mean of the preictals corresponding to the training seizures is used to validate the k^{th} seizure.

For each fold, the performance of the binary classification was evaluated by computing the geometric mean (GM in equation 7.1) between the point sensitivity (SE) and point specificity (SP) (described in Section 2.5.5). The performance for a given set of parameters corresponds to the average of the performance obtained for the three folds. This metric was used to deal with the problem of class imbalance. Then, the set of parameters with the highest performance is chosen.

$$GM = \sqrt{SE \times SP} \tag{7.1}$$

The optimisation of the preictal interval is performed differently according to the approach. In the Control approach, a seizure-specific optimisation was performed

using a grid-search of a set of preictal intervals. In the end, each training seizure is assigned an optimal preictal interval. In literature, the preictal grid-search process occurs at a patient-specific level. However, in this study, a preictal interval was selected for each seizure so that it was possible to compare the results obtained herein with the unsupervised learning studies. To select the optimal preictal for a given seizure, permutations with repetitions of the discrete preictal intervals considered were computed.

In the Hybrid approach, the values obtained with the unsupervised learning methodologies were used (when available), and the grid-search was applied for the remaining seizures as described above. For the ECG-based models, a total of 92 preictal intervals were discovered with the unsupervised learning methods (after excluding patients with less than four seizures and preictal intervals starting after the SPH interval and including only preictal information for the EEG lead seizures). Considering that only the three first seizures of a given patient have been used to train each patient-specific model, it follows that a total of 44 preictal intervals have been used to develop ECG-based prediction models. In the case of the EEG-based models, the unsupervised learning task returned 98 preictal intervals when analysing the univariate linear features (after excluding patients with less than four seizures). A total of 50 preictal intervals (10 from category 3 and 40 from category 6) were used during the training phase.

Training

The second step consisted in training the final patient-specific models using the training dataset, the optimised parameters, and the training mean and standard deviation values to standardise training seizure data.

Quasi-prospective evaluation

Afterwards, the trained models were tested on the unseen data (testing set). For each patient, the preictal period was defined as the average of the values obtained for the training seizures (and obtained with unsupervised learning in the case of the Hybrid approach). The firing power was applied to postprocess the classifier's output and generate alarms using $T = 0.7$. The results were then evaluated using SS and FPR/h and statistically validated using the adapted seizure times surrogate analysis.

7.2.2 Statistical analysis of the results

The statistical analysis performed in this study is detailed in the next subsections.

Assessment of above chance prediction

An adapted version of the seizure times surrogate analysis [172] was applied to determine if the prediction algorithm performed above the chance level. Briefly, for a given seizure data, the seizure onset time was randomly shifted 1000 times within the interictal time (see Section F.1.2 in Appendix F for a more detailed explanation). Above chance performance is observed when the algorithm's seizure sensitivity overcomes the surrogate seizure sensitivity with statistical significance. In this study, a one-tailed one-sample t-test was used, considering a significance level of $\alpha = 0.05$.

Pairwise model comparison of SS and FPR/h

The SS and FPR/h results obtained for each signal (EEG and ECG), and each approach (Control or Hybrid) were assessed regarding normality and further compared in a pairwise fashion using the proper statistical test. In this study, the non-parametric two-sided Mann-Whitney U rank test was used, considering a statistical significance of $\alpha = 0.05$.

Above chance prediction on the whole group of patients

The results obtained for each signal and each approach were investigated in the search for statistically significant above chance prediction in the analysed set of patients [149, 153, 157]. In other words, the null hypothesis that the number of statistically validated patients follows a binomial cumulative distribution was tested. Considering a significance level of $\alpha = 0.05$, the probability of obtaining above chance sensitivities for at least n of N patients is given by:

$$P_{binom}(n, N, \alpha) = \sum_{j \geq n} \binom{N}{j} \alpha^j (1-\alpha)^{N-j} \tag{7.2}$$

Pairwise model comparison of above chance prediction

Lastly, the above chance performance proportions between the pairs of developed models were statistically tested in the search for significant differences. Specifically, a test of proportions was applied under the null hypothesis that, for instance, the proportion of patients with above chance performance for the EEG-based Hybrid model is not significantly different from the ECG-based Hybrid model. A significance level of $\alpha = 0.05$ was considered for this test.

7.3 Results

The results obtained for the four seizure prediction models (EEG- and ECG-based models, each using Hybrid and Control approaches) developed in this study are

presented in this section. Section F.2 in Appendix F contains information regarding the prevalence of the different grid-search parameters in the final prediction models.

7.3.1 Prediction performance

Figure 7.2 shows the SS and above chance performance results obtained by applying each patient-specific prediction model on the testing seizures, independently for EEG and ECG data and Hybrid and Control approaches. When comparing Hybrid and Control approaches for each signal type, it was possible to observe a general concordance regarding the patients for which high SS was obtained. A pairwise comparison of the SS values (e.g., between EEG and ECG for the same approach, or between Hybrid and Control for the same type of signal) yielded: (i) higher SS for the Hybrid approach (when comparing to Control) for EEG (the contrary was observed for the ECG) and (ii) higher SS for the EEG (when comparing to the ECG, for both Hybrid and Control approaches). The differences observed for SS were statistically significant only when comparing the EEG and ECG models for the Hybrid approach (EEG-Hybrid vs EEG-Control: p=0.81; ECG-Hybrid vs ECG-Control: p=0.74; EEG-Hybrid vs ECG-Hybrid: p=0.02; EEG-Control vs ECG-Control: p=0.07).

The values of FPR/h show some variation among signal types (see Figure 7.3). While the FPR/h values obtained for the ECG-based models fitted in the $[0, 0.5]$ interval (except for three patients), that did not occur for the EEG-based models, which showed more scattered values for some patients. No striking difference was

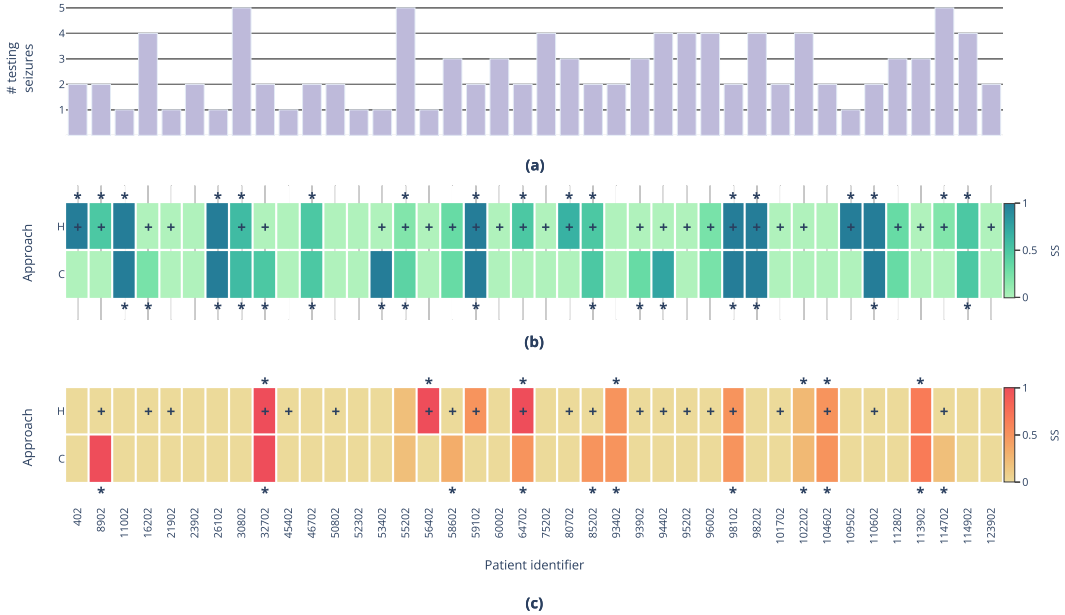

Figure 7.2: Testing results for seizure prediction sensitivity (SS). Panel (a) shows the number of leading seizures tested for each patient. Panels (b) and (c) depict the seizure prediction sensitivity obtained for EEG and ECG data, respectively, and for Hybrid (H) and Control (C) approaches. Asterisk symbols indicate patients with prediction sensitivity above chance level. Plus symbols indicate patients for whom preictal intervals have been identified using unsupervised learning for at least one seizure.

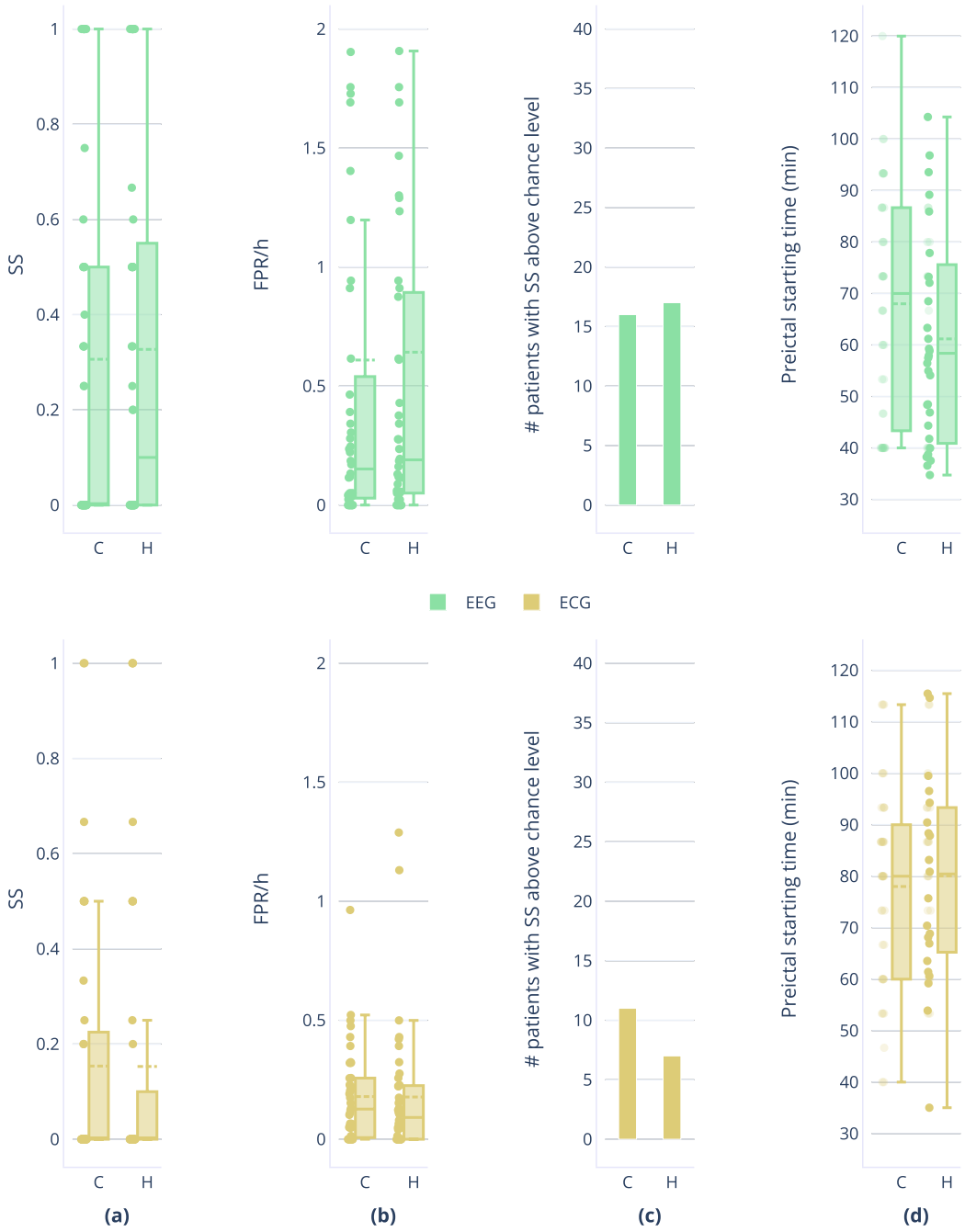

Figure 7.3: Testing results for seizure prediction performance. Performance was evaluated in terms of seizure sensitivity (SS, panel (a)), false prediction rate per hour (FPR/h, panel (b)) and above chance performance (panel (c)) for ECG-based and EEG-based Hybrid (H) and Control (C) models. The preictal starting time before the seizure onset (averaged across seizures) is also presented for each patient (panel (d)). In the boxplots, dots correspond to variables' data points. Solid and dashed lines indicate medians and means, respectively. Box's tops and bottoms correspond to the 75th and 25th percentiles, respectively. Whiskers refer to the span of each variable after discarding outliers. The opaque dots shown for the Hybrid approach in the preictal starting time boxplots indicate averaged preictal intervals for the patients for whom a preictal clustering interval has been found. In the boxplot representing the results of FPR/h for the EEG signal, there are two outliers that are not depicted (7.8 and 8.7 for Hybrid and Control approaches, respectively).

Table 7.2: Results for the statistically validated group of patients.

Signal type	Approach	$\mathbf{P_{binomial}}$	SS	FPR/h	ACL
EEG	Hybrid	$P_{bin}\{17, 40, 0.05\} = 2.2e-12$	0.72±0.30	0.94±1.86	0.42
	Control	$P_{bin}\{16, 40, 0.05\} = 3.0e-11$	0.71±0.29	0.50±0.63	0.40
ECG	Hybrid	$P_{bin}\{7, 40, 0.05\} = 3.4e-3$	0.70±0.30	0.17±0.13	0.17
	Control	$P_{bin}\{11, 40, 0.05\} = 2.9e-6$	0.54±0.26	0.14±0.10	0.28

SS: seizure sensitivity (Mean±SD) in the range $[0, 1]$. FPR/h: false prediction rate per hour (Mean±SD). ACL: ratio of patients with above chance level sensitivity in the range $[0, 1]$.

observed between the FPR/h values obtained for Hybrid and Control approaches for the same signal. The four pairwise model comparisons yielded statistically significant differences only when comparing the EEG and ECG models for the Hybrid approach (EEG-Hybrid vs EEG-Control: p=0.50; ECG-Hybrid vs ECG-Control: p=0.41; EEG-Hybrid vs ECG-Hybrid: p=0.02; EEG-Control vs ECG-Control: p=0.40).

Additionally, as can be seen in Table 7.2, using the Hybrid approach increased the patients with above chance level SS in one patient for EEG-based models and decreased that metric in two patients for the ECG-based models. The percentage of patients performing above chance level was higher for EEG-based models compared to ECG. Differences in the patients' proportions were statistically significant when comparing the EEG and ECG models for the Hybrid approach (EEG-Hybrid vs EEG-Control: p=0.82; ECG-Hybrid vs ECG-Control: p=0.28; EEG-Hybrid vs ECG-Hybrid: p=0.01; EEG-Control vs ECG-Control: p=0.24). Nevertheless, it was possible to reject the null hypothesis that the above chance level seizure sensitivities obtained for each model followed a binomial distribution. This indicates that the ratio of statistically validated patients for each model was significant in the entire group of analysed patients. Also, eleven patients were statistically validated both with EEG- and ECG-based Hybrid models. For Control models, six patients were statistically validated with models using both signal types.

Lastly, it is important to note that high performances were obtained only for one and two patients for ECG- and EEG-based models, respectively (refer to Table 7.3). By high performance, it is meant that, when testing a given model, an SS equal to or above 0.8, an FRP/h of less than 0.15 and an above chance level prediction were obtained. The reference value of 0.15 FPR/h has been suggested for patients under presurgical monitoring [147]. Hybrid and Control models performed similarly in each patient. ECG- and EEG-based models developed for patients 32702 and 98102, respectively, integrated one training seizure having an unsupervised preictal interval. As expected, in the case of the remaining patients, whenever high values of SS were found, high values of FPR/h were often obtained, reflecting the trade-off between these two metrics in seizure prediction models.

7.3.2 Preictal duration

Panel D in Figure 7.3 presents the values of averaged preictal starting time before seizure onset for each patient, for each approach and signal type. In ECG-based models, the boxplots for preictal starting time are more similar across approaches. The difference in distributions between Hybrid and Control approaches becomes more evident for EEG-based models, with more patients showing a preictal interval starting between 40 and 70 minutes before seizure onset. Additionally, preictal intervals start earlier for EEG-based models compared to ECG-based ones.

7.3.3 Metadata analysis

The patient stratification was performed according to the following criteria: (i) patients presenting seizures of one type, (ii) patients with pre-seizure activity annotated by clinicians as rhythmic theta waves, and (iii) seizure vigilance state (patients that only experienced seizures while awake), and (iv) patients that suffered only day-time seizures (as defined in [149,153]). Although other criteria have been considered, only

Table 7.3: Results for the patients with high performance.

Signal type	ID	EEG onset hour (hh/mm/ss)	Seizure type	Starting time* (min)	Train/ Test	SS	FPR/h
ECG	32702	08:25:28	FOIA		Train	H: 1 C: 1	H: 0.10 C: 0.05
		10:22:47	FOIA		Train		
		10:13:13	FOIA	83.3	Train		
		17:03:16	FOIA	79.6	Test		
		09:29:02	FOIA	38.6	Test		
EEG	26102	15:31:37	FOIA		Train	H: 1 C: 1	H: 0.05 C: 0.05
		08:33:50	FOIA		Train		
		07:52:54	FOIA		Train		
		11:36:45	FOIA	16.1	Test		
	98102	07:17:49	FOA		Train	H: 1 C: 1	H: 0.02 C: 0.02
		18:49:53	UC	92.8	Train		
		05:18:58	UC		Train		
		06:11:33	UC		Test		
		04:07:04	FBTC		Test		

Seizure ILAE classification: focal onset aware (FOA), focal onset impaired awareness (FOIA), focal to bilateral tonic-clonic (FBTC), unclassified (UC). H: Hybrid approach. C: control approach. *Values for the putative preictal intervals identified with unsupervised learning. SS: seizure sensitivity, in the range $[0, 1]$. FPR/h: false prediction rate per hour. All seizures occurred when the patient was in the vigilance state of wakefulness. Seizure sensitivity above chance level was observed for all patients.

stratification groups with 10 or more patients were considered here. As shown in Table 7.4, no criterion was found to improve seizure prediction performance.

7.3.4 Grid-search parameters

Appendix F Section F.2 contains information regarding the prevalence of the different grid-search parameters in the final prediction models.

Regarding ECG-based models, it was possible to observe a large agreement among Control and Hybrid approaches which can be largely explained by the order of the feature selection process: feature redundancy assessment followed by feature relevancy evaluation. As the difference between both approaches lies in the definition of the preictal intervals for each seizure, the difference in feature selection will be noticed only in the feature relevancy assessment. As such, around 24 to 27 features are often considered nonredundant in both approaches. From those, the algorithm often selected five relevant features, a selection tendency observed in both approaches. The most prevalent HRV features include linear time-domain features (*RRMin*, *RRMean*, *SDSD*), linear frequency-domain features (*HF Norm* and *VLF Power*) and several nonlinear features (*SampEn*, *RQA ENT*, *RQA L* and *RQA REC*). AUC and ANOVA f-test were the feature selection methods most often chosen in the grid-search step. The cost value of the optimised SVMs models

Table 7.4: Average performance results for all patients and for the stratified groups of patients.

Stratification	#Pt	Hybrid			Control		
		SS	FPR/h	ACL	SS	FPR/h	ACL
FOA | FOIA	10	0.39±0.44 0.15±0.32	0.43±0.49 0.21±0.37	0.10 0.02	0.54±0.42 0.13±0.31	0.32±0.42 0.21±0.27	0.15 0.05
FOIA | FOIA & UC	14	0.37±0.37 0.12±0.30	0.99±2.00 0.13±0.15	0.15 0.05	0.28±0.35 0.26±0.37	0.98±2.22 0.13±0.15	0.10 0.15
Rhythmic theta waves | Rhythmic theta waves & unclear	13	0.32±0.43 0.12±0.21	1.09±2.02 0.30±0.42	0.15 0.02	0.38±0.45 0.08±0.18	1.12±2.26 0.24±0.26	0.12 0.05
Wakefulness	18	0.46±0.46 0.18±0.33	0.89±1.78 0.27±0.36	0.28 0.05	0.37±0.42 0.16±0.32	0.85±1.99 0.22±0.22	0.20 0.10
Day-time (starting at 10pm and ending at 7am)	15	0.15±0.22 0.19±0.31	0.29±0.34 0.09±0.12	0.10 0.12	0.10±0.18 0.26±0.31	0.22±0.31 0.11±0.14	0.08 0.18
Overall	40	0.33±0.39 0.15±0.30	0.64±1.28 0.18±0.27	0.42 0.18	0.31±0.38 0.15±0.27	0.61±1.41 0.18±0.20	0.40 0.28

Results for EEG- (■) and ECG-based (■) models. SS: seizure sensitivity (Mean±SD) in the range $[0, 1]$; FPR/h: false prediction rate per hour (Mean±SD); ACL: ratio of patients with SS above chance level, in the range $[0, 1]$; FOA: focal onset aware seizure; FOIA: focal onset impaired awareness seizure. UC: unclassified seizure. #Pt: number of patients.

was found to take mainly values below 2^{-8}, evidencing the selection of models with larger generalisation ability [297].

The results for the EEG-based prediction models show that in most patients, the models selected 10 or 20 relevant features. Afterwards, the redundancy methods would select mainly five features. All the spectrum of extracted EEG features was important for classification, with exception of the time-domain feature *Skewness*. In terms of electrodes, we observed some prevalence of Pz, P4, T8 and P7. Additionally, there was a clear prevalence of the Kruskal-Wallis H test as a feature relevance method in the EEG-based prediction models. Regarding the SVMs cost value, we observed a striking predominance of low values of C, specifically, the value 2^{-20}.

7.4 Discussion

This study assessed the impact on seizure prediction performance of preictal interval labels obtained using unsupervised learning. To that end, a Control approach was compared with a Hybrid approach. The former corresponds to a common seizure prediction model that defines a preictal interval by performing a grid-search on a range of user-defined preictal intervals. The latter integrates information on unsupervised preictal labels for some seizures and grid-search preictal labels for the seizures for which no unsupervised preictal has been found. The models were developed independently for EEG-based and ECG-based simultaneously acquired data, allowing the comparison of the prediction performance between models integrating brain information and models based on cardiac parameters. All models were tested quasi-prospectively on previously unseen data.

7.4.1 Key aspects

Important aspects of this study are separately discussed in the next subsections.

Performance of prediction models

Using unsupervised preictal interval labels in seizure prediction resulted in above chance prediction in 17 and 7 patients (using EEG and ECG data) compared to using simply a grid-search procedure (16 using EEG data and 11 using ECG data). Despite the lack of statistically significant differences among these proportions, the number of statistically validated patients was significant in the group of 40 patients analysed in this study, for any of the four models. Additionally, high performance (i.e., SS of 0.8 or above, FPR/h below 0.15 and above chance level sensitivity) was obtained in three patients using two EEG- and one ECG-based models. The results show that considering the Hybrid approach did not improve seizure prediction compared to a control method. Nevertheless, we enforce the need to obtain preictal labels using unsupervised learning on data containing a higher number of seizures

for each patient [154]. This method might prove useful when applied to seizures occurring only during the night or day.

When comparing the results obtained for EEG- and ECG-based models for the same approach, it was possible to conclude that with EEG data, more patients were statistically validated, with statistical significance for the Hybrid approach. Also, statistically significant differences were observed among signal types regarding SS and FPR/h for the Hybrid approach. As such, in the analysed dataset, using ECG data to develop prediction models may be helpful for some patients, but still does not compete with the use of EEG recordings in seizure prediction. These results were not surprising [150, 233] given that the brain is the origin of the hypersynchronous neuronal activity characteristic of epilepsy events.

Importantly, developing patient-specific models revealed the expected variability in performance and grid-search selected parameters. Interestingly, in EEG-based models, the selected features varied substantially among patients confirming early speculations on the need to explore patient-specific preictal features [17].

Comparison with state-of-the-art studies

The obtained results were compared with other state-of-the-art studies also using EEG data contained in the EPILEPSIAE database to evaluate prediction models quasi-prospectively [149, 153, 157, 236]. Alvarado-Rojas *et al.* [149] developed a threshold-based seizure prediction model using intracranial EEG data from 53 patients with different types of focal epilepsy (a total of 531 days and 558 seizures). They obtained an SS of 0.48, an FPR/h of 0.95 and three (9.4%) statistically validated patients in the group of 32 patients with only temporal lobe focus seizures. Direito *et al.* [236] reported the analysis of both scalp and intracranial EEG data from 216 patients with seizures occurring in different focal regions (a total of 697 days and 1206 seizures). The developed SVMs prediction models yielded an SS of 0.39, an FPR/h of 0.21 and 10% of patients with sensitivity above chance level, for the scalp EEG recordings (185 patients). The average SS and FPR/h results were stratified according to the focal region, with an SS of 0.38 and an FPR/h of 0.23 for the temporal lobe. In these studies, improved sensitivity was often achieved at the cost of increasing the false prediction rate, with such a trade-off also showing in the current study's results: lower false prediction rate but also lower sensitivity. A striking difference was observed when comparing the ratio of statistically validated patients, with the current study showing a considerably higher percentage of patients with above chance performance. Importantly, authors in [149, 236] applied the random predictor as the statistical validation method instead of the surrogate analysis used herein.

In the other two studies [153, 157], each patient's database ID was provided, allowing for a more direct comparison with results reported in this chapter (refer to

Section F.3 in Appendix F). The reported patient-specific seizure prediction models were developed using scalp EEG data, and evolutionary algorithms [153, 157]. The results in these two studies were compared with the EEG-based Hybrid model for the patients analysed in both studies (i.e., patients analysed in Pinto *et al.* 2021 [153] and with the EEG-based Hybrid model and patients analysed in Pinto *et al.* 2022 [157] and with EEG-based Hybrid model). Consistent results were obtained among these models, with the trade-off between sensitivity and false alarm rate being evident in the observed averaged results. The ratio of statistically validated patients was higher with the EEG-based Hybrid models compared to the other two models. Interestingly, there were four patients (85202, 110602, and 114902) that were statistically validated by the three prediction methodologies under comparison. However, the high-performance values observed for patients 26102 and 98102 using the EEG-based models did not stand out for any of the Pinto *et al.* studies. Such observation might align with the difficulty in identifying the preictal interval and the consequent impact on prediction performance [12]. Importantly, the EEG data used in this study was thoroughly preprocessed to minimise the impact of artefacts in seizure prediction [248]. Specifically, besides using high-pass and notch filters [153, 157], data were denoised using also independent component analysis. Lastly, another difference lies in using all data before seizure onset to train the prediction models. Due to computational constraints, Pinto *et al.* studies [153, 157] used only the four hours before seizure onset to train their prediction models.

Regarding the ECG-based models, no studies report the use of recordings comprised in the EPILEPSIAE database. Recently, a comprehensive study compared EEG- and ECG-based seizure prediction models [150]. The study was conducted to understand the predictive potential of extracerebral modalities currently under study to replace invasive devices. Meisel & Bailey [150] reported similar performance for models based on the power spectral density of ECG signals and models based on the power spectral density of scalp EEG data. Results in this chapter align with this study in the case of the Control approach, for which no statistically significant differences were found between the ECG and EEG models. Interestingly, the performance varies considerably among patients for each signal type, with patients with high performances not overlapping among signal types. Such results suggest the occurrence of the patient-specific brain and cardiac alterations before the seizure onset.

7.4.2 Study limitations

Several aspects should be weighted when interpreting the results in this chapter. Namely, data analysed here were collected while patients were under presurgical evaluation. During the in-hospital stay, patients are submitted to activation procedures (e.g., medication withdrawal or sleep deprivation) to provoke seizures for

diagnosis purposes [167]. Naturally, the seizure frequency during this period is an overestimation of the seizure frequency observed in routine ambulatory monitoring [17, 147]. Consequently, despite tested quasi-prospectively in the held-out seizures, the developed patient-specific prediction models should also be tested in data collected during patient real life.

The results also suggest that a real-life application might only be fruitful for a small number of patients. The prediction performance obtained for the vast majority of patients using the Hybrid models (models with the largest number of statistically validated patients) precludes the integration of such models in warning devices. Note that, despite no correlation has been found between the number of testing seizures and the obtained performance results, eight patients only had one testing seizure, and, on average, 2.57 seizures were tested per patient. Future studies are required to achieve more robust results. Namely, the reported results should be confirmed by analysing long-term data comprising a high number of seizures and a considerable amount of metadata. With such a study, it might be possible to find a strong correlation between a given preictal interval and, e.g., a given seizure type or vigilance state. In that case, prediction models could be tailored for those metadata characteristics, with the possibility of clinical application.

Besides the low sensitivity values, the number of false alarms was also too high to render a real-life application possible. Similarly, despite reporting above chance level performance, many other studies also achieve underperforming results [154,166]. The occurrence of false positives has been suggested to result from the involvement of homeostatic mechanisms or other exogenous factors (e.g., medication) that activate brain processes to resume seizure-free brain activity and prevent seizure occurrence [16, 17]. Another possibility is that the models are raising false alarms in synchrony with circadian rhythms [17, 170]. The interictal epileptiform activity, besides being predominantly modulated by the sleep-wake cycle, has been reported to follow a circadian pattern [65]. As such, it has been suggested that specific models could be trained to identify different types of epileptiform activity [17]. However, this task might be challenging, as even clinicians do not often reach a consensus on the definition of this type of epileptic activity [43].

A similar distribution of false alarms was observed among Control and Hybrid approaches for the same type of signal. These results seem to agree with a recent study [154] suggesting that different prediction algorithms might present a strong correlation regarding the number of false and missing alarms. Although our models only changed regarding the value of the preictal intervals used to train the models, we also agree that there are intrinsic aspects of the data that will equally affect different methodologies (e.g., low number of seizures and marginal representation of different brain states).

The false alarm rate has, therefore, fuelled open discussion [16, 154, 159, 170]. By adopting an “all-or-nothing” perspective (classification into alarm or not), seizure

prediction models are not allowing the occurrence of the mentioned aspects characterising an epileptic brain. Seizure forecasting frameworks can address such concerns by considering the existence of periods of increased seizure likelihood, during which a seizure may or may not occur [16,166]. However, similarly to deterministic models, probabilistic forecast ultimately requires the definition of a threshold to translate a given risk of seizure occurrence into an intervention (e.g., taking rescue medication or behavioural measures) [166]. Given the lack of a ground truth, the precise duration of the proictal state is also hypothesised by researchers [68,154]. The uncertainty regarding these aspects may render the comparison among studies more difficult [154,166].

Forecasting seizures still requires clarification on some critical points before considering a clinical application. For instance, a clinical utility is currently dependent on reaching a consensus on the required accuracy of a seizure forecast [265]. The type of clinical application might also help guide the researcher in developing seizure forecasting or seizure prediction models [166]. However, there is uncertainty about choosing forecasting, prediction or both. Forecasting can, theoretically, be applied alone by providing the patient with a forecasting horizon of, e.g., three days during which a benzodiazepine treatment is administered (reducing habituation and dependence) [159]. In the case of prediction, the patient is warned of an upcoming seizure hours to minutes before the onset, allowing for the intake of a single benzodiazepine and optimally reducing the medication side effects to the minimum possible. A third option, known as a nested approach [68,159,166], is to inform the patient about a period of high seizure risk, during which it is possible to carefully plan daily activities. During that period, the patient can also be warned of a seizure within an interval of hours and minutes that grants enough time to take the rescue medication. When developing prediction models, the false alarm rate per hour remains an important measure to help the clinician decide on the number of false alarms each patient might tolerate.

Another two aspects that deserve attention are related to two assumptions made when developing supervised prediction models. The first is that when performing cross-validation with the training data, the temporal sequence of the seizures is not taken into account. Conversely, in the testing phase, the models are applied to each subsequent seizure, respecting its temporal order. The second aspect concerns one insight from unsupervised learning studies: the alterations observed in features before the seizure onset might not remain until the onset. Similarly, a decrease in seizure likelihood before the seizure onset has also been observed during the proictal state in some seizure forecasting studies [17, 65]. However, the preictal interval, starting when those alterations occur, is assigned as zeros until the seizure onset. Assuming that the preictal alterations increase or, at least, remain unchanged until the seizure onset might mislead the SVMs classifier and underestimate the training performance. Ultimately, these two aspects will influence the choice of the optimal

parameters during grid-search and the resulting testing performance.

7.5 Conclusions

The following sections elaborate on this chapter's final reflections and provide suggestions for further research.

7.5.1 Final reflections

In conclusion, this study provides evidence for the potential of using preictal unsupervised labels when developing supervised seizure prediction models. EEG-based models integrating unsupervised preictal labels provided significantly improved prediction for more patients than the homologous ECG-based model. High prediction performance was identified in three patients (two with EEG-based models and one with ECG-based models). Envisioning future applications with noninvasive devices, the prediction performance among signal types was comprehensively compared. More patients verified an above chance performance using EEG-based models compared to ECG-based models. However, the ECG-based models yielded statistically validated performance for seven patients which was not verified with EEG. These findings support the hypothesis that inter-patient variability might be partially addressed by considering multimodal sources of information [166]. Lastly, exploring preictal alterations in noncerebral sources of information might help devise treatment strategies that more directly address patient concerns on device comfort and stigmatisation.

7.5.2 Future work

This work settles the path for future studies which should address the previously mentioned limitations. Summarily, new seizure prediction studies should attempt to confirm the potential of using preictal labels obtained with unsupervised learning methods to predict seizures. These studies must be conducted on long-term data collected over months to years in real-life conditions. Such conditions are critical to have a significant number of seizures to train the models and increase trust in the returned decisions. Additionally, expanding knowledge on the preictal interval might also be closely dependent on the analysis of chronic data.

Analysis of non-neurological data should also be the focus of new research. This choice meets the patients' requirement for noninvasive seizure prediction and, therefore, for less stigmatising data collection.

Chapter 8

Conclusions

This chapter highlights the main contributions and provides a global balance of the conducted research. Future directions are also discussed here.

8.1 Summary of the main contributions

This thesis presents a systematic study on the potential of unsupervised learning to unravel preictal patterns in electroencephalography (EEG) and electrocardiography (ECG) data. The obtained preictal information was later assessed regarding its capability to improve seizure prediction performance.

In Chapter 5, preictal patterns were sought on heart rate variability data using unsupervised methods. Three-dimensional representations of each three-by-three feature combinations were inspected. The study showed that cardiac-related alterations indicative of a putative preictal interval were observed in 41% of the seizures and 90% of the patients. Despite the low percentage of success, these results indicate that cardiac parameters resulting from altered autonomic function during pre-seizure may convey preictal information complementary to brain-related preictal changes.

In Chapter 6, the characterisation of the preictal interval continued, this time on EEG recordings simultaneously collected with the previously assessed ECG data. This time, the three-dimensional representation of the three components obtained by feature dimensionality reduction was inspected. The results showed preictal clusters in 51% of seizures and 90% of patients. Interestingly, the visual inspection of the clustered signals over time was insightful in the sense that it unravelled distinct distributions in EEG features. Specifically, for some seizures, it was possible to observe multi-clustered distributions, which might indicate the occurrence of multi-brain states. These observations were valuable, on one side, in understanding the seizure-specific profile of the ictogenesis process. On the other side, it was also concluded that the definition of a fixed preictal interval for all seizures annotated for a given patient might be limited in addressing the variability of the seizure generation process in that patient.

Chapter 7 presents the last contribution, where it was hypothesised that the accurate estimation of the preictal interval would improve seizure prediction performance. In addition, the prediction potential of the ECG data was also compared with the EEG. Results indicated that models using annotated preictal intervals using unsupervised learning did not improve seizure prediction, performing comparably to models using preictal grid-search. Conversely, statistically significant differences were found between the performance of EEG- and ECG-based models, when using unsupervised preictal intervals but not when using grid-search preictal intervals. Such finding, evidencing at least that the EEG is not significantly superior to the ECG in the Control approach, is important to keep studying non-neurological preictal changes in patients with drug-resistant epilepsy.

8.2 Added value of contributions and future directions

The exploration of non-neurological data is currently underway as these types of data might more easily be collected either at the hospital or during everyday life. Particularly, epilepsy management is evolving towards the development of wearable devices that collect long-term data from peripheral measurements, including heart rate, electrodermal activity, actigraphy, and temperature [166]. Such endeavours in current research are in line with the preference of people with epilepsy to use less cumbersome and stigmatising acquisition setups [8,21]. Additionally, by considering these systems, broad clinical applications can become a reality in low- to middle-income countries where the burden is more dramatic [25, 26]. Wearable devices likely meet the need for data collection devices that are more comfortable and easily implemented and managed by clinical staff [21].

The exploration of ECG alterations before seizure onset may also provide useful information to the clinician with regard to the treatment options. Namely, it might be helpful to know the patients who show cardiac alterations in ECG to select candidates for a vagus nerve stimulation procedure.

Future research directions concern several aspects. First, the developed seizure prediction models must be prospectively validated on long-term data collected in a real-life scenario. This would be a paramount step to prove the clinical usefulness of the retrospective study conducted along this thesis [12, 166]. Additionally, chronic monitoring complemented with rich patient and seizure metadata is critical to confirm the results reported in this thesis and extract more knowledge.

Second, including the circadian or sleep-wake cycles as input to the prediction models may also improve seizure prediction performance. Such information has been widely used in seizure forecasting frameworks in an attempt to integrate seizure co-modulators manifesting at different temporal scales. In fact, it has been suggested that seizure prediction and seizure forecasting frameworks should be developed as a nested approach [68, 159, 166]. Accordingly, the patient would be informed about

periods of high seizure risk hours to days in advance and about warnings of upcoming seizures minutes to hours in advance. Prediction horizons of days may enable patients to timely plan their lives, including taking medication that would have enough time to take effect. Future studies should then lay the path to such integrated models, which still lack methodological clarifications. Another aspect that should perhaps deserve the main focus concerns the impact of the different prediction horizons (days, hours or minutes) on patients with drug-resistant epilepsy. Epilepsy management will likely require patient-specific adjustments both due to the individuality of brain alterations and the subject's expectations regarding a warning system.

References

[1] Valery L. Feigin, Emma Nichols, Tahiya Alam, Marlena S. Bannick, et al. **Global, regional, and national burden of neurological disorders, 1990–2016: a systematic analysis for the Global Burden of Disease Study 2016**. *The Lancet Neurology*, **18**(5):459–480, 2019. 1, 11

[2] Emanuele Bartolini and Josemir W. Sander. **Dealing with the storm: An overview of seizure precipitants and spontaneous seizure worsening in drug-resistant epilepsy**. *Epilepsy & Behavior*, **97**:212–218, 2019. 1

[3] Yi Wang and Zhong Chen. **An update for epilepsy research and antiepileptic drug development: Toward precise circuit therapy**. *Pharmacology & Therapeutics*, **201**:77–93, 2019. 1, 27, 28

[4] Philippe Ryvlin, Sylvain Rheims, Lawrence J. Hirsch, Arseny Sokolov, and Lara Jehi. **Neuromodulation in epilepsy: state-of-the-art approved therapies**. *The Lancet Neurology*, **20**(12):1038–1047, 2021. 1, 31, 32, 33, 34

[5] Bushra Sultana, Marie-Andrée Panzini, Ariane Veilleux Carpentier, Jacynthe Comtois, et al. **Incidence and Prevalence of Drug-Resistant Epilepsy**. *Neurology*, **96**(17):805–817, 2021. 1, 28

[6] Kenneth D. Laxer, Eugen Trinka, Lawrence J. Hirsch, Fernando Cendes, et al. **The consequences of refractory epilepsy and its treatment**. *Epilepsy & Behavior*, **37**:59–70, 2014. 1, 28, 33, 34

[7] Jerome Engel. **What can we do for people with drug-resistant epilepsy?** *Neurology*, **87**(23):2483–2489, 2016. 1, 28, 29, 31

[8] Sarah A. Janse, Sonya B. Dumanis, Tanya Huwig, Sarah Hyman, et al. **Patient and caregiver preferences for the potential benefits and risks of a seizure forecasting device: A best–worst scaling**. *Epilepsy & Behavior*, **96**:183–191, 2019. 2, 3, 164

[9] Elisa Bruno, Pedro F. Viana, Michael R. Sperling, and Mark P. Richardson. **Seizure detection at home: Do devices on the market match the needs of people living with epilepsy and their caregivers?** *Epilepsia*, **61**(S1):S11–S24, 2020. 2

[10] Paolo Federico. **Functional MRI of the pre-ictal state**. *Brain*, **128**(8):1811–1817, 2005. 2, 38, 70

[11] Elie Bou Assi, Dang K. Nguyen, Sandy Rihana, and Mohamad Sawan. **Towards accurate prediction of epileptic seizures: A review**. *Biomedical Signal Processing and Control*, **34**:144–157, 2017. 2, 37, 39, 40, 43, 48, 62, 66, 67, 70, 73, 75, 78, 79, 120, 139, 148, 255, 256, 263, 264, 291

[12] Levin Kuhlmann, Klaus Lehnertz, Mark P. Richardson, Björn Schelter, and Hitten P. Zaveri. **Seizure prediction — ready for a new era**. *Nature Reviews Neurology*, **14**(10):618–630, 2018. 2, 43, 46, 47, 55, 62, 63, 70, 71, 73, 78, 79, 83, 86, 100, 112, 113, 115, 117, 134, 137, 142, 143, 158, 164

[13] Florian Mormann, Ralph G. Andrzejak, Christian E. Elger, and Klaus Lehnertz. **Seizure prediction: the long and winding road**. *Brain*, **130**(2):314–333, 2007. 2, 36, 37, 38, 39, 40, 42, 43, 47, 70, 71, 73, 75, 79, 83, 84, 117, 120, 139, 255, 256, 257, 264

[14] Florian Mormann, Thomas Kreuz, Christoph Rieke, Ralph G. Andrzejak, et al. **On the predictability of epileptic seizures**. *Clinical Neurophysiology*, **116**(3):569–587, 2005. 2, 37, 39, 71, 72, 73, 113, 120, 132, 137, 139, 213, 214, 255, 262, 263, 264

[15] Dean R. Freestone, Philippa J. Karoly, Andre D. H. Peterson, Levin Kuhlmann, et al. **Seizure Prediction: Science Fiction or Soon to Become Reality?** *Current Neurology and Neuroscience Reports*, **15**(11):73, 2015. 2, 71, 83, 84, 137

[16] Dean R. Freestone, Philippa J. Karoly, and Mark J. Cook. **A forward-looking review of seizure prediction**. *Current Opinion in Neurology*, **30**(2):167–173, 2017. 2, 5, 16, 36, 50, 51, 57, 58, 71, 83, 86, 112, 113, 117, 135, 136, 137, 138, 142, 159, 160

[17] Philippa J. Karoly, Hoameng Ung, David B. Grayden, Levin Kuhlmann, et al. **The circadian profile of epilepsy improves seizure forecasting**. *Brain*, **140**(8):2169–2182, 2017. 2, 39, 64, 68, 71, 76, 77, 78, 80, 87, 91, 135, 136, 138, 157, 159, 160

[18] Thomas Blauwblomme, Premysl Jiruska, and Gilles Huberfeld. **Mechanisms of Ictogenesis**. In Premysl Jiruska, Marco de Curtis,

and John G. R. Jefferys, editors, *International Review of Neurobiology*, **114**, chapter 7, pages 155–185. Academic Press, 1st edition, 2014. 2, 84, 117, 137, 138

[19] Orrin Devinsky. **Effects of Seizures on Autonomic and Cardiovascular Function**. *Epilepsy Currents*, **4**(2):43–46, 2004. 3, 26, 59, 99, 209, 210, 235

[20] K. Jansen and L. Lagae. **Cardiac changes in epilepsy.** *Seizure*, **19**(8):455–460, 2010. 3, 4, 26, 59, 99, 139, 209, 210, 235, 238

[21] Elisa Bruno, Andrea Biondi, and Mark P. Richardson. **Pre-ictal heart rate changes: A systematic review and meta-analysis**. *Seizure*, **55**:48–56, 2018. 3, 60, 61, 94, 99, 109, 164, 209, 210

[22] Ilona Hubbard, Sandor Beniczky, and Philippe Ryvlin. **The Challenging Path to Developing a Mobile Health Device for Epilepsy: The Current Landscape and Where We Go From Here**. *Frontiers in Neurology*, **12**:1737, 2021. 3, 23, 24, 39, 142

[23] Rachel E. Stirling, Mark J. Cook, David B. Grayden, and Philippa J. Karoly. **Seizure forecasting and cyclic control of seizures**. *Epilepsia*, **62**(S1):S2–S14, 2021. 3, 61, 83, 86

[24] Andreas Schulze-Bonhage, Francisco Sales, Kathrin Wagner, Rute Teotonio, et al. **Views of patients with epilepsy on seizure prediction devices**. *Epilepsy & Behavior*, **18**(4):388–396, 2010. 3, 43

[25] Kirsten M. Fiest, Khara M. Sauro, Samuel Wiebe, Scott B. Patten, et al. **Prevalence and incidence of epilepsy**. *Neurology*, **88**(3):296–303, 2017. 3, 164

[26] Roland D. Thijs, Rainer Surges, Terence J. O'Brien, and Josemir W. Sander. **Epilepsy in adults**. *The Lancet*, **393**(10172):689–701, 2019. 3, 29, 30, 31, 33, 35, 164

[27] Chaturbhuj Rathore and Kurupath Radhakrishnan. **Concept of epilepsy surgery and presurgical evaluation**. *Epileptic Disorders*, **17**(1):19–31, 2015. 3

[28] Matthias Ihle, Hinnerk Feldwisch-Drentrup, César A. Teixeira, Adrien Witon, et al. **EPILEPSIAE – A European epilepsy database**. *Computer Methods and Programs in Biomedicine*, **106**(3):127–138, 2012. 4, 93, 94

[29] Juliane Klatt, Hinnerk Feldwisch-Drentrup, Matthias Ihle, Vincent Navarro, et al. **The EPILEPSIAE database: An extensive electroencephalography database of epilepsy patients**. *Epilepsia*, **53**(9):1669–1676, 2012. 4, 93, 94, 138

[30] Robert S. Delamont and Matthew C. Walker. **Pre-ictal autonomic changes**. *Epilepsy Research*, **97**(3):267–272, 2011. 4, 26, 27, 38, 59, 61, 70, 113, 139, 209, 210, 236, 238

[31] Ettore Beghi, Giorgia Giussani, Emma Nichols, Foad Abd-Allah, et al. **Global, regional, and national burden of epilepsy, 1990–2016: a systematic analysis for the Global Burden of Disease Study 2016**. *The Lancet Neurology*, **18**(4):357–375, 2019. 11

[32] Robert S. Fisher, Walter van Emde Boas, Warren Blume, Christian Elger, et al. **Epileptic Seizures and Epilepsy: Definitions Proposed by the International League Against Epilepsy (ILAE) and the International Bureau for Epilepsy (IBE)**. *Epilepsia*, **46**(4):470–472, 2005. 11, 12

[33] Robert S. Fisher, Carlos Acevedo, Alexis Arzimanoglou, Alicia Bogacz, et al. **ILAE Official Report: A practical clinical definition of epilepsy**. *Epilepsia*, **55**(4):475–482, 2014. 12

[34] Andrea. Varsavsky, Iven Mareels, and Mark Cook. *Epileptic seizure and the EEG: Measurement, Models, Detection and Prediction*. CRC Press, Boca Raton, FL, 2011. 12, 16, 18, 20, 22, 38, 39, 40, 205, 206, 240, 260

[35] Jerome. Engel, Marc A. Dichter, and Phulip A. Schwartzkroin. **Basic Mechanisms of Human Epilepsy**. In Jerome. Engel and Timothy A. Pedley, editors, *Epilepsy: a comprehensive textbook*, **I**, chapter 41, pages 495–508. Wolters Kluwer Health/Lippincott Williams & Wilkins, 2nd edition, 2008. 12, 16, 104

[36] Robert S. Fisher, J. Helen Cross, Jacqueline A. French, Norimichi Higurashi, et al. **Operational classification of seizure types by the International League Against Epilepsy: Position Paper of the ILAE Commission for Classification and Terminology**. *Epilepsia*, **58**(4):522–530, 2017. 12, 13, 14, 15, 94

[37] Orrin Devinsky, Annamaria Vezzani, Terence J. O'Brien, Nathalie Jette, et al. **Epilepsy**. *Nature Reviews Disease Primers*, **4**(1):18024, 2018. 12, 13, 15, 20, 27, 28, 30, 33, 34, 35, 39

[38] Ingrid E. Scheffer, Samuel Berkovic, Giuseppe Capovilla, Mary B. Connolly, et al. **ILAE classification of the epilepsies: Position paper of the ILAE Commission for Classification and Terminology**. *Epilepsia*, **58**(4):512–521, 2017. 13, 15, 16

[39] Maeike Zijlmans, Willemiek Zweiphenning, and Nicole van Klink. **Changing concepts in presurgical assessment for epilepsy surgery**. *Nature Reviews Neurology*, **15**(10):594–606, 2019. 13, 22, 29, 30

[40] Elaine C. Wirrell. **Classification of Seizures and the Epilepsies**. In Gregory D. Cascino, Joseph I. Sirven, and William O. Tatum, editors, *Epilepsy*, chapter 2, pages 11–22. John Wiley & Sons, Ltd, 2nd edition, 2021. 13, 14, 16

[41] Renzo Guerrini and Carmen Barba. **Classification, Clinical Symptoms, and Syndromes**. In Simon Shorvon, Renzo Guerrini, Mark Cook, and Samden Lhatoo, editors, *Oxford Textbook of Epilepsy and Epileptic Seizures*, chapter 7, pages 70–80. Oxford University Press, 2012. 14, 16

[42] Roland D. Thijs, Philippe Ryvlin, and Rainer Surges. **Autonomic manifestations of epilepsy: emerging pathways to sudden death?** *Nature Reviews Neurology*, **17**(12):774–788, 2021. 14, 26, 59, 61, 210

[43] Sándor Beniczky, Philippa Karoly, Ewan Nurse, Philippe Ryvlin, and Mark Cook. **Machine learning and wearable devices of the future**. *Epilepsia*, **62**(S2):S116–S124, 2021. 14, 34, 35, 36, 37, 61, 100, 159

[44] Thomas V. Kodankandath, Danny Theodore, and Debopam Samanta. **Generalized Tonic-Clonic Seizure**, 2021. 14, 37

[45] Jerome Engel and Noriko Salamon. **Temporal Lobe Epilepsy**. In *Brain Mapping*, **3**, pages 853–860. Elsevier, 2015. 16

[46] Guido Rubboli and Elena Gardella. **Non-age-Related Focal Epilepsies**. In Oriano Mecarelli, editor, *Clinical Electroencephalography*, chapter 26, pages 445–460. Springer International Publishing, Cham, 2019. 16, 94

[47] Christian E. Elger and Christian Hoppe. **Diagnostic challenges in epilepsy: seizure under-reporting and seizure detection**. *The Lancet Neurology*, **17**(3):279–288, 2018. 16, 17

[48] Benjamin H. Brinkmann, Philippa J. Karoly, Ewan S. Nurse, Sonya B. Dumanis, et al. **Seizure Diaries and Forecasting With**

Wearables: Epilepsy Monitoring Outside the Clinic. *Frontiers in Neurology*, **12**:1128, 2021. 17, 88

[49] Marc G. Leguia, Ralph G. Andrzejak, Christian Rummel, Joline M. Fan, et al. **Seizure Cycles in Focal Epilepsy**. *JAMA Neurology*, **78**(4):454, 2021. 17, 20, 40, 88, 89

[50] Mark J. Cook, Terence J. O'Brien, Samuel F. Berkovic, Michael Murphy, et al. **Prediction of seizure likelihood with a long-term, implanted seizure advisory system in patients with drug-resistant epilepsy: a first-in-man study**. *The Lancet Neurology*, **12**(6):563–571, 2013. 17, 37, 39, 63, 64, 68, 76, 77, 78, 80, 84, 117, 138

[51] Philippa J. Karoly, Dominique Eden, Ewan S. Nurse, Mark J. Cook, et al. **Cycles of self-reported seizure likelihood correspond to yield of diagnostic epilepsy monitoring**. *Epilepsia*, **62**(2):416–425, 2021. 17

[52] Victor Ferastraoaru, Daniel M. Goldenholz, Sharon Chiang, Robert Moss, et al. **Characteristics of large patient-reported outcomes: Where can one million seizures get us?** *Epilepsia Open*, **3**(3):364–373, 2018. 17, 37, 88, 89

[53] J. Bauer and W. Burr. **Course of chronic focal epilepsy resistant to anticonvulsant treatment**. *Seizure*, **10**(4):239–246, 2001. 17, 43

[54] Saba Jafarpour, Lawrence J. Hirsch, Marina Gaínza-Lein, Christoph Kellinghaus, and Kamil Detyniecki. **Seizure cluster: Definition, prevalence, consequences, and management**. *Seizure*, **68**:9–15, 2019. 17, 18, 39

[55] Steve Chung, Jerzy P. Szaflarski, Eun Jung Choi, Jessica Claire Wilson, et al. **A systematic review of seizure clusters: Prevalence, risk factors, burden of disease and treatment patterns**. *Epilepsy Research*, **177**:106748, 2021. 17, 18, 34

[56] Sheryl R. Haut. **Seizure clusters**. *Current Opinion in Neurology*, **28**(2):143–150, 2015. 17, 18, 39

[57] Richard Wennberg. **Introduction to EEG for Nonepileptologists Working in Seizure Prediction and Dynamics**. In Ivan Osorio, Hitten P. Zaveri, Mark G. Frei, and Susan Arthurs, editors, *Epilepsy: The Intersection of Neurosciences, Biology, Mathematics, Engineering, and Physics*, chapter 2, pages 23–39. CRC Press, Boca Raton, FL, 2011. 18, 20, 22, 138, 205, 206

[58] Mike X. Cohen. *Analyzing neural time series data: Theory and practice*. Number 1 in Issues in clinical and cognitive neuropsychology. MIT Press, 2014. 18, 20, 75, 205, 206, 261, 262

[59] Anteneh M. Feyissa, Gregory A. Worrell, and Terrence D. Lagerlund. **EEG and Epilepsy**. In Gregory D Cascino, Joseph I Sirven, and William O Tatum, editors, *Epilepsy*, chapter 6, pages 77–98. John Wiley & Sons, Ltd, 2nd edition, 2021. 18, 20, 22, 30, 36

[60] Md Kafiul Islam, Amir Rastegarnia, and Zhi Yang. **Methods for artifact detection and removal from scalp EEG: A review**. *Neurophysiologie Clinique/Clinical Neurophysiology*, **46**(4-5):287–305, 2016. 18, 66, 67

[61] U. Rajendra Acharya, S. Vinitha Sree, G. Swapna, Roshan Joy Martis, and Jasjit S. Suri. **Automated EEG analysis of epilepsy: A review**. *Knowledge-Based Systems*, **45**:147–165, 2013. 18, 38, 70, 257, 258, 264

[62] Oriano Mecarelli. **Normal Awake Adult EEG**. In *Clinical Electroencephalography*, chapter 9, pages 131–152. Springer International Publishing, Cham, 2019. 18, 20, 120, 137, 138

[63] Saeid Sanei and Jonathon A. Chambers. **EEG Waveforms**. In Saeid Sanei and Jonathon A. Chambers, editors, *EEG Signal Processing and Machine Learning*, chapter 2, pages 15–46. John Wiley & Sons, Ltd, 2nd edition, 2021. 19, 20, 22, 138

[64] Christine B. Baca and John M. Stern. **Scalp EEG in the epilepsy surgery evaluation**. In Simon Shorvon, Emillo Perucca, and Jerome Engel Jr., editors, *The Treatment of Epilepsy*, chapter 57, pages 723–732. John Wiley & Sons, Ltd, Oxford, UK, 2015. 20, 22, 30

[65] Philippa J. Karoly, Vikram R. Rao, Nicholas M. Gregg, Gregory A. Worrell, et al. **Cycles in epilepsy**. *Nature Reviews Neurology*, **17**(5):267–284, 2021. 20, 22, 51, 83, 86, 87, 88, 90, 94, 136, 159, 160

[66] Maxime O. Baud and Vikram R. Rao. **Gauging seizure risk**. *Neurology*, **91**(21):967–973, 2018. 20, 22, 40, 83, 85, 86, 137, 142

[67] Maxime O. Baud, Jonathan K. Kleen, Emily A. Mirro, Jason C. Andrechak, et al. **Multi-day rhythms modulate seizure risk in epilepsy**. *Nature Communications*, **9**(1):88, 2018. 20, 40, 88, 89, 91, 137, 138

[68] Timothée Proix, Wilson Truccolo, Marc G. Leguia, Thomas K. Tcheng, et al. **Forecasting seizure risk in adults with focal epilepsy: a development and validation study**. *The Lancet Neurology*, **20**(2):127–135, 2021. 20, 40, 43, 66, 84, 85, 87, 160, 164

[69] Rachel E. Stirling, Matias I. Maturana, Philippa J. Karoly, Ewan S. Nurse, et al. **Seizure Forecasting Using a Novel Sub-Scalp Ultra-Long Term EEG Monitoring System**. *Frontiers in Neurology*, **12**:1445, 2021. 20, 23, 24, 85, 142

[70] Jamie J. Van Gompel, Katherine Noe, and Richard S. Zimmerman. **Intracranial EEG Monitoring**. In Gregory D Cascino, Joseph I Sirven, and William O Tatum, editors, *Epilepsy*, chapter 21, pages 381–399. John Wiley & Sons, Ltd, 2nd edition, 2021. 20, 22, 23

[71] Oriano Mecarelli. **Electrode Placement Systems and Montages**. In *Clinical Electroencephalography*, chapter 4, pages 35–52. Springer International Publishing, Cham, 2019. 20, 21, 22, 205, 206

[72] Robert Oostenveld and Peter Praamstra. **The five percent electrode system for high-resolution EEG and ERP measurements**. *Clinical Neurophysiology*, **112**(4):713–719, 2001. 21

[73] Paul L. Nunez and Ramesh Srinivasan. **Recording Strategies, Reference Issues, and Dipole Localization**. In Paul L. Nunez and Ramesh Srinivasan, editors, *Electric Fields of the Brain*, chapter 7, pages 275–312. Oxford University Press, 2nd edition, 2006. 20, 205, 206

[74] Maria N. Anastasiadou, Manolis Christodoulakis, Eleftherios S. Papathanasiou, Savvas S. Papacostas, et al. **Graph Theoretical Characteristics of EEG-Based Functional Brain Networks in Patients With Epilepsy: The Effect of Reference Choice and Volume Conduction**. *Frontiers in Neuroscience*, **13**:221, 2019. 20, 205, 206, 261, 262

[75] Andrea Biondi, Viviana Santoro, Pedro F. Viana, Petroula Laiou, et al. **Noninvasive mobile EEG as a tool for seizure monitoring and management: A systematic review**. *Epilepsia*, **63**(5):1041–1063, 2022. 22, 36, 142

[76] Jonas Duun-Henriksen, Maxime Baud, Mark P. Richardson, Mark Cook, et al. **A new era in electroencephalographic monitoring? Subscalp devices for ultra–long-term recordings**. *Epilepsia*, **61**(9):1805–1817, 2020. 22, 23, 24, 35, 36, 37, 142

[77] About Kids Health. **Invasive electroencephalography (EEG) monitoring before epilepsy surgery**, 2017. 23

[78] Soheyl Noachtar and Jan Rémi. **The role of EEG in epilepsy: A critical review**. *Epilepsy & Behavior*, **15**(1):22–33, 2009. 23

[79] Dennis Spencer, Dang K. Nguyen, and Adithya Sivaraju. **Invasive EEG in presurgical evaluation of epilepsy**. In Simon Shorvon, Emillo Perucca, and Jerome Engel Jr., editors, *The Treatment of Epilepsy*, chapter 58, pages 733–755. John Wiley & Sons, Ltd, Oxford, UK, 2015. 22, 23

[80] Hitten P. Zaveri and Mark G. Frei. **Intracranial EEG electrodes, filtering, amplification, digitization, storage, and display**. In Ivan Osorio, Hitten P. Zaveri, Mark G. Frei, and Susan Arthurs, editors, *Epilepsy: The Intersection of Neurosciences, Biology, Mathematics, Engineering, and Physics*, chapter 6, pages 81–93. CRC Press, Boca Raton, FL, 1st edition, 2016. 22

[81] Laura Tassi. **Invasive EEG**. In Oriano Mecarelli, editor, *Clinical Electroencephalography*, chapter 19, pages 319–328. Springer International Publishing, Cham, 2019. 22

[82] Florian Mormann, Ralph G. Andrzejak, and Klaus Lehnertz. **Automated prediction and assessment of seizure prediction algorithms**. In Ivan Osorio, Hitten P. Zaveri, Mark G. Frei, and Susan Arthurs, editors, *Epilepsy: The Intersection of Neurosciences, Biology, Mathematics, Engineering, and Physics*, chapter 11, pages 165–174. CRC Press, Boca Raton, FL, 1st edition, 2016. 23, 36, 37, 38, 39, 40, 41, 42, 43, 70

[83] Norman K. So and Warren T. Blume. **The postictal EEG**. *Epilepsy & Behavior*, **19**(2):121–126, 2010. 23, 37, 38, 120

[84] Stjepana Kovac, Vejay N. Vakharia, Catherine Scott, and Beate Diehl. **Invasive epilepsy surgery evaluation**. *Seizure*, **44**:125–136, 2017. 23

[85] Sigge Weisdorf, Jonas Duun-Henriksen, Marianne J. Kjeldsen, Frantz R. Poulsen, et al. **Ultra-long-term subcutaneous home monitoring of epilepsy—490 days of <scp>EEG</scp> from nine patients**. *Epilepsia*, **60**(11):2204–2214, 2019. 23, 66

[86] Richard E. Klabunde. **Neurohumoral Control of the Heart and Circulation**. In *Cardiovascular Physiology Concepts*, chapter 6, pages 124–147. Lippincott Williams & Wilkins/Wolters Kluwer, 2nd edition, 2012. 24, 26

[87] D. Bruce Foster. **Derivation of the Normal Electrocardiogram**. In *Twelve-Lead Electrocardiography*, chapter 4, pages 17–23. Springer London, London, 2nd edition, 2007. 25

[88] Richard E. Klabunde. **Electrical Activity of the Heart**. In *Cardiovascular Physiology Concepts*, chapter 2, pages 9–40. Lippincott Williams & Wilkins/Wolters Kluwer, 2nd edition, 2012. 25, 26

[89] A. Ulate-Campos, F. Coughlin, M. Gaínza-Lein, I. Sánchez Fernández, et al. **Automated seizure detection systems and their effectiveness for each type of seizure**. *Seizure*, **40**:88–101, 2016. 25, 39, 60, 62

[90] S. Nasehi and H. Pourghassem. **Seizure Detection Algorithms Based on Analysis of EEG and ECG Signals: a Survey**. *Neurophysiology*, **44**(2):174–186, 2012. 25, 34, 35, 256, 263

[91] Rollin McCraty. *Science of the Heart: Exploring the Role of the Heart in Human Performance Volume 2*. HeartMath Institute, Boulder Creek, CA, 2016. 25, 61

[92] Task Force of the European Society of Cardiology Electrophysiology, The North American, and Society of Pacing and Electrophysiology. **Heart Rate Variability**. *Circulation*, **93**(5):1043–1065, 1996. 26, 102, 233, 234, 235, 236, 237, 238, 242

[93] Katherine S. Eggleston, Bryan D. Olin, and Robert S. Fisher. **Ictal tachycardia: The head–heart connection**. *Seizure*, **23**(7):496–505, 2014. 26, 33, 39, 59, 61, 62, 99, 109, 209

[94] Leif Sörnmo and Pablo Laguna. **The Electroencephalogram—A Brief Background**. In Leif Sörnmo and Pablo Laguna, editors, *Bioelectrical Signal Processing in Cardiac and Neurological Applications*, chapter 2, pages 25–53. Elsevier, 1st edition, 2005. 26

[95] Cristian Sevcencu and Johannes J. Struijk. **Autonomic alterations and cardiac changes in epilepsy**. *Epilepsia*, **51**(5):725–737, 2010. 26, 59, 60, 61, 209

[96] Kenneth A. Myers, Shobi Sivathamboo, and Piero Perucca. **Heart rate variability measurement in epilepsy: How can we move from research to clinical practice?** *Epilepsia*, **59**(12):1–10, 2018. 27, 59, 60, 99

[97] Julia C. M. Pottkämper, Jeannette Hofmeijer, Jeroen A. van Waarde, and Michel J. A. M. van Putten. **The postictal state — What do we know?** *Epilepsia*, **61**(6):1045–1061, 2020. 27, 120, 138

[98] Patrick Kwan, Alexis Arzimanoglou, Anne T. Berg, Martin J. Brodie, et al. **Definition of drug resistant epilepsy: Consensus**

proposal by the ad hoc Task Force of the ILAE Commission on Therapeutic Strategies. *Epilepsia*, **51**(6):1069–1077, 2009. 28

[99] Philippe Ryvlin, J. Helen Cross, and Sylvain Rheims. **Epilepsy surgery in children and adults**. *The Lancet Neurology*, **13**(11):1114–1126, 2014. 29, 30, 31

[100] Jerome Engel. **The current place of epilepsy surgery**. *Current Opinion in Neurology*, **31**(2):192–197, 2018. 29, 30, 31

[101] Jerome Engel. **Overview of surgical treatment for epilepsy**. In Simon Shorvon, Emillo Perucca, and Jerome Engel Jr., editors, *The Treatment of Epilepsy*, chapter 56, pages 709–722. John Wiley & Sons, Ltd, Oxford, UK, 2015. 29, 30

[102] Jack Kirby, Veronica M. Leach, Alice Brockington, Phillip Patsalos, et al. **Drug withdrawal in the epilepsy monitoring unit – The patsalos table**. *Seizure*, **75**:75–81, 2020. 30

[103] Sylvain Rheims and Philippe Ryvlin. **Patients' safety in the epilepsy monitoring unit**. *Current Opinion in Neurology*, **27**(2):213–218, 2014. 30

[104] Philippe Ryvlin and Sylvain Rheims. **Predicting epilepsy surgery outcome**. *Current Opinion in Neurology*, **29**(2):182–188, 2016. 30

[105] Susan Spencer and Linda Huh. **Outcomes of epilepsy surgery in adults and children**. *The Lancet Neurology*, **7**(6):525–537, 2008. 31

[106] Paul Boon, Elien De Cock, Ann Mertens, and Eugen Trinka. **Neurostimulation for drug-resistant epilepsy: a systematic review of clinical evidence for efficacy, safety, contraindications and predictors for response**. *Current Opinion in Neurology*, **31**(2):198–210, 2018. 31, 32, 33

[107] Matthew D. Bigelow and Abbas Z. Kouzani. **Neural stimulation systems for the control of refractory epilepsy: a review**. *Journal of NeuroEngineering and Rehabilitation*, **16**(1):126, 2019. 31, 32, 33

[108] Natalia Rincon, Donald Barr, and Naymee Velez-Ruiz. **Neuromodulation in Drug Resistant Epilepsy**. *Aging and disease*, **12**(4):1070, 2021. 31, 32, 33

[109] Andreas Schulze-Bonhage. **Brain stimulation as a neuromodulatory epilepsy therapy**. *Seizure*, **44**:169–175, 2017. 32

[110] The Vagus Nerve Stimulation Study Group. **A randomized controlled trial of chronic vagus nerve stimulation for treatment of**

medically intractable seizures: The Vagus Nerve Stimulation Study Group*. *Neurology*, **45**(2):224–230, 1995. 32

[111] Adrian Handforth, C. M. DeGiorgio, S. C. Schachter, B. M. Uthman, et al. **Vagus nerve stimulation therapy for partial-onset seizures: A randomized active-control trial**. *Neurology*, **51**(1):48–55, 1998. 32

[112] Robert Fisher, Vicenta Salanova, Thomas Witt, Robert Worth, et al. **Electrical stimulation of the anterior nucleus of thalamus for treatment of refractory epilepsy**. *Epilepsia*, **51**(5):899–908, 2010. 32

[113] Martha J. Morrell. **Responsive cortical stimulation for the treatment of medically intractable partial epilepsy**. *Neurology*, **77**(13):1295–1304, 2011. 32

[114] Breanne Fisher, Julie A. DesMarteau, Elizabeth H. Koontz, Seth J. Wilks, and Susan E. Melamed. **Responsive Vagus Nerve Stimulation for Drug Resistant Epilepsy: A Review of New Features and Practical Guidance for Advanced Practice Providers**. *Frontiers in Neurology*, **11**:1863, 2021. 32, 34

[115] Matthew S. Markert and Robert S. Fisher. **Neuromodulation - Science and Practice in Epilepsy: Vagus Nerve Stimulation, Thalamic Deep Brain Stimulation, and Responsive NeuroStimulation**. *Expert Review of Neurotherapeutics*, **19**(1):17–29, 2019. 33, 34

[116] Felice T. Sun and Martha J. Morrell. **The RNS System: responsive cortical stimulation for the treatment of refractory partial epilepsy**. *Expert Review of Medical Devices*, **11**(6):563–572, 2014. 33, 34, 63

[117] Andreas Schulze-Bonhage. **Long-term outcome in neurostimulation of epilepsy**. *Epilepsy & Behavior*, **91**:25–29, 2019. 33, 34

[118] Matthew C. Walker and Simon Shorvon. **Emergency Treatment of Seizures and Status Epilepticus**. In Simon Shorvon, Emillo Perucca, and Jerome Engel Jr., editors, *The Treatment of Epilepsy*, chapter 17, pages 221–244. John Wiley & Sons, Ltd, Oxford, UK, 2015. 34, 39

[119] Peter Wolf, Katia Lin, and Marina Nikanorova. **Non-Pharmacological Therapy of Epilepsy**. In Simon Shorvon, Renzo Guerrini, Mark Cook, and Samden Lhatoo, editors, *Oxford Textbook of Epilepsy and Epileptic Seizures*, chapter 12, pages 135–143. Oxford University Press, 2012. 34, 35

[120] James Cloyd, Sheryl Haut, Enrique Carrazana, and Adrian L. Rabinowicz. **Overcoming the challenges of developing an intranasal diazepam rescue therapy for the treatment of seizure clusters**. *Epilepsia*, **62**(4):846–856, 2021. 34

[121] Sai H. S. Boddu and Sneha Kumari. **A Short Review on the Intranasal Delivery of Diazepam for Treating Acute Repetitive Seizures**. *Pharmaceutics*, **12**(12):1167, 2020. 35

[122] M. René Bouw, Steve S. Chung, Barry Gidal, Aliceson King, et al. **Clinical pharmacokinetic and pharmacodynamic profile of midazolam nasal spray**. *Epilepsy Research*, **171**:106567, 2021. 35

[123] Elizabeth G. Neal, Hannah Chaffe, Ruby H. Schwartz, Margaret S. Lawson, et al. **The ketogenic diet for the treatment of childhood epilepsy: a randomised controlled trial**. *The Lancet Neurology*, **7**(6):500–506, 2008. 35

[124] D. A. J. E. Lambrechts, R. J. A. de Kinderen, J. S. H. Vles, A. J. A. de Louw, et al. **A randomized controlled trial of the ketogenic diet in refractory childhood epilepsy**. *Acta Neurologica Scandinavica*, **135**(2):231–239, 2017. 35

[125] Mona Nasseri, Ewan Nurse, Martin Glasstetter, Sebastian Böttcher, et al. **Signal quality and patient experience with wearable devices for epilepsy management**. *Epilepsia*, **61**(S1):S25–S35, 2020. 35, 36

[126] Mona Nasseri, Tal Pal Attia, Boney Joseph, Nicholas M. Gregg, et al. **Non-invasive wearable seizure detection using long–short-term memory networks with transfer learning**. *Journal of Neural Engineering*, **18**(5):056017, 2021. 36

[127] Ming-Zher Poh, Tobias Loddenkemper, Claus Reinsberger, Nicholas C. Swenson, et al. **Convulsive seizure detection using a wrist-worn electrodermal activity and accelerometry biosensor**. *Epilepsia*, **53**(5):e93–e97, 2012. 36

[128] Christian Meisel, Rima El Atrache, Michele Jackson, Sarah Schubach, et al. **Machine learning from wristband sensor data for wearable, noninvasive seizure forecasting**. *Epilepsia*, **61**(12):2653–2666, 2020. 36, 39, 79, 85

[129] Sándor Beniczky and Jesper Jeppesen. **Non-electroencephalography-based seizure detection**. *Current Opinion in Neurology*, **32**(2):198–204, 2019. 36

[130] Sándor Beniczky, Samuel Wiebe, Jesper Jeppesen, William O. Tatum, et al. **Automated seizure detection using wearable devices: A clinical practice guideline of the International League Against Epilepsy and the International Federation of Clinical Neurophysiology**. *Clinical Neurophysiology*, **132**(5):1173–1184, 2021. 36, 37, 100

[131] Laure Mazzola and Sylvain Rheims. **Ictal and Interictal Cardiac Manifestations in Epilepsy. A Review of Their Relation With an Altered Central Control of Autonomic Functions and With the Risk of SUDEP**. *Frontiers in Neurology*, **12**:642645, 2021. 36, 60

[132] Christian Meisel and Tobias Loddenkemper. **Seizure prediction and intervention**. *Neuropharmacology*, **172**:107898, 2020. 36, 59, 71, 137

[133] Sriram Ramgopal, Sigride Thome-Souza, Michele Jackson, Navah Ester Kadish, et al. **Seizure detection, seizure prediction, and closed-loop warning systems in epilepsy**. *Epilepsy & Behavior*, **37**:291–307, 2014. 36, 37, 39, 60, 62, 70, 264

[134] Mona Nasseri, Tal Pal Attia, Boney Joseph, Nicholas M. Gregg, et al. **Ambulatory seizure forecasting with a wrist-worn device using long-short term memory deep learning**. *Scientific Reports*, **11**(1):21935, 2021. 36, 39, 65, 66, 69, 76, 77, 78, 82, 85, 101

[135] Elisa Bruno, Sara Simblett, Alexandra Lang, Andrea Biondi, et al. **Wearable technology in epilepsy: The views of patients, caregivers, and healthcare professionals**. *Epilepsy & Behavior*, **85**:141–149, 2018. 36

[136] Sara Katherine Simblett, Andrea Biondi, Elisa Bruno, Dominic Ballard, et al. **Patients' experience of wearing multimodal sensor devices intended to detect epileptic seizures: A qualitative analysis**. *Epilepsy & Behavior*, **102**:106717, 2020. 36

[137] Zulfi Haneef, Kaiyuan Yang, Sameer A. Sheth, Fuad Z. Aloor, et al. **Sub-scalp electroencephalography: A next-generation technique to study human neurophysiology**. *Clinical Neurophysiology*, **141**:77–87, 2022. 36, 37

[138] Jonas Munch Nielsen, Dirk Rades, and Troels Wesenberg Kjaer. **Wearable electroencephalography for ultra-long-term seizure monitoring: a systematic review and future prospects**. *Expert Review of Medical Devices*, **18**(sup1):57–67, 2021. 37

[139] Jen Sze Ong, Shuet Nee Wong, Alina Arulsamy, Jessica L. Watterson, and Mohd. Farooq Shaikh. **Medical Technology: A Systematic**

Review on Medical Devices Utilized for Epilepsy Prediction and Management. *Current Neuropharmacology*, **20**(5):950–964, 2022. 37

[140] Jennifer Shum and Daniel Friedman. **Commercially available seizure detection devices: A systematic review**. *Journal of the Neurological Sciences*, **428**:117611, 2021. 37, 60, 100

[141] Judith van Andel, Constantin Ungureanu, Johan Arends, Francis Tan, et al. **Multimodal, automated detection of nocturnal motor seizures at home: Is a reliable seizure detector feasible?** *Epilepsia Open*, **2**(4):424–431, 2017. 37

[142] Robert S. Fisher and Jerome J. Engel. **Definition of the postictal state: When does it start and end?** *Epilepsy & Behavior*, **19**(2):100–104, 2010. 37, 38

[143] Sridhar Sunderam. **How to detect and quantify epileptic seizures**. In Ivan Osorio, Hitten P. Zaveri, Mark G. Frei, and Susan Arthurs, editors, *Epilepsy: The Intersection of Neurosciences, Biology, Mathematics, Engineering, and Physics*, chapter 10, pages 139–164. CRC Press, 1st edition, 2016. 37, 38

[144] Jalil Rasekhi, MohammadReza Karami Mollaei, Mojtaba Bandarabadi, CésarA Teixeira, and António Dourado. **Epileptic seizure prediction based on ratio and differential linear univariate features**. *Journal of Medical Signals & Sensors*, **5**(1):1, 2015. 37, 48, 64, 68, 72, 76, 77, 78, 80, 213, 214, 215, 257

[145] Song Cui, Lijuan Duan, Yuanhua Qiao, and Ying Xiao. **Learning EEG synchronization patterns for epileptic seizure prediction using bag-of-wave features**. *Journal of Ambient Intelligence and Humanized Computing*, pages 1–16, 2018. 38

[146] Meir Bialer, Svein I. Johannessen, René H. Levy, Emilio Perucca, et al. **Seizure detection and neuromodulation: A summary of data presented at the XIII conference on new antiepileptic drug and devices (EILAT XIII)**. *Epilepsy Research*, **130**:27–36, 2017. 38, 39, 42, 43, 61, 62, 209, 210

[147] M. Winterhalder, T. Maiwald, H.U. Voss, R. Aschenbrenner-Scheibe, et al. **The seizure prediction characteristic: a general framework to assess and compare seizure prediction methods**. *Epilepsy & Behavior*, **4**(3):318–325, 2003. 38, 40, 41, 43, 44, 46, 50, 97, 104, 120, 153, 159

[148] Rachel E. Stirling, David B. Grayden, Wendyl D'Souza, Mark J. Cook, et al. **Forecasting Seizure Likelihood With Wearable Technology**. *Frontiers in Neurology*, **12**:1170, 2021. 39, 60, 65, 69, 76, 77, 82, 85, 87

[149] C. Alvarado-Rojas, M. Valderrama, A. Fouad-Ahmed, H. Feldwisch-Drentrup, et al. **Slow modulations of high-frequency activity (40–140 Hz) discriminate preictal changes in human focal epilepsy**. *Scientific Reports*, **4**(1):4545, 2015. 39, 42, 45, 64, 68, 71, 72, 76, 77, 80, 113, 114, 124, 132, 150, 154, 157, 213, 214, 215

[150] Christian Meisel and Kimberlyn A. Bailey. **Identifying signal-dependent information about the preictal state: A comparison across ECoG, EEG and EKG using deep learning**. *EBioMedicine*, **45**:422–431, 2019. 39, 65, 69, 76, 77, 81, 97, 104, 120, 143, 157, 158

[151] Ahmet Remzi Ozcan and Sarp Erturk. **Seizure Prediction in Scalp EEG Using 3D Convolutional Neural Networks With an Image-Based Approach**. *IEEE Transactions on Neural Systems and Rehabilitation Engineering*, **27**(11):2284–2293, 2019. 39, 65, 69, 73, 76, 77, 81

[152] Nhan Duy Truong, Levin Kuhlmann, Mohammad Reza Bonyadi, Damien Querlioz, et al. **Epileptic Seizure Forecasting With Generative Adversarial Networks**. *IEEE Access*, **7**:143999–144009, 2019. 39, 65, 68, 76, 77, 78, 81, 101

[153] Mauro. F. Pinto, Adriana Leal, Fábio Lopes, António Dourado, et al. **A personalized and evolutionary algorithm for interpretable EEG epilepsy seizure prediction**. *Scientific Reports*, **11**(1):3415, 2021. 39, 49, 65, 69, 72, 76, 77, 78, 82, 97, 104, 120, 132, 145, 147, 148, 150, 154, 157, 158, 255, 273, 286, 287, 288, 291, 292, 300, 301

[154] Jens Müller, Hongliu Yang, Matthias Eberlein, Georg Leonhardt, et al. **Coherent false seizure prediction in epilepsy, coincidence or providence?** *Clinical Neurophysiology*, **133**:157–164, 2022. 39, 101, 137, 157, 159, 160

[155] Adriana Leal, Mauro F. Pinto, Fábio Lopes, Anna M. Bianchi, et al. **Heart rate variability analysis for the identification of the preictal interval in patients with drug-resistant epilepsy**. *Scientific Reports*, **11**(1):5987, 2021. 39, 99, 122, 124, 131, 132, 139, 284

[156] Fabio Lopes, Adriana Leal, Julio Medeiros, Mauro F. Pinto, et al. **Automatic Electroencephalogram Artifact Removal Using**

Deep Convolutional Neural Networks. *IEEE Access*, **9**:149955–149970, 2021. 39, 66, 67, 118, 145

[157] Mauro Pinto, Tiago Coelho, Adriana Leal, Fábio Lopes, et al. **Interpretable EEG seizure prediction using a multiobjective evolutionary algorithm**. *Scientific Reports*, **12**(1):4420, 2022. 39, 65, 69, 72, 76, 77, 78, 82, 97, 104, 118, 120, 132, 145, 147, 148, 150, 157, 158, 263, 273, 286, 287, 288, 291, 300, 301

[158] M. Dümpelmann. **Early seizure detection for closed loop direct neurostimulation devices in epilepsy**. *Journal of Neural Engineering*, **16**(4):041001, 2019. 39, 73, 88

[159] Maxime O. Baud, Timothée Proix, Vikram R. Rao, and Kaspar Schindler. **Chance and risk in epilepsy**. *Current Opinion in Neurology*, **33**(2):163–172, 2020. 40, 57, 58, 83, 84, 86, 87, 88, 135, 136, 137, 159, 160, 164

[160] Philippa J. Karoly, Daniel M. Goldenholz, Dean R. Freestone, Robert E. Moss, et al. **Circadian and circaseptan rhythms in human epilepsy: a retrospective cohort study**. *The Lancet Neurology*, **17**(11):977–985, 2018. 40, 51, 88, 89

[161] Maxime Baud and Kaspar Schindler. **Forecasting Seizures: Not Unthinkable Anymore**. *Epileptologie*, **35**:156–161, 2018. 40, 87

[162] Bjrn Schelter, Ralph G. Andrzejak, and Florian Mormann. **Can Your Prediction Algorithm Beat a Random Predictor?** In Björn Schelter, Jens Timmer, and Andreas Schulze-Bonhage, editors, *Seizure Prediction in Epilepsy*, chapter 18, pages 237–248. Wiley, Weinheim, Germany, 2008. 40, 43, 45, 46, 47, 293

[163] Björn Schelter, Matthias Winterhalder, Thomas Maiwald, Armin Brandt, et al. **Testing statistical significance of multivariate time series analysis techniques for epileptic seizure prediction**. *Chaos: An Interdisciplinary Journal of Nonlinear Science*, **16**(1):013108, 2006. 40, 45, 46

[164] Kais Gadhoumi, Jean Marc Lina, Florian Mormann, and Jean Gotman. **Seizure prediction for therapeutic devices: A review**. *Journal of Neuroscience Methods*, **260**(029):270–282, 2016. 40, 43, 264

[165] Björn Schelter, Matthias Winterhalder, Hinnerk Feldwisch genannt Drentrup, Johannes Wohlmuth, et al. **Seizure prediction: The impact of long prediction horizons**. *Epilepsy Research*, **73**(2):213–217, 2007. 41, 97, 104, 120

[166] Maxime O. Baud, Timothée Proix, Nicholas M. Gregg, Benjamin H. Brinkmann, et al. **Seizure forecasting: bifurcations in the long and winding road**. *Epilepsia*, 2022. 43, 63, 84, 159, 160, 161, 164

[167] Sheryl R. Haut, Cynthia Swick, Katherine Freeman, and Susan Spencer. **Seizure Clustering during Epilepsy Monitoring**. *Epilepsia*, **43**(7):711–715, 2002. 43, 159

[168] Hinnerk Feldwisch-Drentrup, Andreas Schulze-Bonhage, Jens Timmer, and Björn Schelter. **Statistical validation of event predictors: A comparative study based on the field of seizure prediction**. *Physical Review E*, **83**(6):066704, 2011. 43, 46, 47

[169] Levin Kuhlmann, Dean Freestone, Alan Lai, Anthony N. Burkitt, et al. **Patient-specific bivariate-synchrony-based seizure prediction for short prediction horizons**. *Epilepsy Research*, **91**(2-3):214–231, 2010. 45

[170] Björn Schelter, Matthias Winterhalder, Thomas Maiwald, Armin Brandt, et al. **Do False Predictions of Seizures Depend on the State of Vigilance? A Report from Two Seizure-Prediction Methods and Proposed Remedies**. *Epilepsia*, **47**(12):2058–2070, 2006. 45, 50, 91, 159

[171] Andreas Schulze-Bonhage. **From moon to earth—ultradian cycles in brain excitability**. *The Lancet Neurology*, **17**(11):930–932, 2018. 46, 88

[172] Ralph G. Andrzejak, Florian Mormann, Thomas Kreuz, Christoph Rieke, et al. **Testing the null hypothesis of the nonexistence of a preseizure state.** *Physical review. E, Statistical, nonlinear, and soft matter physics*, **67**(1 Pt 1):010901, 2003. 46, 47, 48, 150, 292

[173] Ralph G. Andrzejak, Daniel Chicharro, Christian E. Elger, and Florian Mormann. **Seizure prediction: Any better than chance?** *Clinical Neurophysiology*, **120**(8):1465–1478, 2009. 46, 47, 292

[174] Thomas Kreuz, Ralph G. Andrzejak, Florian Mormann, Alexander Kraskov, et al. **Measure profile surrogates: A method to validate the performance of epileptic seizure prediction algorithms**. *Physical Review E*, **69**(6):061915, 2004. 46

[175] César Alexandre Teixeira, Bruno Direito, Mojtaba Bandarabadi, Michel Le Van Quyen, et al. **Epileptic seizure predictors based on computational intelligence techniques: A comparative study with 278 patients**. *Computer Methods and Programs in Biomedicine*, **114**(3):324–336, 2014. 48, 64, 68, 72, 76, 77, 78, 80, 113, 114, 132, 148, 213, 214, 215, 256, 257

[176] Luigi Chisci, Antonio Mavino, Guido Perferi, Marco Sciandrone, et al. **Real-Time Epileptic Seizure Prediction Using AR Models and Support Vector Machines**. *IEEE Transactions on Biomedical Engineering*, **57**(5):1124–1132, 2010. 48

[177] C.A. Teixeira, B. Direito, H. Feldwisch-Drentrup, M. Valderrama, et al. **EPILAB: A software package for studies on the prediction of epileptic seizures**. *Journal of Neuroscience Methods*, **200**(2):257–271, 2011. 48, 75, 147, 264

[178] Cesar Teixeira, Bruno Direito, Mojtaba Bandarabadi, and Antonio Dourado. **Output regularization of SVM seizure predictors: Kalman Filter versus the "Firing Power" method**. In *2012 Annual International Conference of the IEEE Engineering in Medicine and Biology Society*, pages 6530–6533. IEEE, 2012. 48, 49

[179] Yun Park, Lan Luo, Keshab K. Parhi, and Theoden Netoff. **Seizure prediction with spectral power of EEG using cost-sensitive support vector machines**. *Epilepsia*, **52**(10):1761–1770, 2011. 48, 78, 263

[180] Jie Lu, Anjin Liu, Fan Dong, Feng Gu, et al. **Learning under Concept Drift: A Review**. *IEEE Transactions on Knowledge and Data Engineering*, **31**(12):1–1, 2018. 50

[181] João Gama, Indrė Žliobaitė, Albert Bifet, Mykola Pechenizkiy, and Abdelhamid Bouchachia. **A survey on concept drift adaptation**. *ACM Computing Surveys*, **46**(4):1–37, 2014. 50

[182] Alexey Tsymbal, Mykola Pechenizkiy, Pádraig Cunningham, and Seppo Puuronen. **Dynamic integration of classifiers for handling concept drift**. *Information Fusion*, **9**(1):56–68, 2008. 50

[183] Igor Goldenberg and Geoffrey I. Webb. **Survey of distance measures for quantifying concept drift and shift in numeric data**. *Knowledge and Information Systems*, **60**(2):591–615, 2019. 50

[184] Scott Wares, John Isaacs, and Eyad Elyan. **Data stream mining: methods and challenges for handling concept drift**. *SN Applied Sciences*, **1**(11):1412, 2019. 50

[185] Sofia Khan, Lino Nobili, Ramin Khatami, Tobias Loddenkemper, et al. **Circadian rhythm and epilepsy**. *The Lancet Neurology*, **17**(12):1098–1108, 2018. 50, 51, 86, 90, 138

[186] Mark Quigg. **Chronobiology and Sleep: Implications for Seizure Propensity**. In JM Rho, Raman. Sankar, and CE Stafstrom, editors, *Epilepsy: mechanisms, models, and translational perspectives*, chapter 29. CRC Press, Boca Raton, FL, 1st edition, 2010. 50

[187] Chang-Hoon Cho. **Molecular mechanism of circadian rhythmicity of seizures in temporal lobe epilepsy**. *Frontiers in Cellular Neuroscience*, **6**:55, 2012. 50

[188] Wytske AElig Hofstra and Al Wytze de Weerd. **The circadian rhythm and its interaction with human epilepsy: A review of literature**. *Sleep Medicine Reviews*, **13**(6):413–420, 2009. 50, 51

[189] Wytske A Hofstra-Van Oostveen and Al W De Weerd. **Seizures, epilepsy, and circadian rhythms**. *Sleep Medicine Clinics*, **7**(1):99–104, 2012. 51

[190] Philippa J. Karoly, Dean R. Freestone, Ray Boston, David B. Grayden, et al. **Interictal spikes and epileptic seizures: their relationship and underlying rhythmicity**. *Brain*, **139**(4):1066–1078, 2016. 51

[191] Sudhansu Chokroverty. **Overview of Normal Sleep**. In Sudhansu Chokroverty, editor, *Sleep Disorders Medicine*, chapter 2, pages 5–27. Springer New York, New York, NY, 4th edition, 2017. 51, 52

[192] Diego Z. Carvalho, J. Layne Moore, and Erik K. St. Louis. **Sleep, Sleep Disorders, and Epilepsy**. In Gregory D Cascino, Joseph I Sirven, and William O Tatum, editors, *Epilepsy*, chapter 9, pages 133–168. John Wiley & Sons, Ltd, 2nd edition, 2021. 51, 52

[193] Christine Blume, Renata del Giudice, Malgorzata Wislowska, Julia Lechinger, and Manuel Schabus. **Across the consciousness continuum – from unresponsive wakefulness to sleep**. *Frontiers in Human Neuroscience*, **9**(MAR):105, 2015. 52

[194] American Academy of Sleep Medicine. **AASM Manual for the Scoring of Sleep and Associated Events: Rules, Terminology and Technical Specifications**, 2020. 52

[195] Bo Jin, Thandar Aung, Yu Geng, and Shuang Wang. **Epilepsy and Its Interaction With Sleep and Circadian Rhythm**. *Frontiers in Neurology*, **11**:327, 2020. 52

[196] Divyani Garg, Laurel Charlesworth, and Garima Shukla. **Sleep and Temporal Lobe Epilepsy – Associations, Mechanisms and Treatment Implications**. *Frontiers in Human Neuroscience*, **16**:223, 2022. 52

[197] Annie H Roliz and Sanjeev Kothare. **The Interaction Between Sleep and Epilepsy**. *Current Neurology and Neuroscience Reports*, **22**(9):551–563, 2022. 52

[198] Christophe Bernard, Sebastien Naze, Timothée Proix, and Viktor K. Jirsa. **Modern Concepts of Seizure Modeling**. In Premysl Jiruska, Marco de Curtis, and John G. R. Jefferys, editors, *International Review of Neurobiology*, **114**, chapter 6, pages 121–153. Academic Press, 1st edition, 2014. 55, 56

[199] Frédéric Zubler, Andreas Steimer, Heidemarie Gast, and Kaspar A Schindler. **Seizure termination**. In Premysl Jiruska, Marco De Curtis, and John G. R. Jefferys, editors, *International review of neurobiology*, **114**, chapter 8, pages 187–207. Academic Press, 1st edition, 2014. 55, 56, 57

[200] Christophe Trefois, Paul M.A. Antony, Jorge Goncalves, Alexander Skupin, and Rudi Balling. **Critical transitions in chronic disease: transferring concepts from ecology to systems medicine**. *Current Opinion in Biotechnology*, **34**:48–55, 2015. 56

[201] Matias I. Maturana, Christian Meisel, Katrina Dell, Philippa J. Karoly, et al. **Critical slowing down as a biomarker for seizure susceptibility**. *Nature Communications*, **11**(1):2172, 2020. 56, 59

[202] Roxana A. Stefanescu, R.G. Shivakeshavan, and Sachin S. Talathi. **Computational models of epilepsy**. *Seizure*, **21**(10):748–759, 2012. 56

[203] William W. Lytton. **Computer modelling of epilepsy.** *Nature Reviews Neuroscience*, **9**(8):626–637, 2008. 56, 58, 59

[204] Fabrice Wendling, Pascal Benquet, Fabrice Bartolomei, and Viktor Jirsa. **Computational models of epileptiform activity**. *Journal of Neuroscience Methods*, **260**:233–251, 2016. 56

[205] D.R.W. Burrows, É. Samarut, J. Liu, S.C. Baraban, et al. **Imaging epilepsy in larval zebrafish**. *European Journal of Paediatric Neurology*, **24**:70–80, 2020. 56, 57

[206] Viktor K. Jirsa, William C. Stacey, Pascale P. Quilichini, Anton I. Ivanov, and Christophe Bernard. **On the nature of seizure dynamics**. *Brain*, **137**(8):2210–2230, 2014. 57, 58, 59, 135, 137

[207] Alexandros Skourtis-Cabrera. *Epilepsy at different scales: considerations for the medical application of dynamical models*. PhD thesis, Utrecht University, 2021. 57

[208] Michel J.A.M. van Putten and Jeannette Hofmeijer. **Generalized periodic discharges: Pathophysiology and clinical considerations**. *Epilepsy & Behavior*, **49**:228–233, 2015. 57

[209] P. JIRUSKA, F. MORMANN, and J.G.R. JEFFERYS. **NEURONAL AND NETWORK DYNAMICS PRECEDING EXPERIMENTAL SEIZURES**. In *Recent Advances in Predicting and Preventing Epileptic Seizures*, pages 16–29. WORLD SCIENTIFIC, 2013. 57, 58, 59

[210] F. H. L. da Silva, Wouter Blanes, S.N. Kalitzin, Jaime Parra, et al. **Dynamical diseases of brain systems: different routes to epileptic seizures**. *IEEE Transactions on Biomedical Engineering*, **50**(5):540–548, 2003. 57, 58, 135

[211] Fernando L. da Silva, Wouter Blanes, Stiliyan N. Kalitzin, Jaime Parra, et al. **Epilepsies as Dynamical Diseases of Brain Systems: Basic Models of the Transition Between Normal and Epileptic Activity**. *Epilepsia*, **44**(s12):72–83, 2003. 57, 58, 135

[212] Piotr Milanowski and Piotr Suffczynski. **Seizures Start without Common Signatures of Critical Transition**. *International Journal of Neural Systems*, **26**(08):1650053, 2016. 59

[213] Theresa Wilkat, Thorsten Rings, and Klaus Lehnertz. **No evidence for critical slowing down prior to human epileptic seizures**. *Chaos: An Interdisciplinary Journal of Nonlinear Science*, **29**(9):091104, 2019. 59

[214] Maromi Nei. **Cardiac Effects of Seizures**. *Epilepsy Currents*, **9**(4):91–95, 2009. 59, 209, 210

[215] Paulo A. Lotufo, Leandro Valiengo, Isabela M. Benseñor, and Andre R. Brunoni. **A systematic review and meta-analysis of heart rate variability in epilepsy and antiepileptic drugs**. *Epilepsia*, **53**(2):272–282, 2012. 59, 61, 238

[216] Soroor Behbahani. **A Review of Significant Research on Epileptic Seizure Detection and Prediction using Heart Rate Variability**. *Turk Kardiyoloji Dernegi Arsivi - Archives of the Turkish Society of Cardiology*, **46**(5):414–421, 2018. 60, 99, 238, 242

[217] Philippa J. Karoly, Rachel E. Stirling, Dean R. Freestone, Ewan S. Nurse, et al. **Multiday cycles of heart rate are associated with seizure likelihood: An observational cohort study**. *EBioMedicine*, **72**:103619, 2021. 60, 89

[218] Vera Novak, Andrew L. Reeves, Peter Novak, Phillip A. Low, and Frank W. Sharbrough. **Time-frequency mapping of R–R interval during complex partial seizures of temporal lobe origin**. *Journal of the Autonomic Nervous System*, **77**(2-3):195–202, 1999. 60

[219] D. H. Kerem and A. B. Geva. **Forecasting epilepsy from the heart rate signal**. *Medical & Biological Engineering & Computing*, **43**(2):230–239, 2005. 60, 73, 74, 100

[220] Christoph Baumgartner, Johannes P. Koren, and Michaela Rothmayer. **Automatic Computer-Based Detection of Epileptic Seizures**. *Frontiers in Neurology*, **9**(AUG), 2018. 60

[221] Claire Ufongene, Rima El Atrache, Tobias Loddenkemper, and Christian Meisel. **Electrocardiographic changes associated with epilepsy beyond heart rate and their utilization in future seizure detection and forecasting methods**. *Clinical Neurophysiology*, **131**(4):866–879, 2020. 60

[222] Toshitaka Yamakawa, Miho Miyajima, Koichi Fujiwara, Manabu Kano, et al. **Wearable Epileptic Seizure Prediction System with Machine-Learning-Based Anomaly Detection of Heart Rate Variability**. *Sensors*, **20**(14):3987, 2020. 61, 100, 211, 212

[223] Koichi Fujiwara, Miho Miyajima, Toshitaka Yamakawa, Erika Abe, et al. **Epileptic Seizure Prediction Based on Multivariate Statistical Process Control of Heart Rate Variability Features**. *IEEE Transactions on Biomedical Engineering*, **63**(6):1321–1332, 2016. 61, 100, 211, 212

[224] Lucia Billeci, Daniela Marino, Laura Insana, Giampaolo Vatti, and Maurizio Varanini. **Patient-specific seizure prediction based on heart rate variability and recurrence quantification analysis**. *PLOS ONE*, **13**(9):1–21, 2018. 61, 100, 113, 211, 212, 240, 241

[225] Jonatas Pavei, Renan G. Heinzen, Barbora Novakova, Roger Walz, et al. **Early Seizure Detection Based on Cardiac Autonomic Regulation Dynamics**. *Frontiers in Physiology*, **8**:1–12, 2017. 61, 100, 211, 212

[226] Manjari Tripathi and Navita Choudhary. **Significance of Heart Rate Variability in Patients with Epilepsy**. In M. V. Kamath, M. Watanabe, and A. Upton, editors, *Heart Rate Variability (HRV) Signal Analysis: Clinical Applications*, chapter 21, pages 411–424. CRC Press, 1st edition, 2013. 61

[227] Ivan Osorio and B.F.J. Manly. **Probability of detection of clinical seizures using heart rate changes**. *Seizure*, **30**:120–123, 2015. 61

[228] Carolina Varon, Katrien Jansen, Lieven Lagae, and Sabine Van Huffel. **Can ECG monitoring identify seizures?** *Journal of Electrocardiology*, **48**(6):1069–1074, 2015. 62

[229] S. Shmuely, M. van der Lende, R.J. Lamberts, J.W. Sander, and R.D. Thijs. **The heart of epilepsy: Current views and future concepts**. *Seizure*, **44**:176–183, 2017. 62, 209, 210

[230] Buajieerguli Maimaiti, Hongmei Meng, Yudan Lv, Jiqing Qiu, et al. **An Overview of EEG-based Machine Learning Methods in Seizure Prediction and Opportunities for Neurologists in this Field**. *Neuroscience*, **481**:197–218, 2022. 62, 63, 66, 67, 75

[231] **EEG Database — Seizure Prediction Project Freiburg**. 63

[232] Levin Kuhlmann, Philippa Karoly, Dean R. Freestone, Benjamin H. Brinkmann, et al. **Epilepsyecosystem.org: crowd-sourcing reproducible seizure prediction with long-term human intracranial EEG**. *Brain*, **141**(9):2619–2630, 2018. 63, 64, 68, 76, 77, 78, 81

[233] M. Valderrama, C. Alvarado, S. Nikolopoulos, J. Martinerie, et al. **Identifying an increased risk of epileptic seizures using a multi-feature EEG–ECG classification**. *Biomedical Signal Processing and Control*, **7**(3):237–244, 2012. 64, 68, 71, 72, 76, 77, 78, 80, 113, 114, 120, 124, 132, 157, 213, 214, 215, 255

[234] Jalil Rasekhi, Mohammad Reza Karami Mollaei, Mojtaba Bandarabadi, Cesar A. Teixeira, and Antonio Dourado. **Preprocessing effects of 22 linear univariate features on the performance of seizure prediction methods**. *Journal of Neuroscience Methods*, **217**(1-2):9–16, 2013. 64, 68, 72, 76, 77, 78, 80, 213, 214, 215, 257, 263, 264

[235] Mojtaba Bandarabadi, César A. Teixeira, Jalil Rasekhi, and António Dourado. **Epileptic seizure prediction using relative spectral power features**. *Clinical Neurophysiology*, **126**(2):237–248, 2015. 64, 68, 72, 75, 76, 77, 78, 80, 113, 114, 132, 148, 213, 214, 215, 264

[236] Bruno Direito, César A. Teixeira, Francisco Sales, Miguel Castelo-Branco, and António Dourado. **A Realistic Seizure Prediction Study Based on Multiclass SVM**. *International Journal of Neural Systems*, **27**(03):1–15, 2017. 64, 68, 71, 72, 76, 77, 78, 80, 100, 113, 114, 124, 132, 148, 157, 213, 214, 215, 256, 257

[237] Kostas M. Tsiouris, Vasileios C. Pezoulas, Michalis Zervakis, Spiros Konitsiotis, et al. **A Long Short-Term Memory deep learning network for the prediction of epileptic seizures using EEG signals**. *Computers in Biology and Medicine*, **99**:24–37, 2018. 64, 68, 72, 76, 77, 81, 213, 214, 215

[238] Nhan Duy Truong, Anh Duy Nguyen, Levin Kuhlmann, Mohammad Reza Bonyadi, et al. **Convolutional neural networks for seizure prediction using intracranial and scalp electroencephalogram**. *Neural Networks*, **105**:104–111, 2018. 64, 68, 76, 77, 78, 81

[239] Isabell Kiral-Kornek, Subhrajit Roy, Ewan Nurse, Benjamin Mashford, et al. **Epileptic Seizure Prediction Using Big Data and Deep Learning: Toward a Mobile System**. *EBioMedicine*, **27**:103–111, 2018. 65, 68, 76, 77, 81, 91

[240] Hisham Daoud and Magdy A. Bayoumi. **Efficient Epileptic Seizure Prediction Based on Deep Learning**. *IEEE Transactions on Biomedical Circuits and Systems*, **13**(5):804–813, 2019. 65, 68, 73, 76, 77, 78, 81

[241] Yuan Zhang, Yao Guo, Po Yang, Wei Chen, and Benny Lo. **Epilepsy Seizure Prediction on EEG Using Common Spatial Pattern and Convolutional Neural Network**. *IEEE Journal of Biomedical and Health Informatics*, **24**(2):465–474, 2020. 65, 69, 76, 77, 78, 81

[242] Syed Muhammad Usman, Shehzad Khalid, and Zafar Bashir. **Epileptic seizure prediction using scalp electroencephalogram signals**. *Biocybernetics and Biomedical Engineering*, **41**(1):211–220, 2021. 65, 69, 73, 76, 77, 78, 82

[243] Pedro F. Viana, Tal Pal Attia, Mona Nasseri, Jonas Duun-Henriksen, et al. **Seizure forecasting using minimally invasive, ultra-long-term subcutaneous electroencephalography: Individualized intrapatient models**. *Epilepsia*, 2022. 65, 66, 69, 76, 77, 78, 79, 82, 85

[244] Jingwei Zhang, Christos Chatzichristos, Kaat Vandecasteele, Lauren Swinnen, et al. **Automatic annotation correction for wear-**

able EEG based epileptic seizure detection. *Journal of Neural Engineering*, **19**(1):016038, 2022. 66

[245] Kevin T. Sweeney, Tomás E. Ward, and Seán F. McLoone. **Artifact Removal in Physiological Signals—Practices and Possibilities**. *IEEE Transactions on Information Technology in Biomedicine*, **16**(3):488–500, 2012. 66, 67

[246] Jose Antonio Urigüen and Begoña Garcia-Zapirain. **EEG artifact removal—state-of-the-art and guidelines**. *Journal of Neural Engineering*, **12**(3):031001, 2015. 66, 67

[247] Syed Muhammad Usman, Shehzad Khalid, Rizwan Akhtar, Zuner Bortolotto, et al. **Using scalp EEG and intracranial EEG signals for predicting epileptic seizures: Review of available methodologies**. *Seizure*, **71**:258–269, 2019. 67

[248] Fabio Lopes, Adriana Leal, Julio Medeiros, Mauro F. Pinto, et al. **Ensemble Deep Neural Network for Automatic Classification of EEG Independent Components**. *IEEE Transactions on Neural Systems and Rehabilitation Engineering*, **30**:559–568, 2022. 67, 119, 146, 158

[249] Sheryl R. Haut, Charles B. Hall, Thomas Borkowski, Howard Tennen, and Richard B. Lipton. **Clinical features of the pre-ictal state: Mood changes and premonitory symptoms**. *Epilepsy & Behavior*, **23**(4):415–421, 2012. 70

[250] William Stacey, Michel Le Van Quyen, Florian Mormann, and Andreas Schulze-Bonhage. **What is the present-day EEG evidence for a preictal state?** *Epilepsy Research*, **97**(3):243–251, 2011. 70

[251] Mojtaba Bandarabadi, Jalil Rasekhi, César A. Teixeira, Mohammad R. Karami, and António Dourado. **On the proper selection of preictal period for seizure prediction**. *Epilepsy & Behavior*, **46**:158–166, 2015. 71, 72, 113, 114, 132, 135, 213, 214

[252] Heinz Beck and Christian E. Elger. **Epilepsy research: a window onto function to and dysfunction of the human brain**. *Dialogues in Clinical Neuroscience*, **10**(1):7–15, 2008. 73, 137

[253] Michel Le Van Quyen, Jason Soss, Vincent Navarro, Richard Robertson, et al. **Preictal state identification by synchronization changes in long-term intracranial EEG recordings**. *Clinical Neurophysiology*, **116**(3):559–568, 2005. 73, 74, 100, 113, 118, 135, 139

[254] Fali Li, Yi Liang, Luyan Zhang, Chanlin Yi, et al. **Transition of brain networks from an interictal to a preictal state preceding a seizure revealed by scalp EEG network analysis**. *Cognitive Neurodynamics*, **13**(2):175–181, 2019. 73, 74, 100, 113, 118, 135

[255] Mona Nasseri, Vaclav Kremen, Petr Nejedly, Inyong Kim, et al. **Semi-supervised training data selection improves seizure forecasting in canines with epilepsy**. *Biomedical Signal Processing and Control*, **57**:101743, 2020. 73, 74, 100, 118

[256] Alessio Quercia, Thomas Frick, Fabian Emanuel Egli, Nicholas Pullen, et al. **Preictal onset detection through unsupervised clustering for epileptic seizure prediction**. In *2021 IEEE International Conference on Digital Health (ICDH)*, pages 142–147. IEEE, 2021. 73, 74, 100, 113, 118, 135

[257] Pieter van Mierlo, Margarita Papadopoulou, Evelien Carrette, Paul Boon, et al. **Functional brain connectivity from EEG in epilepsy: Seizure prediction and epileptogenic focus localization**. *Progress in Neurobiology*, **121**:19–35, 2014. 75

[258] Guiomar Niso, Ricardo Bruña, Ernesto Pereda, Ricardo Gutiérrez, et al. **HERMES: Towards an Integrated Toolbox to Characterize Functional and Effective Brain Connectivity**. *Neuroinformatics*, **11**(4):405–434, 2013. 75, 261

[259] Katarzyna J. Blinowska. **Review of the methods of determination of directed connectivity from multichannel data**. *Medical and Biological Engineering and Computing*, **49**(5):521–529, 2011. 75

[260] Poomipat Boonyakitanont, Apiwat Lek-uthai, Krisnachai Chomtho, and Jitkomut Songsiri. **A review of feature extraction and performance evaluation in epileptic seizure detection using EEG**. *Biomedical Signal Processing and Control*, **57**:101702, 2019. 75

[261] John P Cunningham and Byron M Yu. **Dimensionality reduction for large-scale neural recordings**. *Nature Neuroscience*, **17**(11):1500–1509, 2014. 78, 139

[262] Benson Mwangi, Tian Siva Tian, and Jair C. Soares. **A Review of Feature Reduction Techniques in Neuroimaging**. *Neuroinformatics*, **12**(2):229–244, 2014. 78

[263] Tal Pal Attia, Pedro F. Viana, Mona Nasseri, Jonas Duun-Henriksen, et al. **Seizure forecasting using minimally -invasive, ul-**

tra long-term subcutaneous EEG: Generalizable cross-patient models. *Epilepsia*, **00**:1–10, 2022. 78, 79

[264] Leon D. Iasemidis. **Epileptic Seizure Prediction and Control**. *IEEE Transactions on Biomedical Engineering*, **50**(5):549–558, 2003. 84, 139

[265] Philippa J. Karoly, Mark J. Cook, Matias Maturana, Ewan S. Nurse, et al. **Forecasting cycles of seizure likelihood**. *Epilepsia*, **61**(4):776–786, 2020. 85, 138, 160

[266] Vikram R. Rao, Marc Leguia, Thomas K. Tcheng, and Maxime O. Baud. **Cues for seizure timing**. *Epilepsia*, **62**(S1):S15–S31, 2021. 88, 90

[267] Jolien S. van Campen, Floris A. Valentijn, Floor E. Jansen, Marian Joëls, and Kees P. J. Braun. **Seizure occurrence and the circadian rhythm of cortisol: a systematic review**. *Epilepsy & Behavior*, **47**:132–137, 2015. 90

[268] Joseph T. Daley and Jennifer L. DeWolfe. **Sleep, Circadian Rhythms, and Epilepsy**. *Current Treatment Options in Neurology*, **20**(11):47, 2018. 90

[269] Soroor Behbahani, Nader Jafarnia Dabanloo, Ali Motie Nasrabadi, Cesar A. Teixeira, and Antonio Dourado. **Pre-ictal heart rate variability assessment of epileptic seizures by means of linear and non-linear analyses**. *Anadolu Kardiyoloji Dergisi/The Anatolian Journal of Cardiology*, **13**(8):797–803, 2013. 100, 114

[270] Jiapu Pan and Willis J. Tompkins. **A Real-Time QRS Detection Algorithm**. *IEEE Transactions on Biomedical Engineering*, **BME-32**(3):230–236, 1985. 101, 234

[271] Fred Shaffer and J. P. Ginsberg. **An Overview of Heart Rate Variability Metrics and Norms**. *Frontiers in Public Health*, **5**:1–17, 2017. 102, 235, 236, 237, 238, 239, 242

[272] A. Voss, Steffen Schulz, Rico Schroeder, Mathias Baumert, and Pere Caminal. **Methods derived from nonlinear dynamics for analysing heart rate variability**. *Philosophical Transactions of the Royal Society A: Mathematical, Physical and Engineering Sciences*, **367**(1887):277–296, 2009. 102, 238, 242

[273] Laura Ferreira and David B. Hitchcock. **A Comparison of Hierarchical Methods for Clustering Functional Data**. *Communications in Statistics - Simulation and Computation*, **38**(9):1925–1949, 2009. 103, 122

[274] Erich Schubert, Jörg Sander, Martin Ester, Hans Peter Kriegel, and Xiaowei Xu. **DBSCAN Revisited, Revisited Why and How You Should (Still) Use DBSCAN**. *ACM Transactions on Database Systems*, **42**(3):1–21, 2017. 103

[275] Martin Ester. **Density-Based Clustering**. In Charu C. Aggarwal and Chandan K. Reddy, editors, *Data Clustering: Algorithms and Applications*, chapter 5, pages 111–126. Chapman & Hall/CRC, 1st edition, 2014. 103, 122

[276] Jörg Sander, Martin Ester, Hans Peter Kriegel, and Xiaowei Xu. **Density-based clustering in spatial databases: The algorithm GDBSCAN and its applications**. *Data Mining and Knowledge Discovery*, **2**(2):169–194, 1998. 103, 122

[277] Hongbo Deng and Jiawei Han. **Probabilistic Models for Clustering**. In Charu C. Aggarwal and Chandan K. Reddy, editors, *Data Clustering: Algorithms and Applications*, chapter 3, pages 61–86. Chapman and Hall/CRC, 1st edition, 2014. 103, 122

[278] Negin Moghim and David W. Corne. **Predicting Epileptic Seizures in Advance**. *PLoS ONE*, **9**(6):1–17, 2014. 105

[279] Hui Xiong and Zhongmou Li. **Clustering Validation Measures**. In Charu C. Aggarwal and Chandan K. Reddy, editors, *Data Clustering: Algorithms and Applications*, chapter 23, pages 572–606. Chapman & Hall/CRC, 1st edition, 2014. 105, 123

[280] Sara Mahallati, James C. Bezdek, Milos R. Popovic, and Taufik A. Valiante. **Cluster tendency assessment in neuronal spike data**. *PLOS ONE*, **14**(11):1–29, 2019. 105

[281] Hinnerk Feldwisch-Drentrup, Matthäus Staniek, Andreas Schulze-Bonhage, Jens Timmer, et al. **Identification of Preseizure States in Epilepsy: A Data-Driven Approach for Multichannel EEG Recordings**. *Frontiers in Computational Neuroscience*, **5**:32, 2011. 120

[282] Klaus Lehnertz, Henning Dickten, Stephan Porz, Christoph Helmstaedter, and Christian E. Elger. **Predictability of uncontrollable multifocal seizures – towards new treatment options**. *Scientific Reports*, **6**(1):24584, 2016. 120

[283] Daniel E. Payne, Philippa J. Karoly, Dean R. Freestone, Ray Boston, et al. **Postictal suppression and seizure durations: A patient-specific, long-term iEEG analysis**. *Epilepsia*, **59**(5):1027–1036, 2018. 120

[284] Leland McInnes, John Healy, and James Melville. **UMAP: Uniform Manifold Approximation and Projection for Dimension Reduction**, 2018. 120

[285] Yingfan Wang, Haiyang Huang, Cynthia Rudin, and Yaron Shaposhnik. **Understanding how dimension reduction tools work: An empirical approach to deciphering T-SNE, UMAP, TriMap, and PaCMAP for data visualization**. *Journal of Machine Learning Research*, **22**:1–73, 2021. 120, 122

[286] Pang-Ning Tan, Michael Steinbach, Anuj Karpatne, and Vipin Kumar. **Cluster Analysis: Basic Concepts and Algorithms**. In *Introduction to Data Mining*, chapter 5, page 866. Pearson Education, 2nd edition, 2019. 122

[287] Sławomir T. Wierzchoń and Mieczysław A. Kłopotek. **Algorithms of Combinatorial Cluster Analysis**. In *Modern Algorithms of Cluster Analysis. Studies in Big Data*, **34**, pages 67–161. Springer, Cham, 2018. 122

[288] Martin Ester, Hans-Peter Kriegel, Jörg Sander, and Xiaowei Xu. **A Density-Based Algorithm for Discovering Clusters in Large Spatial Databases with Noise**. In *Proceedings of the 2nd International Conference on Knowledge Discovery and Data Mining*, pages 226–231, 1996. 122

[289] Ricardo J. G. B. Campello, Davoud Moulavi, and Joerg Sander. **Density-Based Clustering Based on Hierarchical Density Estimates**. In Pei J., Tseng V.S., Cao L., Motoda H., and Xu G., editors, *Advances in Knowledge Discovery and Data Mining. PAKDD 2013. Lecture Notes in Computer Science*, **7819**, pages 160–172. Springer, Berlin, Heidelberg, 2013. 122

[290] Ricardo J. G. B. Campello, Davoud Moulavi, Arthur Zimek, and Jörg Sander. **Hierarchical Density Estimates for Data Clustering, Visualization, and Outlier Detection**. *ACM Transactions on Knowledge Discovery from Data*, **10**(1):1–51, 2015. 122

[291] Ana Catarina Rocha Oliveira. *Sleep-Awake Cycle Evaluation from Long-term EEG Data: Assessing the Impact in Epilepsy Seizure Prediction*. PhD thesis, University of Coimbra, 2021. 127, 270

[292] Michael Brusco, J. Dennis Cradit, and Douglas Steinley. **A comparison of 71 binary similarity coefficients: The effect of base rates**. *PLOS ONE*, **16**(4):e0247751, 2021. 127

[293] Davide Chicco and Giuseppe Jurman. **The advantages of the Matthews correlation coefficient (MCC) over F1 score and accuracy in binary classification evaluation**. *BMC Genomics*, **21**(1):6, 2020. 127

[294] Márcio Flávio Dutra Moraes, Daniel de Castro Medeiros, Flávio Afonso Gonçalves Mourao, Sergio Augusto Vieira Cancado, and Vinicius Rosa Cota. **Epilepsy as a dynamical system, a most needed paradigm shift in epileptology**. *Epilepsy & Behavior*, **121**:106838, 2021. 135, 136

[295] Oriano Mecarelli. **Pathological EEG Patterns**. In Oriano Mecarelli, editor, *Clinical Electroencephalography*, chapter 13, pages 223–235. Springer International Publishing, Cham, 2019. 137

[296] Paul L. Nunez and Ramesh Srinivasan. **Fallacies in EEG**. In Paul L. Nunez and Ramesh Srinivasan, editors, *Electric Fields of the Brain*, chapter 2, pages 56–98. Oxford University Press, 2nd edition, 2006. 138

[297] Zhi-Hua Zhou. **Support Vector Machine**. In *Machine Learning*, chapter 6, pages 129–153. Springer Singapore, Singapore, 2021. 156

[298] Marije van der Lende, Rainer Surges, Josemir W. Sander, and Roland D. Thijs. **Cardiac arrhythmias during or after epileptic seizures**. *Journal of Neurology, Neurosurgery & Psychiatry*, **87**(1):69–74, 2015. 210

[299] Leif Sörnmo and Pablo Laguna. **ECG Signal Processing**. In Leif Sörnmo and Pablo Laguna, editors, *Bioelectrical Signal Processing in Cardiac and Neurological Applications*, chapter 7, pages 453–566. Elsevier, 1st edition, 2005. 233

[300] Gari D. Clifford. **Linear Filtering Methods**. In Gari D. Clifford, Francisco Azuaje, and Patrick E. Mcsharry, editors, *Advanced Methods and Tools for ECG Data Analysis*, chapter 5, pages 135–170. Artech House, 2006. 233

[301] Leif Sörnmo and Pablo Laguna. **ECG Signal Processing: Heart Rate Variability**. In Leif Sörnmo and Pablo Laguna, editors, *Bioelectrical Signal Processing in Cardiac and Neurological Applications*, chapter 8, pages 567–631. Elsevier, 1st edition, 2005. 233, 235, 237, 239

[302] Gari D. Clifford. **Introduction to Feature Extraction**. In Gari D. Clifford, Francisco Azuaje, and Patrick E. Mcsharry, editors, *Advanced Methods and Tools for ECG Data Analysis*, chapter 9, pages 245–268. Artech House, 2006. 233

[303] Gari D. Clifford. **ECG Statistics, Noise, Artifacts, and Missing Data**. In Gari D. Clifford, Francisco Azuaje, and Patrick E. Mcsharry, editors, *Advanced Methods and Tools for ECG Data Analysis*, chapter 3, pages 55–100. Artech House, 2006. 234, 235, 236, 237, 239

[304] Mirja A. Peltola. **Role of editing of R–R intervals in the analysis of heart rate variability**. *Frontiers in Physiology*, **3**:1–10, 2012. 234, 235

[305] Sylvie J. M. van der Kruijs, Kristl E. J. Vonck, Geert R. Langereis, Loe M. G. Feijs, et al. **Autonomic nervous system functioning associated with psychogenic nonepileptic seizures: Analysis of heart rate variability**. *Epilepsy & Behavior*, **54**:14–19, 2016. 236, 238, 239, 242, 251

[306] Athi Ponnusamy, Jefferson L. B. Marques, and Markus Reuber. **Comparison of heart rate variability parameters during complex partial seizures and psychogenic nonepileptic seizures**. *Epilepsia*, **53**(8):1314–1321, 2012. 236, 238, 242, 251

[307] Jacob T. VanderPlas. **Understanding the Lomb–Scargle Periodogram**. *The Astrophysical Journal Supplement Series*, **236**(1):1–28, 2018. 236

[308] Massimiliano de Zambotti, John Trinder, Alessandro Silvani, Ian M. Colrain, and Fiona C. Baker. **Dynamic coupling between the central and autonomic nervous systems during sleep: A review**. *Neuroscience & Biobehavioral Reviews*, **90**:84–103, 2018. 237

[309] Rhenan Bartels, Leonardo Neumamm, Tiago Peçanha, and Alysson Roncally Silva Carvalho. **SinusCor: an advanced tool for heart rate variability analysis**. *BioMedical Engineering OnLine*, **16**(1):1–15, 2017. 237

[310] George E. Billman. **Heart Rate Variability ? A Historical Perspective**. *Frontiers in Physiology*, **2**:1–13, 2011. 237

[311] Tom Kuusela. **Methodological Aspects of Heart Rate Variability Analysis**. In M. V. Kamath, M. Watanabe, and A. Upton, editors, *Heart Rate Variability (HRV) Signal Analysis: Clinical Applications*, chapter 2, pages 9–42. CRC Press, 1st edition, 2013. 237, 239

[312] Mika P. Tarvainen, Juha-Pekka Niskanen, Jukka A. Lipponen, Perttu O. Ranta-aho, and Pasi A. Karjalainen. **Kubios HRV – Heart rate variability analysis software**. *Computer Methods and Programs in Biomedicine*, **113**(1):210–220, 2014. 237

[313] Roberto Maestri, Gian Domenico Pinna, Alberto Porta, Rita Balocchi, et al. **Assessing nonlinear properties of heart rate variability from short-term recordings: are these measurements reliable?** *Physiological Measurement*, **28**(9):1067–1077, 2007. 238

[314] Rosangela Akemi Hoshi, Carlos Marcelo Pastre, Luiz Carlos Marques Vanderlei, and Moacir Fernandes Godoy. **Poincaré plot indexes of heart rate variability: Relationships with other nonlinear variables**. *Autonomic Neuroscience*, **177**(2):271–274, 2013. 238, 239, 240

[315] C.-K. Peng, Shlomo Havlin, H. Eugene Stanley, and Ary L. Goldberger. **Quantification of scaling exponents and crossover phenomena in nonstationary heartbeat time series**. *Chaos: An Interdisciplinary Journal of Nonlinear Science*, **5**(1):82–87, 1995. 239

[316] Madalena D. Costa, Roger B. Davis, and Ary L. Goldberger. **Heart Rate Fragmentation: A New Approach to the Analysis of Cardiac Interbeat Interval Dynamics**. *Frontiers in Physiology*, **8**(MAY):1–13, 2017. 239

[317] Sieven M. Pincus. **Approximate entropy as a measure of system complexity.** *Proceedings of the National Academy of Sciences*, **88**(6):2297–2301, 1991. 239, 260

[318] Joshua S. Richman and J. Randall Moorman. **Physiological time-series analysis using approximate entropy and sample entropy**. *American Journal of Physiology-Heart and Circulatory Physiology*, **278**(6):H2039–H2049, 2000. 239, 260

[319] Alfonso Delgado-Bonal and Alexander Marshak. **Approximate Entropy and Sample Entropy: A Comprehensive Tutorial**. *Entropy*, **21**(6):1–37, 2019. 239, 260

[320] U. Rajendra Acharya, K. Paul Joseph, N. Kannathal, Choo Min Lim, and Jasjit S. Suri. **Heart rate variability: a review**. *Medical & Biological Engineering & Computing*, **44**(12):1031–1051, 2006. 240

[321] Teresa Henriques, Maria Ribeiro, Andreia Teixeira, Luísa Castro, et al. **Nonlinear Methods Most Applied to Heart-Rate Time Series: A Review**. *Entropy*, **22**(3):1–39, 2020. 240, 264

[322] Jaqueline Lekscha and Reik V. Donner. **Phase space reconstruction for non-uniformly sampled noisy time series**. *Chaos: An Interdisciplinary Journal of Nonlinear Science*, **28**(8):1–12, 2018. 240, 260

[323] Matthew B. Kennel, Reggie Brown, and Henry D. I. Abarbanel. **Determining embedding dimension for phase-space reconstruction using a geometrical construction**. *Physical Review A*, **45**(6):3403–3411, 1992. 240, 260

[324] Andrew M. Fraser and Harry L. Swinney. **Independent coordinates for strange attractors from mutual information**. *Physical Review A*, **33**(2):1134–1140, 1986. 240, 260

[325] Michael T. Rosenstein, James J. Collins, and Carlo J. De Luca. **A practical method for calculating largest Lyapunov exponents from small data sets**. *Physica D: Nonlinear Phenomena*, **65**(1-2):117–134, 1993. 240, 260

[326] Peter Grassberger and Itamar Procaccia. **Characterization of Strange Attractors**. *Physical Review Letters*, **50**(5):346–349, 1983. 240, 260

[327] J.-P Eckmann, S. Oliffson Kamphorst, and D. Ruelle. **Recurrence Plots of Dynamical Systems**. *Europhysics Letters (EPL)*, **4**(9):973–977, 1987. 240, 261

[328] N. MARWAN, M. CARMENROMANO, M. THIEL, and J. KURTHS. **Recurrence plots for the analysis of complex systems**. *Physics Reports*, **438**(5-6):237–329, 2007. 241, 261

[329] Norbert Marwan and Charles L. Webber. **Mathematical and Computational Foundations of Recurrence Quantifications**. In Jr. C. Webber and N. Marwan, editors, *Recurrence Quantification Analysis. Understanding Complex Systems.*, chapter 1, pages 3–43. Springer, Cham, 2015. 241, 261

[330] Isabelle Guyon and André Elisseeff. **An Introduction to Feature Extraction**. In Isabelle Guyon, Steve Gunn, Masoud Nikravesh, and Lotfi A. Zadeh, editors, *Feature Extraction Foundations and Applications*, **207**, chapter 1, pages 1–25. Springer Berlin Heidelberg, Berlin, Heidelberg, 2006. 245

[331] Robin D. Thomas, Nathan C. Moses, Erin A. Semple, and Adam J. Strang. **An efficient algorithm for the computation of average mutual information: Validation and implementation in Matlab**. *Journal of Mathematical Psychology*, **61**:45–59, 2014. 245

[332] P. A. Estevez, M. Tesmer, C. A. Perez, and J. M. Zurada. **Normalized Mutual Information Feature Selection**. *IEEE Transactions on Neural Networks*, **20**(2):189–201, 2009. 245

[333] Robert S. Witte and John S. Witte. **Describing Relationships: Correlation**. In *Statistics*, chapter 6, pages 107–125. John Wiley & Sons, Inc., 11 edition, 2016. 247

[334] Yulong Sheng. **Wavelet Transform**. In Alexander D. Poularikas, editor, *Transforms and Applications Handbook*, chapter 10, pages 1–10. CRC Press, 3rd edition, 2010. 257

[335] Oliver Faust, U. Rajendra Acharya, Hojjat Adeli, and Amir Adeli. **Wavelet-based EEG processing for computer-aided seizure detection and epilepsy diagnosis**. *Seizure*, **26**:56–64, 2015. 257

[336] Elisabeth Ruiz-Padial and Antonio J. Ibáñez-Molina. **Fractal dimension of EEG signals and heart dynamics in discrete emotional states**. *Biological Psychology*, **137**:42–48, 2018. 258

[337] Tame N. J. Kawe, Shabah M. Shadli, and Neil McNaughton. **Higuchi's fractal dimension, but not frontal or posterior alpha asymmetry, predicts PID-5 anxiousness more than depressivity**. *Scientific Reports*, **9**(1):19666, 2019. 258

[338] Srdjan Kesić and Sladjana Z. Spasić. **Application of Higuchi's fractal dimension from basic to clinical neurophysiology: A review**. *Computer Methods and Programs in Biomedicine*, **133**:55–70, 2016. 258, 264

[339] Espen A. F. Ihlen. **Introduction to Multifractal Detrended Fluctuation Analysis in Matlab**. *Frontiers in Physiology*, **3**:141, 2012. 258, 259

[340] R. M. Bryce and K. B. Sprague. **Revisiting detrended fluctuation analysis**. *Scientific Reports*, **2**(1):315, 2012. 258

[341] Jorge Luis Morales Martínez, Ignacio Segovia-Domínguez, Israel Quiros Rodríguez, Francisco Antonio Horta-Rangel, and Guillermo Sosa-Gómez. **A modified Multifractal Detrended Fluctuation Analysis (MFDFA) approach for multifractal analysis of precipitation**. *Physica A: Statistical Mechanics and its Applications*, **565**:125611, 2021. 258

[342] Lihan Tang, Ning Xie, Menglian Zhao, and Xiaobo Wu. **Seizure Prediction Using Multi-View Features and Improved Convolutional Gated Recurrent Network**. *IEEE Access*, **8**:172352–172361, 2020. 258, 264

[343] Debdeep Sikdar, Rinku Roy, and Manjunatha Mahadevappa. **Epilepsy and seizure characterisation by multifractal analysis of**

EEG subbands. *Biomedical Signal Processing and Control*, **41**:264–270, 2018. 258, 264

[344] E. Serrano and A. Figliola. **Wavelet Leaders: A new method to estimate the multifractal singularity spectra**. *Physica A: Statistical Mechanics and its Applications*, **388**(14):2793–2805, 2009. 258, 264

[345] Lucas Gabriel Souza França, Pedro Montoya, and José Garcia Vivas Miranda. **On multifractals: a non-linear study of actigraphy data**. *Physica A: Statistical Mechanics and its Applications*, **514**:612–619, 2017. 258

[346] Rohit Bose, Sawon Pratiher, and Soumya Chatterjee. **Detection of epileptic seizure employing a novel set of features extracted from multifractal spectrum of electroencephalogram signals**. *IET Signal Processing*, **13**(2):157–164, 2019. 258, 259

[347] Igor Freitas Cruz and Jaime Sampaio. **Multifractal Analysis of Movement Behavior in Association Football**. *Symmetry*, **12**(8):1287, 2020. 258

[348] U. Rajendra Acharya, Filippo Molinari, S. Vinitha Sree, Subhagata Chattopadhyay, et al. **Automated diagnosis of epileptic EEG using entropies**. *Biomedical Signal Processing and Control*, **7**(4):401–408, 2012. 260

[349] U. Rajendra Acharya, H. Fujita, Vidya K. Sudarshan, Shreya Bhat, and Joel E.W. Koh. **Application of entropies for automated diagnosis of epilepsy using EEG signals: A review**. *Knowledge-Based Systems*, **88**:85–96, 2015. 260

[350] U. Rajendra Acharya, Yuki Hagiwara, and Hojjat Adeli. **Automated seizure prediction**. *Epilepsy & Behavior*, **88**:251–261, 2018. 260, 264

[351] Payam Shahsavari Baboukani, Ghasem Azemi, Boualem Boashash, Paul Colditz, and Amir Omidvarnia. **A novel multivariate phase synchrony measure: Application to multichannel newborn EEG analysis**. *Digital Signal Processing*, **84**:59–68, 2019. 261

[352] Tetsuo Kida, Emi Tanaka, and Ryusuke Kakigi. **Multi-Dimensional Dynamics of Human Electromagnetic Brain Activity**. *Frontiers in Human Neuroscience*, **9**(JAN2016):713, 2016. 261, 262

[353] Florian Mormann, Ralph G. Andrzejak, Thomas Kreuz, Christoph Rieke, et al. **Automated detection of a preseizure state based on**

a decrease in synchronization in intracranial electroencephalogram recordings from epilepsy patients. *Physical Review E*, **67**(2):021912, 2003. 262

[354] Piotr Mirowski, Deepak Madhavan, Yann LeCun, and Ruben Kuzniecky. **Classification of patterns of EEG synchronization for seizure prediction**. *Clinical Neurophysiology*, **120**(11):1927–1940, 2009. 262

[355] Mikail Rubinov and Olaf Sporns. **Complex network measures of brain connectivity: Uses and interpretations**. *NeuroImage*, **52**(3):1059–1069, 2010. 262, 263

[356] Klaus Lehnertz, Christian Geier, Thorsten Rings, and Kirsten Stahn. **Capturing time-varying brain dynamics**. *EPJ Nonlinear Biomedical Physics*, **5**:2, 2017. 262

[357] Anis Malekzadeh, Assef Zare, Mahdi Yaghoobi, and Roohallah Alizadehsani. **Automatic Diagnosis of Epileptic Seizures in EEG Signals Using Fractal Dimension Features and Convolutional Autoencoder Method**. *Big Data and Cognitive Computing*, **5**(4):78, 2021. 264

[358] Anis Malekzadeh, Assef Zare, Mahdi Yaghoobi, Hamid-Reza Kobravi, and Roohallah Alizadehsani. **Epileptic Seizures Detection in EEG Signals Using Fusion Handcrafted and Deep Learning Features**. *Sensors*, **21**(22):7710, 2021. 264

[359] Sami Auno, Leena Lauronen, Juha Wilenius, Maria Peltola, et al. **Detrended fluctuation analysis in the presurgical evaluation of parietal lobe epilepsy patients**. *Clinical Neurophysiology*, **132**(7):1515–1525, 2021. 264

[360] Nikita S. Frolov, Vadim V. Grubov, Vladimir A. Maksimenko, Annika Lüttjohann, et al. **Statistical Properties and Predictability of Extreme Epileptic Events**. *Scientific Reports*, **9**(1):7243, 2019. 264

[361] Mario Giovanni Terzano, Liborio Parrino, Adriano Sherieri, Ronald Chervin, et al. **Atlas, rules, and recording techniques for the scoring of cyclic alternating pattern (CAP) in human sleep**. *Sleep Medicine*, **2**(6):537–553, 2001. 270

[362] A. L. Goldberger, L. A. N. Amaral, L. Glass, J. M. Hausdorff, et al. **PhysioBank, PhysioToolkit, and PhysioNet: Components of a New Research Resource for Complex Physiologic Signals**. *Circulation*, **101**(23):e215–e220, 2000. 270

[363] Reza Boostani, Foroozan Karimzadeh, and Mohammad Nami. **A comparative review on sleep stage classification methods in patients and healthy individuals**. *Computer Methods and Programs in Biomedicine*, **140**:77–91, 2017. 271, 272

[364] Khald Aboalayon, Miad Faezipour, Wafaa Almuhammadi, and Saeid Moslehpour. **Sleep Stage Classification Using EEG Signal Analysis: A Comprehensive Survey and New Investigation**. *Entropy*, **18**(9):272, 2016. 271, 272

[365] Jason Brownlee. **Feature Selection**. In *Data preparation for machine learning*, chapter 11, pages 111–118. v1.1 edition, 2020. 272

[366] Jason Brownlee. **Tour of Model Evaluation Metrics**. In *Imbalanced Classification with Python*, chapter 4, pages 36–47. v1.2 edition, 2020. 272

Appendix A

Background concepts in detail

This chapter extends on two aspects from the background section, namely, the electroencephalography (EEG) acquisition montage (Section A.1) and the concept of true and false alarms (Section A.2).

A.1 EEG acquisition montage

Bipolar montage corresponds to the measurement of the voltage difference between two electrodes, that are usually placed along chains and are, therefore, close to each other (see Figure 2.4). Referential montages, despite being also a bipolar arrangement, involve measuring the voltage differences between each electrode and a reference electrode, that is more distant from the active electrodes. In practice, online acquisition of scalp EEG recordings is obtained using a referential montage, i.e., by subtracting the voltage from a single reference electrode and the remaining active electrodes. Given that such referencing is a linear transformation of voltage potentials, the recordings are typically re-referenced offline, either using a bipolar or a referential montage [34,58,71,73]. Offline references used in referential montage can be obtained from: (i) a common reference such as the linked mastoids, the ear lobes, or the vertex electrode (Cz) or (ii) averaging over some or all signals that have been recorded from other scalp electrodes (average common reference) [34,57,58,71,73,74].

The choice of the referencing montage (bipolar vs referential), as well as the reference electrode in referential montage, lead to differences in scalp EEG recordings that may cloud the interpretation of the further analysis. For instance, the voltages captured by a reference electrode will impact the voltages recorded by all other active electrodes. The choice of the reference electrode strongly influences further analysis in the sense that if the reference electrode is severely contaminated with noise, so will the obtained scalp EEG signals [58]. A bad choice of the reference electrode is also reflected in the values of connectivity measures such as correlation, coherency and phase synchronisation [57]. Notwithstanding, there is no electrode placement that ideally would provide a reference electrode free from electrical artefacts (zero

potential reference) [34, 58, 71, 73].

The number of electrodes available for acquisition may help decide which re-referencing montage to choose. With a low number of electrodes (e.g., the 10-20 system), the bipolar montage is considered the best choice to record scalp EEG [73]. In this montage, the pairs of electrodes are closer to each other, this way providing more accurate estimates of the local electric field and thus better spatial resolution. The larger the distance between electrodes, the higher the contribution of distant, volume-conducted, electric fields to the signal acquired at a given electrode site [57, 71, 73]. Conversely, subtracting the average of all channels to each channel is more efficient when scalp EEG has been acquired using a large number of electrodes (128 or more). The higher the number of electrodes, the more accurate will be the estimate of the field distribution across the entire head (the reference average potential will tend to zero) [34, 71, 73, 74].

A.2 Examples of false and true alarms

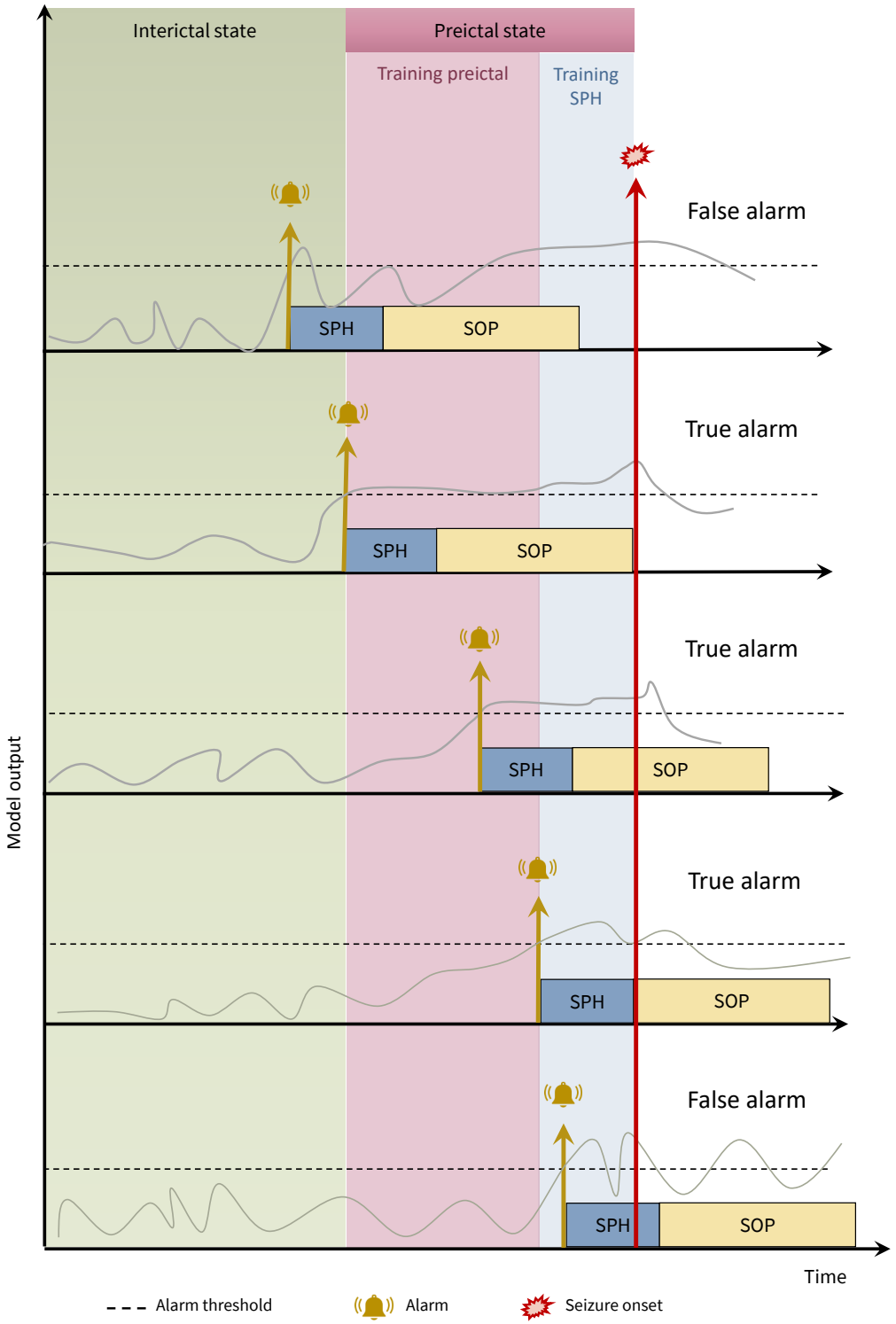

Figure A.1: Examples of false and true alarms. Despite assuming a preictal state manifesting as altered brain dynamics until the seizure onset (biological perspective), a seizure prediction model is trained by considering a preictal interval of the same length as the SOP. The patient perspective implies that when an alarm is raised, the patient can take preventive measures during the SPH and expect a seizure to occur within the SOP.

Appendix B

State of the art article information

B.1 Changes in heart rate during seizures

Heart rate (HR) changes have been widely reported during epileptic seizures. Some studies document episodes of tachycardia and bradycardia, and others simply report a statistically significant increase or decrease in HR, respectively [93].

Ictal heart rate increase

Sinus tachycardia has been typically observed during the ictal period in the majority of seizures (up to 100% of seizures and in 38-100% of epileptic patients), beginning just before (in the range of 0.7-49.3 seconds), during or after seizure onset and usually asymptomatically (it is typically associated with palpitations but not with clinical signs such syncope) [20, 93, 229].

Most studies evaluated HR changes in seizures arising from the temporal lobe [21, 93]. Nevertheless, when differences among lobes were inspected, tachycardia was more frequently observed in seizures originating from the temporal lobe when compared to extratemporal lobe seizures [20, 21, 93]. Early research suggested the hemispheric lateralisation of the autonomic cardiovascular function. Namely, some studies showed that ictal tachycardia was more frequently observed in the right hemisphere, indicating that this hemisphere would predominantly modulate sympathetic responses [19, 20, 30, 95, 214]. However, recent surveys concluded that more studies are required to verify this hypothesis [21, 93, 146]. Lastly, temporal lobe seizures have also been associated with earlier and longer periods of increased HR compared to other seizure locations [19, 93, 95].

HR alterations are predominantly detected from the electroencephalography (EEG) seizure onset onwards [93, 146, 214]. In some seizures, those alterations persisted for minutes up to hours after seizure offset [214]. Additionally, several studies

show increasing HR seconds before seizure onset (median onset of 10.7 seconds, in up to 36% of seizures) [21].

Regarding seizure type, an increase in HR is often seen for focal onset impaired awareness (FOIA) and generalised tonic-clonic seizures. However, a greater and longer-lasting HR increase is observed for the latter compared to the former [30, 42, 146, 214].

Ictal heart rate decrease

Bradycardia episodes, although the most frequent clinically relevant arrhythmias are considerably less frequent in epileptic seizures than in tachycardias (occurs in less than 2% of seizures). A severe decrease in HR can lead to asystole and syncope (and subsequent falls, fractures and/or traffic accidents), a clear indicator of ictal bradycardia [19, 20, 42, 214].

Ictal asystole has been reported to occur exclusively in focal onset seizures, mainly in patients with temporal lobe epilepsy (TLE) and 0.32% of people with drug-resistant focal epilepsy [42, 214, 229, 298]. Despite the limited understanding regarding the brain mechanisms generating ictal asystole, this event is thought to arise from: (i) direct stimulation of the autonomous nervous system (ANS) or (ii) fear (or other behavioural effects) induced by the seizure and subsequent cardioinhibition and vasodilation [42, 229].

B.2 Extra information on heart rate variability studies

Table B.1 presents information on seizure prediction studies based on heart rate variability (HRV) data. All studies were conducted in patients with drug-resistant epilepsy (DRE), under presurgical monitoring.

Table B.1: Database information on HRV-based seizure prediction studies.

Study	Patients	Seizures	Interictal time	Preictal time
Fujiwara *et al.* 2016 [223]	14 patients with DRE	11 awakening seizures	38.4 h of total interictal time	15 min
Pavei *et al.* 2017 [225]	12 patients with temporal lobe DRE	34 focal seizures	7.8 h of total interictal training time and 47.4 h total interictal testing time	10 min
Billeci *et al.* 2018 [224]	15 patients with temporal lobe DRE	38 FOIA, FBTC and generalised seizures	57 h of total interictal time	15 min
Yamakawa *et al.* 2020 [222]	7 patients with focal DRE and 7 healthy controls	14 FOA, FOIA and FBTC seizures	40 h of total interictal time	15 min

DRE: drug-resistant epilepsy. FBTC: focal to bilateral tonic-clonic seizure. FOIA: focal onset impaired awareness seizure. FOA: focal onset aware seizure.

Table B.2: Methodology information on HRV-based seizure prediction studies.

Study	Feature extraction	Feature selection	Classifier	Partitioning
Fujiwara *et al.* 2016 [223]	**Time-domain:** MeanNN, SDNN, RMSSD, TP, NN50; **Frequency-domain:** LF_n^3, HF_n^3, LF_n/HF_n^3	-	Patient-specific, Multivariate Statistical Process Control (MSPC)	n.s.
Pavei *et al.* 2017 [225]	**Time-domain:** SDNN, RMSSD; **Frequency-domain:** LF, HF; **Non-linear:** SampEn, Poincaré plot (CSI and CVI)	-	SVM with Gaussian kernel	Leave-one-out cross-validation
Billeci *et al.* 2018 [224]	**Time-domain:** MeanNN, RMSSD, SDNN, NN50, pNN50, VarNN; **Frequency-domain:** LF_n^3, HF_n^3, LF_n/HF_n^3; **Non-linear:** COSEn (Coefficient of Sample Entropy), KFD, Poincaré plot (SD1, SD2, CSI, CVI), RQA (Rec, Det, L_{max}, Lam, TT, Ent).	Stepwise regression analysis	Patient-specific. SVM with RBF kernel	Five-fold cross validation training. Additionally, for patients with 3 or more seizures, double cross-validation.
Yamakawa *et al.* 2020 [222]	**Time-domain:** MeanNN, SDNN, RMSSD, NN50, VarNN; **Frequency-domain:** TP, LF, HF, LF/HF	-	Multivariate Statistical Process Control (MSPC)	n.s.

n.s.: not specified

B.3 Extra information on preictal grid-search studies

Table B.3: Database information on studies inspecting different preictal durations.

Study	Database	Patients	Electrodes	EEG type
Mormann *et al.* 2005 [14]*	Bonn	5	All electrodes	iEEG
Valderrama *et al.* 2012 [233]	EPILEPSIAE	12 with focal DRE	All electrodes	sEEG, iEEG, ECG
Rasekhi *et al.* 2013 [234]	EPILEPSIAE	10	3 in focal region and 3 far from local region (?)	sEEG, iEEG
Teixeira *et al.* 2014 [175]	EPILEPSIAE	278	F7, FZ, F8, T5, PZ, T6; 6 random; 6 in focal region	sEEG, iEEG
Alvarado-Rojas *et al.* 2014 [149]	EPILEPSIAE	53 with focal DRE	All electrodes	sEEG, iEEG
Rasekhi *et al.* 2015 [144]	EPILEPSIAE	10	3 in focal region and 3 far from local region	sEEG, iEEG
Bandarabadi *et al.* 2015 [251]*	EPILEPSIAE	18 with focal DRE	2 in focal region	sEEG, iEEG
Bandarabadi *et al.* 2015 [235]	EPILEPSIAE	24	3 in focal region and 3 far from local region	sEEG, iEEG
Direito *et al.* 2017 [236]	EPILEPSIAE	216	F7, FZ, F8, T5, PZ, T6; 6 random; 6 in focal region	sEEG, iEEG
Tsiouris *et al.* 2018 [237]	CHB-MIT	23 with DRE	18	sEEG

The asterisk indicates a statistical rather than an algorithm approach. DRE: drug-resistant epilepsy. iEEG: intracranial EEG. sEEG: scalp EEG.

Table B.4: Preprocessing information on studies inspecting different preictal durations.

Study	Sliding window (seconds)	Overlap (%)	Filtering	SPH (minutes)
Mormann *et al.* 2005 [14]*	17 - 20.5	0	0.5 - 85 Hz band-pass	n.s.
Valderrama *et al.* 2012 [233]	5	0	n.s.	n.s.
Rasekhi *et al.* 2013 [234]	5	0	50 Hz notch	n.s.
Teixeira *et al.* 2014 [175]	5	0	50 Hz notch	10
Alvarado-Rojas *et al.* 2014 [149]	60	0	Filtered in the bands of interest: 0.5 Hz to 140 Hz	n.s.
Rasekhi *et al.* 2015 [144]	5	0	50 Hz notch	n.s.
Bandarabadi *et al.* 2015 [251]*	8	50	50 Hz notch	n.s.
Bandarabadi *et al.* 2015 [235]	5	0	50 Hz notch	n.s.
Direito *et al.* 2017 [236]	5	0	50 Hz notch	10
Tsiouris *et al.* 2018 [237]	5	0	None	n.s.

The asterisk indicates a statistical rather than an algorithm approach. n.s.: not specified.

Table B.5: Feature information on studies inspecting different preictal durations.

Study	Univariate		Bivariate	
	Linear	Nonlinear	Linear	Nonlinear
Mormann *et al.* 2005 [14]*	×	×	×	×
Valderrama *et al.* 2012 [233]	×			
Rasekhi *et al.* 2013 [234]	×			
Teixeira *et al.* 2014 [175]	×			
Alvarado-Rojas *et al.* 2014 [149]		×		
Rasekhi *et al.* 2015 [144]	×		×	
Bandarabadi *et al.* 2015 [251]*	×			
Bandarabadi *et al.* 2015 [235]	×			
Direito *et al.* 2017 [236]	×			
Tsiouris *et al.* 2018 [237]	×		×	

The asterisk indicates a statistical rather than an algorithm approach.

Table B.6: Classification information on studies with preictal interval grid-search.

Study	Partitioning	Classifier	Regularisation	Statistical validation
Valderrama *et al.* 2012 [233]	Training: first half. Testing: second half.	Patient-specific SVM	Computing the mode in a sliding window	Seizure time surrogates
Rasekhi *et al.* 2013 [234]	Training: first 3 seizures. Testing: the remaining.	Patient-specific SVM	Firing power	n.s.
Teixeira *et al.* 2014 [175]	Training: first 2-3 seizures. Testing: the remaining.	Patient-specific, ANN, SVM	Firing power	n.s.
Alvarado-Rojas *et al.* 2014 [149]	Training: first 2-4 seizures. Testing: the remaining.	Patient-specific thresholding	Kalman filter	Analytic random predictor
Rasekhi *et al.* 2015 [144]	Training: first 3 seizures. Testing: the remaining.	Patient-specific SVM	Firing power	Analytic random predictor
Bandarabadi *et al.* 2015 [235]	Training: first 3 seizures. Testing: the remaining.	Patient-specific SVM	Firing power	Analytic random predictor
Direito *et al.* 2017 [236]	Training: 2-3 seizures. Testing: the remaining.	Patient-specific SVM	Firing power	Analytic random predictor
Tsiouris *et al.* 2018 [237]	n.s.	Patient-specific LSTM	n.s.	n.s.

n.s.: not specified.

Appendix C

Database seizure metadata

The metadata information concerning each seizure contained in the group of patients from the EPILEPSIAE database analysed in this thesis is presented here.

Accordingly, Table C.1 contains information regarding each seizure's metadata. Namely, each seizure is characterised in terms of electroencephalography (EEG) seizure onset hour, vigilance state at the onset and ILAE classification.

Given the extension of this table, the information regarding the final preictal intervals identified for each seizure in Chapters 5 and 6 was also provided.

The preictal intervals identified in the electrocardiography (ECG) data were selected according to the time continuity and duration (see Section 5.2.5). Information regarding the starting time before seizure onset, duration and time continuity are presented in *brown* colour in Table C.1.

In the case of EEG, the table presents the preictal intervals, in *teal* colour, found for either category 3 or 6, that were later used to perform preictal interval comparison among modalities and studies (refer to Sections E.4.5 and E.4.6, respectively). The preictal intervals identified in the EEG data were selected according the preictal cluster density and duration (as described in Section E.4.5).

Additionally, Table C.1 also comprises information regarding the percentage of time during which noisy segments have been identified in each seizure's 4.5 hours of EEG data. These noisy segments do not contain neurological information, but rather flat lines or saturated signal for instance caused by electrode detachment.

Table C.1: Dataset description regarding data preceding each seizure.

S	ID	EEG onset	VS	ILAE Class	Noise (%)	Starting time* (min)	Duration* (min)	Density* (%)	Starting time* (min)	Duration* (min)	Time* continuity
1	402	22:45:26	W	FOIA	3.1	111.5	17.9	94.91			
2	402	21:27:34	W	FBTC	4.0	26.2	8.2	88.00			
3	402	02:13:30	W	FOIA	9.3						
4	402	08:53:21	W	FBTC	10.8	73.3	56.5	98.37	107.3	78.2	Discontinuous
5	402	08:57:27	W	FOIA	3.3	56.9	46.9	100.00			
6	8902	23:51:14	W	UC	10.7				126.5	6.9	Discontinuous
7	8902	23:03:23	W	FOIA	5.4	65.1	55.1	98.49			
8	8902	05:37:05	W	FOIA	2.1						
9	8902	00:35:56	W	FOIA	7.5						
10	8902	05:10:26	W	FOIA	0.0				127.7	4.8	Continuous
11	11 002	00:00:10	W	UC	7.1				11.7	1.9	Discontinuous
12	11 002	06:38:01	R	FOIA	0.1						
13	11 002	15:16:42	W	FOIA	19.3						
14	11 002	08:18:49	W	FOIA	9.3						
15	11 002	15:40:32	W	FOA	–	–	–	–			

S: seizure index. ID: patient identifier. VS: Seizure vigilance state: wakefulness (W), NREM sleep stage I (N1), NREM sleep stage II (N2), REM sleep stage (R). Seizure ILAE classification: focal onset aware (FOA), focal onset impaired awareness (FOIA), focal to bilateral tonic-clonic (FBTC), unclassified (UC). Noise: percentage of time gap between the 10-minute preprocessed segments. *Values for the putative preictal intervals identified with unsupervised learning. EEG study preictal information. ECG study preictal information. '-': lead seizure only in ECG study.

Continued on next page

S	ID	EEG onset	VS	ILAE Class	Noise (%)	Starting time* (min)	Duration* (min)	Density* (%)	Starting time* (min)	Duration* (min)	Time* continuity
16	16 202	04:34:07	W	UC	0.0	35.8	25.8	100.00	37.8	3.2	Continuous
17	16 202	06:05:10	W	FBTC	0.4				86.9	4.8	Continuous
18	16 202	05:07:14	W	UC	0.3	111.7	35.0	95.24	15.2	2.3	Continuous
19	16 202	18:48:33	W	FOIA	11.2	21.4	4.4	100.00	36.5	4.8	Continuous
20	16 202	03:34:35	W	FOIA	0.3						
21	16 202	13:50:31	W	FOIA	2.1	94.4	9.9	100.00			
22	16 202	19:27:39	W	FOIA	5.9	22.8	9.9	82.50	96.1	9.1	Continuous
23	21 902	16:16:43	W	UC	6.1						
24	21 902	08:40:51	W	FOIA	7.2	58.6	34.7	90.16	37.7	3.5	Continuous
25	21 902	20:32:56	W	FOIA	9.2	45.4	34.5	84.53	111.5	2.2	Discontinuous
26	21 902	06:50:12	R	FOIA	0.2				42.6	5.4	Continuous
27	23 902	10:18:13	W	FOA	10.9						
28	23 902	20:50:38	W	FOA	12.6	14.2	4.2	96.08			
29	23 902	11:18:12	W	FOA	27.9						
30	23 902	16:48:02	W	FOA	6.8	20.1	4.3	94.23			
31	23 902	22:17:22	W	FOA	11.0	25.6	7.1	94.25			
32	26 102	15:31:37	W	FOIA	2.5						

S: seizure index. ID: patient identifier. VS: Seizure vigilance state: wakefulness (W), NREM sleep stage I (N1), NREM sleep stage II (N2), REM sleep stage (R). Seizure ILAE classification: focal onset aware (FOA), focal onset impaired awareness (FOIA), focal to bilateral tonic-clonic (FBTC), unclassified (UC). Noise: percentage of time gap between the 10-minute preprocessed segments. *Values for the putative preictal intervals identified with unsupervised learning. EEG study preictal information. ECG study preictal information. '-': lead seizure only in ECG study.

Continued on next page

S	ID	EEG onset	VS	ILAE Class	Noise (%)	Starting time* (min)	Duration* (min)	Density* (%)	Starting time* (min)	Duration* (min)	Time* continuity
33	26 102	08:33:50	W	FOIA	2.3						
34	26 102	07:52:54	W	FOIA	4.0				25.9	4.8	Continuous
35	26 102	11:36:45	W	FOIA	4.1	16.1	6.1	86.49	52.2	5.6	Discontinuous
36	30 802	04:33:31	R	FOA	0.0						
37	30 802	04:52:24	W	FOA	3.5						
38	30 802	10:58:12	N2	FOA	10.6	63.5	53.5	95.80			
39	30 802	22:58:11	W	FOA	2.5	89.8	9.8	84.75	20.5	12.0	Continuous
40	30 802	05:49:34	W	FOA	0.0				44.3	2.8	Continuous
41	30 802	02:48:42	R	FOA	1.4				83.5	1.6	Continuous
42	30 802	07:48:06	N2	FOA	0.1						
43	30 802	03:15:10	N2	FOA	0.3						
44	32 702	08:25:28	W	FOIA	5.2				12.5	2.8	Continuous
45	32 702	10:22:47	W	FOIA	2.6						
46	32 702	10:13:13	W	FOIA	10.8	24.2	8.2	85.86	83.3	4.9	Continuous
47	32 702	17:03:16	W	FOIA	20.0				79.6	4.3	Continuous
48	32 702	09:29:02	W	FOIA	4.2	90.5	14.7	98.83	38.6	4.8	Continuous
49	45 402	01:48:55	W	FOIA	5.9				106.1	2.6	Discontinuous

S: seizure index. ID: patient identifier. VS: Seizure vigilance state: wakefulness (W), NREM sleep stage I (N1), NREM sleep stage II (N2), REM sleep stage (R). Seizure ILAE classification: focal onset aware (FOA), focal onset impaired awareness (FOIA), focal to bilateral tonic-clonic (FBTC), unclassified (UC). Noise: percentage of time gap between the 10-minute preprocessed segments. *Values for the putative preictal intervals identified with unsupervised learning. EEG study preictal information. ECG study preictal information. '-': lead seizure only in ECG study.

Continued on next page

S	ID	EEG onset	VS	ILAE Class	Noise (%)	Starting time* (min)	Duration* (min)	Density* (%)	Starting time* (min)	Duration* (min)	Time* continuity
50	45 402	08:11:29	W	FOIA	3.8	54.9	44.9	95.00	37.9	32.3	Discontinuous
51	45 402	14:56:37	W	FOA	7.3						
52	45 402	15:13:34	W	FOIA	4.8	67.8	10.0	95.00			
53	46 702	15:56:40	W	FOA	2.7				18.5	3.7	Discontinuous
54	46 702	06:16:40	N2	FOIA	0.9				68.7	1.7	Continuous
55	46 702	17:06:57	W	FOIA	4.0						
56	46 702	02:02:23	N2	FBTC	4.1				36.1	2.1	Continuous
57	46 702	06:45:59	W	FOIA	3.6				78.1	63.9	Discontinuous
58	50 802	02:44:39	W	FOIA	0.3				78.8	17.8	Discontinuous
59	50 802	06:37:35	N2	UC	0.2				103.7	4.6	Discontinuous
60	50 802	12:39:04	N2	UC	3.5				90.1	2.6	Discontinuous
61	50 802	22:50:41	N2	FOIA	7.5	30.7	20.4	97.93			
62	50 802	01:18:38	W	FBTC	0.5						
63	52 302	06:29:39	W	UC	1.7						
64	52 302	11:31:13	W	FOA	10.2						
65	52 302	16:27:47	W	UC	–	–	–	–			
66	52 302	02:31:34	N1	UC	8.9						

S: seizure index. ID: patient identifier. VS: Seizure vigilance state: wakefulness (W), NREM sleep stage I (N1), NREM sleep stage II (N2), REM sleep stage (R). Seizure ILAE classification: focal onset aware (FOA), focal onset impaired awareness (FOIA), focal to bilateral tonic-clonic (FBTC), unclassified (UC). Noise: percentage of time gap between the 10-minute preprocessed segments. *Values for the putative preictal intervals identified with unsupervised learning. EEG study preictal information. ECG study preictal information. '-': lead seizure only in ECG study.

Continued on next page

S	ID	EEG onset	VS	ILAE Class	Noise (%)	Starting time* (min)	Duration* (min)	Density* (%)	Starting time* (min)	Duration* (min)	Time* continuity
67	52 302	09:53:02	W	UC	15.0						
68	53 402	19:09:46	W	FOA	–	–	–	–			
69	53 402	08:16:32	W	FOA	2.8	23.8	8.8	100.00			
70	53 402	05:46:33	N2	FOA	2.9	18.0	4.7	81.03			
71	53 402	19:02:38	W	FOA	15.8	48.6	9.7	99.15			
72	53 402	09:17:43	W	FOIA	8.8						
73	55 202	07:02:49	W	FOIA	0.2				13.1	7.7	Discontinuous
74	55 202	09:55:11	W	FOIA	9.1						
75	55 202	18:15:11	W	FOA	5.4	52.4	9.9	100.00			
76	55 202	08:09:27	W	UC	1.8	60.4	47.4	95.71	19.0	2.8	Continuous
77	55 202	17:47:47	W	UC	1.4						
78	55 202	09:57:39	W	FOA	17.3	75.6	9.9	91.67			
79	55 202	15:34:54	W	UC	7.6				103.4	1.9	Discontinuous
80	55 202	14:11:59	W	FOIA	7.8	18.2	8.2	92.93			
81	56 402	08:17:30	W	UC	3.8	23.1	9.2	100.00	27.6	13.8	Continuous
82	56 402	21:11:53	W	UC	4.5						
83	56 402	01:30:23	W	UC	–	–	–	–			

S: seizure index. ID: patient identifier. VS: Seizure vigilance state: wakefulness (W), NREM sleep stage I (N1), NREM sleep stage II (N2), REM sleep stage (R). Seizure ILAE classification: focal onset aware (FOA), focal onset impaired awareness (FOIA), focal to bilateral tonic-clonic (FBTC), unclassified (UC). Noise: percentage of time gap between the 10-minute preprocessed segments. *Values for the putative preictal intervals identified with unsupervised learning. EEG study preictal information. ECG study preictal information. '-': lead seizure only in ECG study.

Continued on next page

S	ID	EEG onset	VS	ILAE Class	Noise (%)	Starting time* (min)	Duration* (min)	Density* (%)	Starting time* (min)	Duration* (min)	Time* continuity
84	56 402	09:13:46	W	UC	4.9	64.6	9.9	96.67			
85	56 402	06:29:39	W	FBTC	0.4				22.5	15.0	Discontinuous
86	56 402	10:47:36	W	FBTC	–	–	–	–			
87	58 602	09:11:25	W	FOIA	4.8	28.9	18.9	100.00	46.9	39.3	Discontinuous
88	58 602	03:29:21	R	FOIA	3.5	79.5	69.5	96.53	72.0	1.7	Continuous
89	58 602	19:52:52	W	FOIA	4.3	58.9	9.9	98.33			
90	58 602	09:01:07	W	FOIA	0.6	29.8	19.8	99.16			
91	58 602	15:41:02	W	FOIA	7.8	17.5	7.5	63.33			
92	58 602	20:06:30	W	FOIA	–	–	–	–			
93	58 602	02:31:58	N2	FOIA	4.4	74.4	64.4	48.00	36.2	26.5	Discontinuous
94	59 102	08:54:51	W	FOA	10.5	110.7	100.7	99.10	128.9	15.9	Discontinuous
95	59 102	15:41:55	W	FOIA	27.2	40.6	24.0	80.97			
96	59 102	09:56:35	W	FOIA	13.6						
97	59 102	19:51:41	W	FOIA	4.9				124.9	30.0	Discontinuous
98	59 102	21:12:26	W	FOA	4.7	22.4	11.7	78.01			
99	60 002	02:45:01	N1	FOIA	0.0	46.6	36.6	92.97	50.7	1.7	Continuous
100	60 002	02:22:55	W	FOIA	2.7	29.7	19.7	86.50			

S: seizure index. ID: patient identifier. VS: Seizure vigilance state: wakefulness (W), NREM sleep stage I (N1), NREM sleep stage II (N2), REM sleep stage (R). Seizure ILAE classification: focal onset aware (FOA), focal onset impaired awareness (FOIA), focal to bilateral tonic-clonic (FBTC), unclassified (UC). Noise: percentage of time gap between the 10-minute preprocessed segments. *Values for the putative preictal intervals identified with unsupervised learning. EEG study preictal information. ECG study preictal information. '-': lead seizure only in ECG study.

Continued on next page

S	ID	EEG onset	VS	ILAE Class	Noise (%)	Starting time* (min)	Duration* (min)	Density* (%)	Starting time* (min)	Duration* (min)	Time* continuity
101	60 002	12:21:36	W	FOIA	5.4	43.4	13.5	66.87			
102	60 002	05:40:53	R	UC	0.4						
103	60 002	00:17:54	R	FOIA	3.8						
104	60 002	22:18:46	N1	FOIA	1.5	28.1	11.7	74.65			
105	64 702	13:53:39	W	FOA	7.4	41.3	9.9	98.33			
106	64 702	04:23:21	W	FBTC	4.5	47.0	9.4	89.47	49.6	1.9	Discontinuous
107	64 702	18:59:43	W	FBTC	6.8	32.3	9.9	90.00			
108	64 702	19:50:01	W	FBTC	9.9	18.6	8.6	96.15	112.9	2.2	Continuous
109	64 702	03:41:27	N2	FBTC	1.4						
110	75 202	23:37:38	N2	FOA	4.7	28.8	12.1	63.01			
111	75 202	01:10:45	N2	FOA	6.9	92.8	5.3	87.69			
112	75 202	21:33:44	W	UC	9.6	40.9	14.5	58.00			
113	75 202	19:27:00	W	FOA	4.4						
114	75 202	09:46:19	W	FOA	13.3	18.3	7.7	80.65			
115	75 202	17:43:46	W	FOA	15.5						
116	75 202	06:25:19	W	FOA	3.2	16.0	6.0	94.44			
117	80 702	05:03:56	W	FOIA	0.0						

S: seizure index. ID: patient identifier. VS: Seizure vigilance state: wakefulness (W), NREM sleep stage I (N1), NREM sleep stage II (N2), REM sleep stage (R). Seizure ILAE classification: focal onset aware (FOA), focal onset impaired awareness (FOIA), focal to bilateral tonic-clonic (FBTC), unclassified (UC). Noise: percentage of time gap between the 10-minute preprocessed segments. *Values for the putative preictal intervals identified with unsupervised learning. EEG study preictal information. ECG study preictal information. '-': lead seizure only in ECG study.

Continued on next page

S	ID	EEG onset	VS	ILAE Class	Noise (%)	Starting time* (min)	Duration* (min)	Density* (%)	Starting time* (min)	Duration* (min)	Time* continuity
118	80 702	08:43:22	W	FOIA	0.3	35.9	9.9	98.33	31.9	26.0	Discontinuous
119	80 702	20:43:38	W	UC	4.6	29.3	9.6	89.66	73.8	17.5	Discontinuous
120	80 702	07:46:14	W	FOIA	2.1				16.1	7.4	Discontinuous
121	80 702	12:27:44	W	UC	–	–	–	–			
122	80 702	17:54:17	W	FBTC	3.9	97.3	11.1	100.00	43.8	24.6	Discontinuous
123	80 702	08:53:56	W	FOIA	3.7	37.6	27.6	97.28	37.2	29.5	Continuous
124	81 102	20:48:50	W	FOIA	3.6	61.3	51.3	98.35			
125	81 102	01:05:05	W	FOA	–	–	–	–	54.3	2.2	Continuous
126	81 102	10:30:03	W	FOA	–	–	–	–			
127	81 102	10:44:57	W	FOA	8.3	24.3	11.7	87.14			
128	81 102	10:42:15	W	FOIA	8.4	38.8	26.6	93.44			
129	85 202	23:37:05	N2	FOIA	3.1				92.2	5.7	Continuous
130	85 202	16:51:04	W	FOIA	6.7	69.3	9.9	95.83			
131	85 202	04:24:27	W	UC	0.0	50.3	40.3	96.69	50.0	8.7	Continuous
132	85 202	16:08:00	W	UC	2.6	58.8	48.8	91.81			
133	85 202	01:51:40	W	UC	1.3	34.8	24.8	98.66	29.9	22.3	Continuous
134	93 402	22:17:50	N2	FBTC	4.3						

S: seizure index. ID: patient identifier. VS: Seizure vigilance state: wakefulness (W), NREM sleep stage I (N1), NREM sleep stage II (N2), REM sleep stage (R). Seizure ILAE classification: focal onset aware (FOA), focal onset impaired awareness (FOIA), focal to bilateral tonic-clonic (FBTC), unclassified (UC). Noise: percentage of time gap between the 10-minute preprocessed segments. *Values for the putative preictal intervals identified with unsupervised learning. EEG study preictal information. ECG study preictal information. '-': lead seizure only in ECG study.

Continued on next page

S	ID	EEG onset	VS	ILAE Class	Noise (%)	Starting time* (min)	Duration* (min)	Density* (%)	Starting time* (min)	Duration* (min)	Time* continuity
135	93 402	10:21:34	N2	FOIA	2.3						
136	93 402	23:20:24	N2	FOIA	6.4						
137	93 402	00:59:09	N2	UC	4.2	88.3	78.3	96.38			
138	93 402	06:26:26	N2	UC	3.6				118.9	41.0	Discontinuous
139	93 902	08:39:52	W	FOA	1.4	36.8	26.8	99.03	37.6	29.9	Discontinuous
140	93 902	16:02:21	W	FOIA	4.8	106.5	6.0	97.26			
141	93 902	02:31:07	N2	FBTC	3.2	32.5	22.5	91.83	69.1	5.3	Continuous
142	93 902	18:48:40	W	FOIA	21.8	25.1	11.9	87.41	52.9	28.0	Discontinuous
143	93 902	04:02:38	N2	FOIA	0.2				38.4	2.0	Continuous
144	93 902	09:21:33	W	UC	10.8	64.7	10.1	98.36	112.5	94.8	Discontinuous
145	94 402	15:29:22	W	FOA	3.9	29.2	6.4	66.67			
146	94 402	11:02:56	W	UC	11.5	83.0	20.7	100.00	44.3	35.9	Continuous
147	94 402	18:05:40	W	FOIA	5.7	29.7	9.9	100.00			
148	94 402	01:36:02	N2	UC	1.8	119.9	109.9	98.63			
149	94 402	16:10:53	W	FOA	8.5	18.7	8.7	96.19			
150	94 402	02:48:18	N2	UC	4.2	32.8	22.7	98.90	48.8	1.6	Continuous
151	94 402	08:16:30	W	FOA	2.9	94.8	76.3	99.89			

S: seizure index. ID: patient identifier. VS: Seizure vigilance state: wakefulness (W), NREM sleep stage I (N1), NREM sleep stage II (N2), REM sleep stage (R). Seizure ILAE classification: focal onset aware (FOA), focal onset impaired awareness (FOIA), focal to bilateral tonic-clonic (FBTC), unclassified (UC). Noise: percentage of time gap between the 10-minute preprocessed segments. *Values for the putative preictal intervals identified with unsupervised learning. EEG study preictal information. ECG study preictal information. '-': lead seizure only in ECG study.

Continued on next page

S	ID	EEG onset	VS	ILAE Class	Noise (%)	Starting time* (min)	Duration* (min)	Density* (%)	Starting time* (min)	Duration* (min)	Time* continuity
152	95 202	01:28:09	N2	FBTC	11.0	29.6	19.6	99.15	32.5	27.2	Continuous
153	95 202	15:00:18	N2	FOIA	8.7				110.1	84.7	Discontinuous
154	95 202	01:35:24	N2	FOIA	3.2						
155	95 202	14:13:22	N2	FOIA	3.3	24.5	9.8	88.24	80.9	2.5	Continuous
156	95 202	23:30:29	N2	UC	9.1	21.8	11.8	86.62			
157	95 202	23:55:21	N2	FOIA	5.9	38.8	28.8	89.88			
158	95 202	00:04:20	N2	UC	11.2	52.2	42.2	97.83	121.0	2.8	Discontinuous
159	96 002	17:10:35	W	FOIA	3.9	79.2	30.0	66.67	85.1	41.0	Discontinuous
160	96 002	10:26:53	W	FOIA	11.7	18.5	8.5	98.06			
161	96 002	17:46:44	W	FOIA	1.8	30.4	9.9	100.00			
162	96 002	00:05:44	W	FOIA	5.7	79.8	69.8	96.06			
163	96 002	00:44:10	W	UC	4.3	84.3	74.3	93.62	12.7	3.4	Continuous
164	96 002	18:57:18	W	FOIA	1.3	49.6	9.9	100.00			
165	96 002	06:20:01	W	FOIA	0.2	25.2	15.2	99.45	27.7	18.2	Continuous
166	98 102	07:17:49	W	FOA	3.2				49.0	2.6	Discontinuous
167	98 102	18:49:53	W	UC	0.4	92.8	9.9	100.00			
168	98 102	05:18:58	W	UC	1.3						

S: seizure index. ID: patient identifier. VS: Seizure vigilance state: wakefulness (W), NREM sleep stage I (N1), NREM sleep stage II (N2), REM sleep stage (R). Seizure ILAE classification: focal onset aware (FOA), focal onset impaired awareness (FOIA), focal to bilateral tonic-clonic (FBTC), unclassified (UC). Noise: percentage of time gap between the 10-minute preprocessed segments. *Values for the putative preictal intervals identified with unsupervised learning. EEG study preictal information. ECG study preictal information. '-': lead seizure only in ECG study.

Continued on next page

S	ID	EEG onset	VS	ILAE Class	Noise (%)	Starting time* (min)	Duration* (min)	Density* (%)	Starting time* (min)	Duration* (min)	Time* continuity
169	98 102	06:11:33	W	UC	2.1				8.9	2.7	Continuous
170	98 102	04:07:04	W	FBTC	2.7						
171	98 202	04:50:27	W	FOIA	4.5						
172	98 202	20:38:46	W	FOIA	6.0	45.4	7.6	94.62			
173	98 202	07:16:40	W	FOIA	2.2						
174	98 202	12:16:11	W	FBTC	8.7	83.8	9.9	93.28	25.0	15.4	Continuous
175	98 202	01:22:11	W	FOIA	3.9						
176	98 202	07:55:06	W	FOIA	6.4	24.9	9.9	99.17			
177	98 202	16:57:19	W	UC	5.6				119.0	2.0	Continuous
178	101 702	07:35:40	W	FOIA	2.8						
179	101 702	12:29:53	W	FOIA	5.8	28.9	9.9	100.00	121.0	3.3	Continuous
180	101 702	19:33:06	W	FOIA	3.6	120.0	87.9	66.53			
181	101 702	07:35:22	N2	FOIA	4.4				122.9	2.4	Continuous
182	101 702	20:26:01	W	FOIA	3.5	115.9	47.1	44.52	108.6	1.8	Discontinuous
183	102 202	22:50:21	N2	FOA	5.9	97.7	87.7	72.61	8.2	3.1	Continuous
184	102 202	15:36:30	W	UC	10.5						
185	102 202	05:47:03	N2	FOIA	3.3						

S: seizure index. ID: patient identifier. VS: Seizure vigilance state: wakefulness (W), NREM sleep stage I (N1), NREM sleep stage II (N2), REM sleep stage (R). Seizure ILAE classification: focal onset aware (FOA), focal onset impaired awareness (FOIA), focal to bilateral tonic-clonic (FBTC), unclassified (UC). Noise: percentage of time gap between the 10-minute preprocessed segments. *Values for the putative preictal intervals identified with unsupervised learning. EEG study preictal information. ECG study preictal information. '-': lead seizure only in ECG study.

Continued on next page

S	ID	EEG onset	VS	ILAE Class	Noise (%)	Starting time* (min)	Duration* (min)	Density* (%)	Starting time* (min)	Duration* (min)	Time* continuity
186	102 202	22:14:59	W	UC	10.9	35.6	25.6	77.27	36.6	11.5	Discontinuous
187	102 202	14:07:10	W	FOA	4.5				18.0	1.8	Continuous
188	102 202	06:16:20	N2	FOIA	0.9						
189	102 202	15:54:20	W	UC	7.5						
190	104 602	15:35:45	W	FOIA	18.8						
191	104 602	23:46:07	N2	FBTC	5.5				53.7	46.7	Discontinuous
192	104 602	06:24:56	N2	FBTC	0.3						
193	104 602	12:30:01	N2	FBTC	6.4						
194	104 602	22:44:07	N2	UC	8.6						
195	109 502	10:00:00	W	FOIA	14.5	23.2	9.0	52.29			
196	109 502	19:42:33	W	FOIA	8.4	31.4	17.3	93.78			
197	109 502	02:17:20	N1	FOIA	–	–	–	–	56.5	1.6	Continuous
198	109 502	07:56:09	W	UC	1.6				12.3	2.4	Continuous
199	109 502	10:17:37	W	UC	16.2				54.6	2.7	Discontinuous
200	110 602	10:20:41	W	FOIA	6.3						
201	110 602	17:39:56	W	FOIA	3.7				105.3	2.4	Discontinuous
202	110 602	08:30:09	W	FOIA	8.5				14.7	5.4	Continuous

S: seizure index. ID: patient identifier. VS: Seizure vigilance state: wakefulness (W), NREM sleep stage I (N1), NREM sleep stage II (N2), REM sleep stage (R). Seizure ILAE classification: focal onset aware (FOA), focal onset impaired awareness (FOIA), focal to bilateral tonic-clonic (FBTC), unclassified (UC). Noise: percentage of time gap between the 10-minute preprocessed segments. *Values for the putative preictal intervals identified with unsupervised learning. EEG study preictal information. ECG study preictal information. '-': lead seizure only in ECG study.

Continued on next page

S	ID	EEG onset	VS	ILAE Class	Noise (%)	Starting time* (min)	Duration* (min)	Density* (%)	Starting time* (min)	Duration* (min)	Time* continuity
203	110 602	21:34:00	W	FOIA	3.1	29.6	16.3	89.29	106.1	28.6	Discontinuous
204	110 602	11:28:35	W	FOA	15.4				33.3	23.0	Discontinuous
205	112 802	17:05:49	W	UC	1.6	36.1	9.8	54.62	74.8	25.6	Discontinuous
206	112 802	07:49:43	W	FOIA	6.5						
207	112 802	15:36:04	W	UC	4.7						
208	112 802	06:52:41	W	FOIA	0.0				23.2	14.5	Discontinuous
209	112 802	11:54:45	W	FOIA	13.5				25.8	7.5	Continuous
210	112 802	08:39:39	W	UC	6.5	38.6	19.9	98.75	125.6	1.8	Continuous
211	113 902	23:32:27	W	UC	6.4	37.1	25.2	89.97			
212	113 902	16:55:50	W	FOIA	6.6	23.4	9.9	98.33			
213	113 902	05:17:05	N2	FOIA	1.4						
214	113 902	13:46:12	W	FOIA	9.2	27.1	17.1	66.99	93.5	1.7	Discontinuous
215	113 902	22:40:46	N2	UC	5.0	14.8	4.8	98.31			
216	113 902	10:00:18	W	UC	–	–	–	–	55.2	3.8	Continuous
217	113 902	16:53:42	W	FOIA	7.6	76.0	66.0	99.09	86.6	50.0	Discontinuous
218	114 702	20:52:30	W	FOIA	6.9				53.1	43.8	Discontinuous
219	114 702	14:45:03	W	FOIA	14.6	29.9	10.4	93.60	32.7	9.3	Continuous

S: seizure index. ID: patient identifier. VS: Seizure vigilance state: wakefulness (W), NREM sleep stage I (N1), NREM sleep stage II (N2), REM sleep stage (R). Seizure ILAE classification: focal onset aware (FOA), focal onset impaired awareness (FOIA), focal to bilateral tonic-clonic (FBTC), unclassified (UC). Noise: percentage of time gap between the 10-minute preprocessed segments. *Values for the putative preictal intervals identified with unsupervised learning. EEG study preictal information. ECG study preictal information. '-': lead seizure only in ECG study.

Continued on next page

S	ID	EEG onset	VS	ILAE Class	Noise (%)	Starting time* (min)	Duration* (min)	Density* (%)	Starting time* (min)	Duration* (min)	Time* continuity
220	114 702	04:09:15	W	UC	0.0						
221	114 702	09:50:10	W	FOIA	14.2	41.4	20.0	100.00			
222	114 702	14:27:45	W	FOIA	7.6						
223	114 702	11:03:08	W	FOIA	4.8	116.0	9.9	96.67			
224	114 702	02:21:45	N2	FOIA	–	–	–	–			
225	114 702	13:27:36	W	FOIA	3.5	77.6	11.6	91.43			
226	114 702	21:04:57	W	FOIA	2.3						
227	114 902	08:30:29	W	FOA	9.0	43.8	33.8	75.48			
228	114 902	14:42:32	W	FOIA	2.1						
229	114 902	19:42:40	W	FOIA	1.8						
230	114 902	05:59:33	N2	FBTC	1.5						
231	114 902	17:18:54	W	UC	6.8						
232	114 902	11:52:26	W	FOIA	6.5				129.2	2.2	Continuous
233	114 902	09:27:30	W	FOIA	9.2						
234	123 902	02:52:47	N2	FBTC	0.0						
235	123 902	01:38:19	N2	FBTC	1.3	45.3	35.3	94.58			
236	123 902	02:11:22	R	FOIA	3.0				12.9	2.9	Discontinuous

S: seizure index. ID: patient identifier. VS: Seizure vigilance state: wakefulness (W), NREM sleep stage I (N1), NREM sleep stage II (N2), REM sleep stage (R). Seizure ILAE classification: focal onset aware (FOA), focal onset impaired awareness (FOIA), focal to bilateral tonic-clonic (FBTC), unclassified (UC). Noise: percentage of time gap between the 10-minute preprocessed segments. *Values for the putative preictal intervals identified with unsupervised learning. EEG study preictal information. ECG study preictal information. '-': lead seizure only in ECG study.

Continued on next page

S	ID	EEG onset	VS	ILAE Class	Noise (%)	Starting time* (min)	Duration* (min)	Density* (%)	Starting time* (min)	Duration* (min)	Time* continuity
237	123 902	18:57:10	W	FOIA	1.0	85.0	9.9	86.67			
238	123 902	15:22:45	W	FOIA	3.2				84.3	3.2	Continuous

S: seizure index. ID: patient identifier. VS: Seizure vigilance state: wakefulness (W), NREM sleep stage I (N1), NREM sleep stage II (N2), REM sleep stage (R). Seizure ILAE classification: focal onset aware (FOA), focal onset impaired awareness (FOIA), focal to bilateral tonic-clonic (FBTC), unclassified (UC). Noise: percentage of time gap between the 10-minute preprocessed segments. *Values for the putative preictal intervals identified with unsupervised learning. EEG study preictal information. ECG study preictal information. '-': lead seizure only in ECG study.

Appendix D

ECG unsupervised learning study

This chapter presents extended details on the electrocardiography (ECG) preprocessing and heart rate variability (HRV) computation (Section D.1), the HRV feature extraction (Section D.2), the feature redundancy study (Section D.3) and the pseudocode to select meaningful clustering solutions (Section D.4).

D.1 Extracting HRV from ECG

D.1.1 ECG signals preprocessing

The ECG preprocessing step (represented in Figure D.1) started by inspecting 5-minute non-overlapping windows of the ECG raw data. According to the Task Force of the European Society of Cardiology and the North American Society of Pacing and Electrophysiology, five minutes is considered to be the minimum time interval required to compute HRV metrics [92]. In each 5-minute window, a notch filter (IIR filter design and zero-phase distortion by forward and backward filtering) was applied at 50 Hz frequency to remove the powerline interference [299].

The next step consisted of applying the Discrete Wavelet Transform (DWT) to the 5-minute non-overlapping windows, to obtain the frequencies of interest in ECG as well as to remove its baseline wander. Each window underwent a multilevel one-dimensional wavelet analysis, using a mother wavelet belonging to the biorthogonal family (*bior3.3*). This mother wavelet very closely resembles the morphology of the QRS complex [300]. As a result, 10 frequency bands were obtained (10 decomposition levels and 10 approximation levels). From the wavelet analysis, two frequency bands were further inspected: the approximation coefficient containing frequency content up to 45 Hz, and the approximation coefficient containing frequency components up to 0.8 Hz. The latter, comprising the baseline wander frequency components, was then subtracted from the former [299, 301, 302].

Subsequently, a R-peak detection algorithm, based on the Pan & Tompkins algorithm [270] was used to identify the R-peaks in each 5-minute non-overlapping window. Similarly to Pan & Tompkins, two thresholds were computed. The first one corresponds to the application of a two-second moving average filter to the moving-window integration (using a 0.2 second window). The second one consists of a baseline threshold intended to prevent the analysis of lead-off periods. In other words, to prevent the moving average threshold from reaching zero, a baseline threshold was defined, corresponding to the minimum of the moving average threshold plus 10% of the difference between the median and the minimum of that threshold (defined experimentally). In this way, it was possible to improve the algorithm's robustness regarding the specific characteristics of the ECG of each lead and each patient.

The ECG signals were then inspected regarding the identification of noisy segments. Towards that end, a simple thresholding approach was developed, based on the computation of two measures in each 5-minute window: the first detail coefficient, returned by the DWT and the zero-crossing rate. The latter was particularly useful in identifying for instance periods of lead-off signal.

D.1.2 RR interval series editing

The RR interval series is obtained by computing the time intervals between adjacent QRS complexes, taking the R-peak as the reference fiducial point [303, 304]. At this point, it is important to note the distinction between normal-to-normal (NN) intervals and RR intervals. The former are observed between adjacent heartbeats resulting from sinus node depolarisations, whereas the latter comprises all interbeat intervals, including both the NN intervals and abnormal intervals [92]. Abnormal RR intervals are obtained by analysing false beats introduced by (i) physiological artefact in the form of ectopic beats, also known as premature beats, and (ii) technical artefact originated by problems in signal acquisition, e.g., subject movement or

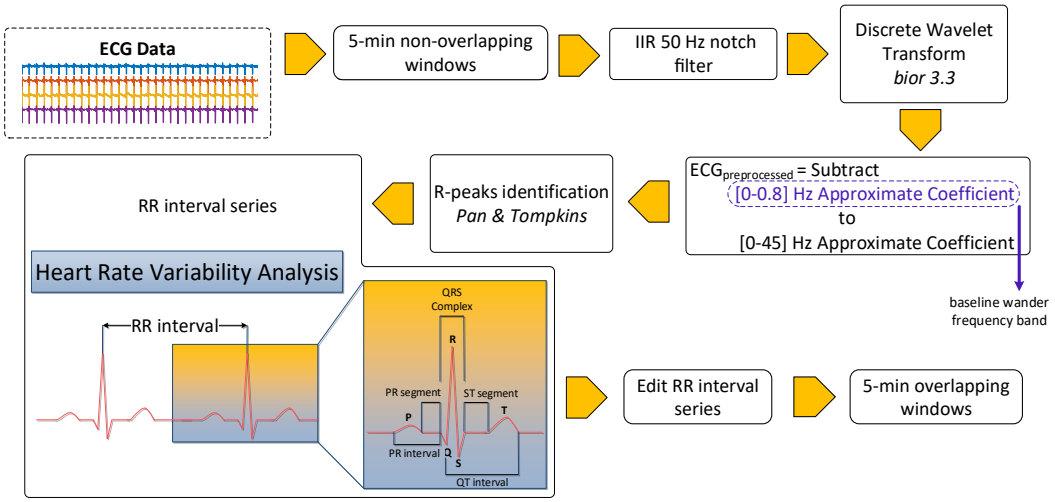

Figure D.1: ECG preprocessing and RR interval series extraction.

electrode detachment, or by the emergence of false positives or false negatives during peak detection phase [301,303,304]. The presence of ectopic beats has been reported to undermine the HRV analysis specifically by leading to an overestimation of the values of power in the low frequency (LF) and high frequency (HF) frequency bands (described in Section D.2.2), and consequently of the LF to HF ratio [303, 304].

To prevent the analysis of abnormal RR intervals, a simple criteria has been included in this HRV analysis: if a given RR interval falls outside the range of 20% around the mean of the previous 10 RR intervals, then either it is removed or it is replaced by an interpolated RR interval value. This criterion has been built on the assumption that abrupt changes in the heart rate (HR) are unlikely to occur during sinus node activity [301]. When the abnormal RR interval is higher than the range of values previously mentioned, it is replaced using linear interpolation [301, 303, 304].

From now on, the ECG signals were spanned using a 5-minute (300 seconds) window with 98.33% (295 seconds) of overlapping. The RR intervals corresponding to that 5-minute window were pulled from RR interval series, being ready for HRV-feature computation. This means that each feature sample corresponds to a time increase of five seconds. The overlap percentage was set in order to, in a future study, allow for the fusion of information from both ECG and electroencephalography (EEG) data. EEG recordings are typically analysed with a five second non-overlapping spanning window.

Furthermore, if more than 80% of the RR interval series, comprised in a 5-minute window, contains abnormal RR intervals, that window is considered as noise and no features are extracted from it [304]. RR interval and NN intervals notation will henceforth be used interchangeably to denote corrected RR intervals.

D.2 HRV feature engineering

HRV captures the variability of the intervals between consecutive R-peaks. Such short-term oscillations reflect the neurocardiac function or, in other words, the modulation of the heart-brain interactions. In fact, an HRV analysis is typically conducted to inspect the influence of the autonomous nervous system (ANS) on the sinoatrial node and, this way, to assess the relative balance between the sympathetic and parasympathetic branches of the ANS (sympatho-vagal balance) [92, 271]. The computation of the HRV features is intended to capture the influence of the two branches of the ANS, sympathetic and parasympathetic, responsible for maintaining homeostasis. Studies have demonstrated that, when the sympathetic nervous activity is triggered during seizures, it typically results in increased HR and blood pressure, and possible occurrence of tachycardia and tachypnea [19, 20]. When the parasympathetic response predominates, for a considerably low number of seizures, the normal cardiorespiratory function is altered with regard to the decreasing of heart and respiration rates and also blood pressure [19, 20].

All HRV features used in this study are presented in Table D.1, with additional details regarding (i) the units of measurement; (ii) the minimum length of clean ECG signal required to compute these HRV-derived features; (iii) the number of missing values obtained for each feature resulting from the existence of noisy 5-minute windows; (iv) which ANS response has been associated with each feature (it can be both) according to the literature and (v) the computational time required to compute each feature.

D.2.1 HRV linear time domain features

Time domain measures of HRV are the simplest to obtain, as they are basically the result of the application of descriptive statistical methods. These measures are considered robust to a previous preprocessing of the RR interval series towards artefact and/or ectopic beat removal [303]. Two types of features can be derived from the RR interval series: (i) from the series of RR intervals; and (ii) from the time series resulting from the difference between successive RR intervals [92].

The following time-domain features were computed:

- $NN50$: number of RR intervals that last more than 50 ms.
- $pNN50$: percentage of RR intervals that last more than 50 ms.
- $SDNN$: standard deviation of RR intervals.
- $RMSSD$: square root of the mean squared differences of successive RR intervals.
- $SDSD$: standard deviation of the differences between successive RR intervals.
- $RRMean$, $RRMin$, $RRMax$ and $RRVar$: respectively, mean, minimum, maximum and variance of the RR interval time series.

SDNN corresponds to the standard deviation of the RR intervals, which is equivalent to the square root of variance and, therefore, to the total power of the frequency spectrum in a given signal segment. This measure captures the cyclic components introducing variability in the ECG segment under analysis. It is important to highlight that, as the total variance of the HRV is known to increase with the length of the ECG segment, the SDNN will also be influenced by that factor. Consequently, to perform comparisons among SDNN measures, it is mandatory that the different segments analysed have the same length [92, 271].

The time domain HRV features are often used as indicators of parasympathetic activity (RMSSD, NN50, pNN50 and SDSD) and overall autonomic responses (SDNN) [30, 92, 305, 306].

D.2.2 HRV linear frequency domain features

The HRV frequency analysis was performed by computing the Lomb-Scargle periodogram [307]. This nonparametric estimation method was chosen to handle the un-

evenly sampled RR interval series, without requiring data interpolation and, hence, do not assuming any underlying model. Using this method, it is possible to avoid the shifting of the spectral peaks towards the low frequency components and, therefore, the overestimation of the total power present in LF and HF bands [301, 303].

The frequency spectrum (see Figure D.2) is inspected towards the assessment of three different spectral components: very low frequency (VLF) in the 0.0033-0.04 Hz range, LF corresponding to the 0.04-0.15 Hz band, and the HF component found in the 0.15-0.4 Hz range [92, 271, 301, 303]. The power in LF and HF frequency bands can be normalised to the $Total\,power - VLF\,power$ entity, yielding LF norm and HF norm and thus emphasising the influence each branch of the ANS has on the HRV regulation. Equivalently, by normalising the frequency bands, it is possible to decrease the impact of the changes in the Total power, particularly on the values of LF and HF powers. Furthermore, it also allows for direct comparisons of power measures between two subjects. In fact, significant differences were reported between the values of Total power and power in each frequency band, among healthy subjects [92, 308–312].

Eight features were then extracted from the frequency spectrum of each 5-minute window:

- $Total\,power$: window's total power.
- $VLF\,power$: power in the very low frequency band.
- $LF\,power$: power in the low frequency band.
- $HF\,power$: power in the high frequency band.
- $LF/HF = \dfrac{LF\,power}{HF\,power}$.

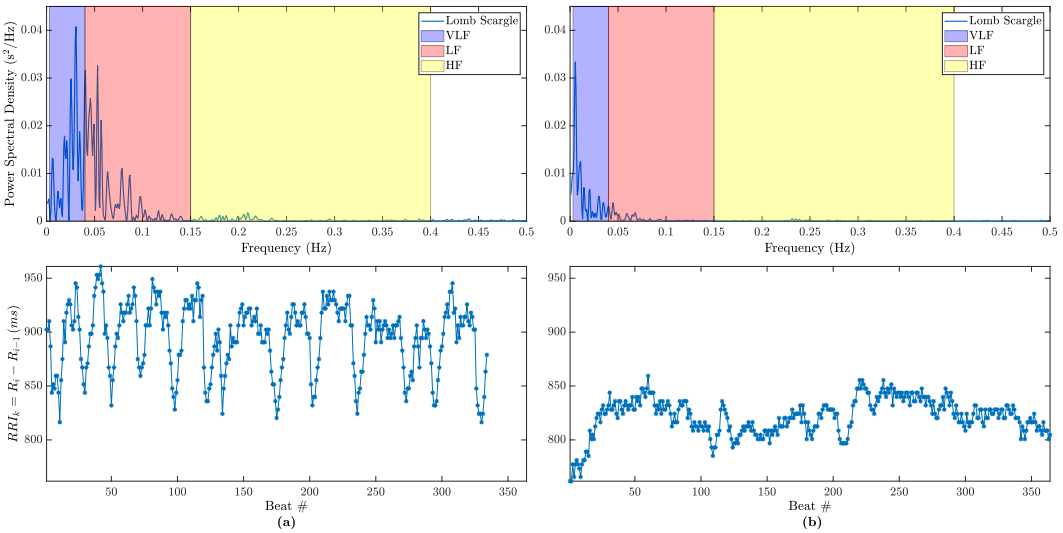

Figure D.2: Example of frequency analysis. The frequency spectrum was computed for two 5-minute windows ranging from (a) 78 to 73 minutes and (b) 26 to 21 minutes before seizure onset, respectively, for the first seizure of patient 2.

- $LF\,norm = \dfrac{LF\,power}{Total\,power - VLF\,power}$.
- $HF\,norm = \dfrac{HF\,power}{Total\,power - VLF\,power}$.

Additionally, HF spectral component (or respiratory sinus arrhythmia), as the name suggests, captures HR variations associated with the respiratory cycle, therefore, reflecting the vagal or parasympathetic activity. Conversely, LF component has not yet been associated with a clear interpretation. While it is considered by the majority of the research community as an indicator of sympathetic activation, other studies suggest that LF power may be influenced by both parasympathetic and sympathetic nervous systems. As a result, the ratio of LF to HF powers (typically assumed to characterise sympatho-vagal balance) and the VLF power remain HRV features that are not to date known to clearly manifest activity from either branch [20, 92, 215, 216, 305, 306]. Finally, Total power is useful in capturing the variance of all the RR intervals [306].

D.2.3 HRV nonlinear features

HRV is known to be the result of the complex interactions between haemodynamic, electrophysiological and humoral body functions. Additionally, the influence of the autonomic and central nervous systems' controlling actions will also be reflected in HRV metrics [92, 272]. A nonlinear analysis might provide new complimentary information regarding such complex interactions. Nonlinear indices, even though not being regarded to directly capture ANS responses and, therefore, having a less clear interpretation comparing to linear measures, are known to provide higher reliability (repeatability) across measurements, when compared to linear ones [30, 313]. A considerable set of nonlinear features was assembled and is described briefly below.

From the Poincaré plot representation (see Figure D.3), obtained by computing a scatter plot of each RR interval against the previous one [271, 314], it is possible to derive three features:

- SD_1: standard deviation of the line perpendicular to the line of identity in the

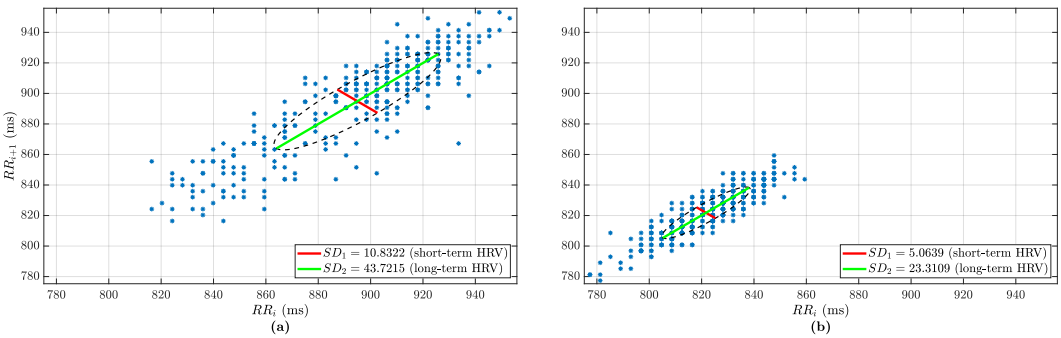

Figure D.3: Examples of Poincaré plot representations. These were computed for two 5-minute windows ranging from (a) 78 to 73 minutes and (b) 26 to 21 minutes before seizure onset, respectively, for the first seizure of patient 2.

Poincaré plot or, in other words, the width of the ellipse fitted to that plot.

- SD_2: standard deviation of the line of identity in the Poincaré plot, therefore measuring the length of the ellipse fitted to that plot.
- SD_1/SD_2: ratio of SD_1 to SD_2.

In other words, SD_1 and SD_2 can be regarded as measures of short- and long-term RR interval variability, respectively. Accordingly, SD_1 translates parasympathetic activity, whereas SD_2 captures overall HRV [305]. Lastly, the unpredictability of the RR interval series can be determined by computing SD_1/SD_2 [271].

The computation of the remaining nonlinear features, which will be described hereafter, assumes that the RR interval series is evenly sampled. As such, a cubic spline interpolation was performed on the irregularly sampled RR interval series. This method was reported to introduce the lowest error when computing LF and HF powers [303]. An RR interval time series was obtained, characterised by a sampling frequency of 4 Hz that allows for spectral components up to 2 Hz to be captured, according to the Nyquist theorem [301, 303, 311].

Detrended fluctuation analysis (DFA) was performed to explore the extent of long-range correlations in the RR interval time series for different time scales and, this way, to inspect the fractal scaling properties of HRV [314–316]. Particularly, two scaling exponents were returned from DFA:

- DFA slope α_1 ($DFA\,\alpha_1$): short-term fluctuations, within the 4-11 heartbeats range.
- DFA slope α_2 ($DFA\alpha_2$): long-term fluctuations, over the 11-64 heartbeats range.

Two entropy measures were computed and stand as measures of regularity and complexity of a time series:

- Approximate entropy ($ApEn$).
- Sample entropy ($SampEn$).

By inspecting these features, it is possible to know what is the likelihood that similar sequences found for m points, within a tolerance, r, will also be found for $m + 1$ points. Both measures require, therefore, the definition of the number of points, m, comprised in the sequences further compared, and the tolerance value, r, for which matches are accepted. In an HRV analysis, value of m parameter is typically set to 2. The tolerance, taken as the similarity criterion, was set to $0.2 \times SD$, SD corresponding to the standard deviation of the 5-minute window of the interpolated RR interval signal (of length N) [311,317–319]. A detailed description of the remaining process to compute these measures can be found in Delgado-Bonal and Marshak paper [319]. Low values of ApEn or SampEn are related to the existence of patterns, whereas high values can be found for less predictable and more complex processes [318].

By using the information of an RR interval time series to reconstruct the underlying m-dimensional dynamical system, it is possible to compute the following features:

- Correlation dimension (CD).
- Largest Lyapunov exponent (LLE).

The former quantifies the complexity of the system, whereas the latter provides information regarding the overall predictability of the system, i.e., the evolution of the trajectories in the phase space. A zero value of LLE can be found for periodic signals, whilst more chaotic systems are associated with an increase of the LLE [34, 314, 320]. Similarly, an increase in complexity corresponds to an increase in the value of CD [34, 321]. To compute such measures, the reconstruction of the underlying system's phase space from the available measured data (RR interval time series) must be performed. In this study, the two parameters required for phase space reconstruction, the embedding dimension, m, and the time delay, τ, were estimated (for each 5-minute window) using the False Nearest Neighbour algorithm and first local minimum of the average mutual information method, respectively [322–324]. The LLE was then obtained using Rosenstein *et al.* (1993) [325] method, which is one of the most widely used for this purpose, whereas CD was computed based on Grassberger & Procaccia (1983) [326] method.

A recurrence quantification analysis (RQA) is typically conducted to find hidden periodicities in the aforementioned phase space trajectory. Such information can be accessed by computing the recurrence plot (RP) of a given time series [327]. The first step to obtain such representation is to compute the square matrix with dimensions $N \times N$ (known as colour recurrence plot and depicted in Figure D.4), containing the pairwise Euclidean distance (given by the norm $||\cdot||$) between all samples of the trajectory, N, in the m-dimensional space [224, 320]. Afterwards, a threshold distance ε is used to define a sphere centred at the state x_i. If x_j falls within that sphere, then the Heaviside function $\Theta(\cdot)$ decides for $R_{i,j} = 1$, meaning the

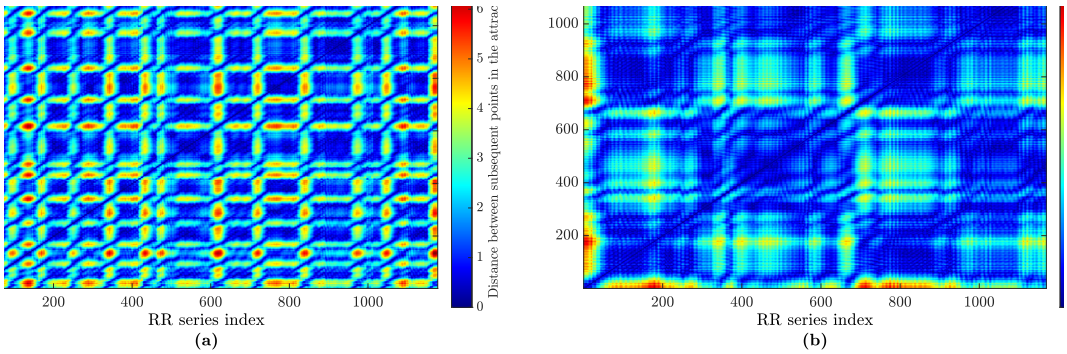

Figure D.4: Examples of colour recurrence plots. These were computed for two 5-minute windows ranging from (a) 78 to 73 minutes and (b) 26 to 21 minutes before seizure onset, respectively, for the first seizure of patient 2.

states are close to each other. Otherwise, $R_{i,j} = 0$. This binary matrix, symmetric along the identity line, can therefore be visualised in a black ($R_{i,j} = 1$) and white plot ($R_{i,j} = 0$), the RP. In this study, the value of ε was estimated for each 5-minute window, corresponding to 10% of the maximum phase space diameter [328]. The RQA returned seven RP measures of complexity, which quantify recurrence point density and indicate the existence of diagonal and/or vertical lines in the RP. A comprehensive description of the computation of these measures can be found in [224, 328, 329]. The following RQA features were derived:

- Recurrence rate (REC).
- Determinism (DET).
- Average diagonal line length (L).
- Length of the longest diagonal line (L_{max}).
- Laminarity (LAM).
- Trapping time (TT).
- Shannon entropy (ENT).

Table D.1: Extended information on HRV-derived features.

	Features	Units	ML (s)	MVs (%)	Characterisation	Computational Time (s)
Linear/Time domain	NN50	count	150	0.09	STV, PSA [92]	$(1.1 \pm 9.5) \times 10^{-4}$
	pNN50	%	150	0.09	STV, PSA [92]	
	SDNN	ms	300	0.16	OV [92, 305, 306]	
	RMSSD	ms	150	0.09	STV, PSA [92, 305, 306]	
	SDSD	ms	150	0.09	STV, PSA [92]	
	RRMean	ms	150	0.09		
	RRMin	ms	150	0.09		
	RRMax	ms	150	0.09		
	RRVar	ms	150	0.09		
Linear/Frequency domain	Total power	ms^2	300	0.16	OV [92, 305, 306]	0.03 ± 0.03
	VLF power	ms^2	300	0.16	LTV [216]	
	LF power	ms^2	150	0.09	SA [216, 306]	
	HF power	ms^2	150	0.09	STV, PSA [216]	
	LF/HF	–	150	0.09	SVB [216]	
	LF norm	n.u.	150	0.09	SA	
	HF norm	n.u.	150	0.09	STV, PSA	
Nonlinear	SD_1	ms	150	0.09	STV, PSA [271, 272]	$(4.8 \pm 40.4) \times 10^{-5}$
	SD_2	ms	150	0.09	OV [271, 272]	
	SD_1/SD_2	–	150	0.09	SVB [271]	
	DFA α_1	–	300	0.16	STV [272]	$(4.4 \pm 1.6) \times 10^{-3}$
	DFA α_2	–	300	0.16	LTV, SA [272]	
	ApEn	–	180	0.10	STV, PSA [272]	0.03 ± 0.02
	SampEn	–	150	0.09	SVB [272]	$(1.2 \pm 0.5) \times 10^{-3}$
	LLE	–	300	0.16		0.8 ± 0.2
	CD	–	300	0.16		2.1 ± 12.5
	RQA (REC, L, TT, DET, LAM, ENT, L_{max})	–	150	0.09		1.3 ± 3.6

s: seconds; ms: milli seconds; n.u.: normalised units; ML: minimum length of clean ECG recordings required to compute each feature [92, 271]; MVs: percentage ratio of the number of missing values (i.e., 5-minute windows contaminated with noise and therefore not having the ML required) to the total of 658,784 5-minute windows (238 seizures times 2768 5-minute windows) analysed for each feature. Each feature can be characterised in terms of (i) ANS branch activation: sympatho-vagal balance (or sympathetic-parasympathetic), SVB; sympathetic activity, SA; and parasympathetic activity, PSA; and (ii) short-term variability, STV and long-term variability, LTV or (iii) overall variability (OV). Computational time (averaged over all 5-minute windows) is presented as the average ± standard deviation.

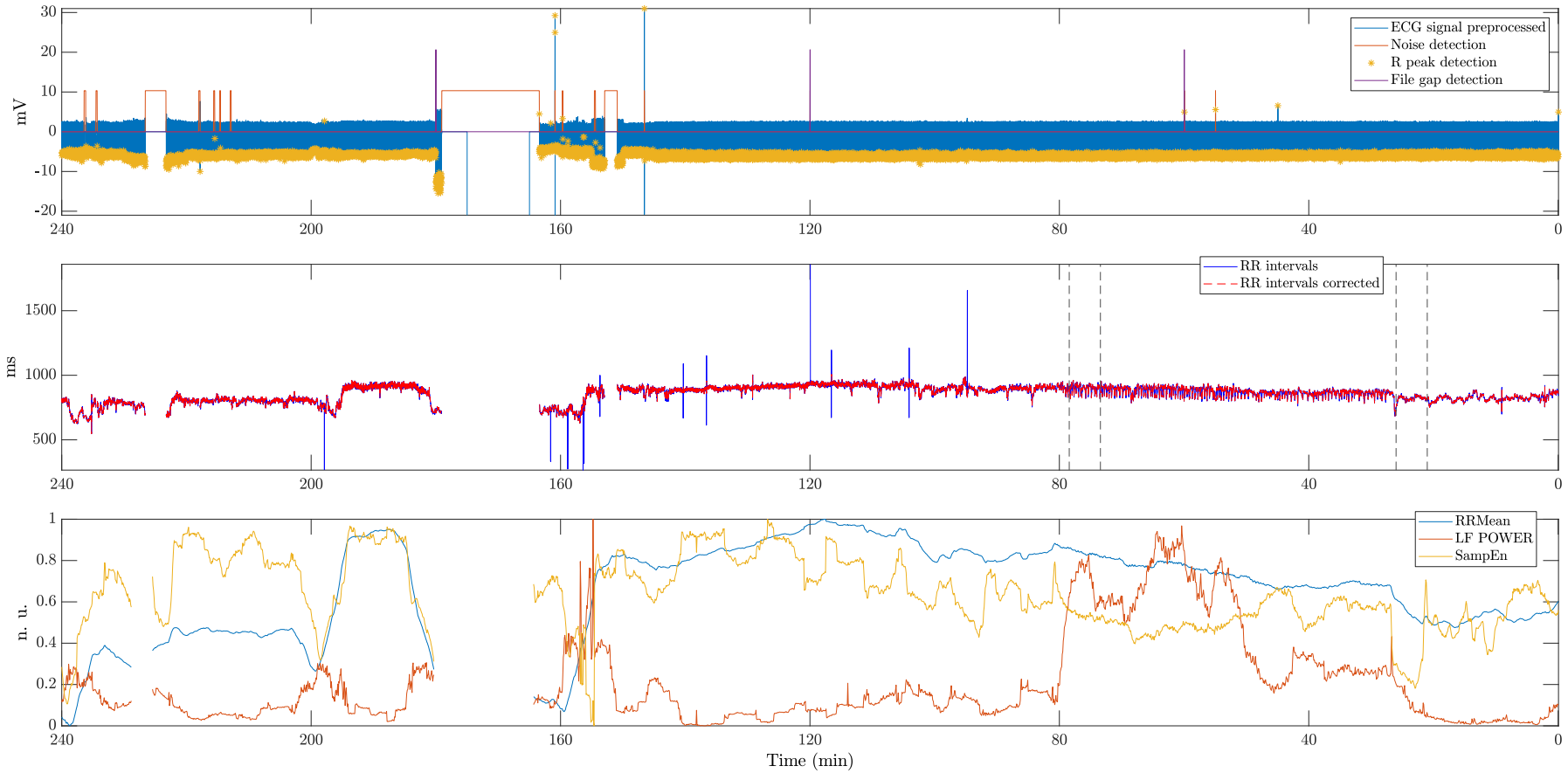

Figure D.5: Example of the results returned for: (i) preprocessing and noise detection (top plot); (ii) RR interval series editing (middle plot); and (iii) HRV feature engineering (bottom plot) steps, for the first seizure of patient 2 (identified by 8902 in Table 4.1). The feature combination $c = 2159$, corresponding to features RRMean, LF Power and SampEn, is depicted. Seizure onset occurs at 0 min, as the x-axis represents the time anticipating seizure onset. The vertical dashed lines indicate the location of the 5-minute windows depicted in Figures D.2, D.3 and D.4.

D.3 Feature redundancy study

Aside from the main study that aims at characterising the preictal interval, the present feature redundancy study was also performed in order to understand which features are able to capture the different ANS responses (sympathetic and parasympathetic, respectively). Towards that end, it would be interesting to inspect the correlation (or linear dependence) and general statistical dependence existing among each pair of features. Naturally, it is expected that some may present similar behaviour because, despite being envisaged to capture different data patterns, those features are all derived from HRV time series analysis and from similar signal processing methods (e.g., NN50 and pNN50, ApEn and SampEn).

As can be concluded from Table D.1, there is a stronger evidence in the relevant literature for some features regarding its capability to capture activity of parasympathetic and sympathetic autonomic branches (e.g., SDNN, RMSSD and Total Power). Feature redundancy evaluation was introduced here to reduce the variability associated with the interpretation of remaining features.

D.3.1 Methodology

Feature redundancy was evaluated over two directions in the three-dimensional matrix, $M \in \mathbb{R}^3$, obtained from the feature engineering step and of dimensions $F \times S \times W$:

$f = 1 : F, \quad F = 32$ features;

$s = 1 : S, \quad S = 238$ seizures;

$w = 1 : W, \quad W = 2,768$ 5-minute 98.33% overlapping windows.

Specifically, correlation and mutual information were assessed for all combinations of two features in $F = 32$ feature dataset:

$c = 1 : C, \quad C = 496$ combinations of two features resulting from C_2^F.

In order to handle the existence of redundant features, both correlation and average mutual information (AMI) between each pair of features were assessed for:

1. each 5-minute overlapping window, w, meaning over all seizures ($X = x_1, x_2, x_3, ..., x_S$ and $Y = y_1, y_2, y_3, ..., y_S$). Given the minimum four hour interval between subsequent seizures, it was assumed that each seizure is an independent event.

2. each seizure, s, meaning over all 5-minute overlapping windows ($X = x_1, x_2, x_3, ..., x_W$ and $Y = y_1, y_2, y_3, ..., y_W$). By performing the study over the feature's time series, it is possible to take into account inter-seizure variability.

The following explanations regarding the computation of features' redundancy are exemplified for point 1. previously enumerated, even though the results will be presented for both substudies.

On one hand, linear correlation, given by Pearson's correlation coefficient (PCC), provides information regarding the existence of negative or positive linear relationship between the variables considered [330].

$$PCC = \frac{1}{S-1}\sum_{i=1}^{S}\left(\frac{x_i-\mu_X}{\sigma_X}\right)\left(\frac{y_i-\mu_Y}{\sigma_Y}\right) = \frac{cov(X,Y)}{\sigma_X\sigma_Y}. \tag{D.1}$$

On the other hand, AMI is useful in evaluating features' statistical inter dependency or dependence on another variable [331,332]. It translates into computing the amount of information that is possible to obtain from a random variable, given the knowledge of another. According to equation (D.2), AMI requires the estimation of the joint probability density function $\hat{p}_{XY}$ and the marginal probability density functions $\hat{p}_X(x_i)$ and $\hat{p}_Y(y_i)$ using kernel density estimators. This kernel approach was chosen over the widely used histogram estimators of the theoretical probabilities, as large estimation errors can result from the latter [332]. The advantages of the kernel estimation over histograms were thoroughly presented by Thomas *et al.* (2014) [331].

$$AMI = \frac{1}{S}\sum_{i=1}^{S} ln\left\{\frac{\hat{p}_{XY}(x_i,y_i)}{\hat{p}_X(x_i)\hat{p}_Y(y_i)}\right\}. \tag{D.2}$$

It is important to note that finding connections in PCC corresponds to find those very connections in AMI graph whereas the opposite may not happen.

Both PCC and AMI were inspected for each 2-combinations of features for each 5-minute window of data and stored in two bi-dimensional matrices of size $[C \times W]$, respectively. Each matrix was inspected regarding the number of windows for which PCC and AMI were found to exceed a given threshold. In other words, a given feature combination was considered redundant if a minimum number of windows was found to have PCC or AMI superior to the respective thresholds (see Section D.3.1.1). Finally, correlation and mutual information among features were represented in graph plots, with the nodes referring to the explored features and the edges containing information about the number of 5-minute windows that verified PCC and AMI higher than the respective thresholds.

D.3.1.1 On choosing PCC and AMI thresholds

The origin of both PCC and AMI thresholds is explained in Figure D.6 and D.7, respectively. For each measure, a linear discriminant analysis was applied in order to find the threshold for which the discrimination between samples was maximum, while keeping reasonable ratio of the samples comprised in the two remaining groups. The

resulting values of sensitivity (SE) and specificity (SP) were assessed on the ROC curve.

$$SE = \frac{TP}{TP + FN}. \tag{D.3}$$

$$SP = \frac{TN}{TN + FP}. \tag{D.4}$$

Given that, as the threshold increases the number of samples in the resulting two groups of data becomes strongly unbalanced, the geometric mean (GM) was also presented.

$$GM = \sqrt{SE^2 + SP^2}. \tag{D.5}$$

The threshold for each measure corresponds to the first maximum of GM for which a ratio, R, between the number of samples in the group of data crossing the tested thresholds, $th = 0.01, 0.02, 0.03, ..., 1$, and the total number of samples,

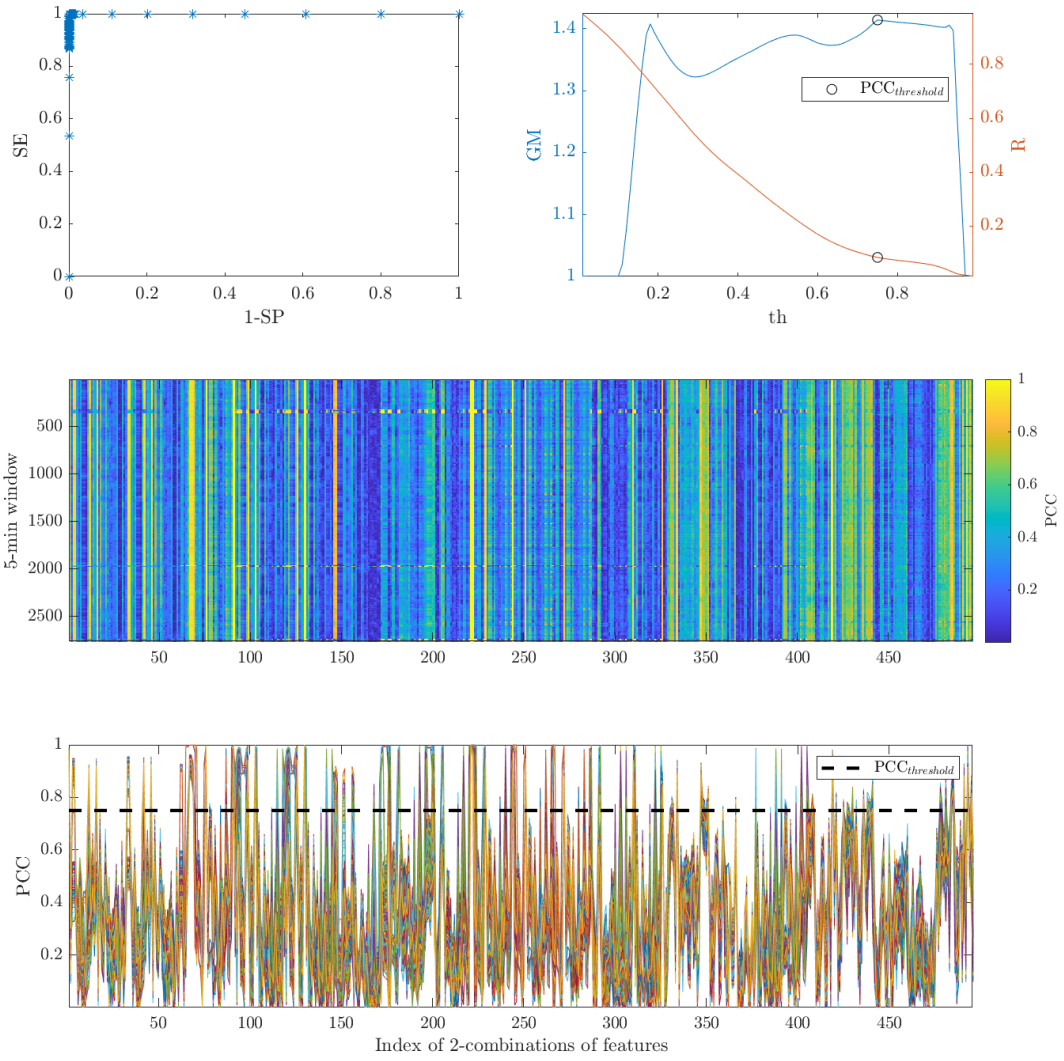

Figure D.6: Selection of PCC threshold.

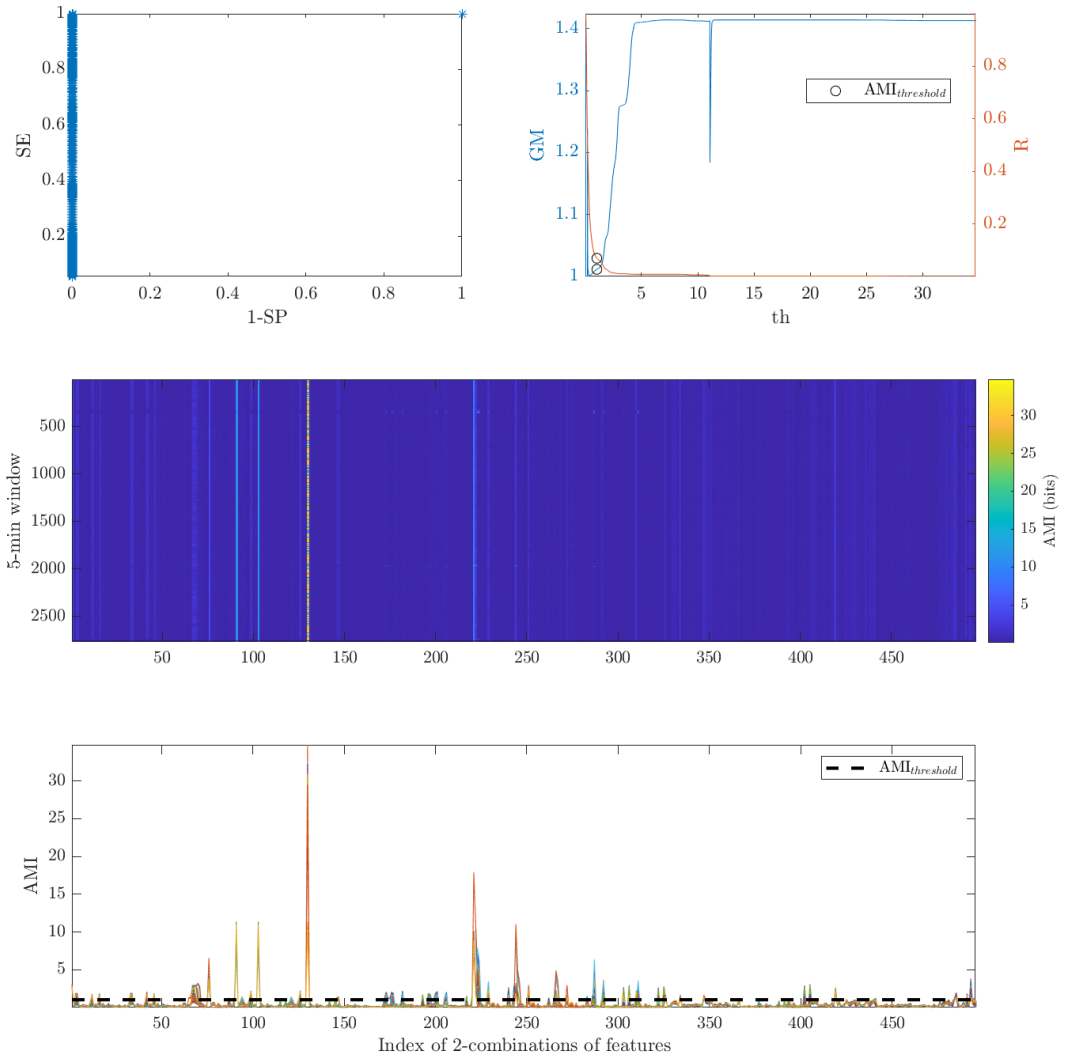

Figure D.7: Selection of AMI threshold.

$N = 496 \times 2768$, was higher than 5%.

$$R = \frac{\sum_{c=1}^{C} \sum_{w=1}^{W} \delta(c, w)}{N}, \tag{D.6}$$

where

$$\delta(c, w) = \begin{cases} 1, & \text{if } PCC >= th_i, \\ 0, & otherwise \end{cases}. \tag{D.7}$$

For PCC, a threshold of 0.75 was obtained which is in accordance with literature. Typically, two variables are said to be strongly correlated if a correlation of more than 0.8 is found [333]. Regarding AMI, a threshold of 1 bit was found to comply with the previous requirements.

Additionally, given the fact that PCC > 0.75 and AMI > 1 bit did not manifest for all 5-minute overlapping windows of a given feature combination, an analysis was performed in order to define a minimum number of 5-minute windows for which to

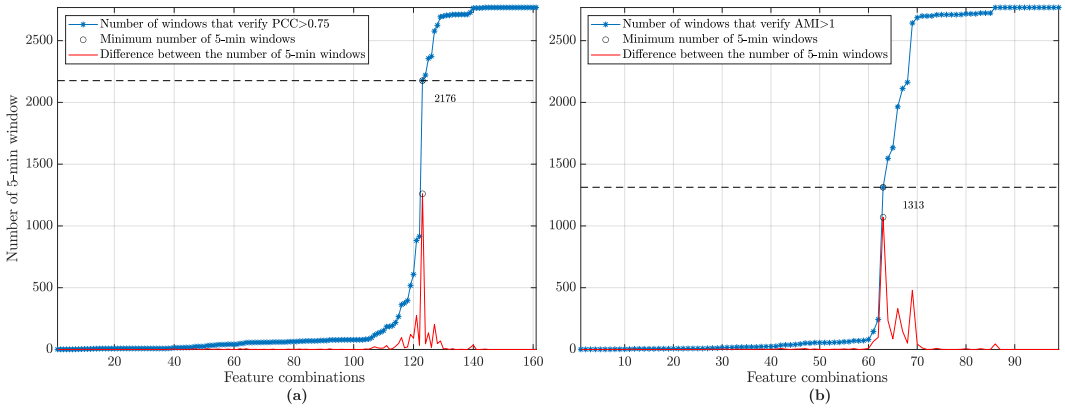

Figure D.8: Determination of the minimum number of 5-minute overlapping windows indicating redundancy. Above these window thresholds, redundant information, i.e, for which PCC > 0.75 and AMI > 1 bit, can be found for each pair of features.

consider the existence of redundant information. The minimum number of windows for which to observe PCC > 0.75 and AMI > 1 bit between two features was set to the number of windows with the highest difference from the previous one (namely, 2176 and 1313 for PCC and AMI, as can be seen in Figure D.8).

D.3.2 Results

Representations of correlation and mutual information between features over seizures and over the features' time series are depicted in Figure D.9 and D.10, respectively.

D.3.2.1 Analysis of redundancy over seizures

The colour of the edges in Figure D.9 provides information regarding the number of 5-minute windows for which values of PCC and AMI were higher than 0.75 and 1 bit, respectively. It should be noted that, PCC and AMI feature redundancy assessment is presented for a minimum number of windows, verifying the threshold conditions (PCC > 0.75 and AMI > 1 bit). In other words, it was often observed that redundant information was not present in all 5-minute windows, for a given feature combination, evidencing the existence of time intervals with different dynamics. In sum, the results of feature redundancy obtained for PCC > 0.75 and AMI > 1 bit were observed for a minimum number of 5-minute windows, namely, 2176 and 1313, respectively.

By taking close inspection of the results obtained for PCC (see Figure D.9 (a)), it is possible to observe that features such as Total Power, VLF Power, RRVar, SD_2, and SDNN are strongly correlated, in the sense that a correlation of more than 0.75 was found for all 2,768 5-minute windows. Another cluster of correlated features can also be found in the graph, indicating some level of correlation between features SDSD, SD_1, HF Power, NN50, pNN50 and RMSSD. According to Table 1, HF Power, RMSSD, SDSD, SDNN, SD_1 and SD_2 are features associated with the

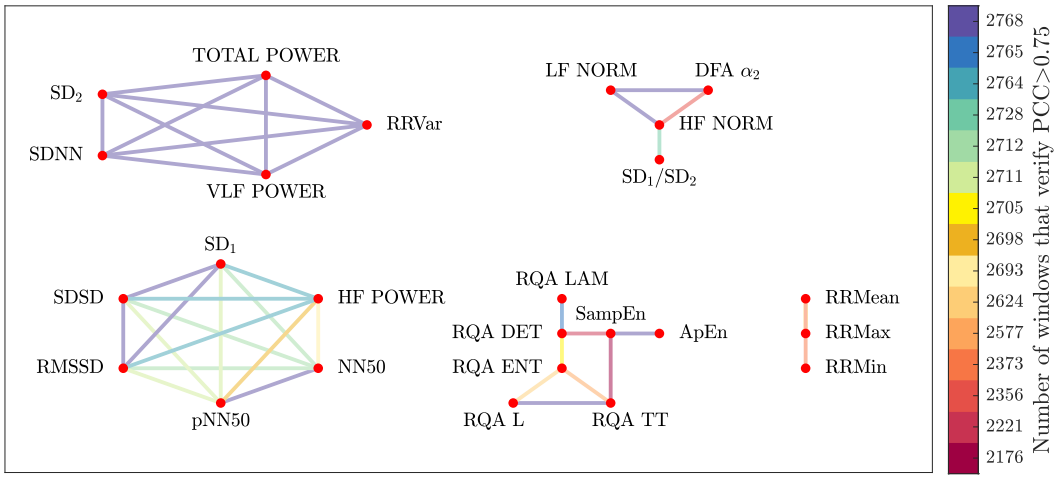

(a)

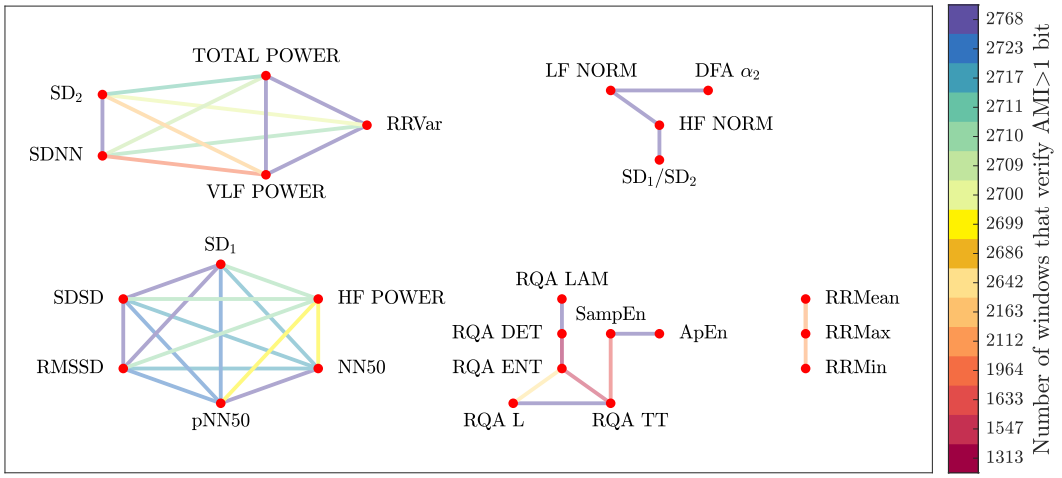

(b)

Figure D.9: Graph representation of features' (a) correlation and (b) mutual information across time windows. Each edge colour provides information regarding the number of 5-minute windows for which (a) a Pearson's correlation coefficient (PCC) of more than 0.75 and (b) average mutual information (AMI) superior to 1 bit between the features was observed.

short-term HRV, which is indeed represented in the graph.

A similar scenario was returned when analysing AMI (see Figure D.9 (b)), with the same groups of features shown in the graph. Comparing to PCC, AMI presented weaker dependencies among features in the sense that the amount of shared information was verified for a lower number of 5-minute windows. In fact, relationships HF Norm/DFA α_2 and RQA DET/SampEn were not even present in AMI graph.

Additionally, while some of the correlation and mutual information relationships were somehow expected, there are others that might suggest the action of parasympathetic or sympathetic autonomic branches. For instance, strong connections such as the ones between (i) SampEn and ApEn, (ii) NN50 and pNN50, (iii) RQA DET, RQA LAM, RQA L and RQA TT, (iv) RRMean, RRMin and RRMax; and (v) RMSSD and SDSD, may be the reflection of similar computational approach (e.g., different content extracted from the difference of successive RR intervals, for the

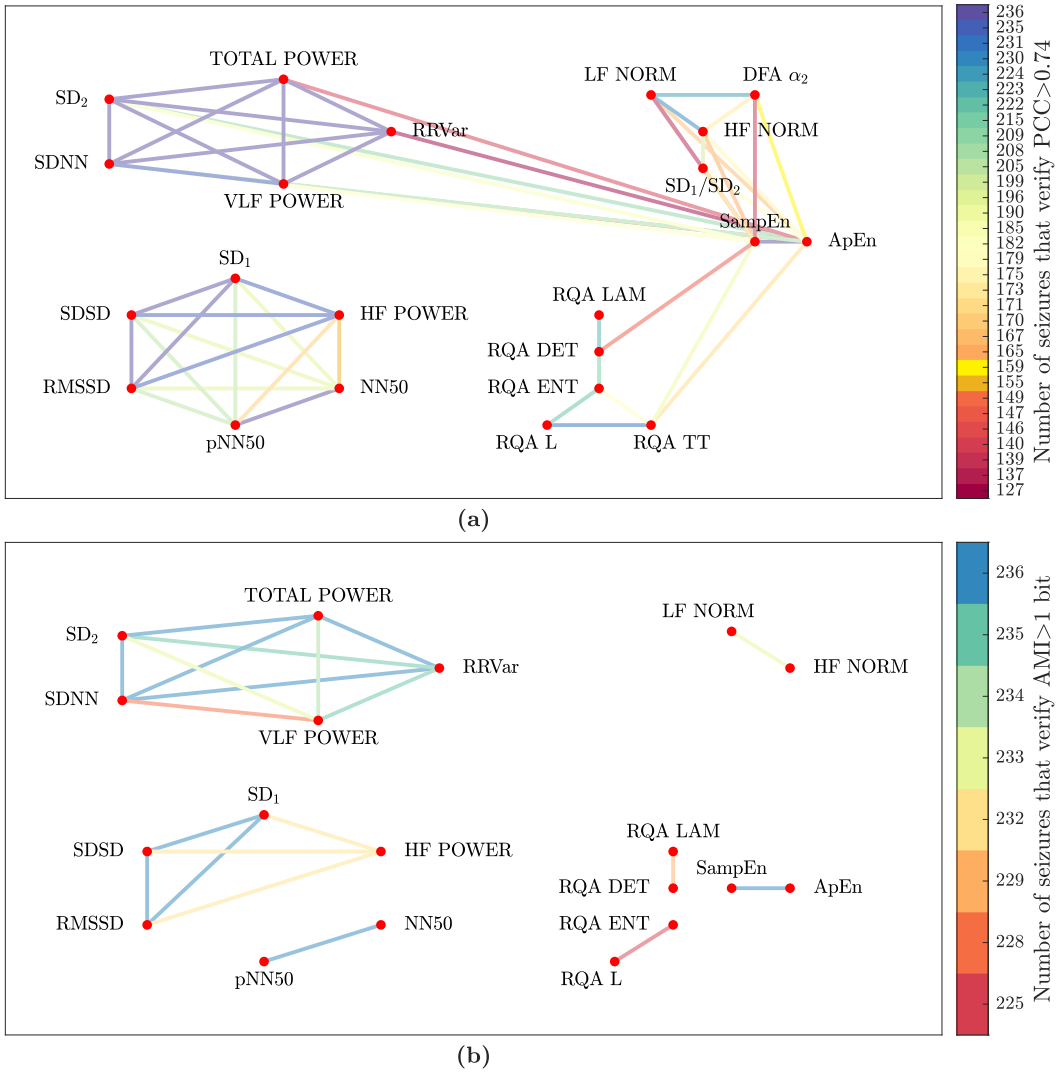

Figure D.10: Graph representation of features' (a) correlation and (b) mutual information across seizures. Each edge colour provides information regarding the number of seizures for which (a) a Pearson's correlation coefficient (PCC) of more than 0.74 and (b) average mutual information (AMI) superior to 1 bit between the features was observed.

latter case). It is also interesting to notice the cluster behaviour of the connections between features both in PCC and AMI, which seem to unveil new associations that could be useful in providing new interpretations of features (and therefore in filling white spaces in feature characterisation in Table D.1). There are two groups, forming a hexagon and a pentagon, comprising time- and frequency-domain as well as Poincaré features. For the case of the hexagonal group and according to the characterisation of features in Table 1, all features (SDSD, SD_1, HF Power, NN50, pNN50 and RMSSD) are associated with short-term variability and eventually the engagement of the parasympathetic autonomic branch. The pentagonal group, on the other side, contains features VLF Power and RRVar, not yet clearly associated to a given physiological interpretation, which are connected with Total Power and SDNN and SD_2. While SDNN has been reported to manifest overall variability, SD_2 has been

associated with both short-term and long-term variability. It is worth noting that Total Power and VLF Power are separated from the remaining frequency-domain features, as well as RRVar from RRMean, RRMin and RRMax group, SDNN from the time-domain features and SD_2 from SD_1. It might indicate that these measures of HRV belonging to the pentagon are related to the sympatho-vagal balance, therefore capturing overall variability [305, 306].

The LF Norm, DFA α_2, HF Norm and SD_1/SD_2 group raises debate as well. In fact, LF Norm (sympathetic activity) and HF Norm (short-term variability indicating parasympathetic activity) are showing separated from the remaining frequency-derived features and are related with nonlinear features DFA α_2 (long-term variability) and SD_1/SD_2 (sympatho-vagal balance).

As for the connection found between a few RQA measures and SampEn in both PCC and AMI graphs, it is in line with what is being measured. In fact, both RQA and SampEN quantify regularity/periodicity in a time series. Contrarily to ApEn, SampEn does not count self-matches which might explain why ApEn is not connected to RQA features.

D.3.2.2 Analysis of redundancy over time series

A similar analysis was performed in order to assess the features' redundancy over time. For this substudy, it must be noticed that more samples (W) are used to compute the PCC and AMI between each feature combination, when comparing to the previous study. As consequence, more reliable estimations of the variables distributions are obtained.

As can be seen in Figure D.10, the results obtained for PCC and AMI are quite similar to the ones obtained when assessing redundancy over seizures. One of the major differences lies in the new correlations involving SampEn and ApEn. Additionally, when looking at the AMI graph, it is possible to observe the decrease of some feature dependencies, comparing to Figure D.9, indicating a low level of redundancy among features within each seizure.

D.4 Preictal interval search using unsupervised learning

Algorithm 1 Selecting clustering solutions

1. Initialise accepted solutions set $A_1 = []$;
2. For $c = 1$ to C:
   (a) Set condition 1: clustering solution comprising two clusters.
   (b) Set condition 2: clustering solution evaluated with $DI >= 0.15$.
   (c) Set condition 3: DBSCAN clustering solution not containing noisy samples.
   (d) Set condition 4: clustering solution containing smaller cluster with 20 or more samples.
   (e) Set condition 5: clustering solution containing smaller cluster starting after 120 minutes.
   (f) If (condition 1 & condition 2 & condition 3 & condition 4 & condition 5)
      i. Accept clustering solution stored in A_1.
   (g) Else
      i. Discard clustering solution.

Algorithm 2 Selecting clustering solutions based on time continuity and duration

1. Initialise accepted solutions $A_2 = []$.
2. Initialise matrix $M = cell(A, 2)$ with information on clustering solution.
   For $a = 1$ to A_1:
   (a) If smaller cluster is continuous over time
      i. $M(a, 1) =$ "*continuous*".
      ii. Find the solution(s) with the smaller cluster comprising the highest number of samples, save it in A_2 and register the number of samples in $M(a, 2)$.
   (b) Else
      i. $M(a, 1) =$ "*discontinuous*".
      ii. Find the solution(s) with the smaller cluster comprising the highest number of samples, save it in A_2 and register the number of samples in $M(a, 2)$.

Algorithm 3 Stratifying clustering solutions in time and selecting clustering solutions based on time continuity and duration

1. Initialise accepted solutions sets for each of the intervals under analysis.
   $A_{[40,0]} = []$
   $A_{[80,40]} = []$
   $A_{[120,80]} = []$
2. For $a = 1$ to A_2:
   (a) If smaller cluster located in [40, 0] interval before seizure
      i. Save solution in $A_{[40,0]}$.
   (b) Elseif smaller cluster located in [80, 40] interval before seizure
      i. Save solution in $A_{[80,40]}$.
   (c) Elseif smaller cluster located in [120, 80] interval before seizure
      i. Save solution in $A_{[120,80]}$.
   (d) Else
      i. Discard clustering solution.
   (e) Select solutions in $A_{[40,0]}$ according to Algorithm 2.
   (f) Select solutions in $A_{[80,40]}$ according to Algorithm 2.
   (g) Select solutions in $A_{[120,80]}$ according to Algorithm 2.

Appendix E

EEG unsupervised learning study

This chapter presents additional information on the electroencephalography (EEG) extracted features (Section E.1), the feature data preparation (Section E.2), the sleep-wake cycle model (Section E.3) and, finally, the extended results for the unsupervised learning study (Section E.4).

E.1 EEG feature engineering

There is a vast amount of literature spanning the different groups of features typically extracted from EEG. The next subsections describe the univariate linear, univariate nonlinear and multivariate features considered in this study according to the state of the art [11,13]. The frequency bands considered in univariate linear and multivariate feature extraction comprise delta (0.5-4 Hz), theta (4-8 Hz), alpha (8-13 Hz), beta (13-30 Hz), and gamma (30-47 Hz) [11,13,233].

E.1.1 Univariate linear features

A total of 42 features were extracted from each 5-second window and each EEG channel [11,13,233].

E.1.1.1 Time-domain univariate linear features

Statistical measures

Five statistical measures were considered in this study: normalised and non-normalised (with respect to the maximum value in each window) mean amplitude [153], standard deviation, skewness, and kurtosis [11,14].

These measures are meant to capture information regarding the amplitude distribution of a given time series. Symmetric and asymmetric amplitude distribu-

tions translate to zero and non-zero skewness, respectively. The relative flatness (or peakedness) of the amplitude distribution is reflected in the value of kurtosis [13].

Hjorth parameters

Hjorth parameters, activity, mobility and complexity, were conceptualised as clinically useful tools to quantitatively describe the EEG [13]. Activity is given by the variance of a given time series, $y(t)$:

$$Activity = var(y(t)) \tag{E.1}$$

Mobility corresponds to the variance of the slopes of a time series normalised by the variance of that time series:

$$Mobility = \sqrt{\frac{var(y'(t))}{var(y(t))}} \tag{E.2}$$

Complexity quantifies the variance of the rate of slope changes of a time series with reference to an ideal sine curve. The more similar is the time series to a pure sine wave, the more approximate will be the value of complexity to 1.

$$Complexity = \frac{Mobility(y'(t))}{Mobility(y(t))} \tag{E.3}$$

Decorrelation time

The decorrelation time corresponds to the time at which the first zero-crossing of the autocorrelation function occurs. The samples in a time series are less correlated as the time of the first zero-crossing approaches zero. The decorrelation time is, therefore, an indicator of signal periodicity. Considering the extreme case of a white noise signal, it theoretically presents a zero value of decorrelation time [175, 236].

E.1.1.2 Frequency-domain univariate linear features

The frequency spectrum was computed using Welch's power spectral density estimate (see Figure E.1 (c)-(d)). Five frequency bands were considered: delta (0.5-4 Hz), theta (4-8 Hz), alpha (8-13 Hz), beta (13-30 Hz), and gamma (30-47 Hz) [11]. The power and the relative power in each of those frequency bands were extracted. The relative power corresponds to dividing the power in each of these frequency bands by the total power of the time series [11, 90, 175, 236].

- Spectral power in each frequency band (delta, theta, alpha, beta, and gamma).
- Total power.
- Relative spectral power in each frequency band (delta, theta, alpha, beta, and gamma).

- Alpha peak frequency.
- Spectral edge frequency and power (at 50%).
- Mean frequency.
- Power ratios between frequency bands (delta/alpha, delta/beta, delta/gamma, delta/theta, theta/alpha, theta/beta, theta/gamma, alpha/beta, alpha/gamma, beta/gamma, beta/(alpha+theta), and theta/(alpha+beta)).
- Energy of wavelet coefficients obtained using discrete wavelet transform and Daubechies (db4) mother wavelet at five levels of decomposition (detail coefficients D1: 64-128 Hz, D2: 32-64 Hz, D3: 16-32 Hz, D4: 8-16 Hz, D5: 4-8 Hz, and approximation coefficient A5: 0-4 Hz).

Spectral edge frequency and power

Typically, the power spectrum of an EEG signal is characterised by a predominance of power in the 0 to 40 Hz frequency band. The spectral edge frequency, f_{50}, is a measure of the power spectrum distribution that consists of the minimum frequency for which it is possible to obtain 50% of the spectral power up to 40 Hz, $P_{40\,Hz}$ [13].

$$f_{50} = min\left\{ f* \;\middle|\; \sum_{f=0\,Hz}^{f*} p_f > P_{40\,Hz} \cdot 0.50 \right\} \tag{E.4}$$

The spectral edge power corresponds to the power spectrum area below the spectral edge frequency [175, 234, 236].

Energy of wavelet coefficients

The wavelet transform has been used as an alternative to the FFT analysis as it allows for multiresolution time-frequency decomposition. Particularly, the discrete wavelet transform (DWT) decomposes a given time series into approximation and detail coefficients yielding the first level of decomposition. The approximation coefficients in every level are further decomposed into the next level of approximation and detail coefficients. The DWT coefficients are obtained by applying the mother wavelet to a given time series at different translations and scales. The first levels correspond to the time series' high frequency content, whereas the last levels contain low frequencies [61, 175, 334, 335]. Given that the dataset under analysis contains data sampled at 256 Hz, the DWT decomposition was conducted using Daubechies (db4) [175, 236, 335] mother wavelet at five decomposition levels: detail coefficients D1 (64-128 Hz), D2 (32-64 Hz), D3 (16-32 Hz), D4 (8-16 Hz), D5 (4-8 Hz), and approximation coefficient A5 (0-4 Hz) [144]. At last, the energy of each decomposition level and of the last approximation level was computed [175].

E.1.2 Univariate nonlinear features

A total of 29 univariate nonlinear features were extracted from each 5-second window and EEG channel:

Higuchi's fractal dimension

Higuchi's fractal dimension (HFD) is a fractal measure of the irregularity and self-similarity of a given signal [61, 336, 337]. HFD corresponds to the slope of the linear fit between a log-log plot of the length and different scales of a given 5-second EEG window. This feature requires the definition of a free parameter (k_{max}) corresponding to the maximum number of scales that have been analysed. In this study, this parameter was set to 100 as a result of an estimation process that evaluated a range of k_{max} values and assessed when the corresponding values of fractal dimension reached a plateau [336–338].

Monofractal detrended fluctuation analysis

Monofractal detrended fluctuation analysis (DFA) was performed to explore the extent of long-range correlations in the EEG 5-second windows for different time scales [339, 340]. Two scaling exponents were returned from DFA analysis: (i) DFA slope α_1 ($DFA\alpha_1$) corresponding to short-term fluctuations, within the 10-32 sample range and (ii) DFA slope α_2 ($DFA\alpha_2$) corresponding to long-term fluctuations, over the 32-128 sample range [339].

Multifractal detrended fluctuation analysis

Multifractal detrended fluctuation analysis (MFDFA) is a generalisation of the DFA method, which is computed for a single scale or fractal dimension. This method explores the possibility that different fractal patterns may describe the fractal structure of the EEG segments. Three measures were obtained from the multifractal spectrum: width, the abscissa value of the apex, and the asymmetry parameter [339, 341, 342]. The asymmetry parameter measures the multifractal spectrum symmetry: a symmetric spectrum corresponds to a zero value of the asymmetry parameter; an asymmetric spectrum that is left- or right-skewed yields a positive or negative value of the asymmetry parameter [343].

Multifractal 1-D Wavelet Leader estimates

Multifractal 1-D Wavelet Leader estimates is an alternative method based on wavelet analysis to estimate the multifractal spectrum [344]. Eleven measures characterising the multifractal spectrum were extracted, [344–347] as can be seen in Figure E.1 (e)-(f). An asymmetrical spectrum is obtained when the structure of the time series is not sensitive to the local fluctuations with (i) large magnitudes (long right tail)

or (ii) small magnitudes (left long tail). When the time series contains high and low fluctuation components presenting a similar scaling complexity, the multifractal spectrum takes a symmetrical shape [339, 346].

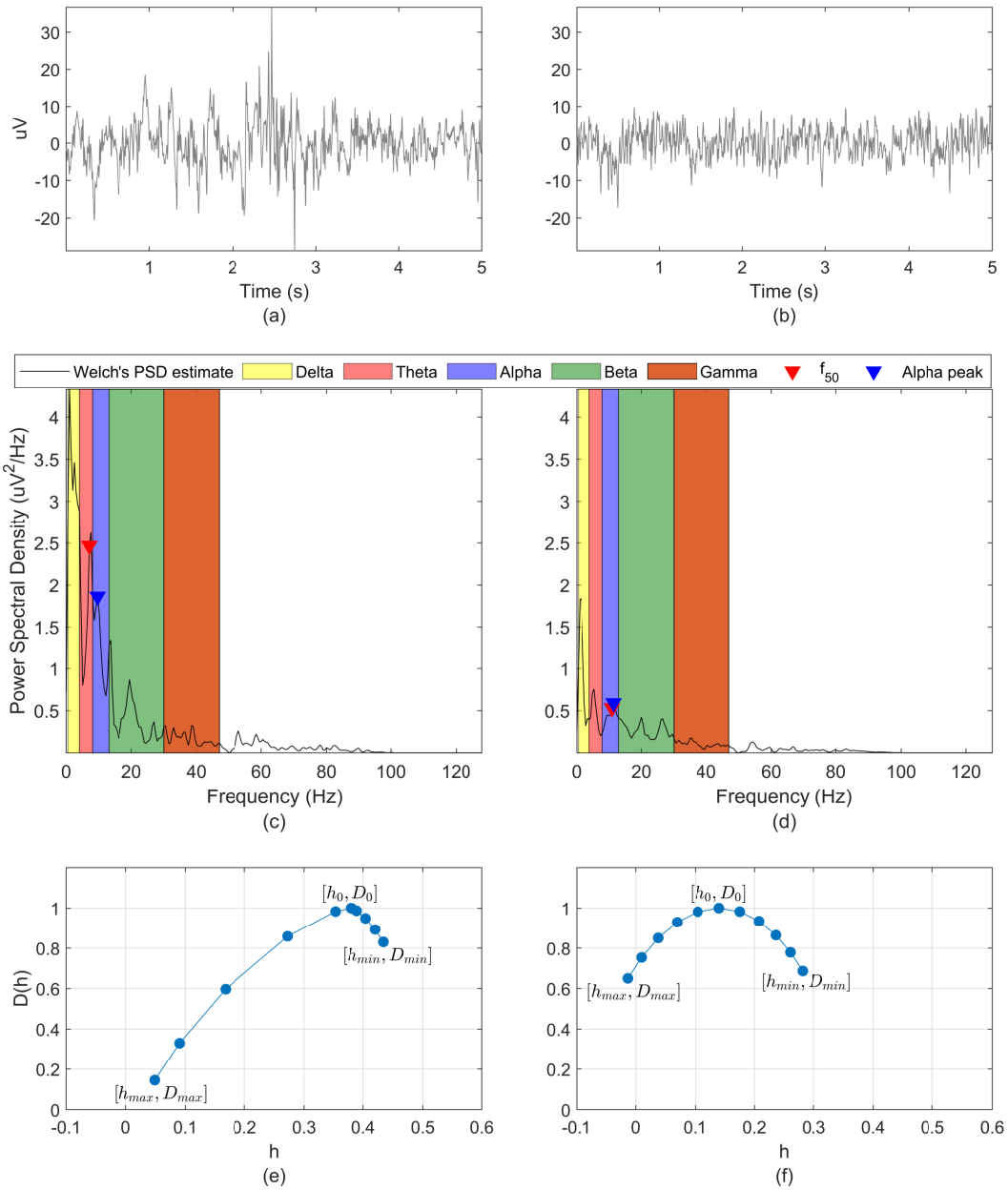

Figure E.1: Example of two 5-second EEG windows located (a) 4.5 hours and (b) 5 minutes before the onset of the first seizure of patient 402. The frequency spectrum (c)-(d) and the multifractal spectrum (e)-(f) have been obtained for both windows. The multifractal spectrum has been computed using the `dwtleader` Matlab function. Eleven measures were saved for each 5-second window: h_{min}, h_{max}, D_{min}, D_{max}, h_0, spectrum width $\Delta h = h_{max} - h_{min}$, $\Delta D = D_{max} - D_{min}$, $h_0 - h_{min}$, $h_{max} - h_0$, $D_0 - D_{max}$, and $D_0 - D_{min}$.

Approximate and sample entropies

Approximate and sample entropies quantify the regularity and the complexity of a time series [348–350]. By inspecting these features, it is possible to know the likelihood that similar sequences found for m points, within a tolerance, r, will also be found for $m + 1$ points. Both measures require the definition of the number of points, m, comprised in the sequences further compared, and the tolerance value, r, for which matches are accepted. Parameter m is equal to 2 [349]. The tolerance, taken as the similarity criterion, was set to $0.2 \times SD$, SD corresponding to the standard deviation of the 5-second EEG window (of length N) [317–319, 349].

Correlation dimension and largest Lyapunov exponent

The correlation dimension (CD) and the largest Lyapunov exponent (LLE) were obtained from the reconstruction of the underlying m-dimensional dynamical system. The former quantifies the complexity of a system, whereas the latter provides information regarding the overall predictability of that system, i.e., the evolution of the trajectories in the phase space. Periodic signals are associated with null values of LLE, whereas chaotic systems display increased values of the LLE [34]. Similarly, an increase in complexity corresponds to an increase in the value of CD [34]. These measures were obtained through the reconstruction of the underlying system's phase space. In this study, the two parameters required for phase space reconstruction, the embedding dimension, m, and the time delay, τ, were estimated (for each 5-second window) using the False Nearest Neighbour algorithm and the first local minimum of the average mutual information method, respectively (refer to Figure E.2) [322–324]. The LLE was then obtained using the Rosenstein *et al.* (1993) [325] method, which is one of the most widely used for this purpose, whereas CD was computed based on the Grassberger & Procaccia (1983) [326] method.

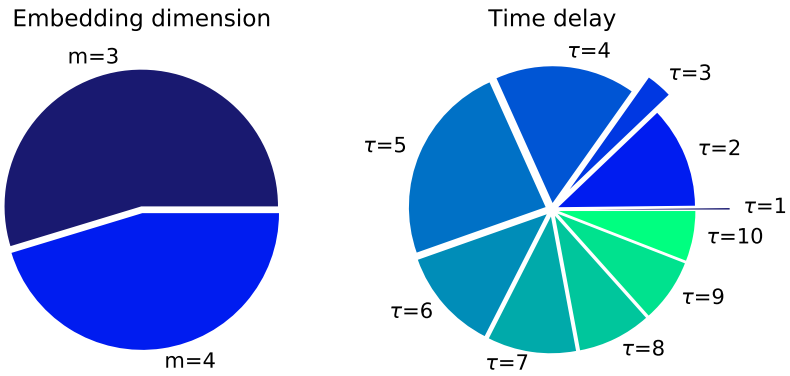

Figure E.2: Frequency of phase space reconstruction parameters in the present study. The embedding dimension, m, and the time delay, τ, were estimated for each 5-second window using the False Nearest Neighbour algorithm and the first local minimum of the average mutual information method.

Recurrence quantification analysis

A recurrence quantification analysis (RQA) provides information regarding hidden periodicities in the aforementioned phase space trajectory. Such information can be accessed by computing the recurrence plot (RP) of a given time series [327]. The first step to obtaining such representation is to compute the square matrix with dimensions $N \times N$ (known as the colour recurrence plot), containing the pairwise Euclidean distance (given by the norm $||\cdot||$) between all samples of the trajectory, N, in the m-dimensional space. Afterwards, a threshold distance ε is used to define a sphere centred at the state x_i. If x_j falls within that sphere, then the Heaviside function $\Theta(\cdot)$ decides for $R_{i,j} = 1$, meaning the states are close to each other. Otherwise, $R_{i,j} = 0$. This binary matrix, symmetric along the identity line, can therefore be visualised in a black ($R_{i,j} = 1$) and white plot ($R_{i,j} = 0$), the RP. In this study, the value of ε was estimated for each 5-second non-overlapping window, corresponding to 10% of the maximum phase space diameter [328]. The RQA returned seven RP measures of complexity, which quantify recurrence point density and indicate the existence of diagonal and/or vertical lines in the RP [328, 329]. The following RQA features were computed:

- Recurrence rate (REC).
- Determinism (DET).
- Average diagonal line length (L).
- Length of the longest diagonal line (L_{max}).
- Laminarity (LAM).
- Trapping time (TT).
- Shannon entropy (ENT).

E.1.3 Multivariate features

A total of 495 multivariate features were computed and are described below. First, bivariate measures were computed for all EEG channel pairs. Then graph measures were extracted from the obtained connectivity matrices.

Undirect connectivity measures (per frequency band)

- Circular omega complexity [351].
- Circular correlation [351].
- Intersite phase clustering [58, 258].
- Phase lag index [58, 74, 258, 352].
- Weighted phase lag index [58, 74, 352].

- Debiased weighted phase lag index [58, 352].
- Spearman's correlation coefficient [58].
- Spearman's correlation coefficient for instantaneous power [58].
- Normalised cross-correlation [14, 74, 353, 354].
- Normalised cross-correlation for instantaneous power [14, 353, 354].

Direct connectivity measures (per frequency band)

- Phase slope index [58, 352].

Graph indexes for undirect connectivity measures

With the exception of circular omega complexity (which are already a multivariate measure of connectivity), all the remaining bivariate features were analysed using the following graph measures. These are measures of local and global connectivity [58, 74, 355, 356]:

- Assortativity (A).
- Characteristic path length (CPL).
- Global efficiency (GE).
- Modularity (M).
- Mean network degree (MD).
- Mean strength (MS).
- Mean closeness centrality (MCC).

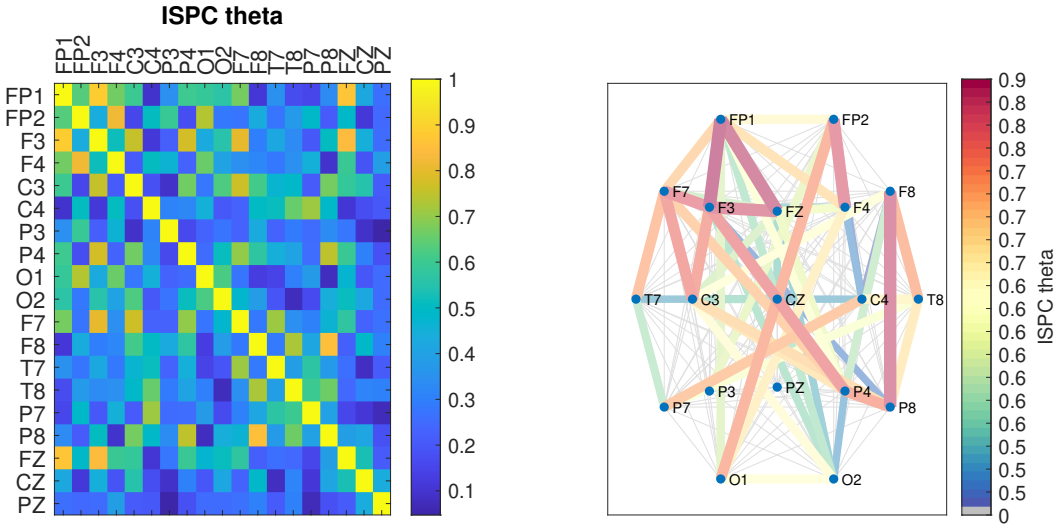

Figure E.3: Connectivity matrix obtained for theta band intersite phase clustering for the 5-second EEG window located 4.5 hours before the onset of the first seizure of patient 402. Grey edges indicate non-significant interaction strengths.

- Mean betweenness centrality (MBC).
- Transitivity (T).
- Mean weighted clustering coefficient (WGCC).

Graph indexes for direct connectivity measures

The following graphs measures were extracted from the connectivity matrix of the phase slope index bivariate feature [355]:

- Assortativity (A).
- Characteristic path length (CPL).
- Global efficiency (GE).
- Modularity (M).
- Mean strength (MS).
- Mean betweenness centrality (MBC).
- Mean incloseness centrality (MCIC).
- Mean outcloseness centrality (MCOC).

E.1.4 Feature significance in seizure prediction studies

Most of the univariate linear features described above have been widely used in the context of seizure prediction. For instance, statistical measures have been shown to significantly change during the preictal period compared to the interictal state [11, 14, 90, 234]. The preictal interval has been associated with a decrease in the variance and an increase in the kurtosis [11]. Hjorth parameters (mobility and complexity) were also reported to increase during the preictal interval [14]. The decorrelation time was documented to decrease near the seizure onset [11]. Pinto *et al.* concluded that Hjorth mobility and skewness were highly discriminating features, often selected by their evolutionary seizure prediction model [157].

Extracting frequency-domain univariate linear features has been extensively performed in seizure prediction [11]. Mormann *et al.* [14] showed a decrease in delta band power during the preictal period, accompanied by a relative increase of power in the other subbands. Park *et al.* documented gamma frequency bands to be the most discriminating features when classifying interictal and preictal samples [179]. Pinto *et al.* reported theta band relative power and mean normalised frequency as the most frequently extracted features by their seizure prediction model. Spectral edge frequency at 75% of the spectrum was later reported by the same authors to arise as a highly discriminating feature in seizure prediction [157].

Additionally, univariate nonlinear features have been investigated in seizure prediction. The LLE, CD, fractal dimension, recurrence quantification analysis, and

approximate and sample entropies are frequently considered to develop prediction models [11, 13, 61, 133, 177, 350]. Mormann *et al.* [14] observed an increase of the LLE 30 minutes before seizure onset. In this study, different measures of fractal dimension were extracted. Higuchi's fractal dimension has already been used in the context of seizure prediction [61, 338]. The DFA has been mainly used to measure the long-range correlation of the electrocardiogram [321]. In epilepsy, DFA has been often considered to identify the disease characteristics [357, 358] and for the non-invasive localisation of the epileptic zone before presurgical evaluation [359]. More recently, some attempts have been documented on the use of DFA in seizure prediction studies [342, 360]. Initially, the monofractal perspective on the EEG oscillations was typically addressed by a monofractal DFA analysis. However, the nonstationary nature of EEG demands a multifractal DFA that contemplates the existence of large and small fluctuations [343, 357]. Besides adding a multifractal DFA, the method of multifractal 1-D Wavelet Leader estimates was also considered. This decision was supported by the simplicity of the methods' implementation (the `dwtleader` Matlab function was used) associated with the potential of simultaneously characterising multifractal properties and exploring wavelet self-similarity structures [344].

Even though uncertainty exists as to whether nonlinear features bring discriminatory power or not, there are some studies indicating that higher prediction performance can be obtained by combining linear and nonlinear features [164]. Moreover, a method that is able to capture the nonlinear nature of EEG signals may provide valuable insight into brain dynamics [61].

The inspection of multivariate features in this study is supported by some studies reporting increased prediction performance when using bivariate features, in comparison with univariate linear features [14, 235]. Although multivariate features were analysed, these are global measures computed from graphs of bivariate measures. It is important to note that using bivariate measures as input to the feature reduction methods would result in a considerable increase in the feature reduction computational time (as a total of 7695 bivariate features would be analysed).

Ultimately, when studies conducted a feature selection step in the seizure prediction methodology, high inter-patient variability is often observed [234, 235]. This further motivates the inclusion of different types of features in this study.

E.2 EEG feature data preparation

After feature extraction, the feature datasets obtained for each feature group (univariate linear, univariate nonlinear, and multivariate) and each seizure were inspected. Specifically, constant and quasi-constant features were sought in the three feature groups. Constant (corresponding to features that have the same value for all 5-second windows) and quasi-constant features (corresponding to features for which more than half of the values are equal) were discarded from further analysis.

Given that constant and quasi-constant features were sought for each seizure independently, the feature dataset after discarding constant and quasi-constant features could differ among seizures. That was only verified for the multivariate feature group. In fact, no constant features were found for univariate linear and univariate nonlinear features. Alpha peak frequency, decorrelation time and spectral edge frequency (at 50%) were the quasi-constant features removed over all channels and seizures from the univariate linear feature group. The remaining univariate linear features were selected (not discarded) over all channels and seizures. RQA feature L_{max} was the only quasi-constant feature found across all channels for the univariate nonlinear feature group. The remaining univariate nonlinear features were selected over all channels and seizures.

For the multivariate feature group, the feature dataset (resulting after discarding constant and quasi-constant features) would differ from seizure to seizure. Based on that, information regarding the constant, quasi-constant and the features that showed across all seizures is provided in Table E.1. A total of 15 (3.0%), 111 (22,4%), and 216 (43.6%) constant, quasi-constant, and selected (over all channels and seizures) multivariate features were identified, respectively.

Table E.1: Information regarding the constant, quasi-constant and selected (not discarded over all channels and seizures) multivariate EEG features.

Feature	Graph index	Delta	Theta	Alpha	Beta	Gamma
Circular omega complexity	—	■	■	■	■	■
Circular correlation	A	■	■	■	■	■
	CPL	■	■	■	■	■
	GE	■	■	■	■	■
	M		■	■	■	■
	MBC	■	■	■	■	■
	MCC	■	■	■	■	■
	MD	■	■	■	■	■
	MS	■	■	■	■	■
	T	■	■	■	■	■
	WGCC	■	■	■	■	■
Spearman's correlation coefficient	A	■	■			
	CPL	■	■	■	■	■
	GE	■	■	■		
	M	■	■	■		
	MBC		■	■	■	■
	MCC	■				
	MD		■	■	■	■
	MS	■	■	■		
	T	■				
	WGCC	■				
Spearman's correlation coefficient for instantaneous power	A	■				
	CPL	■	■	■	■	■
	GE	■				
	M	■				
	MBC	■	■	■	■	■
	MCC					■
	MD	■	■	■		■
	MS	■				
	T	■				
	WGCC	■				

Continued on next page

Feature	Graph index	Delta	Theta	Alpha	Beta	Gamma
Normalised cross-correlation	A	■	■	■		
	CPL	■	■	■	■	■
	GE	■	■	■	■	
	M	■	■	■		
	MBC	■	■	■	■	■
	MCC	■				
	MD	■	■	■	■	■
	MS	■	■	■	■	
	T	■				
	WGCC	■				
Normalised cross-correlation for instantaneous power	A	■	■	■		
	CPL	■	■	■	■	■
	GE	■	■	■	■	
	M	■	■	■		
	MBC	■	■	■	■	■
	MCC	■				
	MD	■	■	■	■	■
	MS	■	■	■	■	
	T	■				
	WGCC	■				
Phase lag index	A	■	■	■	■	■
	CPL	■				
	GE	■				
	M	■				
	MBC	■	■	■		
	MCC	■				
	MD	■	■	■		
	MS	■				
	T	■	■			
	WGCC	■				

Continued on next page

Feature	Graph index	Delta	Theta	Alpha	Beta	Gamma
Weighted phase lag index	A	■	■	■		
	CPL	■	■	■	■	■
	GE	■	■	■		
	M	■	■			■
	MBC	■	■	■	■	■
	MCC	■				■
	MD	■	■	■	■	■
	MS	■	■	■		
	T	■	■		■	■
	WGCC	■	■		■	■
Debiased weighted phase lag index	A	■			■	■
	CPL	■	■	■	■	■
	GE	■			■	■
	M	■			■	■
	MBC	■	■	■	■	■
	MCC	■			■	■
	MD	■	■	■	■	■
	MS	■			■	■
	T	■				
	WGCC	■				
Intersite phase clustering	A	■	■	■	■	■
	CPL	■	■	■	■	■
	GE	■	■	■	■	■
	M		■	■	■	■
	MBC	■	■	■	■	■
	MCC	■	■	■	■	
	MD	■	■	■	■	■
	MS	■	■	■	■	■
	T	■	■	■	■	
	WGCC	■	■	■	■	

Continued on next page

Feature	Graph index	Delta	Theta	Alpha	Beta	Gamma
Phase slope index	A					
	CPL					
	GE					
	M					
	MS					
	MBC					
	MCIC					
	MCOC					

Constant (■), quasi-constant (■) and selected (■) multivariate features.

E.3 Sleep-wake cycle detection

A sleep-wake classifier was designed to distinguish between periods during which the patient is awake (stage of wakefulness) or sleeping (stage of sleep) [291]. The details regarding the classifier's development are provided below.

E.3.1 Database

The EPILEPSIAE database contains scalp EEG recordings accompanied by information regarding the vigilance state of the patient only at the onset of the experienced seizures. This type of information is not provided over the remaining time of monitoring. So, even though this database's content was used to search for preictal brain activity, an appropriate database had to be considered to develop a sleep-wake classifier. The Cyclic Alternating Pattern (CAP) EEG activity database [361, 362], known as CAP Sleep database, and online available at PhysioNet (https://physionet.org/content/capslpdb/1.0.0/), was selected for this study. The database comprises manual sleep annotations over scalp EEG recordings collected from patients with epilepsy. With these data, a sleep-wake model was built and further applied to the EPILEPSIAE data considered for the unsupervised search of the preictal interval. This way, it could be possible to understand the influence of the sleep-wake cycle, computed over the 4.5 hours before each seizure's onset, on the obtained results.

CAP Sleep database contains multimodal recordings that have been visually inspected and annotated by expert neurologists according to Rechtschaffen and Kales (R&K) rules. The resulting manual annotations include wakefulness (W), NREM sleep stages (N1-4), REM sleep stage (R), and body movements (MT).

The multimodal recordings were collected from healthy subjects and subjects presenting different neurological conditions. For this study, data from 33 patients with nocturnal frontal lobe epilepsy (19 male; age range: 16-67 years; mean age: 31 ± 11 years) were selected. Besides the requirement of analysing data from patients diagnosed with epilepsy, the selected data also fulfilled a second criterion. Specifically, only scalp EEG recordings for which the most common combination of channels could be found were considered herein.

Table E.2 presents the information about each patient comprised in the selected CAP Sleep database. The analysed scalp EEG recordings were acquired with a sampling frequency of 128 or 512 Hz at the Sleep Disorders Center of the Ospedale Maggiore of Parma, in Italy. The electrodes were placed according to the International 10-20 System, resulting in 12 EEG channels organised in a bipolar montage: FP2-F4, F4-C4, C4-P4, P4-O2, FP1-F3, F3-C3, C3-P3, P3-O1, F8-T4, T4-T6, F7-T3, and T3-T5. In total, the recordings used to develop the sleep-wake detection model contain approximately 29 hours of wakefulness state and 244 hours of sleep

state.

E.3.2 Preprocessing

According to the files' information, the EEG signals from the CAP Sleep database were already filtered using a 50 Hz notch filter to remove the power-line interference and a 0.5-30 Hz bandpass filter.

Additionally, since the EEG recordings were collected with either 128 or 512 Hz sampling frequency, the signals sampled at 512 Hz were downsampled to 128 Hz.

E.3.3 Feature extraction

The first step consisted in segmenting the EEG signals into epochs of 30 seconds without overlap. This segment length was chosen since: (i) each sleep annotation included in the CAP Sleep database refers to 30 seconds of the data, and (ii) this period is widely adopted by Automatic Sleep Stage Classification (ASSC) studies [363, 364].

Afterwards, 22 univariate linear features [363, 364], listed below, were extracted from each epoch and each of the 12 EEG channels:

- Statistical moments (mean, variance, skewness, and kurtosis).
- Hjorth parameters (mobility and complexity).
- Relative spectral power in the following frequency bands: delta (0.5-4 Hz), theta (4-8 Hz), alpha (8-13 Hz) and beta (13-27 Hz).
- Spectral edge frequency and spectral edge power (50%, 75% and 90%).
- Energy of wavelet coefficients obtained using Daubechies (db4) mother wavelet at five levels of decomposition (detail coefficients D1: 32-64 Hz, D2: 16-32 Hz, D3: 8-16 Hz, D4: 4-8 Hz, D5: 2-4 Hz, and approximation coefficient A5: 0-2 Hz).

E.3.4 Feature selection and classification

Supported by state of the art regarding ASSC studies, a patient-independent analysis was implemented, assuming the existence of common neuronal characteristics underlying wakefulness and sleep stages among different subjects. The selected CAP Sleep dataset was randomly split into training and testing sets, with 70% of patients used to train the model and the remaining 30% to test it. In sum, the testing phase was based on unseen data from 10 patients.

Each 30-second epoch was assigned one of two classes: wakefulness or sleep. The wakefulness label corresponds to the original annotations provided with the CAP Sleep database. The sleep label was assigned when NREM and REM sleep stages were originally annotated. Segments of data not containing manual CAP sleep annotations were removed.

As the CAP Sleep database recordings were collected mainly at night while patients were sleeping, there is a considerable imbalance between sleep and wakefulness classes (244 hours of sleep state versus 29 hours of the wakefulness state). The class imbalance was addressed by implementing random undersampling, i.e., obtaining an equal number of segments for each class by randomly selecting segments from the majority class, sleep in this case, and further discarding the remaining segments from the training dataset. Given that EEG time series are under analysis, a restriction was imposed to the segment selection process. Namely, considering that the number of segments from the minority class, in this case, wakefulness, is given by n, the entire set of sleep segments was divided into n groups and one sleep segment was randomly selected from each group, discarding the remaining segments. This way, it was possible to maintain the sequential chronology and representativeness of data.

The feature selection method corresponds to a filter method that provides a feature ranking from which it is possible to select the k most discriminative features. The Analysis of Variance (ANOVA) f-test was used to estimate the degree of linear dependency between each feature and the target classes [365]. In order to find the most suitable number of features, k, to be selected, a grid-search procedure was implemented.

ASSC studies indicate a widely used classifier, the Support Vector Machine (SVM) classifier, shown to outperform other classifiers [363,364]. An SVM classifier was used, considering a linear kernel that requires tuning the cost hyperparameter C, achieved via grid-search.

The grid-search step was then implemented to find the optimal parameters to train the SVM classifier. Specifically, 85 combinations of 5 values of k (10, 20, 30, 40, and 50 features) and 17 values of C (2^C, $C[-20, ... -2, 0, 2, ..., 12]$) were explored. The best combination (k, C) was obtained with a Leave-One(Subject)-Out Cross-Validation strategy where each of the 23 patients considered for the training phase was left out for validation. Accordingly, each time a patient was left out for validation, the remaining 22 patients were used to train the classifier. Performance was evaluated based on the sensitivity (SS) and specificity (SP) as follows: $\sqrt{SS \times SP}$ [366]. In order to deal with the stochasticity of the undersampling process, each iteration was performed 31 times. In sum, for each combination (k, C), a final performance is obtained by averaging performances over the 23 iterations and 31 classifiers within each iteration. After evaluating all the combinations (k, C), the combination with the highest average performance yields the optimal parameters. Finally, 31 classifiers were trained using the tuned k and C parameters, obtained from the grid-search, and the entire training dataset (23 patients). Similarly to grid-search, 31 classifiers were trained to address the stochasticity inherent to the undersampling process. Additionally, as explained in the next section, these 31 classifiers were used in the testing phase, where a majority voting system was used to

obtain the final classification.

E.3.5 Out-of-sample classification

In the testing phase, the sleep-wake cycle classifier was assessed regarding the out-of-sample performance in an unseen dataset comprising data from 10 patients.

Whenever the trained sleep-wake model is applied to new, unseen data, the following steps are performed: (i) standardisation of the new data using the z-score parameters (mean and standard deviation) from the training data, (ii) selection of the most discriminative features identified in training phase from the testing dataset, (iii) application of the trained SVM classifier using the C value from grid-search. The 31 classifiers obtained during training are therefore applied to the testing dataset, resulting in 31 output predictions for each sample. The final classifier output results from the classifier ensemble, which consists of a majority voting system. For the case of a binary problem as the sleep/wake detection, the predominant class corresponds to the one for which at least 16 predictions have been made. Therefore, having an odd number of classifiers (31) was used to avoid ties in the final classifier output.

The entire training and testing process is repeated 30 times to deal with the stochasticity of training and testing data splitting [153, 157]. With 30 executions, there is stronger statistical confidence in the results. The obtained testing sensitivity and specificity, each averaged over the 30 executions, is 92.9%±1.6% and 91.4%±3.1%, respectively.

The final model used to obtain the sleep-wake cycle in the EPILEPSIAE dataset corresponds to the sleep-wake model with the best training performance among the 30 executions (sensitivity and specificity of 93.4% and 92.6%, respectively).

Table E.2: Dataset description regarding each patient selected from CAP Sleep database.

P	ID	Sex	Age (years)	Wakefulness time (hh:mm)	Sleep time (hh:mm)	Sampling frequency (Hz)
1	nfle1	F	16	00:11	07:50	512
2	nfle2	F	41	01:39	06:29	512
3	nfle3	M	29	01:07	08:09	512
4	nfle4	M	18	00:31	08:48	512
5	nfle5	F	22	01:08	07:39	512
6	nfle6	F	32	00:11	06:33	128
7	nfle7	M	26	00:34	08:44	512
8	nfle10	M	18	01:04	06:51	128
9	nfle11	M	31	00:13	08:16	128
10	nfle12	F	67	00:48	08:05	512
11	nfle13	F	36	00:20	07:50	512
12	nfle14	M	35	01:34	06:10	512
13	nfle15	F	29	00:48	07:49	512
14	nfle16	F	30	00:54	07:37	512
15	nfle17	M	25	01:57	05:27	512
16	nfle18	M	25	02:42	06:12	512
17	nfle19	M	25	00:10	07:24	128
18	nfle21	M	27	00:38	08:58	512
19	nfle22	F	42	01:21	07:45	512
20	nfle23	M	20	00:42	07:18	128
21	nfle24	M	39	00:20	06:53	512
22	nfle26	M	38	01:13	06:53	128
23	nfle28	F	28	01:30	07:42	512
24	nfle29	F	36	02:01	05:23	512
25	nfle30	F	26	01:08	07:01	512
26	nfle31	M	33	00:23	07:04	128
27	nfle34	M	26	00:35	07:51	512
28	nfle35	M	44	01:07	06:06	512
29	nfle36	F	18	00:06	08:13	512
30	nfle37	M	16	00:10	07:40	512
31	nfle38	M	31	00:18	07:07	512
32	nfle39	M	24	00:59	07:22	512
33	nfle40	F	60	00:19	08:48	512

P: patient index. ID: patient identifier. Sex: female (F) or male (M). nfle: nocturnal frontal lobe epilepsy.

E.4 Results for unsupervised learning

This section presents the results obtained after performing feature dimensionality reduction and clustering tasks.

E.4.1 Results for clustering solution categorisation

Categorisation performed by each of the five members comprising my epilepsy research team is presented for multivariate (Table E.3), univariate linear (Table E.4), univariate nonlinear (Table E.5), and control univariate linear reduced data (Table E.6).

Figure E.4 depicts the number of seizures for which less than 3, 3, 4, or 5 votes have been observed after the categorisation task. When less than 3 votes would be obtained for a given seizure, the expert team would gather and discuss over the category that should be assigned to that seizure. Importantly, the figure also shows the number of seizures that were assigned a given category with the vote of Expert 1, whom performed the first visual inspection. Figure E.5 depicts the number of categories that resulted from this team discussion.

Table E.3: Multivariate reduced data categorisation by the five experts.

Expert	Cat. 1	Cat. 2	Cat. 3	Cat. 4	Cat. 5	Cat. 6
1	106 (46.9%)	11 (4.9%)	23 (10.2%)	1 (0.4%)	77 (34.1%)	8 (3.5%)
2	89 (39.4%)	8 (3.5%)	22 (9.7%)	0 (0.0%)	94 (41.6%)	13 (5.8%)
3	84 (37.2%)	8 (3.5%)	24 (10.6%)	10 (4.4%)	86 (38.1%)	14 (6.2%)
4	106 (46.9%)	8 (3.5%)	23 (10.2%)	2 (0.9%)	68 (30.1%)	19 (8.4%)
5	66 (29.2%)	37 (16.4%)	24 (10.6%)	0 (0.0%)	52 (23.0%)	47 (20.8%)
Final cat.	**104 (46.0%)**	**9 (4.0%)**	**22 (9.7%)**	**1 (0.4%)**	**79 (35.0%)**	**11 (4.9%)**

Table E.4: Univariate linear reduced data categorisation by the five experts.

Expert	Cat. 1	Cat. 2	Cat. 3	Cat. 4	Cat. 5	Cat. 6
1	34 (15.0%)	27 (11.9%)	18 (8.0%)	4 (1.8%)	58 (25.7%)	85 (37.6%)
2	42 (18.6%)	21 (9.3%)	25 (11.1%)	7 (3.1%)	58 (25.7%)	73 (32.3%)
3	34 (15.0%)	16 (7.1%)	30 (13.3%)	10 (4.4%)	66 (29.2%)	70 (31.0%)
4	38 (16.8%)	25 (11.1%)	32 (14.2%)	5 (2.2%)	54 (23.9%)	72 (31.9%)
5	14 (6.7%)	10 (4.8%)	15 (7.2%)	3 (1.4%)	32 (15.4%)	134 (64.4%)
Final cat.	**38 (16.8%)**	**21 (9.3%)**	**19 (8.4%)**	**5 (2.2%)**	**61 (27.0%)**	**82 (36.3%)**

Table E.6: Control univariate linear reduced data categorisation by the five experts.

Expert	Cat. 1	Cat. 2	Cat. 3	Cat. 4	Cat. 5	Cat. 6
1	18 (38.3%)	13 (27.7%)	5 (10.6%)	4 (8.5%)	5 (10.6%)	2 (4.3%)
2	24 (51.1%)	10 (21.3%)	6 (12.8%)	2 (4.3%)	0 (0.0%)	5 (10.6%)
3	19 (40.4%)	10 (21.3%)	9 (18.1%)	4 (8.5%)	2 (4.3%)	3 (6.4%)
4	19 (40.4%)	10 (21.3%)	10 (21.3%)	4 (8.5%)	2 (4.3%)	2 (4.3%)
5	25 (53.2%)	6 (12.8%)	9 (19.1%)	2 (4.3%)	3 (6.4%)	2 (4.3%)
Final cat.	**21 (44.7%)**	**10 (21.3%)**	**8 (17.0%)**	**4 (8.5%)**	**2 (4.3%)**	**2 (4.3%)**

Table E.5: Univariate nonlinear reduced data categorisation by the five experts.

Expert	Cat. 1	Cat. 2	Cat. 3	Cat. 4	Cat. 5	Cat. 6
1	81 (35.8%)	40 (17.7%)	23 (10.2%)	4 (1.8%)	58 (25.7%)	20 (8.8%)
2	87 (35.8%)	25 (11.1%)	26 (11.5%)	13 (5.8%)	56 (24.8%)	19 (8.4%)
3	67 (29.6%)	28 (12.4%)	25 (11.1%)	18 (8.0%)	69 (30.5%)	19 (8.4%)
4	85 (37.6%)	27 (11.9%)	31 (13.7%)	6 (2.7%)	54 (23.9%)	23 (10.2%)
5	53 (23.5%)	50 (22.1%)	19 (8.4%)	3 (1.3%)	48 (21.2%)	53 (23.5%)
Final cat.	**79 (35.0%)**	**32 (14.2%)**	**26 (11.5%)**	**5 (2.2%)**	**63 (27.9%)**	**21 (9.3%)**

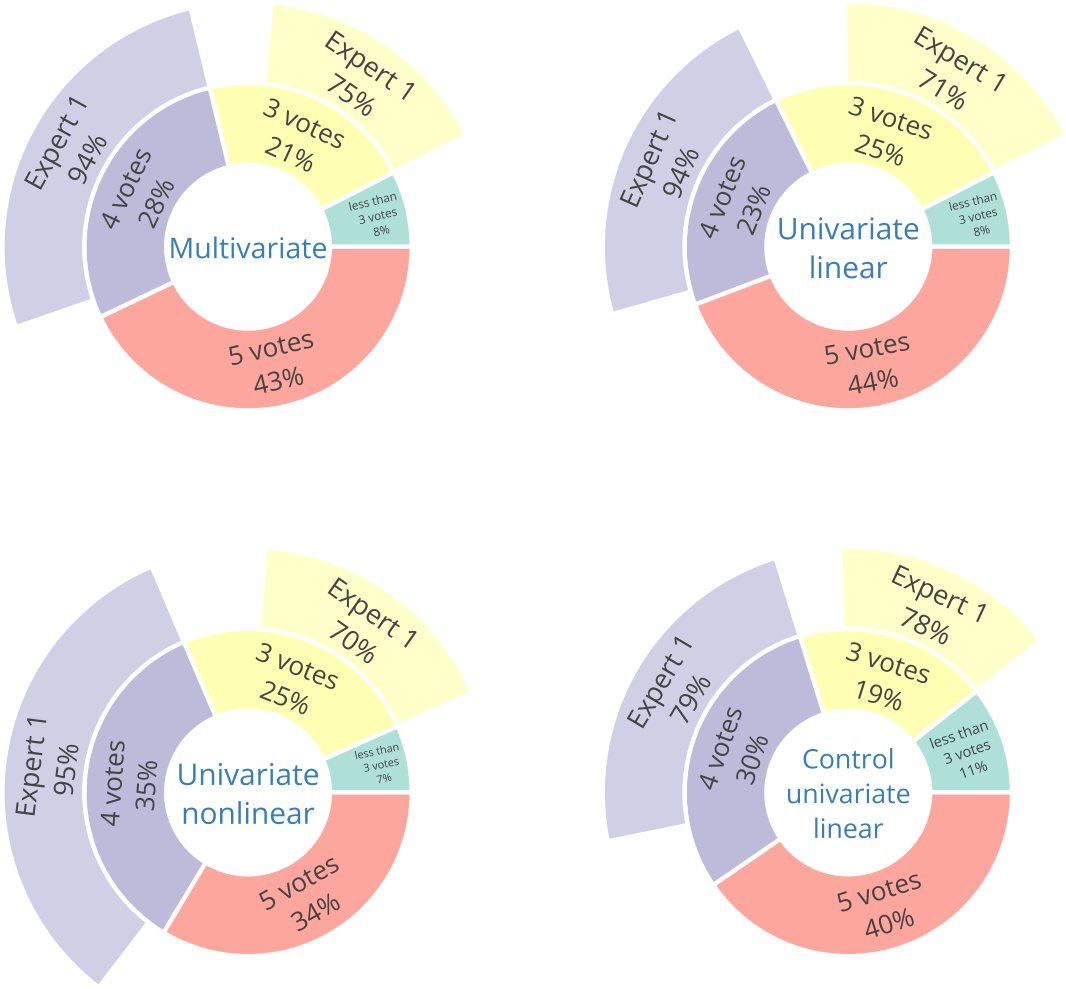

Figure E.4: Number of votes obtained for each seizure and each feature group after the categorisation task.

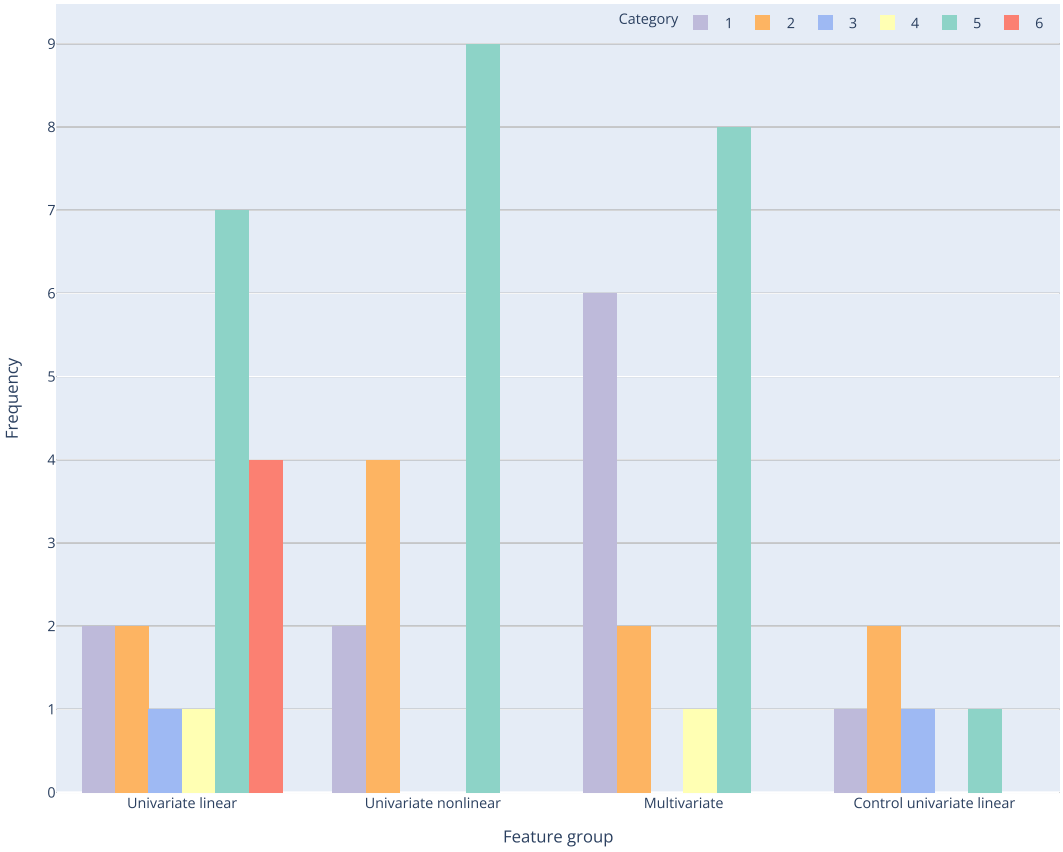

Figure E.5: Number of categories assigned after team member discussion over the categorisation for which less than three votes were obtained. The number of seizures for which the final category was assigned with the vote of Expert 1 (involved in the first inspection of the data) is depicted.

E.4.2 Results for control intervals

In this section presents the results for the analysis of control intervals. Figures E.6 show some examples of seizure distribution para certain patients. The lead seizures, the analysed 4.5 hours of data preceding seizures and the control intervals are depicted. Figures for all patients are provided in the GitHub page.

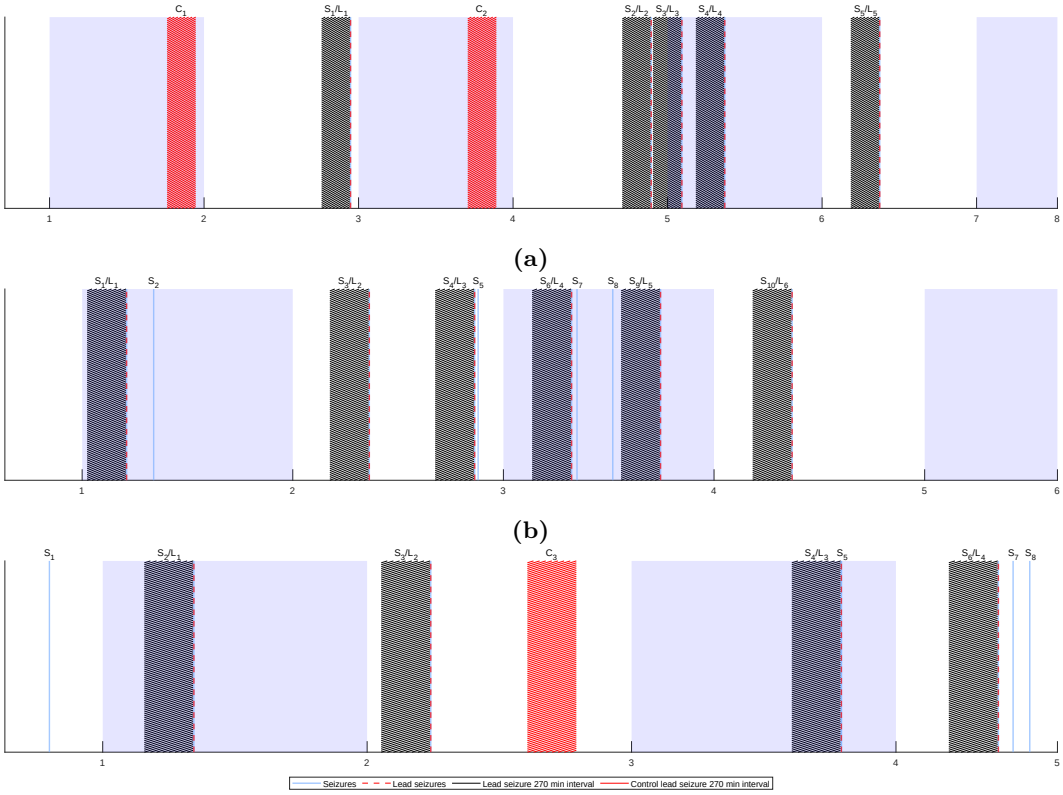

Figure E.6: Seizure distribution for patients (a) 402, (b) 80702 and (c) 53402. White and purple rectangles identify each subsequent day. In (a) the 4.5-hour interval was analysed for all seizures while only two 4.5-hour control intervals were analysed. In (b) the 4.5-hour interval was analysed for six seizures while no 4.5-hour control intervals were analysed. In (c) the 4.5-hour interval was analysed for four seizures while only one 4.5-hour control interval was analysed.

Table E.7 shows the categories assigned to the two 4.5-hour intervals analysed for each seizure: the one preceding the onset and the control interval. This analysis was conducted for the univariate linear feature group. The seizures categorised as 3 or 6 in the 4.5-hour interval preceding the onset are indicated in bold.

Table E.7: Categorisation results for the 4.5 hours of data before seizure and for the corresponding control interval.

	ID	S	Category	Category control		ID	S	Category	Category control		ID	S	Category	Category control
1	**402**	**1**	**6**	**1**	**17**	**58602**	**2**	**3**	**3**	**33**	**98102**	**2**	**3**	**3**
2	**402**	**2**	**3**	**1**	**18**	**59102**	**5**	**6**	**1**	34	98102	3	5	1
3	8902	1	5	4	**19**	**60002**	**1**	**6**	**1**	35	98202	1	4	1
4	11002	1	5	1	**20**	**64702**	**2**	**6**	**2**	**36**	**98202**	**2**	**6**	**1**
5	21902	1	5	1	**21**	**75202**	**1**	**3**	**3**	**37**	**102202**	**1**	**6**	**6**
6	23902	3	2	1	22	85202	1	5	4	**38**	**109502**	**1**	**6**	**3**
7	30802	1	5	2	23	93402	1	5	1	39	109502	4	5	2
8	32702	1	5	1	**24**	**93402**	**4**	**3**	**2**	40	110602	1	5	1
9	45402	1	1	4	25	93902	1	5	2	41	110602	3	4	2
10	50802	1	1	1	26	93902	2	1	1	**42**	**112802**	**1**	**6**	**1**
11	50802	3	5	1	**27**	**93902**	**3**	**6**	**3**	43	112802	4	1	5
12	52302	1	5	1	**28**	**94402**	**1**	**6**	**1**	44	112802	6	4	3
13	**53402**	**3**	**3**	**5**	**29**	**94402**	**2**	**6**	**2**	**45**	**113902**	**1**	**6**	**4**
14	56402	2	1	1	**30**	**95202**	**1**	**6**	**2**	46	123902	1	2	1
15	**56402**	**3**	**3**	**2**	**31**	**95202**	**7**	**6**	**3**	47	**123902**	**2**	**6**	**4**
16	**58602**	**1**	**6**	**3**	**32**	**96002**	**7**	**6**	**6**					

ID: patient identifier. S: seizure index.

E.4.3 Visual representation of preictal characteristics

Figures E.7, E.8, E.9 and E.10 display a visual representation of the results for the preictal identification using unsupervised learning.

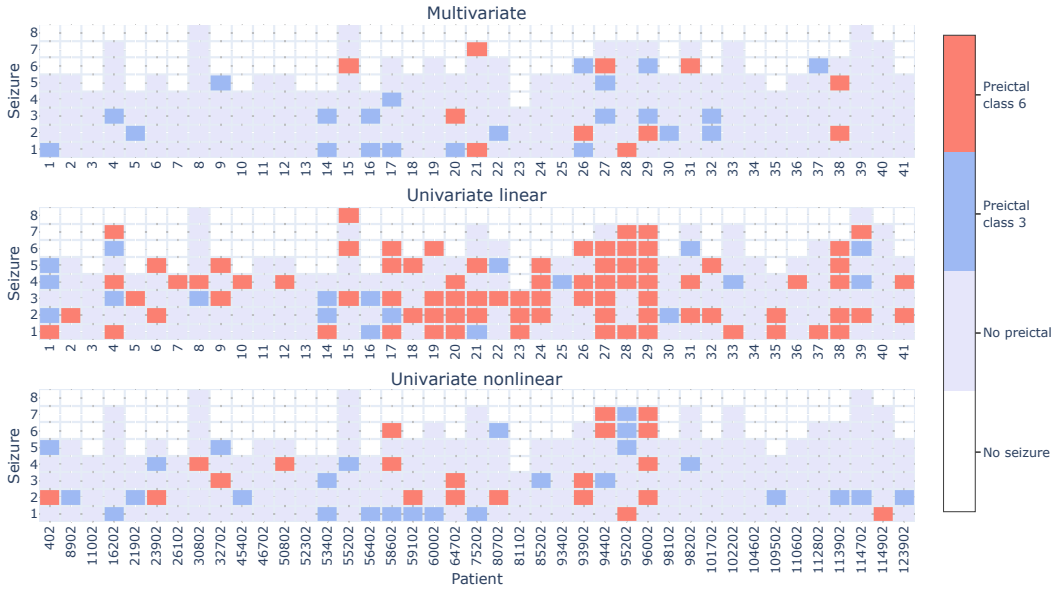

Figure E.7: The results correspond to the evidence of preictal interval found for classes 3 and 6, for the three group of features. Regarding multivariate features, the preictal interval was found for 20 patients (49%) and for 33 seizures (15%). Regarding univariate linear features, the preictal interval was found for 36 patients (88%) and for 101 seizures (45%). Regarding univariate nonlinear features, the preictal interval was found for 29 patients (71%) and for 47 seizures (21%). Multivariate features provided evidence for preictal interval for an additional four seizures, when comparing to univariate features.

Figure E.8: Preictal starting time before seizure onset across patients and seizures.

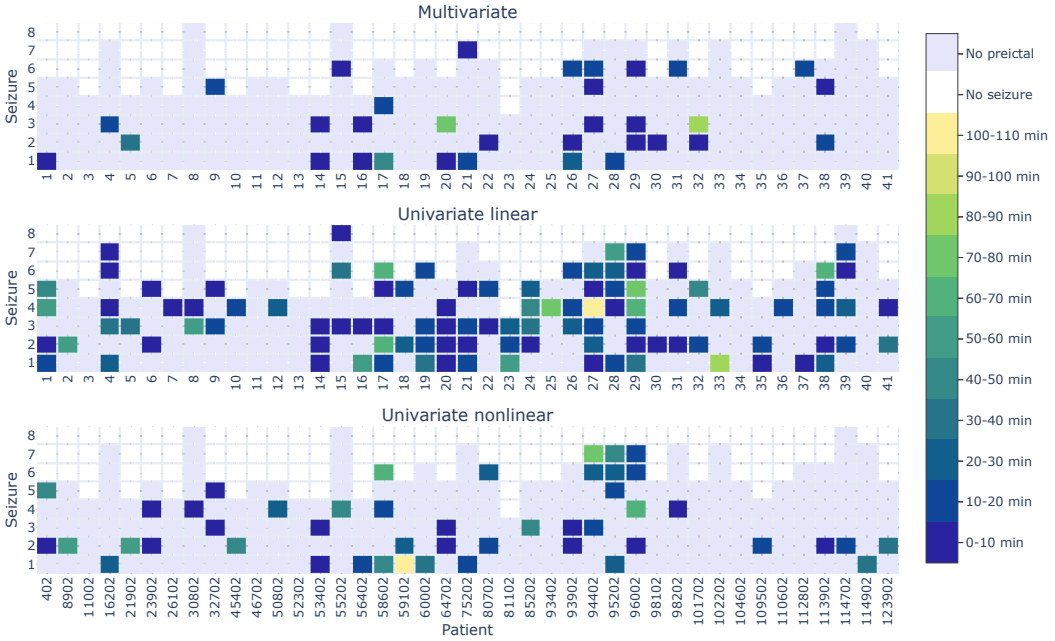

Figure E.9: Preictal duration across patients and seizures.

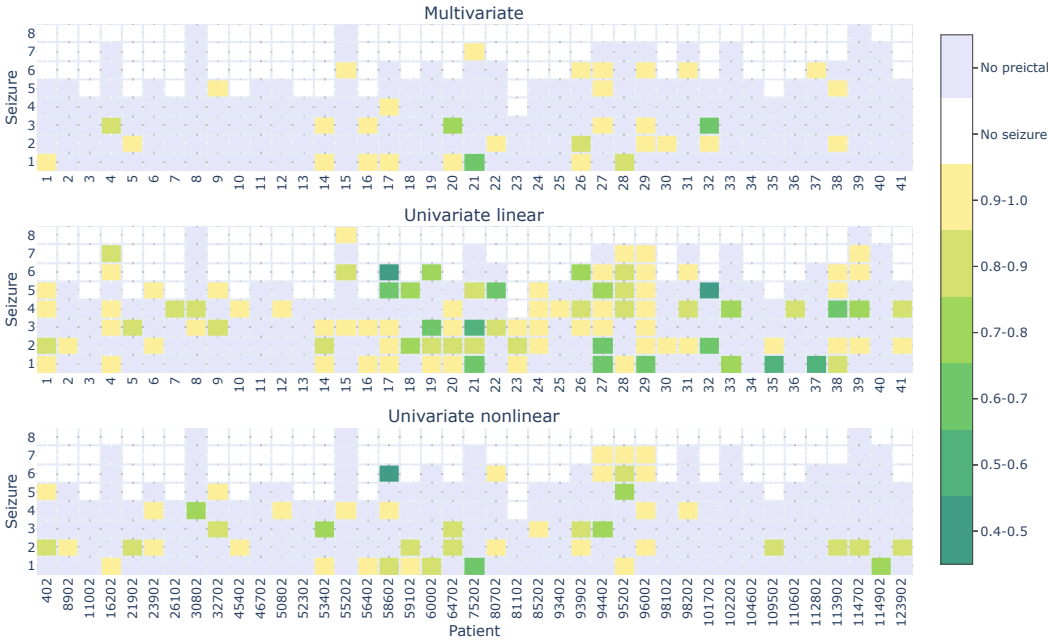

Figure E.10: Preictal cluster density across patients and seizures.

E.4.4 Prevalence of clustering methods

Figure E.11 presents the prevalence of the clustering methods explored in this study. The frequency of each method was assessed for each group of features. The analysis was conducted considering all categories and only categories 3 and 6, where preictal-like behaviour was identified.

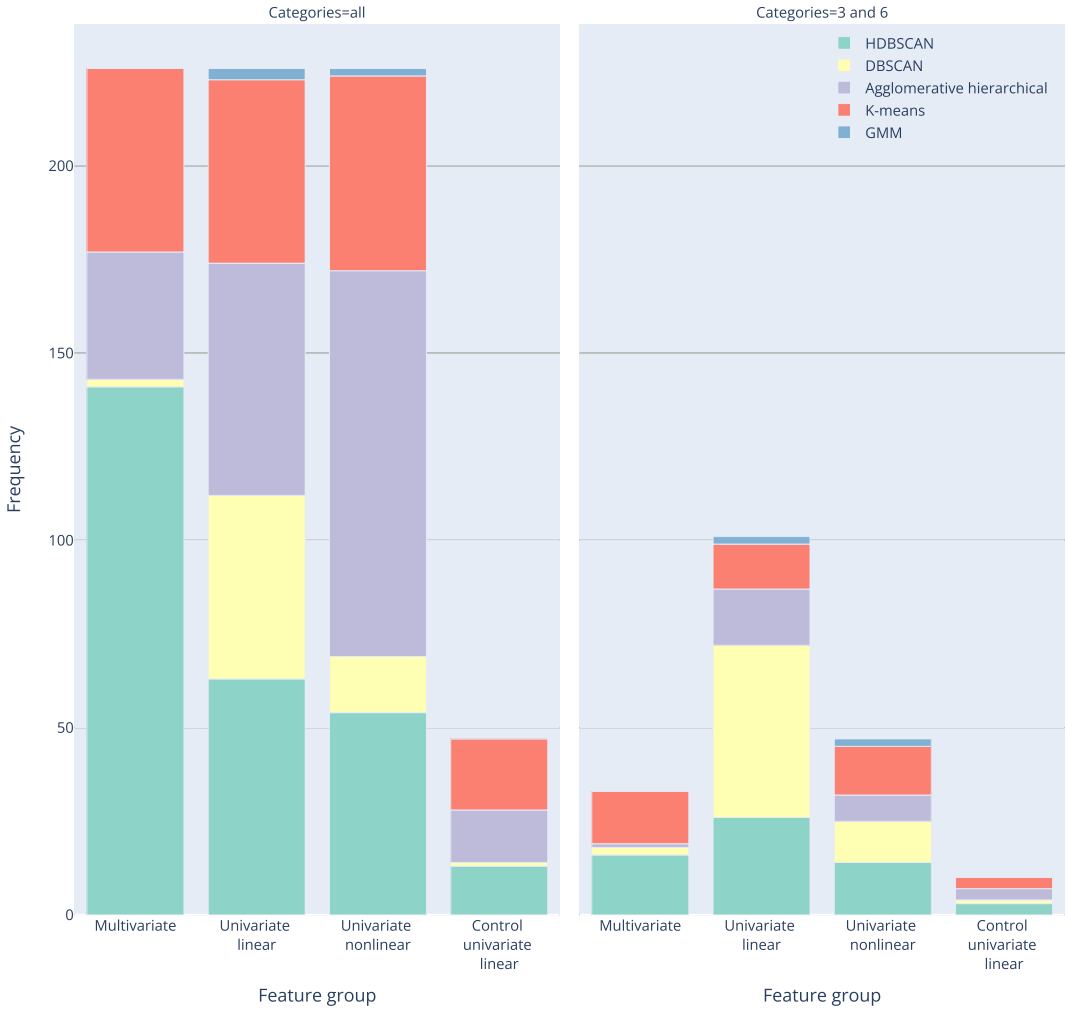

Figure E.11: Frequency of each clustering method computed for each feature group, for all categories and for only categories 3 and 6.

E.4.5 Preictal comparison between EEG and ECG

Figure E.12 presents information regarding the existence of a putative preictal state in EEG and electrocardiography (ECG) data. Additionally, the identified preictal intervals were also characterised in terms of starting time before seizure onset for each modality (see Figure E.13).

The preictal intervals identified in the ECG data were selected according to the time continuity and duration (see Section 5.2.5).

In the case of EEG, the preictal intervals represented in this section were found for either category 3 or 6. It is important to note that when preictal patterns were observed for more than one group of features a final interval had to be chosen. The final preictal interval was chosen according to its characteristics. The first criterion was based on the preictal density as a preictal interval with higher density means that the vast majority (or even all) of the samples belong to the preictal state and there are fewer "jumps" to the remaining clusters. A preictal interval associated with a higher density means that a more evident and permanent change occurs before the seizure onset [155]. The second criterion, used when two preictal intervals had the same density, consisted in choosing a preictal interval based on the duration. In other words, for preictal intervals with different duration, the one with the highest duration was chosen as it provided more statistical confidence in the presence of a preictal state [155]. Lastly, when after these two criteria, two preictal intervals with the same density and duration still occurred, a third criterion was used to select the final interval. Namely, the third criterion consisted of choosing preictal intervals starting near the seizure onset. This means that the patient has to wait less time for the seizure to occur, reducing the impact of larger waiting times on the patient's anxiety levels.

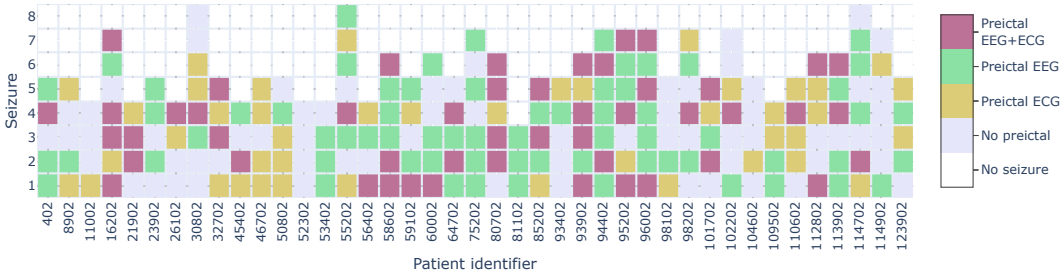

Figure E.12: Results for preictal interval identification. The preictal interval was found for (i) 37 patients (90%) and 116 seizures (51%) in EEG data and (ii) 36 patients (88%) and 92 seizures (41%) in ECG data. Preictal behaviour was found in both EEG and ECG in 22% of the analysed lead seizures (seizures separated from 4.5 hours from the preceding seizure).

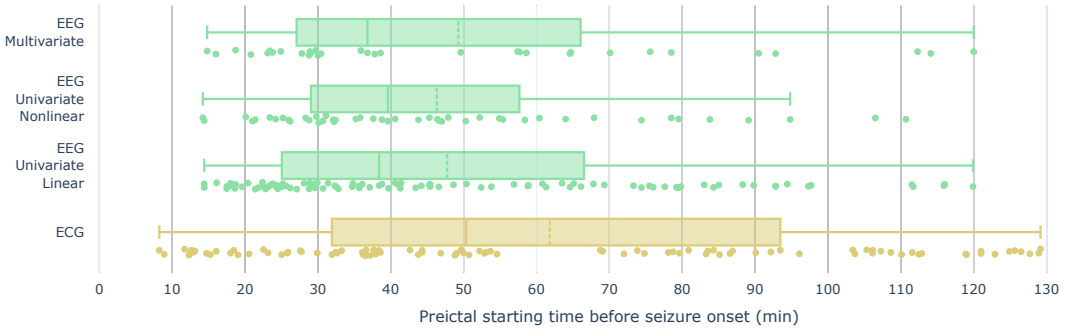

Figure E.13: Results for preictal interval characterisation in terms of starting time before seizure EEG onset, when preictal patterns were found in the analysed EEG lead seizures. Dots correspond to the values of preictal starting time. Solid and dashed lines indicate medians and means, respectively. Box's tops and bottoms indicate the 75th and 25th percentiles, respectively. Whiskers refer to the span of preictal starting time after discarding outliers.

E.4.6 State-of-the-art preictal comparison

Figure E.14 and Table E.8 present the comparison between the preictal intervals obtained using unsupervised learning and the preictal intervals obtained using grid-search supervised learning. This comparison was made for two studies [153, 157] reporting preictal grid-search during seizure prediction model training using the EPILEPSIAE database. The authors provided identification numbers for each patient, allowing for a patient-wise comparison of preictal starting time. In Pinto *et al.* 2021 study [153], the authors present the training results for different values of SOP in their supplementary material. The values that were used to perform the study comparison correspond to the average preictal (SOP plus 10 minutes SPH) interval with the highest value of training fitness. Additionally, when the fitness values were equal for different average preictal intervals, the average preictal interval that starts closer to the seizure onset was chosen, as it means that the patient has to wait less time for a seizure to occur.

The average preictal interval found using unsupervised learning was obtained for each patient by averaging over the starting time of the identified preictal intervals (which were often not found for all seizures of a patient). The criteria to get a final preictal interval when preictal intervals were found for more than one groups of features was clarified in Appendix C.

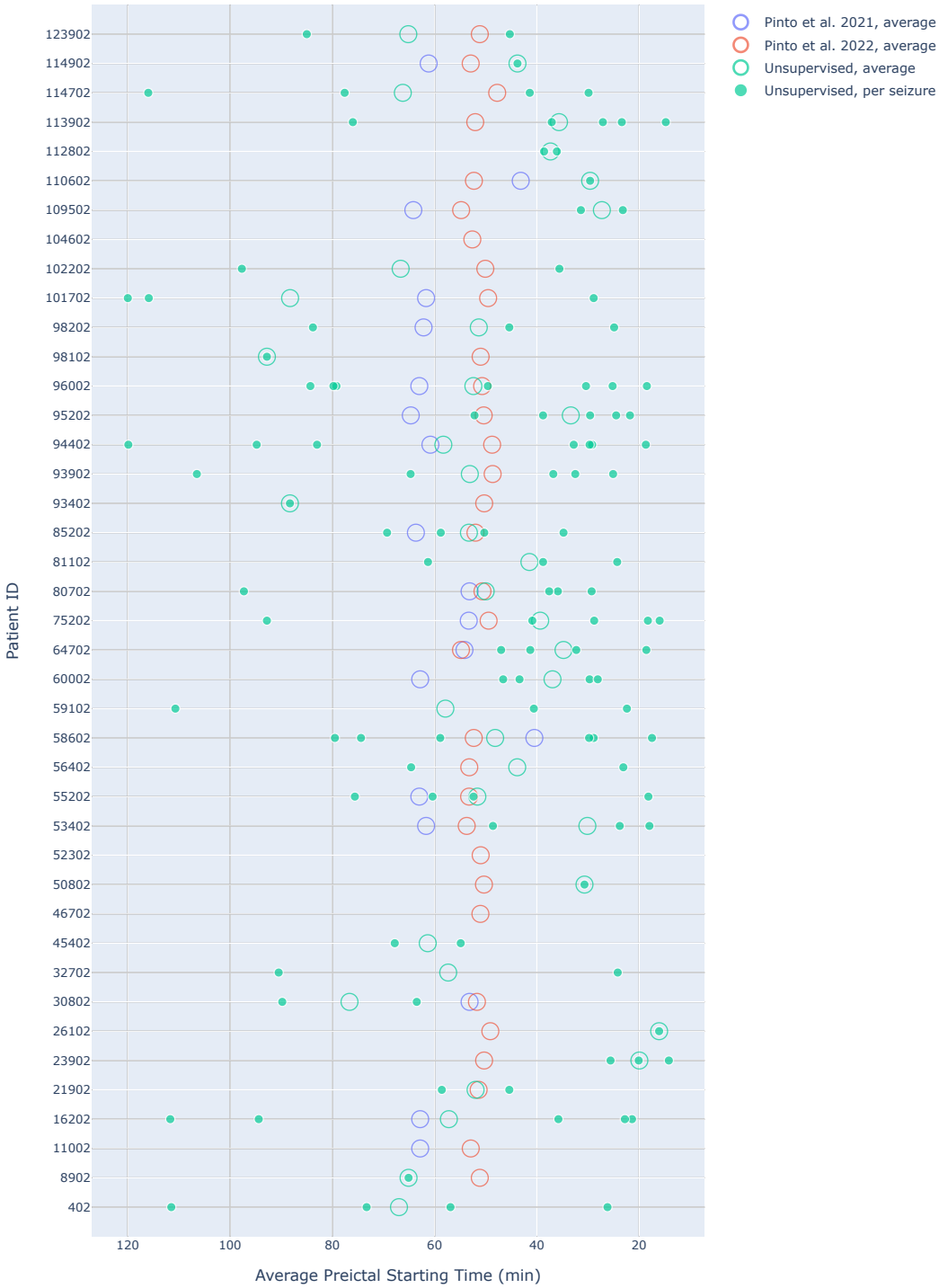

Figure E.14: Representation of the preictal starting time before onset found using unsupervised learning (classes 3 and 6) and using preital grid-search in the two studies by Pinto *el al.* [153, 157].

Table E.8: Comparison of the preictal starting time before seizure onset found using unsupervised learning versus using grid-search supervised learning.

P	ID	Pinto *et al.* 2021		Pinto *et al.* 2022		Unsupervised preictal study			
		Mean	SD	Mean	SD	Mean	SD	#LSz	#PLSz
1	402					56.63	21.49	5	4
2	8902			51.17	9.08	65.10		5	1
3	11 002	62.83	3.34	52.94	10.65			4	0
4	16 202	62.83	3.58			39.02	31.56	7	5
5	21 902			51.40	9.55	54.70	13.15	4	2
6	23 902			50.33	10.39	19.97	5.70	5	3
7	26 102			49.11	7.34	16.10		4	1
8	30 802	53.17	3.02	51.73	8.31	76.65	18.60	8	2
9	32 702					19.30	6.93	5	2
10	45 402					61.35	9.12	4	2
11	46 702			51.05	8.08			5	0
12	50 802			50.36	7.44	30.70		5	1
13	52 302			51.00	8.17			4	0
14	53 402	61.67	2.69	53.73	7.61	26.53	10.18	4	3
15	55 202	63.00	3.56	53.26	9.34	51.63	24.25	8	4
16	56 402			53.23	6.88	45.30	27.29	4	2
17	58 602	40.50	1.50	52.35	11.14	48.17	26.21	6	6
18	59 102					57.90	46.62	5	3
19	60 002	62.83	2.79			36.95	9.41	6	4
20	64 702	54.17	3.67	54.85	7.57	27.43	11.44	5	4
21	75 202	53.33	2.98	49.45	8.64	45.20	33.05	7	4
22	80 702	53.17	2.41	50.65	8.26	48.13	33.05	6	4
23	81 102					41.47	18.64	3	3
24	85 202	63.67	2.56	52.02	11.45	51.78	15.30	5	4
25	93 402			50.31	8.29	88.30		5	1
26	93 902			48.66	7.89	49.70	38.09	6	4
27	94 402	60.83	1.86	48.76	9.00	57.90	40.35	7	7
28	95 202	64.67	2.87	50.41	10.48	32.94	12.48	7	5
29	96 002	63.00	3.06	50.72	7.60	46.71	32.27	7	7
30	98 102			51.01	8.16	92.80		5	1
31	98 202	62.17	2.79			41.37	14.87	7	3
32	101 702	61.67	2.69	49.54	8.12	72.40	61.52	5	2
33	102 202			50.09	8.40	66.65	43.91	7	2
34	104 602			52.63	8.68			5	0
35	109 502	64.17	3.44	54.82	8.58	27.30	5.80	4	2
36	110 602	43.17	3.98	52.32	8.01	29.60		5	1
37	112 802					36.10		6	1
38	113 902			52.06	7.22	35.68	23.92	6	5
39	114 702			47.77	7.98	66.23	38.91	8	4
40	114 902	61.17	2.48	52.95	8.07	43.80		7	1
41	123 902			51.17	9.63	65.15	28.07	5	2
Mean		58.53		51.31		50.06			
SD		7.08		1.73		28.92			

P: patient index. ID: patient identifier. SD: standard deviation. Empty cells indicate that patients were not analysed in Pinto *et al.* studies [153, 157]. Empty cells found in unsupervised preictal learning indicate patients for which no preictal interval was identified. #LSz: number of lead seizures analysed in study. #PLSz: number of lead seizures with preictal interval.

E.5 Metadata analysis

The metadata analysis was performed for each feature group to infer about the influence of seizure characterising variables on the preictal identification results. As shown in Table C.1, vigilance state, onset hour, and ILAE seizure classification are categorical variables, whereas the noise variable is a continuous numerical variable.

First, the Kruskal-Wallis statistical test was computed between the pairs of categorical and numerical variables indicated in Table E.9. The returned p-values indicated that the Kruskal-Wallis test rejected the null hypothesis that the pairs of variables came from the same distribution at a 1% significance level.

The bias-corrected Cramér's V measure was computed to verify the association between each pair of categorical variables. Cramér's V values vary from 0 (corresponding to no association between the variables) to 1 (complete association). The Cramér's V measure corresponds to the absolute value of the phi coefficient when the two variables under study are binary variables. The results in Table E.9 show that no pair of categorical variables verifies any association.

Table E.9: Metadata analysis for the output of the preictal study for each seizure.

		Preictal	**Multivariate**	**Univariate linear**	**Univariate nonlinear**
		0: No preictal; 1: Preictal	0: No preictal; 1: Category 3 preictal; 2: Category 6 preictal		
Vigilance state	0: FOIA 1: FOA 2: FBTC 3: UC	0.14†	0.09†	0.03†	0.00†
ILAE classification	0: W, 1: N1 2: N2, 3: R	0.00†	0.00†	0.00†	0.06†
Onset hour	24 categories	0.38†	0.20†	0.26†	0.22†
Noise		1.21e-56*	1.09e-72*	2.05e-51*	5.44e-68*

Seizure vigilance state: wakefulness (W), NREM sleep stage I (N1), NREM sleep stage II (N2), REM sleep stage (R). Seizure ILAE classification: focal onset aware (FOA), focal onset impaired awareness (FOIA), focal to bilateral tonic-clonic (FBTC), unclassified (UC). *Cramér's V association measure. †p-value of the Kruskal-Wallis statistical test.

A second analysis (see Table E.10) was performed to evaluate the possible association between the continuous preictal characteristics (duration, density, and starting time) and the categorical (vigilance state, ILAE classification, and onset hour) and continuous (percentage of noise) metadata variables.

The results for the Kruskal-Wallis statistical test between the pairs of categorical and continuous variables indicate that the null hypothesis that the pairs of variables came from the same distribution was rejected for all but one pair of variables, at a 5% significance level. Even though the null hypothesis has not been rejected when Kruskal-Wallis statistical test was applied to the pair onset hour and multivariate

preictal duration, it is important to note that this group contains 33 samples (preictal was found for the data of 33 seizures) and 16 categories (16 discrete hours from the 24 hour discretization period where seizure onset occurred).

Finally, the Pearson's correlation coefficient was computed between the continuous variables: the percentage of noise and each of the preictal characteristics (starting time, duration, and density) found for the seizures assigned categories 3 and 6 (see Table E.10). The results indicate that no correlation was found between the obtained preictal characteristics and the percentage of noise in the EEG signals.

Table E.10: Metadata analysis for the seizures for which a preictal interval has been observed (categories 3 and 6).

Metadata variable	Feature group	Preictal duration	Preictal density	Preictal starting time
Vigilance state	Multivariate (W and N2)	2.80e-13†	2.84e-13†	2.88e-13†
	Univariate linear (all categories)	7.31e-37†	9.91e-37†	7.35e-37†
	Univariate nonlinear (W, N1, and N2)	7.80e-18†	8.08e-18†	7.81e-18†
ILAE classification	Multivariate (all categories)	1.92e-12†	3.03e-12†	1.97e-12†
	Univariate linear (all categories)	0.29e-34†	1.23e-34†	0.29e-34†
	Univariate nonlinear (all categories)	3.47e-17†	4.33e-17†	3.47e-17†
Onset hour	Multivariate (16 categories)	**0.14**†	0.34e-11†	4.95e-11†
	Univariate linear (all categories)	0.02†	2.33e-29†	6.00e-29†
	Univariate nonlinear (18 categories)	3.89e-05†	2.15e-14†	0.18e-14†
Noise	Multivariate	4.51‡	2.88‡	15.05‡
	Univariate linear	11.27‡	9.00‡	22.94‡
	Univariate nonlinear	9.46‡	23.74‡	0.97‡

Seizure vigilance state: wakefulness (W), NREM sleep stage I (N1), NREM sleep stage II (N2), REM sleep stage (R). Seizure ILAE classification: focal onset aware (FOA), focal onset impaired awareness (FOIA), focal to bilateral tonic-clonic (FBTC), unclassified (UC). †p-value of the Kruskal-Wallis statistical test (values above the 5% level of significance are in bold). ‡ Pearson's correlation coefficient. The preictal was found for 33, 101, and 47 seizures for the multivariate, univariate linear, and univariate nonlinear feature groups.

Appendix F

Seizure prediction study

This appendix provides a detailed description of some methodological aspects of the seizure prediction pipeline (in Section F.1) as well as a comprehensive analysis of the results of the seizure prediction study (in Section F.2).

F.1 Patient-specific seizure prediction

Details on the developed seizure predictions models (Hybrid and Control) are exposed here. Figure F.2 also presents a schematic of the steps followed during model development.

F.1.1 Classification

For classification, a linear support vector machines (SVMs) classifier trained after performing a class balancing process was chosen. Long-term data used in seizure prediction is a striking example of class imbalance: the interictal interval is typically considerable longer than the preictal interval. To address this problem, weights were assigned to each class according to class frequency [153, 157]. Namely, each class weight is inversely proportional to the class's frequency. The weight corresponding to class i, W_i, is given by

$$W_i = \frac{N_S}{N_C N_{S_i}}, \tag{F.1}$$

where N_S is the total number of samples, N_C is the number of classes under analysis (interictal and preictal), and N_{S_i} is the total number of samples belonging to each class i. Thus, since preictal samples occur more rarely, weights corresponding to this class are higher.

A linear SVMs classifier was used in this study due to its lower computational complexity when compared to nonlinear classifiers. It is one of the most popular classifiers in seizure prediction [11]. Additionally, it only requires the optimisation of one parameter, the cost C. This is a regularisation parameter that controls the trade-

off between sample misclassification and effective data separability. Specifically, large values of C entail getting a smaller-margin hyperplane in optimisation, whereas small values of C will yield a larger-margin separating hyperplane, even if at cost of more samples being misclassified. In other words, small values of C will result in a larger-margin hyperplane, at cost of some misclassifications and, therefore, with less overfit to the training data (improved generalisation ability). Conversely, larger values of C lead to a smaller-margin hyperplane, meaning less misclassified samples and, therefore, lower training error.

F.1.2 Statistical Validation

To ensure that the prediction models performed above the chance level, a statistical validation was carried out using a bootstrapping method based on the seizure time surrogates [172]. The latter is a Monte Carlo based method which consists in randomly shuffling the original labels of inter-seizure intervals annotated in continuous electroencephalography (EEG) recordings.

In this study, this method was adapted in order to ascertain the performance above the chance level when testing the prediction models for each seizure independently. Thus, for each seizure, the seizure onset time was randomly shifted 1000 times within the interictal time preceding it. Each of the 1000 surrogates' sensitivity was calculated for each randomisation by comparing the surrogate target to the alarms obtained when testing the prediction methodologies (see Figure F.1).

By shuffling the original seizure time for each seizure independently, the bootstrapping method takes into account the nonrandom occurrence of seizures. For instance, if 10 hours of data are recorded for a given seizure and 30 hours for another seizure, generating two random seizure times within the entire recording of 40 hours would not be so rigorous [153].

Additionally, another issue is being dealt with by removing the postictal samples from each inter-seizure interval and randomly positioning the seizure onset time within the postictal free inter-seizure feature time series. Specifically, such a procedure addresses the problem of postictal manifestations in the EEG time series/features after the seizure offset that induces time-dependencies in the prediction models when evaluated continuously [173].

The distribution of surrogate sensitivities was then compared to the sensitivity obtained with the corresponding prediction model, using a one-tailed one-sample t-test. The null hypothesis that the performance obtained with a given seizure prediction algorithm is superior to the performance obtained with the surrogate predictor was tested. A given methodology performs better than chance if its performance is higher than the surrogate performance with statistical significance, i.e., if the null hypothesis is rejected, considering a significance level $\alpha = 0.05$.

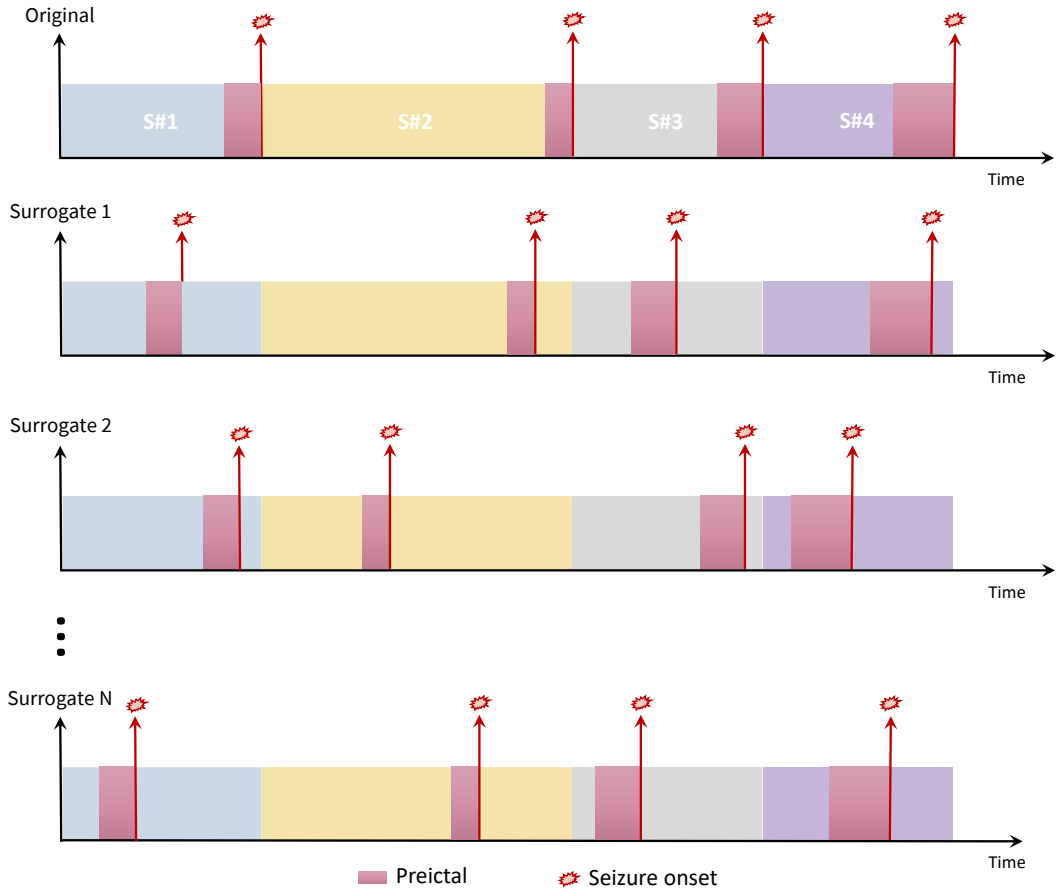

Figure F.1: Example of seizure times surrogate analysis. The position of the preictal interval in the original target data was randomly shuffled N times yielding N surrogate target vectors, with $N = 1000$. Adapted from Schelter *et al.* 2008 [162].

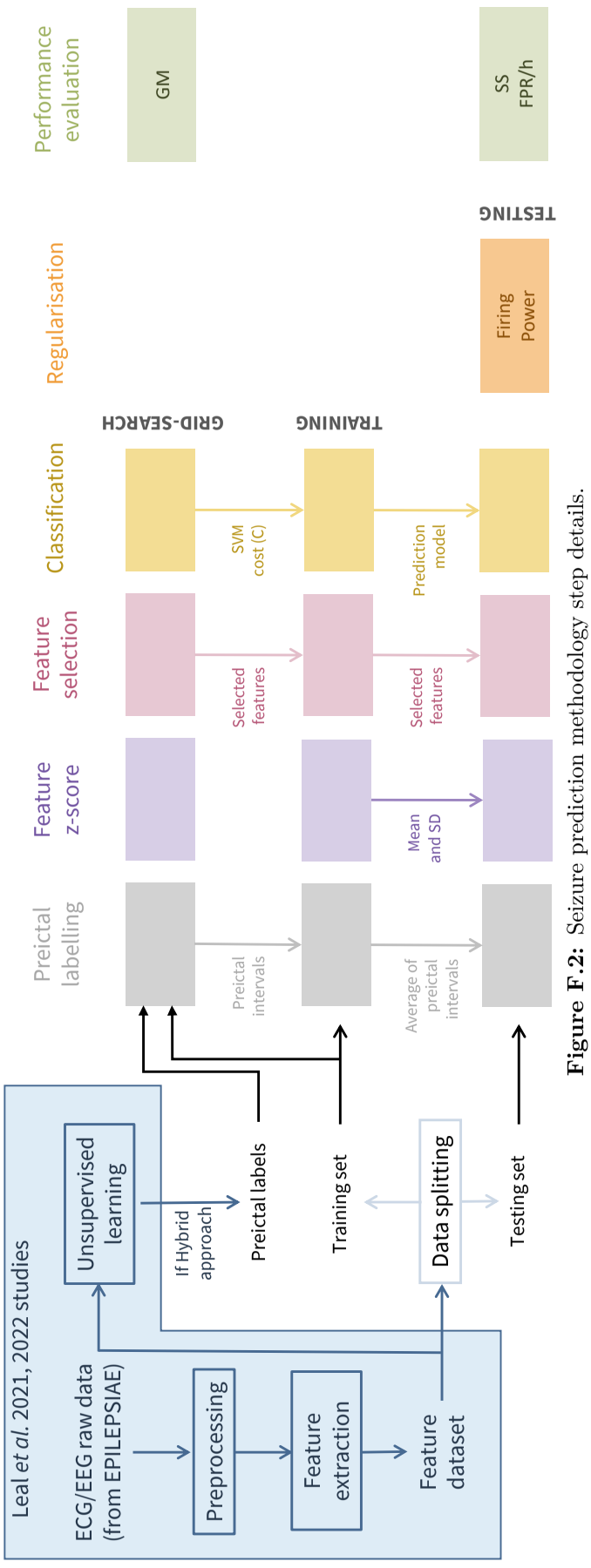

Figure F.2: Seizure prediction methodology step details.

F.2 Results for grid-search model parameters

The results regarding the selected parameters in the grid-search step are presented here.

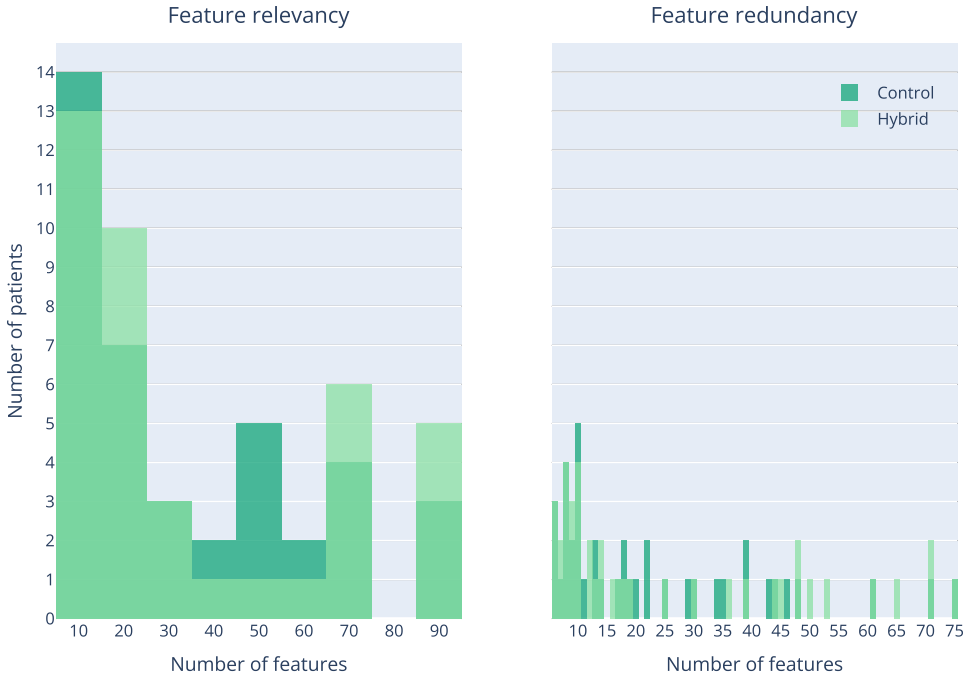

(a)

(b)

Figure F.3: Histograms showing the number of relevant and nonredundant features selected for (a) EEG and (b) ECG, for each approach (according to the order of the feature selection steps followed for each signal).

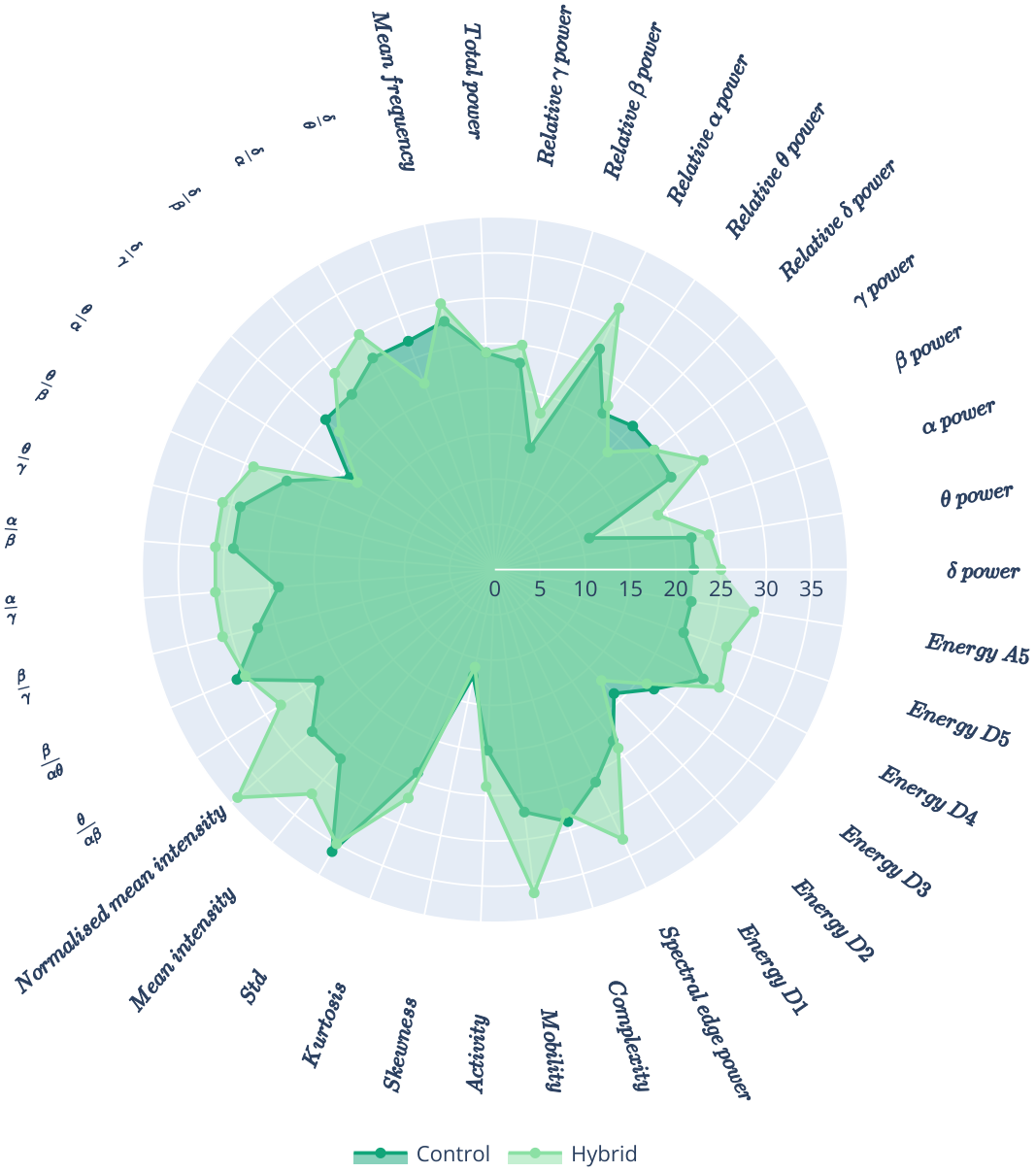

Figure F.4: Radar plot showing the prevalence of each EEG univariate linear feature in the feature dataset obtained after feature selection.

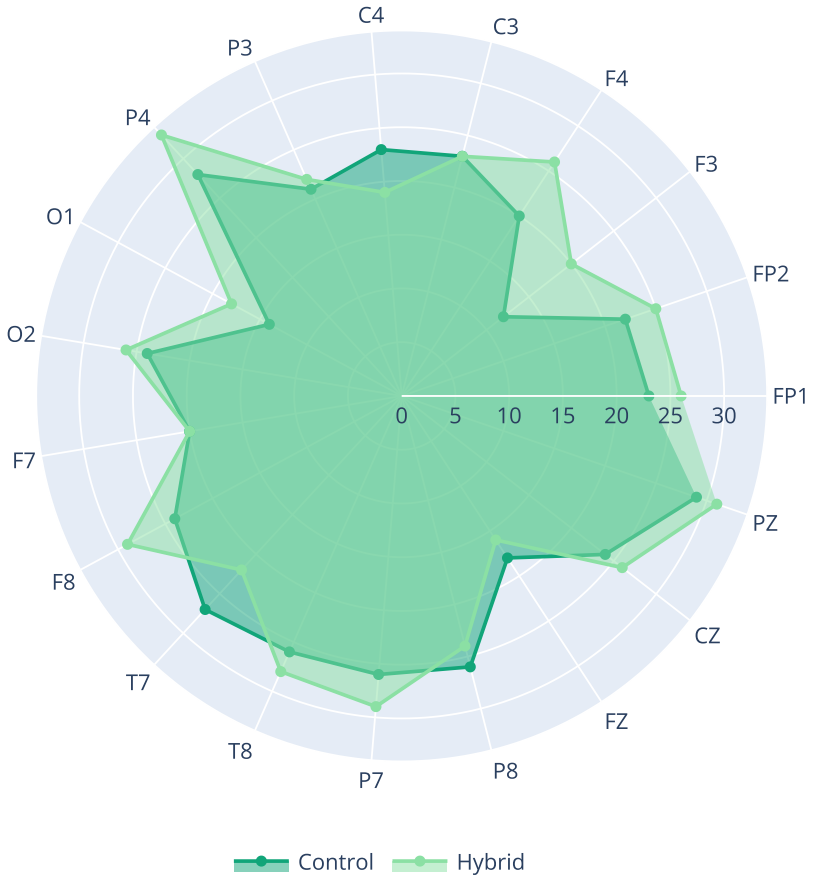

Figure F.5: Radar plot showing the prevalence of each EEG channel in the feature dataset obtained after feature selection.

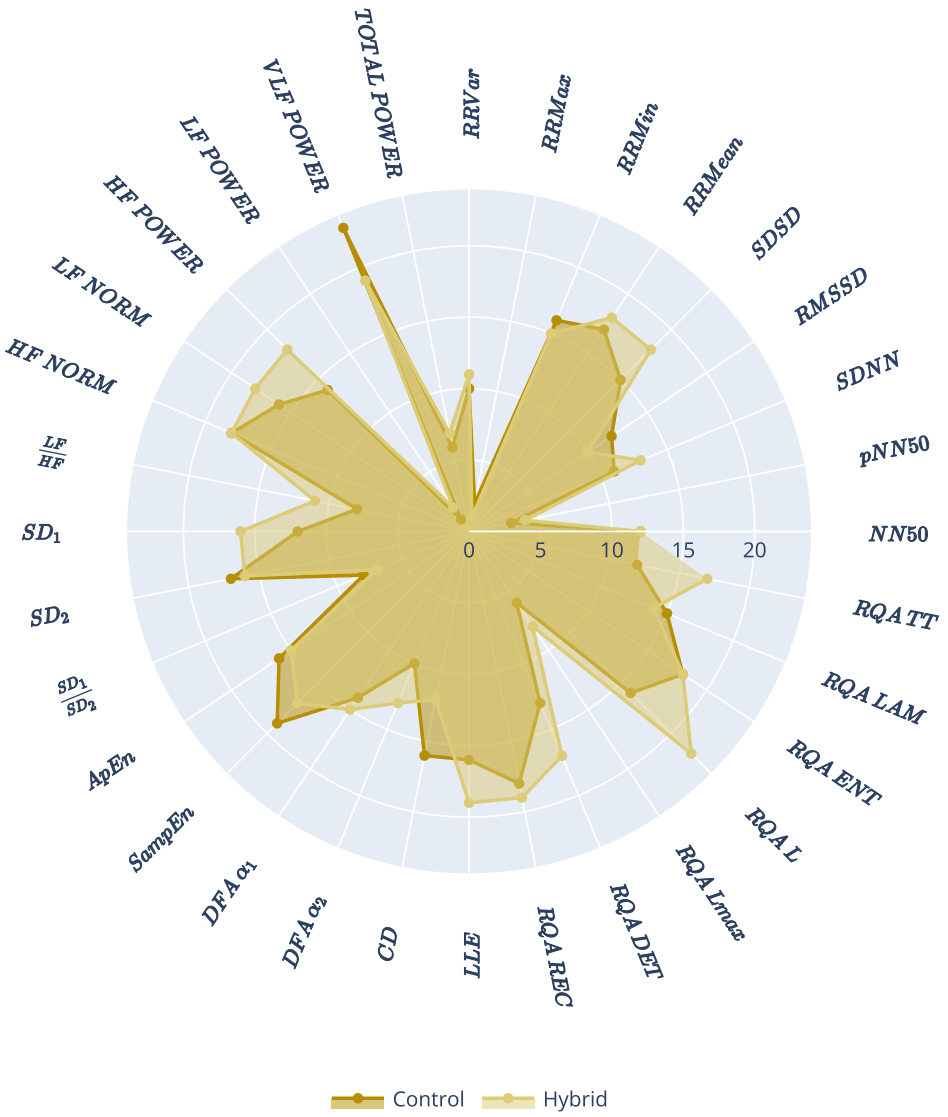

Figure F.6: Radar plot showing the prevalence of each HRV feature in the feature dataset obtained after feature selection.

Figure F.7: Radar plots showing the prevalence of the SVM parameter cost C and the feature relevance method (FR Method) across the patient-specific seizure prediction models.

F.3 Study comparison

This section comprises a prediction performance comparison between the results returned by the EEG-based Hybrid model developed in this thesis and Pinto *et al.* evolutionary algorithm [153] and Pinto *et al.* multiobjective evolutionary algorithm [157].

The average values in Table F.1 were computed for the patients analysed by both EEG-based Hybrid model and Pinto *et al.* 2021 [153] evolutionary algorithm as well as for the patients analysed by both EEG-based Hybrid model and Pinto *et al.* 2022 [157] multiobjective evolutionary algorithm.

Table F.1: Average performance results across patients in each Pinto *et al.* study.

Prediction model	#Pt	SS	FPR/h	ACL
EEG Hybrid model	19	0.40±0.39	0.92±1.76	0.53
Pinto *et al.* 2021 model [153]		0.37±0.24	0.69±0.46	0.37
EEG Hybrid model	32	0.30±0.37	0.65±1.41	0.44
Pinto *et al.* 2022 model [157]		0.18±0.12	0.21±0.07	0.38

#Pt: number of patients; SS: seizure sensitivity (Mean±SD) in the range [0, 1]; FPR/h: false prediction rate per hour (Mean±SD); ACL: ratio of patients with above chance level sensitivity in the range [0, 1].

Table F.2: Performance comparison between EEG Hybrid model, Pinto *et al.* 2021 [153], and Pinto *et al.* 2022 [157], for each patient.

P	ID	EEG Hybrid			Pinto *et al.* 2021			Pinto *et al.* 2022		
		SS	FPR/h	ACL	SS	FPR/h	ACL	SS	FPR/h	ACL
1	402	1.00	0.27	1						
2	8902	0.50	0.28	1				0.20	0.16	0
3	11 002	1.00	1.69	1	0.12	0.37	0	0.00	0.27	0
4	16 202	0.00	0.12	0	0.13	0.39	0			
5	21 902	0.00	0.00	0				0.00	0.18	0
6	23 902	0.00	0.00	0				0.08	0.22	0
7	26 102	1.00	0.05	1				0.13	0.34	0
8	30 802	0.60	0.34	1	0.44	0.63	0	0.19	0.19	0
9	32 702	0.00	0.00	0						
10	45 402	0.00	0.05	0						
11	46 702	0.50	0.00	1				0.25	0.28	1
12	50 802	0.00	0.23	0				0.03	0.22	0
13	52 302	0.00	1.76	0				0.01	0.24	0
14	53 402	0.00	0.61	0	0.67	0.34	1	0.30	0.26	1
15	55 202	0.20	0.13	1	0.70	0.53	1	0.18	0.23	0
16	56 402	0.00	0.19	0				0.05	0.14	0
17	58 602	0.33	1.30	0	0.38	2.14	0	0.05	0.25	0
18	59 102	1.00	1.29	1						
19	60 002	0.00	0.00	0	0.37	1.06	0			
20	64 702	0.50	0.43	1	0.05	0.73	0	0.08	0.14	0
21	75 202	0.00	0.09	0	0.80	0.93	1	0.19	0.14	0
22	80 702	0.67	1.47	1	0.31	0.69	0	0.10	0.14	0
23	85 202	0.50	0.06	1	0.43	0.35	1	0.42	0.25	1
24	93 402	0.00	0.91	0				0.11	0.32	0
25	93 902	0.00	0.06	0				0.37	0.23	1
26	94 402	0.00	0.00	0	0.23	0.82	0	0.13	0.36	0
27	95 202	0.00	0.87	0	0.00	0.45	0	0.09	0.16	0
28	96 002	0.25	0.38	0	0.33	0.69	0	0.16	0.22	0
29	98 102	1.00	0.02	1				0.32	0.11	1
30	98 202	1.00	2.23	1	0.24	0.76	0			
31	101 702	0.00	0.05	0	0.15	0.42	0	0.34	0.24	1
32	102 202	0.00	0.02	0				0.22	0.18	1
33	104 602	0.00	0.94	0				0.33	0.26	1
34	109 502	1.00	7.84	1	0.83	1.35	1	0.11	0.14	0
35	110 602	1.00	0.61	1	0.47	0.33	1	0.37	0.20	1
36	112 802	0.33	1.90	0						
37	113 902	0.00	0.16	0				0.28	0.07	1
38	114 702	0.20	0.11	1				0.16	0.35	1
39	114 902	0.50	0.19	1	0.36	0.18	1	0.33	0.10	1
40	123 902	0.00	0.00	0				0.07	0.14	0

P: patient index. ID: patient identifier. SS: seizure sensitivity in the range $[0, 1]$; FPR/h: false prediction rate per hour; ACL: above chance level sensitivity in the range $[0, 1]$;